SURFACE CRACKS IN METALS AND THEIR CHARACTERISATION USING RAYLEIGH WAVES.

LEONARD JOHN BOND.

Thesis submitted for the degree of

Doctor of Philosophy.

The Department of Physics.

THE CITY UNIVERSITY.

February 1978.

CONTENTS.

Page.

Appendices.

LIST OF TABLES.

LIST OF FIGURES.

ACKNOWLEDGEMENTS.

I would like to thank all the members of the Research Group in Ultrasonics, of the Department of Physics, and particularly my supervisor Dr. A.H.Seville for all his guidance, and Mr J.P.Weight who built much of the electronics used in the Group's Central Ultrasonics Test Equipment.

I would like to thank the British Gas Corporation for their financial support throughout this project and Mr R.F.Lumb, of the Engineering Research Station (British Gas), for his guidance and providing a practical understanding of ultrasonic testing.

I would like to thank Dr. Almoga Ilan, a colleague by correspondence, formerly of the Department of Geophysics and Planetary Sciences, Tel-Aviv University, and since the summer of 1977 with the Group at City, whose studies, together with those of the other members of the Tel-Aviv Group, laid the foundations for much of the present study.

I would like to thank Professor E.Harnik, of the Hebrew University, Jerusalem, for his discussions and guidance with the supporting experimental studies, during his period of sabbatical leave spent with the Group at City in 1976/77.

Finally I would like to thank my wife for her support and encouragement; and her help in checking the original manuscripts of this thesis.

ABSTRACT.

The development of broadband pulsed ultrasonic Rayleigh wave methods in nondestructive testing, has been greatly hindered by the lack of an analytical description of the propagation and scattering of the waves.

The present study presents a review of the previous work on Rayleigh waves in all the fields where they are of interest, in geophysics, seismology, civil engineering, nondestructive testing and high frequency electronics.

A series of mathematical models, which use finite difference approximations, are then presented and used to provide both visual and quantative numerical descriptions of the propagation, interaction and scattering of Rayleigh waves with a range of single-medium configurations, the half, quarter and three-quarter spaces, up and down steps, and open slots, and the two-media configurations of welded quarter spaces and the filled slot.

The techniques of finite difference modelling have not previously been applied to Rayleigh wave nondestructive testing problems and in addition to this new application of the basic technique, extensions to the range of nodal formulations are made, including the presentation of a new second order approximation for the free surface/interface node for welded quarter spaces.

The results obtained with the numerical models are tested by a series of practical experiments on aluminium and steel test blocks. The model results were found to be in agreement with those given by the practical experiments and with those of previous workers who have used numerical, analytical, experimental and visualisation techniques, where they exist.

Following from the analysis of the results of the numerical and experimental work in this study, the author proposes a development in experimental methods for the characterisation of surface features using the advantages of new transducers.

Suggestions are made for extending and improving the basic finite difference methods and for the range of configurations which could be studied.

LIST OF SYMBOLS.

V_c Compressional wave velocity.

V_s Shear wave velocity.

V_r Rayleigh wave velocity.

$\underline{U}$ Displacement vector.

U_1, U_2 components of displacement vector, where,

$U_1(i,j,k)$ is the horizontal displacement

$U_2(i,j,k)$ is the vertical displacement

i is the X_1 index

j is the X_2 index

k is the t (time) index

X_1, X_2 are spatial coordinates with increments d and h respectively.

t is the time coordinate with increment s.

τ is the Cartesian stress tensor, components T_{11}, T_{12}, T_{21} & T_{22}.

λ_j, μ_j are Lame constants

ρ_j density, where j defines the media in two media problems.

G is the shear modulus.

σ is Poisson's ratio.

$\underline{P}$ is the instantaneous power flow vector per unit area.

$\underline{F}$ a matrix with components defined when used.

λ wavelength.

K is a wavenumber where $K = 2\pi/\lambda$

f is frequency where $f = \omega/2\pi$.

other parameters are defined where they are used.

1. INTRODUCTION.

Over recent years there has been an increasing interest in the initial testing and in-service inspection of many engineering products, particularly in relation to such items as aircraft, oilrigs, pressure vessels and pipelines. (Thompson 1976, Lumb 1977)

For this purpose a wide range of nondestructive testing techniques has been developed, for both defect location and sizing. These have included the use of X-rays, electromagnetic induction and dye penetration, with the addition, in recent years, of the increasingly important methods which use ultrasonic waves. There is a wide range of methods of ultrasonic testing which use the different types of elastic waves and display the resulting information in a variety of ways. (Curtis 1975)

In all nondestructive testing much effort is concentrated on the measurement of component thickness and crack depth, and this is particularly so in ultrasonic testing. The present study considers the field of crack depth determination using ultrasonic Rayleigh waves, and concentrates particularly on the problems of providing an understanding of the interaction and scattering of pulsed Rayleigh surface waves at various surface features. The aim of the study is to provide sufficient understanding of the interaction and scattering of Rayleigh waves to enable the characterisation of surface cracks in metals. This information on defect dimensions, when linked with fracture mechanics, should enable better predictions to be made for critical defect size.

Surface waves, including Rayleigh waves, occur not only in metals undergoing nondestructive testing; they are a class of waves of interest to a wide range of workers from a group of very diverse fields. It is found that the interaction of surface waves, and in particular the interaction of Rayleigh waves with surface features, is a subject of study in geophysics, seismology, civil engineering, and high frequency electronic engineering, in addition to the nondestructive testing interest, with the range

in wavelengths going from submillimetre to many tens of kilometres and targets ranging from submillimetre cracks in crystals to geophysical features such as rift valleys and continental boundaries.

Behind all the work in these different fields of study is a common mathematics, which is a subject for study in its own right. This considers the equations which describe the propagation, interaction and scattering of elastic waves.

Although the motivation for the present study has come from the field of nondestructive testing, it is shown in this thesis that the original mathematical interest in Rayleigh waves came mainly from workers in geophysics and seismology and more recently from those working on surface acoustic wave devices.

The background to the present study is thus provided by an extensive body of literature, covering experimental, analytical and numerical work, which crosses all the fields mentioned above. This material is presented in Section 2 of the thesis. As the present study originated in the field of nondestructive testing it is against applications in this field that all the literature is considered. In nondestructive testing, Rayleigh waves have been used to study a wide range of surface and near-surface parameters, with considerable interest being concentrated on the measurement of crack depth; this is reviewed in Section 2.5.

The present combined mathematical and experimental study followed from a piece of experimental work by Morgan (1973), who was the author's predecessor with The Research Group in Ultrasonics of The City University. Morgan studied the interaction of broadband pulses of Rayleigh waves with slots, applying ultrasonic spectroscopic techniques. In seeking to gain a better understanding of these interactions, Morgan looked for a satisfactory theory, but did not find a complete one. In fact the problem of providing a mathematical description of the interaction and resulting scattered pulses for broadband pulses with features of the order of a wavelength, such as a slot, cannot in general be solved using analytical techniques.

It was the lack of a theory which set the present study in motion which has resulted in the numerical model and supporting experimental work which is reported in this thesis.

A range of alternative numerical methods are considered in

Section 3 and the selection of finite difference methods is made for use in a numerical model which can describe the type of wave problem considered by Morgan. That is, to consider the propagation, interaction and resulting scattered pulses for the interaction of broadband pulses, short time domain signals, of ultrasonic Rayleigh waves with slots, and to give the full wave solution, including mode conversion.

The details of the mathematical method, finite difference approximation, which is used exclusively in this study, are given in Section 4 and the supporting appendices. The power of this method is shown by the work of the mathematical seismology group of the late Professor Alterman from the mid 1960's to the present day, although their work has mainly considered body wave sources, (Alterman & Lowenthal 1972) and by the study in connection with surface acoustic wave devices by Munasinghe (1973). It is from this school of finite difference modelling that the present study has developed. The resulting computer programs are considered in Section 6; the results being presented in Section 7.

To test the results of the numerical models a series of practical broadband measurements have been made on specially produced test blocks. In these experiments, wedge transducers are used together with a new edge contact transducer the basic form of which was invented by Professor Harnik, whilst he was working with the author and using the ultrasonic test equipment of the Research Group in Ultrasonics of The City University. (Harnik 1978) The 'Harnik' type probe was developed by the author in the course of the present study and the probes used are considered in Section 8.2.

The present study draws methods and results from all fields where Rayleigh waves have been studied and presents these together with the results obtained in the present study, in Section 9.

The previous studies, reviewed in Section 2 of this thesis, confirm the statements by Ottaviani (1971) that the analytical solution for elastic waves on a quarter space presents "almost insurmountable difficulties" and by Morgan (1973), that no satisfactory model for the reflection (of Rayleigh waves) from a slot exists, in that no analytical description of the propagation and scattering of Rayleigh waves by such surface features as slots, single corners or steps has been found.

Following from the use of finite difference models for elastic wave propagation in geophysics, a new application of the method is presented in providing models of pulsed Rayleigh wave propagation and scattering by surface features on a nondestructive testing scale and this has provided a significant step toward the quantitative understanding of these interactions.

In addition to the new application of the finite difference technique, improvements in the details of the schemes, together with a new second order nodal formulation for the free surface/interface node, for welded quarter spaces, are presented. The use of the improved boundary node schemes, when used with a Ricker type pulse of Rayleigh waves, have made possible a reduction to 16 for the number of nodes per wavelength used and improved the accuracy for the whole scheme. This compares with 32 nodes per wavelength used by Munasinghe (1973). Using the new formulations for boundary nodes, the distance travelled by pulses is better than 1 % when compared with the distances given by ray theory. This compares with travel distance accuracy of the order of 5 % using the old formulations. Pulse distortion with distance travelled is also reduced with the new schemes.

The use of 16 nodes per wavelength, as compared with 32 in other studies, has resulted in the use of a quarter of the number of nodes being used to model the same size space, when measured in wavelengths, or a corresponding increase in the size of object which can be modelled with a set core requirement and job run time.

The finite difference method provides the displacements at every point on the grid in the region studied, and this enables a range of methods to be used to analyse the system and establish such parameters as reflection and transmission coefficients for the single medium geometries of quarter and three-quarter spaces steps and open slots, and the two media geometries of welded quarter spaces and filled slots. In all computer model runs numerical visualisation type displays, which are after Munasinghe (1973) and others, have been improved so as to resolve the waves that are in the stsyem.

The results given by the finite difference models are found to be in good agreement with the experimental results obtained by measurements on test blocks and the results of previous analytical numerical, experimental and photoelastic visualisation studies,

where these exist.

This present study, which started as a direct result of the phrase about Rayleigh waves by Morgan (1973) ,"that no satisfactory model for the reflection from a slot exists", has provided a series of models which follow the propagation and scattering of pulsed Rayleigh waves on half, quarter and three-quarter spaces, up and down steps, open slots, at welded quarter spaces and filled slots These now form the basis for understanding a range of nondestructive testing type problems with both numerical visualisation and quantative numerical results in a single method.

From the consideration of the results of the present study, presented in Section 9, the author has been able to propose a development in the methods which use Rayleigh waves for the characterisation of surface features, using the advantages of the new Harmik (1977) transducers. The proposed method is presented in Section 9.11.

2. BACKGROUND MATERIAL FOR THE PRESENT STUDY.

2.1 Introduction.

This section presents the background against which the present work was performed, as given in the literature and by information obtained by direct contacts with workers in the various fields where Rayleigh waves are of interest. It includes outlines of the previous work with Rayleigh waves and it also presents some definitions which are of direct interest in the present study.

The starting point for the collection of this material was provided by the literature search by Tolley (1972) and the work by Morgan (1973).

In Section 2.2 an introduction to elastic waves and particularly to Rayleigh waves is given which considers the fields where they are studied and gives some of their basic properties. This is followed by Section 2.3 which gives the basic analytical equations for elastic waves in a solid and those specifically for a Rayleigh wave together with the related boundary conditions and some other useful equations.

A review of the material from all fields of study, for a series of idealised geometries is presented in Section 2.4 in order of increasing complexity, and is collected according to the configuration upon which the Rayleigh waves are propagating and being scattered. This is followed by Section 2.5 which considers practical Rayleigh wave measurements with detailed consideration of the specific problem of crack depth measurement being given in Section 2.5.1.

The final part of this section, sub-section 2.6, presents a brief review and introduction to ultrasonic spectroscopy.

2.2 Rayleigh waves.

There are many types of elastic waves which can occur in an elastic solid, on the free surface of a solid, or at an interface between two media where one or both of which is a solid. In each case the waves that will propagate have their own distinctive properties and these waves, which fall into distinct classes, are named according to where the wave propagates, in the body of the medium, at the surface or at an interface, are all accustic or mechanical vibrations. (Graff 1975)

The waves that propagate through the bulk of the medium are called body waves; those which propagate near a free surface, with their energy confined within a few wavelengths of the surface, propagating parallel with the surface, are called surface waves, while those waves that propagate along an interface between two media are called interface waves. Included at the back of this thesis is an appendix, Appendix A, which names some of the basic elastic waves and defines them in terms of their components of displacement.

When an elastic wave is incident on a free surface, an interface, a void or an inclusion, in the case of a body wave, or a surface feature such as a step, a slot or a crack in the case of a surface wave, energy can pass from one form of wave to another. This phenomenon is known as mode conversion. The amount of energy that is converted to or from a particular mode is dependent on the exact form of the incident pulse and the target configuration.

Rayleigh waves are the form of surface waves which have only longitudinal components of displacement in the direction of propagation and transverse components of displacement normal to the free surface; they are named after their first investigator Lord Rayleigh (1885). For a Rayleigh wave there is no energy propagation in the plane of the surface upon which the wave is travelling other than in the original direction of propagation. When a plane wavefront of Rayleigh waves is incident on plane features, normal to the direction of propagation, this effectively reduces the equations which describe them to equations in terms of two spatial dimensions and time. The restriction to studies of systems which allow the reduction to two spatial dimensions is

normal in geophysics, and it is shown in Section 8, in the supporting experimental studies, that this restriction is valid and useful in the present study. The basic equations of motion for two spatial dimensions are given in Section 2.3.

Rayleigh waves are now under active investigation in four fields of study; geophysics/seismology, civil engineering, electronics and nondestructive testing. While the mathematical problems involved in describing the interaction and scattering of waves by features are the same for the four fields, the wavelengths as well as the dimensions of the feature, range over many orders of magnitude, as is shown in Table 1.

Subject	Wave-length	Frequency	Feature size	Order of magnitude
Geophysics	40 km	0.05 Hz	1000 km	10^6 m
Seismology	-	-	10-100 m	10^2 m
Civil Eng.	10 m	100's Hz	1-10's m	10 m
N.D.T.	1-100 mm	25 kHz - 5 MHz	1-10's mm	10^{-3}m
Electronics	0.05 mm	40 MHz -	0.01 mm	10^{-5}m

Range of wavelengths and orders of magnitude of feature size in Rayleigh wave studies.

TABLE 1.

At the long wavelength end of the range are the waves of interest to the geophysicist, which are generated by earthquakes and underground nuclear explosions, where wavelengths are tens of kilometres. This is of particular importance as at these wavelengths the propagation of very destructive high energy pulses is possible over large distances, hence causing damage at large distances from an earthquake epicentre. (Ewing et al 1957) Pulses from geophysical sources also give information about source mechanism and provide a means of studying features comparable with the size of continents.

On an intermediate geophysical/seismological scale there is interest in Rayleigh waves by two groups. These are, firstly investigators who perform local structural investigations using explosive sources and investigate features of the order of metres at ranges from tens of metres to kilometres. The second group are

the civil engineers who, when near an earthquake belt, are required to consider the interaction of Rayleigh waves with large structures such as dams. (Davis & West 1973)

The civil engineer has also to consider vibration-generated Rayleigh waves with wavelengths of the order of tens of metres which are produced by large machines, and which result in requirements for isolation by means of either screening trenches or sheet piling. (Woods 1968)

On a shorter wavelength scale is the region of interest to the nondestructive tester who considers the interaction of Rayleigh waves with features of the order of a wavelength, the wavelength being a few millimetres. (At 1 MHz on Aluminium, Rayleigh waves have a wavelength of about 3 mm.)

The shortest wavelength region is that of interest to the electronic engineer who works in the over ten megahertz region, which has sub-millimetre wavelength. In this region Rayleigh waves are used in circuit components; this field expanded greatly in the 1960's with the growth of surface semiconductor devices. The velocities and consequently the wavelengths of surface waves are five orders of magnitude smaller than the corresponding values for electromagnetic waves of the same frequency and this is shown by the values given in Table 2.

Type of wave.	Vel. in m/sec.	Wavelength in m.
E.M. radiation.	3.0×10^{8}	3.0×10^{2}
Rayleigh wave on aluminum.	2.9×10^{3}	2.9×10^{-3}

Rayleigh and electromagnetic wave velocities and wavelengths at 1 MHz

TABLE 2.

The energy in the surface wave travels in vibrations close to the surface and with this and the slower wave velocities there is the possibility for a wide range of circuit components including waveguides, filters and delay lines for operation in the megahertz region and higher. (White 1970)

Of all the fields of Rayleigh wave study the most recently expanding area of interest is that of nondestructive testing, with the application of Rayleigh waves as a tool for surface and near

surface inspection. These applications of Rayleigh waves are considered in Section 2.5.

In the quest to obtain more information from a signal than can be obtained by considering some form of time display of displacements, signal spectral content is now considered and in nondestructive testing this technique is known as ultrasonic spectroscopy. This method of signal study, which was first described by Gericke (1965) and has been extensively developed at TCU (Brown 1973), uses short time domain pulses of wide bandwidth (now from 0.5 - 20 MHz or higher) as the transmitted signal and spectrum analysis is performed on the transmitted pulse and/or a reference reflected signal and the received scattered pulses, which by comparison, and in some cases complex signal processing, provide more information about a target than is available with conventional ultrasonic testing. This technique, which was first applied to Rayleigh wave nondestructive testing studies by Morgan (1973), is considered further in Section 2.6.

The mechanisms involved in Rayleigh wave scattering by various types of discontinuties are of fundamental importance to all who study Rayleigh waves in practical situations. Thus the study of Rayleigh wave problems concerning scattering from simple targets set in or on isotropic materials, together with such two media problems as that of welded quarter spaces should, when understood, provide a firm basis for considering interactions with real defects. Following a presentation of the basic analytical equations in Section 2.3 the previous work concerning scattering by idealised targets is considered in Section 2.4.

2.3 Basic analytical equations and boundary conditions.

In all analytical or numerical studies of Rayleigh waves, the basic equations, with appropriate changes in scale and material parameters, are common to all the fields of interest. This section presents the basic analytical equations which describe motion in an elastic solid and those which describe a Rayleigh wave, together with the appropriate boundary conditions and some useful relations connecting some of the material parameters.

The equations are presented in two groups, firstly those which describe wave propagation in an elastic solid and secondly

those which describe the Rayleigh wave.

For all elastic wave propagation the vector equation of motion, in a perfectly elastic, homogeneous, isotropic medium is obtained from Hooke's Law and Newton's Second Law of Motion, (Sommerfeld 1950, Ewing et al 1957);

$$\frac{\partial^2 \underline{U}}{\partial t^2} = V_c^2 \text{ grad .(div } \underline{U} \text{)} - V_s^2 \text{ curl . curl } \underline{U} \qquad 2.3.1$$

where $\underline{U}$ is the displacement vector,

V_c is the compressional bulk wave velocity,

V_s is the shear bulk wave velocity,

t is time.

This equation 2.3.1, for a two dimensional system, as for Rayleigh waves, simplifies to a form that was given by Viktorov (1967), which are the basic equations of motion for the horizontal (x) and vertical (y) components of displacement V and U;

$$\frac{\partial^2 V}{\partial t^2} = V_c^2 \frac{\partial^2 V}{\partial x^2} + V_s^2 \frac{\partial^2 V}{\partial y^2} + (V_c^2 - V_s^2) \frac{\partial^2 U}{\partial x \partial y} \qquad 2.3.2$$

$$\frac{\partial^2 U}{\partial t^2} = V_c^2 \frac{\partial^2 U}{\partial y^2} + V_s^2 \frac{\partial^2 U}{\partial x^2} + (V_c^2 - V_s^2) \frac{\partial^2 V}{\partial x \partial y} \qquad 2.3.3$$

The velocities of the shear and compressional waves can be written in terms of the Lamé constants;

$$V_s^2 = \frac{\mu}{\rho} \quad ; \quad V_c^2 = \frac{\lambda + 2\mu}{\rho} \qquad 2.3.4$$

Using the equivalents given as equation 2.3.4 the equations of motion can be written in an alternative form which is often used in seismology, (Alterman & Karal 1968);

$$\begin{aligned} \frac{1}{V_s^2} \frac{\partial^2 V}{\partial t^2} &= \frac{\partial^2 V}{\partial y^2} + \frac{\lambda + 2\mu}{\mu} \frac{\partial^2 V}{\partial x^2} + \frac{\lambda + \mu}{\mu} \frac{\partial^2 U}{\partial x \partial y} \\ \frac{1}{V_c^2} \frac{\partial^2 U}{\partial t^2} &= \frac{\partial^2 U}{\partial x^2} + \frac{\mu}{\lambda + 2\mu} \frac{\partial^2 U}{\partial y^2} + \frac{\lambda + \mu}{\lambda + 2\mu} \frac{\partial^2 V}{\partial x \partial y} \end{aligned} \qquad 2.3.5$$

In considering wave motion in an elastic solid it should be noted that the elastic strains involved in the motion may be computed by partial differentation with respect to displacements and that the elastic stresses can be computed from the strains by applying Hooke's Law.

To describe fully a wave motion in an elastic solid, it is necessary to specify the boundary conditions for both free surfaces and material interfaces and these can be considered in terms of displacements and components of the Cartesian stress tensor.

In the present study only three independent components of the Cartesian stress tensor ($\underline{\tau}$) are involved. (Munasinghe 1973)

The stress is defined by the relation;

$$\underline{\tau} = \underline{G} \cdot \underline{U} \qquad 2.3.6$$

where $\underline{G}$ is the shear modulus.

The components of the shear modulus are;

$$\underline{G} = \begin{bmatrix} V_c^2\,\partial/\partial x & (V_c^2 - 2V_s^2)\,\partial/\partial y \\ V_s^2\,\partial/\partial y & V_s^2\,\partial/\partial x \\ (V_c^2 - 2V_s^2)\,\partial/\partial x & V_c^2\,\partial/\partial y \end{bmatrix} \qquad 2.3.7$$

and the components of the Cartesian stress tensor are;

$$\underline{\tau} = \begin{bmatrix} T_{11} \\ T_{12} \\ T_{22} \end{bmatrix} ; \quad \begin{aligned} T_{11} &= V_c^2 \frac{\partial V}{\partial x} + (V_c^2 - 2V_s^2)\frac{\partial U}{\partial y} \\ T_{12} = T_{21} &= V_s^2 \left(\frac{\partial V}{\partial y} + \frac{\partial U}{\partial x}\right) \\ T_{22} &= V_c^2 \frac{\partial U}{\partial y} + (V_c^2 - 2V_s^2)\frac{\partial V}{\partial x} \end{aligned} \qquad 2.3.8$$

A full treatment of the stress tensor, which describes the components of stress resolved parallel to the co-ordinate axes, is given by Graff (1975).

The boundary conditions are of generalised Neumann type, involving linear combinations of the first degree spatial

derivatives of displacements at all boundaries, with, across material interfaces, the additional condition of requiring the displacements to be continuous. These conditions are set out as equations 2.3.9 to 2.3.13, where T_{11}, T_{12}, T_{21} and T_{22} are components of the Cartesian stress tensor and V and U are displacements.

In the absence of bodily rotation,

$$T_{21} = T_{12} \quad \text{everywhere.} \qquad 2.3.9$$

At a free surface there is zero stress;

For a horizontal free surface, $T_{21} = T_{22} = 0$ 2.3.10

For a vertical free surface, $T_{11} = T_{12} = 0$ 2.3.11

At a material interface both stresses and displacements are continuous;

For a horizontal interface,

V and U , T_{21} and T_{22} are both continuous 2.3.12

For a vertical interface,

V and U , T_{11} and T_{12} are both continuous 2.3.13

In addition to the basic elastic equations, to set up a wave propagation problem it is necessary to specify some initial conditions including the detailed formulation of the wave pulse. The analytic equations for the harmonic Rayleigh wave are now considered with the detailed formulation of the Rayleigh wave pulse used in the model presented in Section 4.4 and Appendix H.

The theory for a Rayleigh wave on a free surface of an elastic solid is well known and was first investigated by Lord Rayleigh (1885). Since that time full theories, including both continuous and transient wave analysis, have been presented by a number of authors including Ewing et al (1957), Morgan (1973) and Graff (1975). In this study only an outline is given for the derivations of the basic equations for the case of an harmonic Rayleigh wave.

The basic equations which describe the harmonic Rayleigh wave are obtained from the equations of motion and the boundary conditions for a free surface.

The basic equations of motion for the bulk of the medium, in the case of an isotropic, homogeneous and perfectly elastic solid can be written in the form;

$$\frac{\partial^2 \phi}{\partial x^2} + \frac{\partial^2 \phi}{\partial y^2} = \frac{1}{V_c^2} \frac{\partial^2 \phi}{\partial t^2}$$

$$\frac{\partial^2 \chi}{\partial x^2} + \frac{\partial^2 \chi}{\partial y^2} = \frac{1}{V_s^2} \frac{\partial^2 \chi}{\partial t^2} \qquad 2.3.14$$

where ϕ and χ are potentials for the compressional and shear waves respectively.

The components of displacement V and U along the x and y axes respectively, given in terms of potentials, are;

$$V = \frac{\partial \phi}{\partial x} + \frac{\partial \chi}{\partial y}$$

$$U = \frac{\partial \phi}{\partial y} - \frac{\partial \chi}{\partial x} \qquad 2.3.15$$

The resulting components of stress are those which have been given as the Cartesian stress tensor, equation 2.3.8.

When the condition for a stress free surface is substituted into expressions for the potentials; a linked pair of equations is obtained which can be combined into an expression which has a characteristic equation that, after transformation reduces to the form;

$$\eta^6 - 8\eta^4 + 8(3 - 2\mathcal{U}^2)\eta^2 - 16(1 - \mathcal{U}^2) = 0 \qquad 2.3.16$$

where $\eta = Vr/Vs$; $\mathcal{U} = Vs/Vc$.

This equation, equation 2.3.16, is a cubic in η^2 and is known as the Rayleigh wave equation, as it is from the roots that the value of the Rayleigh wave velocity (V_r) is obtained. The roots of the equation can be obtained by the use of the techniques for the solution of a cubic equation.

As equation 2.3.16 is a cubic in η^2 there are six roots, the Rayleigh wave velocity is given by the root which satisfies

the condition for the ratio of the Rayleigh wave to shear wave velocities;

$$1 > V_r / V_s > 0$$

It is found that the roots are dependent on Poisson's ratio (σ) and that when;

$\sigma > .263$ there is 1 real root and two complex conjugate roots.

$\sigma < .263$ there are three real roots.

In the case of three real roots it is found that in two cases the constants required in the pair of equations which give equation 2.3.16 are complex.

For all real media Poisson's ratio is subject to the restriction;

$$0 < \sigma < 0.5$$

and this condition ensures that only one root will satisfy the restriction on the values for the V_r/V_s ratio.

A useful approximation for the value of the Rayleigh wave root has been given by Bergmann (1949) which provides a method for rapid calculation of the Rayleigh wave velocity.

$$\frac{V_r}{V_s} = \left[\frac{0.87 + 1.12\,\sigma}{1 + \sigma} \right] \qquad 2.3.17$$

The values obtained from equation 2.3.17, for given Poisson's ratio are plotted against Poisson's ratio and given as Figure 2.1. Cook and Valkenburg (1954) have calculated the values of the roots of equation 2.3.16 to three significant figures and when compared with the values given by equation 2.3.17 there is found to be a maximum error of less than 1 %.

The ratio of the shear and compressional wave velocities can be given in terms of Poisson's ratio and this is given as;

$$\frac{V_s}{V_c} = \left[\frac{1 - 2\,\sigma}{2 - 2\,\sigma} \right]^{1/2} \qquad 2.3.18$$

The values obtained for the ratio (V_s/V_c) given by the

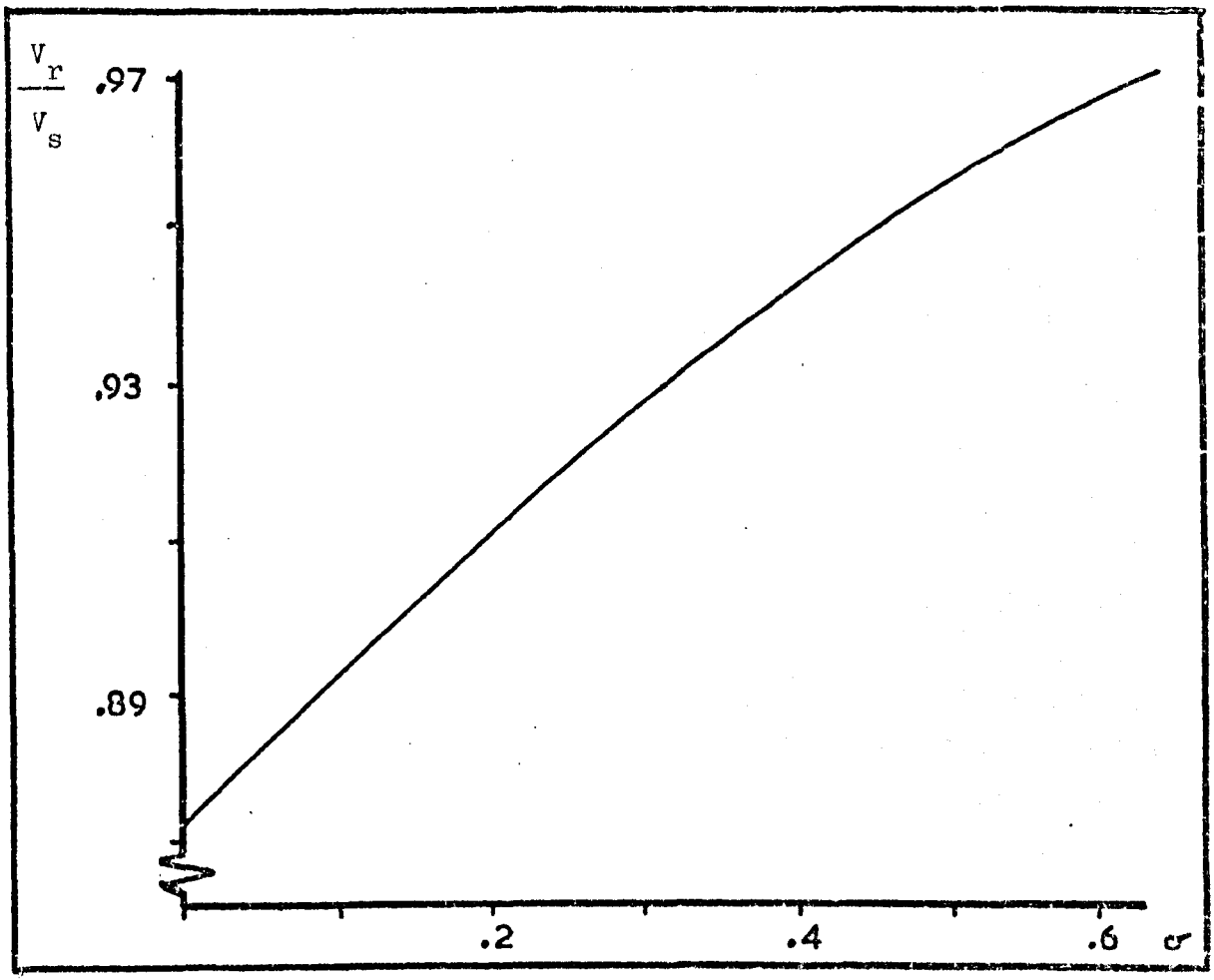

Graph to show values of the ratio Vr/Vs against Poisson's ratio (σ)

FIGURE 2.1

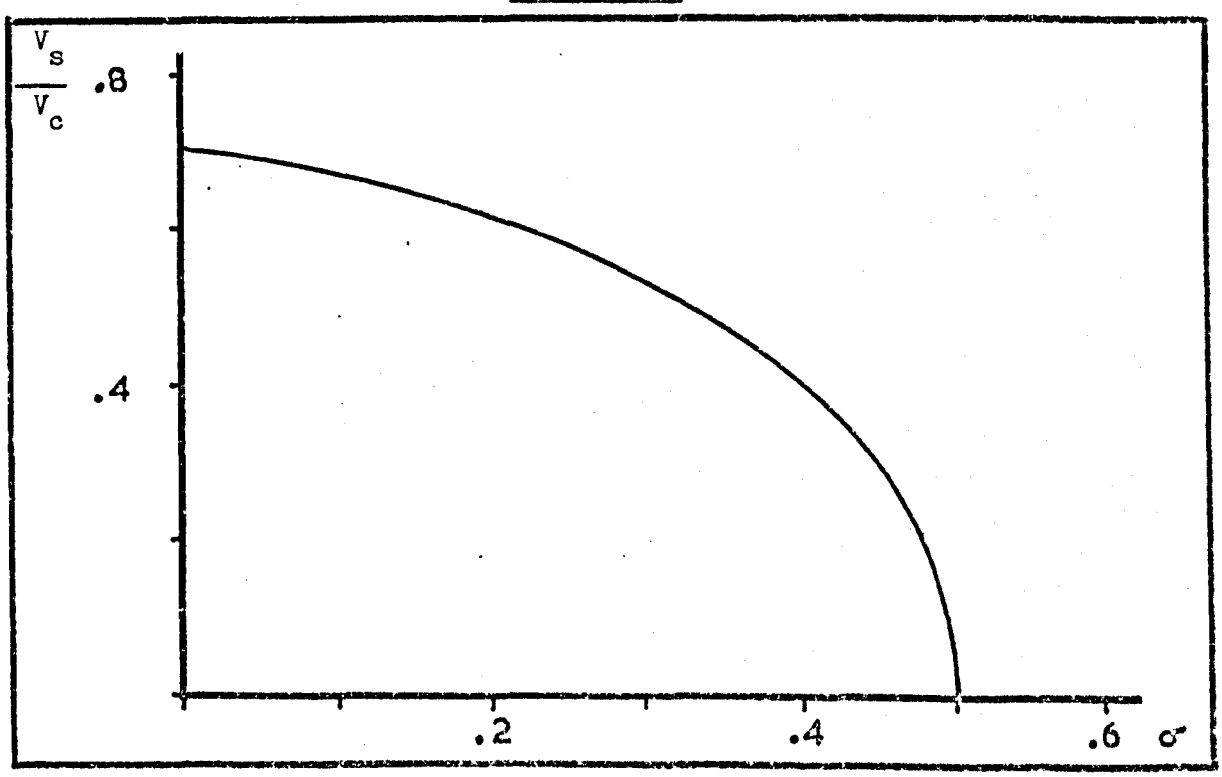

Graph to show values of the ratio Vs/Vc against Poisson's ratio (σ)

FIGURE 2.2

equation 2.3.18 are plotted against Poisson's ratio and shown as Figure 2.2. The value of this ratio (V_s/V_c) is found to be linked with stability for a finite difference scheme and this is considered in Section 4.5.

A further useful relationship is that between Poisson's ratio and the Lamé constants and this is, (Cottrell 1964, p114);

$$\sigma = \frac{\lambda}{2(\lambda+\mu)} \qquad 2.3.19$$

A full consideration of the interrelation of the elastic constants is given by many authors including Mow and Pao (1971).

The equations for the displacements of harmonic Rayleigh waves are obtained upon solution of the equations of motion subject to the free surface boundary conditions. In the case of a perfectly elastic homogeneous, isotropic medium for wave propagation, in the case where the elastic strains produce only small deformations, the equations which describe the decay of the vertical and horizontal components with depth are;

$$U = A\,\frac{2\,(1 - V_r^2/V_c^2)^{\frac{1}{2}}\,(1 - V_r^2/V_s^2)^{\frac{1}{2}}}{2 - V_r^2/V_s^2}\, e^{-\frac{2\pi}{\psi}(1 - \frac{V_r^2}{V_s^2})^{\frac{1}{2}} Z} - e^{-\frac{2\pi}{\psi}(1 - \frac{V_r^2}{V_c^2})^{\frac{1}{2}} Z} \sin(\omega t + kx)$$

$$V = -A\,\frac{2\,(1 - V_r^2/V_c^2)^{\frac{1}{2}}}{2 - V_r^2/V_s^2}\, e^{-\frac{2\pi}{\psi}(1 - \frac{V_r^2}{V_s^2})^{\frac{1}{2}} Z} - (1 - \frac{V_r^2}{V_c^2})^{\frac{1}{2}}\, e^{-\frac{2\pi}{\psi}(1 - \frac{V_r^2}{V_c^2})^{\frac{1}{2}} Z} \cos(\omega t + kZ)$$

2.3.20

The values obtained with these equations, 2.3.20, for two different media are shown as Figure 2.3, with the depth ($Z = y/\gamma$) shown normalised against wavelength (ψ).

Rayleigh waves, in the case of a homogeneous, isotropic, perfectly elastic half-space, consist of two inhomogeneous waves,

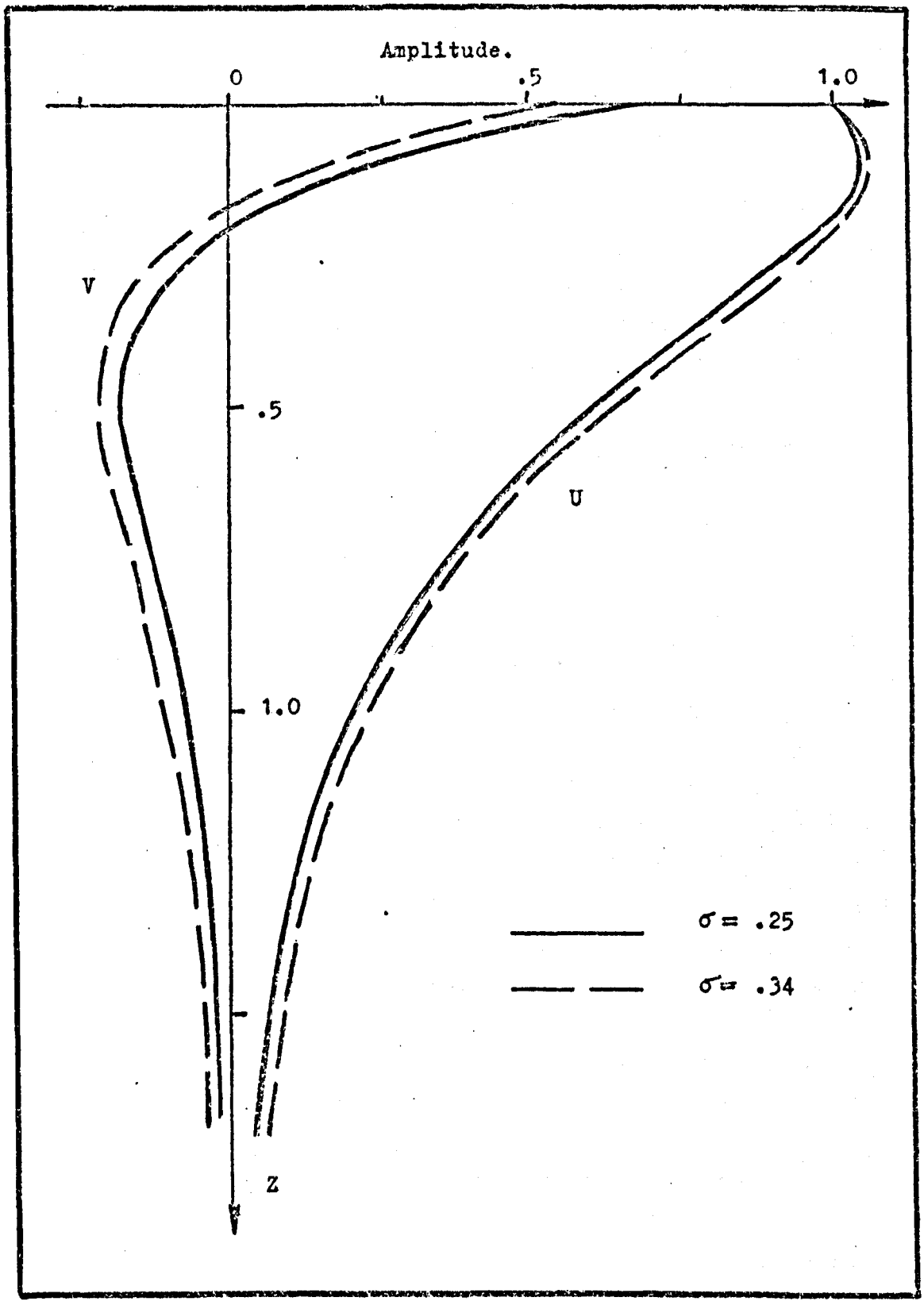

The decay of displacements with depth (Z) for the harmonic Rayleigh wave, given by the analytic equations, at the points of maximum surface displacement.

FIGURE 2.3

one compressional (longitudinal displacements) and one shear (transverse displacements) which propagate along the boundary with identical phase velocities. The displacement amplitude and energy decay rapidly with depth.

In summary, for a pulse of Rayleigh waves in an elastic solid, the problem is in the category of propagation problems which are basically hyperbolic in form, (Ames 1969) and they can be made well posed (Courant and Hilbert 1962) in the sense of having unique solutions which depend continuously on the auxiliary data such as the initial conditions.

Having defined some of the properties and equations which describe Rayleigh wave propagation, attention now turns to consider the previous work which has been performed on Rayleigh wave scattering from idealised targets of increasing complexity.

2.4 Previous work on simple geometries.

This section presents a collection of the analytical, experimental and numerical studies for continuous, pulses and semicontinuous Rayleigh waves, as presented in the literature in all the fields where they are studied. It considers the studies on idealised geometries which form the background to this present study and it is according to the geometry that the material is presented.

This present study has confirmed that although there have been numerous theoretical and experimental studies, with in some cases support from numerical models and or Schlieren or photoelastic visualization, exact analytical solutions are only possible for a few special cases, such as the Rayleigh wave on a half-space. (Ewing et al 1957) It has also shown that no adequate theory exists for predicting the resulting scattered pulses for wideband pulses of Rayleigh waves incident on general surface breaking features, with dimensions of the order of a wavelength.

The geometries reviewed in Sections 2.4.1 to 2.4.6 are shown in Figure 2.4, and they are presented in order of increasing complexity. The results from the various studies reported in general in this section are considered in more detail in Section 9, together with the results from the present study.

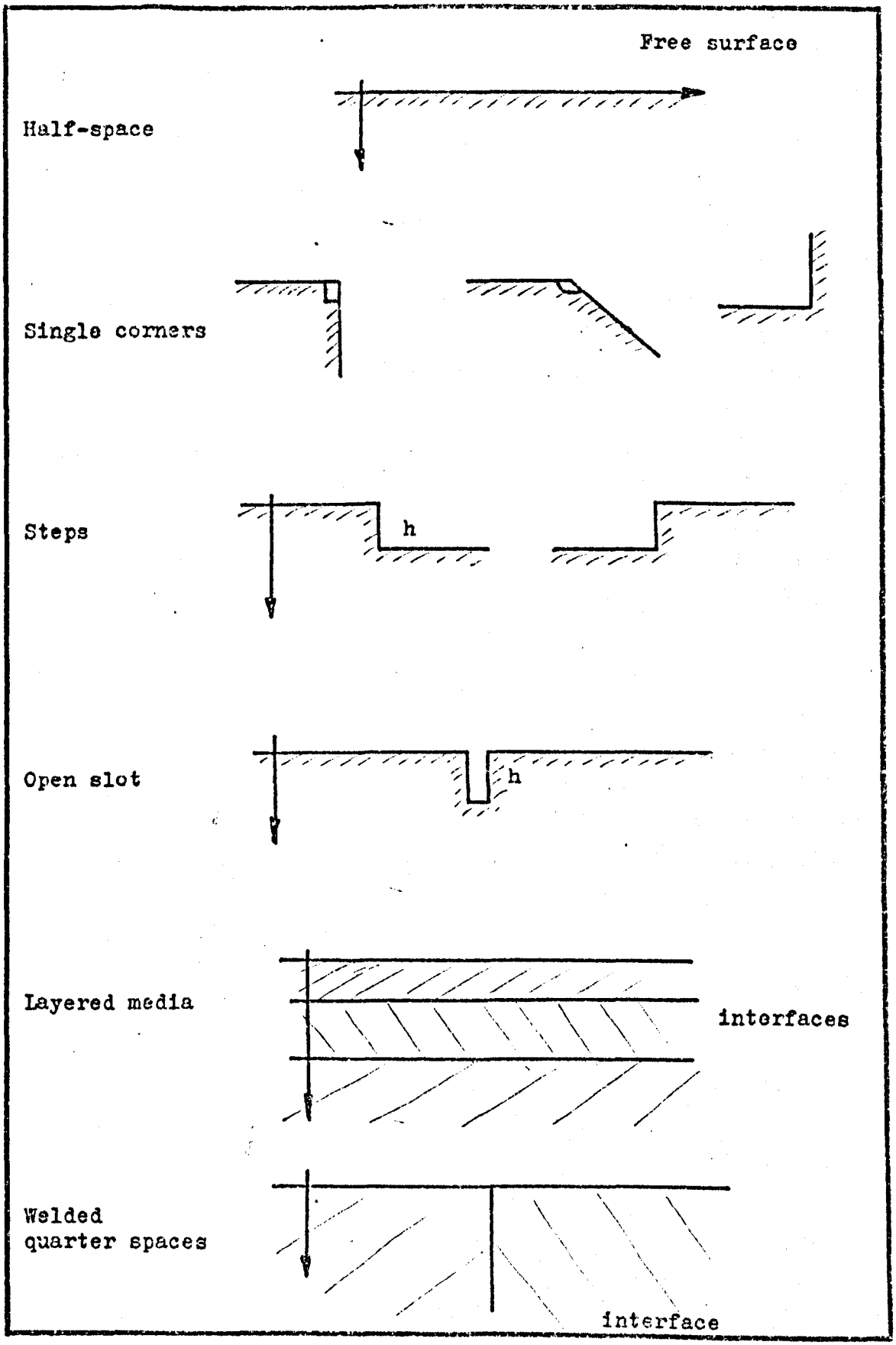

The simple geometries considered in the literature review.

FIGURE 2.4

2.4.1 Rayleigh waves on a half-space.

Rayleigh waves were first demonstrated theoretically to propagate at the free surface of an elastic solid by Lord Rayleigh in 1885. (Rayleigh 1885)

The behaviour of Rayleigh waves on half-spaces is of considerable importance, in that, along with the layered half-space which is considered in Section 2.4.5, it is one of the few cases where an exact analytical solution is available. These solutions have been considered by many authors including Ewing et al (1957) and Graff (1975). The half-space exact solution is of importance in that it provides an analytical form for testing any model for pulsed Rayleigh wave propagation, with the detailed equations for the case of the harmonic Rayleigh wave given in Section 2.3.

In the special case of the solid which is perfectly elastic homogeneous and isotropic, the velocity of propagation is independent of frequency and the waves travel without attenuation in the direction of propagation. In practice on metals at megahertz frequencies it is found that over distances of tens of wavelengths Rayleigh waves will propagate very close to nondispersively when surface roughness is less than .001 of a wavelength.

The problems of measurement on nonideal surfaces which have features such as roughness, suffer attenuation of the propagating waves, and this is considered in Section 2.5 with the practical applications of Rayleigh waves.

2.4.2 Rayleigh waves at single corners.

Fundamental to obtaining an understanding of what scattered pulses can be expected from the interaction of a Rayleigh wave and a defect, is the understanding of those which result from an interaction with a single corner. An idealised form of the scattering which results from a single corner of angle between 80° and 160° struck by a pulse of Rayleigh waves is shown as Figure 2.5. The pulses obtained are transmitted and reflected pulses of Rayleigh waves and two mode converted pulses, one each of shear and compressional waves, which represent energy losses from the Rayleigh waves in the system. The percentage energy loss as well as the energy in each of the Rayleigh wave pulses is

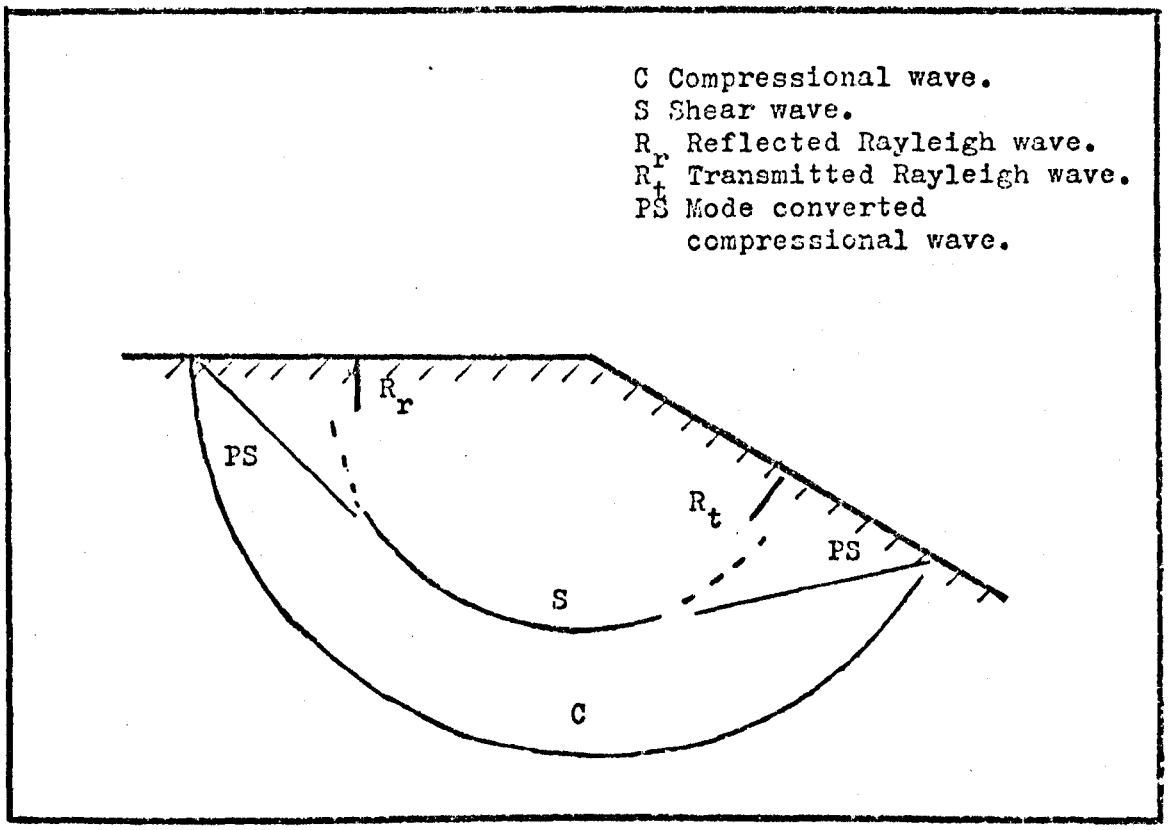

The pulses resulting from a general Rayleigh wave interaction at a corner between 80° and 160°.

FIGURE 2.5

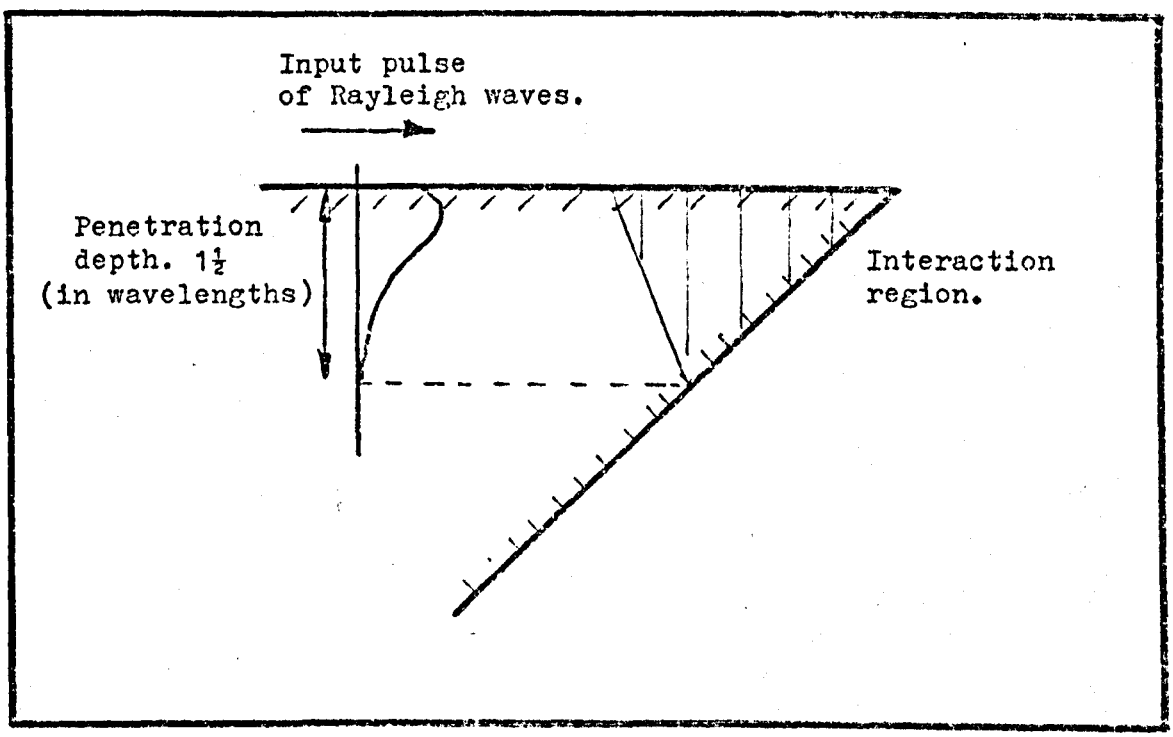

A Rayleigh wave at a corner on a wedge of less than 80°.

FIGURE 2.6

dependent on the exact angle and shape of the corner.

For the wedge of angle less than 80°, as shown in Figure 2.6, the incident, reflected and transmitted pulses, together with the mode converted pulses, have a very complex interaction which occurs not just at the corner but at the two surfaces and in the bulk of the medium in the region near the corner. This is because a Rayleigh wave has a finite penetration depth, of about one and a half wavelengths, as shown in Figure 2.3, which gives the region of interaction.

In practical experiments the sharpness of the corner considerably affects the pulse/corner interaction: a corner which has a radius of curvature of more than about two wavelengths produces no reflected or mode converted waves, the pulses just passing from one surface to the other without change of shape.

There have been numerous studies of single corners and they have covered all angles from 0° to 360°. Many of these studies originate in the field of geophysics as it is the single corner, in the acute wedge configuration as it occurs in the Earth, which is of considerable significance as a producer of non-coherent seismic noise. (Knopoff & Gangi 1960)

The previous studies of wedges are now considered in four groups; those which have measured transmission and reflection coefficients experimentally; those which have sought to provide an analytical expression which fits the experimental results; those which visualise the interaction in a glass or plastic model and those which try to model the scattering using a numerical method.

a. Experimental studies on wedges.

There have been a range of experimental attempts to establish transmission and reflection coefficients for different wedge angles, on different materials and at different frequencies. The earliest study was performed by de Bremecker (1958) who used piezo-electric transducers on a range of polystyrene wedges with angles from 0° to 180°, working at frequencies between 20 and 200 kilohertz. Similar experiments have been performed by Viktorov (1967) working on Dural blocks with wedge angles between 12° and 170°, using 10 μsec pulses of 2.7 MHz Rayleigh waves. There have been studies on aluminium blocks by Knopoff and Gangi (1960), for wedge angles from 0° to 360°, and by Pilant et al (1964) on wedges with angles

between 0° and 180°, working with broadband signals from 50 to 400 kHz.

A further experimental study is that by Haydl (1974) who has made measurements for 90° corners on gallium arsenide at frequencies from 20 to 200 MHz.

b. Analytical studies on wedges.

The second group of studies are those which seek to produce an analytical curve in agreement with the experimental results. These include studies by Knopoff and Gangi (1960) for 0° to 360° wedges and Hudson and Knopoff (1964) who used a Green's function approach and also considered wedges with angles from 0° to 360°. These studies were followed by a paper by Mal and Knopoff (1965) who improved on the approximations in the Hudson and Knopoff (1964) paper. Viswanathan et al (1971, 1973) have recomputed the Hudson and Knopoff (1964) curves. Calculations have also been performed by Kane and Spence (1963) who obtained an approximate expression for the transmitted pulse using an iterative procedure for angles from 0° to 180° and this has been followed by the work of Yoneyama and Nishida (1976) using the same method.

In addition to the treatments of general wedges there has been some work on the quarter space, the single 90° corner, with Lapwood (1961), using an integral transform formulation, having developed first order expressions for incident and transmitted waves.

When the various theories are compared with each other and with the experimental results, it is found that agreement between the different studies is far from good. (Morgan 1973) The problems in comparison are increased by the fact that in many of the studies different methods and materials have been used. Also in the analytical work the methods used in most cases involve approximation.

The reflection and transmission coefficients for 90° and 270° corners have now been obtained by a number of workers and the values obtained are compared in Section 9 with the results from the present study.

There have also been studies of body wave interactions on wedges which result in mode converted pulses of Rayleigh waves and of particular interest is the experimental work by Gangi (1967) who determined compressional (P)/ Rayleigh wave conversion coefficients for aluminium wedges with a range of wedge angles.

c. Visualization studies on wedges.

In attempts to provide insight into the wave corner interactions in the bulk of the medium some work has been performed using photoelastic visualization which shows the stress patterns in transparent media; these are considered further in Section 2.4.7. (Henzi & Dally 1971, Hall 1976)

d. Numerical studies on wedges.

In seeking to provide a more quantitative understanding of the interaction of Rayleigh waves with corners and the resulting scattered pulses some workers have turned their attention to consider approximate and numerical methods, as is illustrated by the work of Alsop and Goodman (1972) who have used a finite element method for semicontinuous waves on a quarter space. Work by Munasinghe and Farnell (1972) and Cuozzo et al (1977) on quarter and three-quarter spaces has applied the finite difference method to pulses and semicontinuous Rayleigh wave propagation respectively. The approximate mathematical and numerical methods are considered in detail in Section 3.

There are many body wave studies but in general these are beyond the scope of this present study; however further consideration is given, in Section 3, to the numerical methods which have application to surface wave problems.

2.4.3 Rayleigh waves at steps.

It is apparent that the interaction with a step configuration is going to be more complex than that with a single corner. The addition of a second corner at some distance from the first introduces a spatial dimension, in addition to pulse penetration depth into the system, and this makes the interaction become wavelength dependent, or rather dependent on the ratio of the feature dimension or dimensions to pulse wavelength or wavelengths. All wavelength dependence is in addition to and linked with material parameter dependent effects.

For a feature consisting of combinations of 90° and 270° corners separated by distances greater than two wavelengths it is sufficient to consider the pulse as interacting with each corner separatelyand in turn; the separate signals from each corner may

be identified in the time domain, as is shown in Section 8, and the problem in principle reduces to one of sucessive application of reflection and transmission coefficients, with energy losses to the other modes.

However, when the corners are closer together than two wavelengths, as for a shallow step, this simple approach is inadequate and the interaction must be considered as a whole. The problem has become wavelength dependent and analytically insoluble for step heights of the order of a wavelength.

The geometries considered by previous workers have, in general removed additional angular dependence from the step problem and restricted consideration to the step change in elevation with a 90° and a 270° corner which have a given vertical separation, on a single homogeneous isotropic medium, as is shown in Figure 2.7.

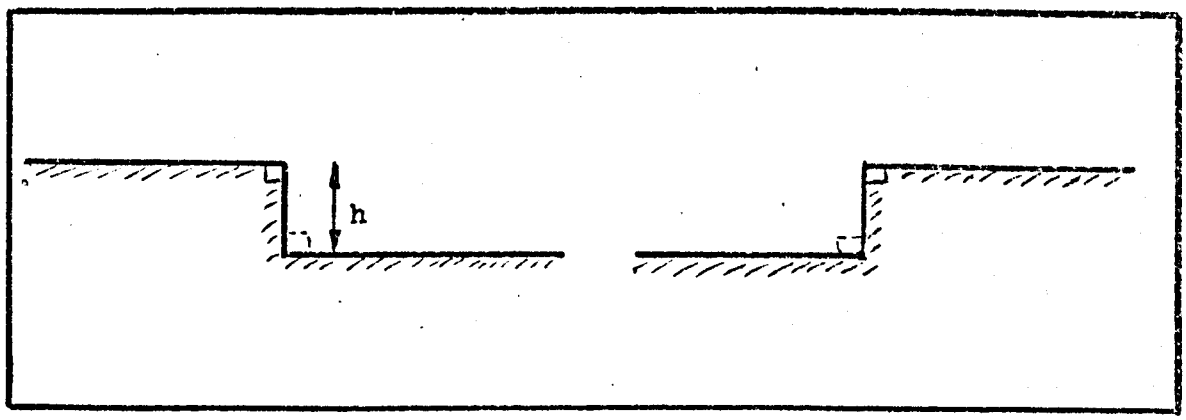

Step changes in elevation on homogeneous media.

FIGURE 2.7.

An exception to the restriction to single media configurations is made in some surface acoustic wave device related studies where the elevated medium is of a second type, giving a configuration such as a layer of aluminium over silicon.

The previous work on steps can be considered in three groups, according to the step height (h) to pulse wavelength (ψ) ratio h/ψ.

a. Step height to wavelength ratio (h/ψ) less than 0.1.

The first group of studies, those with h/ψ less than 0.1, are mainly linked with surface acoustic wave device studies. In this range of step heights some analytical perturbation techniques have application, as is shown by the work of Sabina and Willis (1977)

and Mal and Knopoff (1965)

For very shallow steps, up to h/ψ of 0.02, Li (1974) has applied a transmission line representation. There have also been a number of experimental studies in this range.

b. Step height to wavelength ratio (h/ψ) of the order of one.

The second group of studies which consider studies with the step height to wavelength ratio h/ψ from about 0.2 to 2.0 include, at the bottom end of the range approximate analytical methods, and across the whole range both experimental and numerical studies.

It is in this group of h/ψ ratio values that many geophysical studies fall including those by Drake (1972) using finite element methods to study waves at continental boundaries.

An approximate variational method, which has application up to h/ψ of about 0.5, has been applied by McGarr and Alsop (1967) to studies on media with high Poisson's ratios.

The finite difference method has been applied by Munasinghe (1973) to both up and down step pulsed wave problems, mainly considering waves on polystyrene or aluminium/quartz layered configurations and the details of the method used are considered in Sections 3 and 4. A further study of Rayleigh waves at steps using finite difference methods has been made by Cuozzo et al (1977), but they have considered semicontinuous waves and not pulses.

A series of experimental measurements have been performed by Frost et al (1975), on steps in aluminium blocks, using a new type of noncontact surface wave transducer.

There have also been studies using visualization techniques and these include work by Dally and Lewis (1968) who considered steps in the range from 0 to 1.5 h/ψ. This has been followed by further work which has been presented by Hentzi and Dally (1971).

c. Step height to wavelength ratio (h/ψ) greater than two.

The third group of studies are those where the wavelength dependence has been removed, in that deep steps are considered and an example of this is found in the work by Mal and Knopoff (1965) which uses a Green's Function approximation for deep steps.

In general there is little overlap between the various groups of studies and within the groups the direct comparison of results is difficult as the studies tend to either be using different media or calculate or measure different parameters.

There are however four studies of the down step for h/ψ of the order of unity which can be used to test models and results in the present study and these are considered in Section 9 together with the results of the present study.

2.4.4 Rayleigh waves at slots normal to a surface.

The extension of studies from up and down steps to slots is of considerable importance as the slot is an idealised open crack and it is cracks which are of particular interest in nondestructive testing.

As with the studies of steps the previous work on slots tends to fall into distinct classes according to the slot depth (h) to wavelength (ψ) ratio h/ψ and it is in order of increasing values of this ratio that previous work is now considered.

a. Slot depth to wavelength ratio (h/ψ) less than one.

Much work has been performed relating to surface acoustic wave devices for a range of shallow slots of different depths and profile with the slot considered both as a single feature and as a multi-slot array. Examples of these mixed experimental and theoretical studies are found in the work by Tuan (1975), who considered the bulk waves generated by Rayleigh waves incident on surface slots, and in those by Rykunov and Tkhukh (1972) and Tuan and Perekh (1975).

A further study on shallow slots is that by Ronnekliev and Souquet (1975) who studied slots one twentieth of a wavelength deep and half a wavelength wide, at 1.15 megahertz, cut in aluminum blocks.

There has been some numerical work using finite difference methods to model the interaction and scattering of Rayleigh waves by slots, as occur in surface acoustic wave devices. The two main groups of studies in this field are those by Munasinghe (1973) and Cuozzo et al (1977). The work by Munasinghe (1973) has considered pulsed Rayleigh waves at wide layered slots, the width (w) being greater than 1.5 ψ and with depths (h) up to 0.8 ψ, of the type shown in Figure 2.8. The study by Cuozzo et al (1977) has considered a semicontinuous wave source with either single or arrays of wide shallow slots.

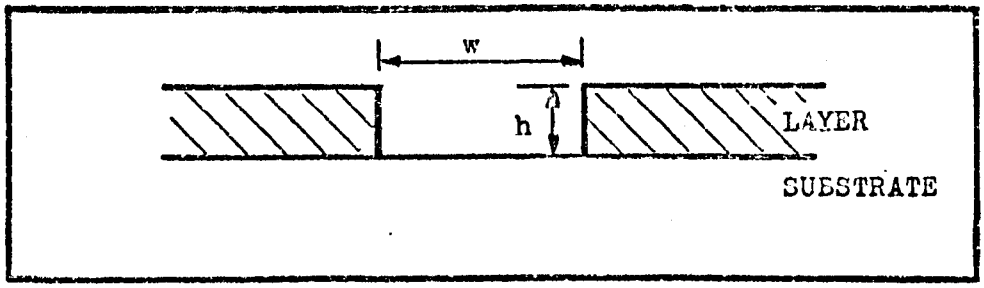

The layered wide slot, as considered by Munasinghe.

FIGURE 2.8.

b. Slot depth to wavelength ratio (h/ψ) of the order of one.

The second group of studies are those where the slot depth is of the order of a wavelength and it is in this range that several studies have been performed on either aluminum or aluminum alloy test pieces. An early attempt to establish transmission and reflection coefficients is that by Viktorov (1967) who measured the incident, transmitted and reflected signals from a slot which was made progressively deeper.

In many cases of practical interest, slot depth is less than two wavelengths and the measurement of depth from identifying time domain signals is not possible.

It is in this range that the studies by Morgan (1973) fall; he applied ultrasonic spectroscopy to the pulses scattered by milled slots in aluminum alloy blocks, that are both normal and at slanting angles to the surface. The information relating to target dimensions is still in the scattered pulses, if a broadband incident pulse is used, and is obtainable using the technique of ultrasonic spectroscopy, which is considered in Section 2.6. The interpretation of Morgan's (1973) results was greatly hindered by the lack of a theory, and it is as a direct result of this problem that the present study was undertaken.

c. Slot depth to wavelength ratio (h/ψ) greater than 1.5.

As for a step, the scattering of a Rayleigh wave pulse by a slot results in separate identifiable pulses in the time domain only when target dimensions are greater than about two pulse wavelengths, that is the wavelength dependence has been removed and each corner acts as a scattering centre. For a deep slot or crack with a point tip where there are three distinct scattering centres it must be at least 1.5 ψ deep for identification of signals in the time domain and this is the case in the crack depth measurement studies reported in Section 2.5.

In a further attempt to gain a better understanding of the interaction of Rayleigh waves with deep slots and the resulting scattered pulses, photoelastic visualization studies have been performed by Reinhardt and Dally (1970) and Hall (1976) and these show the complex pattern of pulses that results.

There is all too little published work on slots to provide the starting point to build the bridge to enable the understanding of scattering by real defects and hence defect characterisation. The previous experimental work on real situations is presented in Section 2.5.

Although reflection and transmission coefficients have been measured for a few slots and the scattered waves studied for particular features only a few general trends for the reflection coefficients and the expected pulses have been published. The slot configuration is one which requires considerable work to establish a more general understanding of the scattered pulses which will be generated: this is especially so if extension is to be made to cracks or slots which are not normal to the surface. The results of previous studies on slots are considered further in Section 9 together with the results of the present study which are presented in Sections 7 and 8.

2.4.5 Rayleigh waves on layered media.

The geophysical importance of the layered configuration is obvious because of the basic layered nature of the Earth's structure. It is also of importance in electronics because the basic form of surface acoustic wave devices is a layered structure, built on a crystal substrate.

Although these configurations do not come under consideration as surface features, in this study, they constitute the simplest type of multimedia problems. As the present study is intended to cover some two media configurations, a review of previous work on layered structures is of value, particularly with a view to extensions to filled slot problems.

The layered half-space is of particular importance as it is one of the configurations for which analytical solutions are available and these are given by a number of authors including Ewing et al (1957).

In addition to the basic analytical studies the work on layered media, as with other configurations, falls into distinct classes according to dimensions, in this case layer thickness (h) to wavelength (ψ) ratio h/ψ.

a. Layer thickness to wavelength ratio (h/ψ) less than 0.5.

This group of studies includes those relating to thin metal layers on crystal substrates, as occur in surface acoustic wave devices; the thickness of the layer often being less than 0.5 wavelengths. These studies are mainly experimental and are covered by an extensive literature which has been considered by White (1970) and Farnell and Adler (1972).

It is in this group of studies that the numerical model developed by Munasinghe (1973) falls. This model uses a finite difference method to model pulsed Rayleigh wave propagation on layered structures consisting of an aluminum layer 0.3 wavelengths thick on fused quartz.

b. Layer thickness to wavelength ratio greater than 1.5.

These are mainly geophysical and seismological studies which have considered both surface and body waves on layered configurations (Herrtra 1964, Fuchs & Muller 1977). The majority of geophysical studies are beyond the scope of the present work; they consider the analysis of travel times, with much of the work following that by Gutenberg (1951). The methods used in these studies are considered in Section 3.

Two main groups of numerical methods, those which use finite elements and those which use finite differences, have been applied to some of the geophysical and surface acoustic wave device studies with layered configurations.

The finite element method has an extensive literature in seismology with much of the recent seismological work following from a report by Waas (1972). The application of finite elements to Rayleigh wave problems is presented in a paper by Lysmer and Drake (1972), although the method is not applied to pulsed wave problems.

The finite difference studies have a longer history but the geophysical configurations with thick layers have tended in the main to consider body sources and follow the methods of Alterman and Karal (1968). Much of this work is reviewed in the paper by Alterman and Loewenthal (1972).

There have also been studies of waves in layered spheres and cylinders, both in geophysics and in connection with nondestructive testing problems. These have used ray theory and numerical methods. An example of the nondestructive testing studies is the work by Rose (1971) which considers elastic waves in pipe sections using a ray theory; these methods are considered further in Section 3.

2.4.6 Rayleigh waves on welded quarter spaces.

As with several of the configurations considered in Sections 2.4.1 to 2.4.5 the geometry of welded quarter spaces, which has a free surface with an interface normal to it which separates two media, is of considerable importance in geophysics as it occurs in a locked fault or similar configuration; and its understanding is necessary if extensions are to be made to any theory or model so as to consider more complex configurations.

This geometry, which has no characteristic dimension, has previously been considered by experimental, analytical and numerical methods. The majority of previous work has been in geophysics, because of the interest in, and importance of, the natural forms of the configuration. Previous studies have considered the scattering of both body and surface waves, but in the present review and study attention is concentrated on the surface wave work.

A theoretical study has been performed by Viswanathan (1966), who proposed a solution by an approximate iterative method using integral transforms.

A more recent study, on welded quarter spaces of perspex and polystyrene, has been performed by McCarr and Alsop (1967), who have made experimental measurements and produced theoretical results using an approximate variational method which has produced reflection and transmission coefficients. Measurements have been made by Munasinghe (1973), using the same media as those used by McCarr and Alsop (1967), in a finite difference model, the details of which are considered in Section 4.3. The results from these studies are presented and discussed in Section 9, together with the results of the present study.

When a Rayleigh wave interacts with an interface, as in welded

quarter spaces, an interface wave known as a Stoneley wave, in addition to mode converted shear and compressional waves can be generated if the conditions for existence will permit and this travels down the interface away from the free surface, decaying exponentially away from the boundary (Stoneley 1924).

There are a large number of possible combinations of different media from which a pair of welded quarter spaces can be produced, or occur in nature, but measurements have only been made experimentally for a few cases. The finite difference method provides a method for measuring the scattered waves for combinations of different media which have not, or cannot be considered experimentally; this geometry is considered in Sections 7 and 9.

2.4.7 The limitations of experimental methods used to study Rayleigh waves.

Following a consideration of the various simple geometries on which studies have been made for Rayleigh wave propagation and scattering, some general comments can be made concerning the limitations of experimental methods and these are now presented.

As is seen from Sections 2.4.1 to 2.4.6 there have been a wide range of studies of Rayleigh waves, but experimental measurements fall into two groups, those which measure surface displacements, giving seismograms in geophysics/seismology and time domain displays in nondestructive testing, and those which visualise the waves in an interaction using a transparent model of the configuration to provide a sectional presentation.

a. Displacement measurements.

The experimental measurement of surface displacements in all the fields where Rayleigh waves are of interest can only provide information about the wave at the surface. Although the details of the methods of measurement vary considerably the state of the waves below the surface is not directly given. The details of some of the practical problems faced by the nondestructive tester in performing surface measurements are considered in Section 8.

The problem then with experimental displacement measurement is that even on test blocks, where there is the possibility of detection for mode converted pulses which reach other surfaces,

the body of the medium, and the waves in it, cannot be seen or measured.

b. Visualization measurements.

In seeking to overcome the limitation of only being able to make direct measurement on waves at the surface attention has turned to methods of visualizing waves in the body of the medium.

Two main techniques are used to visualise ultrasonic pulses in transparent models of the configurations of interest and these are Schlieren and photoelastic visualisation.

Both of these methods, although powerful techniques, require the production of special models, which are expensive, and a new model is required for each configuration. In the case of Schlieren studies a special glass is required for the models which is both difficult to produce and work. There is also the permanent problem of trying to match the model material parameters, such as elastic constants, with those of a real material tested with ultrasonic waves, such as steel.

Schlieren visualization in the published work has been primarily concerned with body waves, as in the work of Baborovsky et al (1973) which considers shear wave interactions with surface features, surface waves are seen to propagate as low energy secondary pulses. Also in this work by Baborovsky et al (1973) a computer model has been produced which, although not giving a rigorous treatment of the interactions, does provide one direct link between experimental and model work.

The visualization methods, although they present well the complex wave patterns which exist in a test configuration, do not easily give direct measures of the relative energies in the various waves.

The requirement for achieving a better understanding of Rayleigh wave interactions and scattering is for a method which will give both the numerical information about displacements that is given experimentally only for surface displacements, and provides a visual representation of the complex patterns of wave fronts which are seen in the visualization studies.

In seeking to achieve at least some of these aims attention has turned to consider mathematical methods and these are reviewed in Section 3.

2.5 Practical applications of Rayleigh wave studies.

This section considers the practical applications and natural situations where Rayleigh waves occur. The material is presented in two parts, the first is a general review and the second, which is given as Section 2.5.1, is a detailed consideration of the application of Rayleigh waves to the practical problem of crack depth measurement.

In all the studies which were considered in Section 2.4 the literature reviewed considered experimental, analytical or numerical studies of Rayleigh wave propagation on either laboratory test pieces, in near perfect configurations, or mathematical studies on ideal materials in perfect configurations. However in practical situations where Rayleigh waves occur in nature, and are used in devices or in nondestructive testing, the waves are interacting with real surface features which are often complex. In many real situations with smooth surfaces nondispersive propagation is possible. This is not always the case and practical surfaces may introduce attenuation and increase background noise levels in systems.

Rayleigh waves, as considered in Sections 2.2, 2.3 and 2.4, can be considered to be nondispersive in an isotropic, homogeneous medium which has a smooth surface for propagation. As outlined in Section 2.2 for the long wavelength pulses that occur as a result of earthquakes and underground nuclear explosions, the Earth, although not perfect, can propagate high energy pulses of Rayleigh waves over large distances; thousands of kilometres. For this reason Rayleigh waves occur as strong pulses on seismograms, with local features such as hills only perturbing a pulse or wavetrain and large features like continental boundaries producing scattering which increases non-coherent seismic noise. Even with the scattering losses the seismic pulses have enough energy to give information about their source and the material through which they have travelled.

Also with reference to the seismic Rayleigh and other wave pulses, in addition to local damage in a belt of seismic activity, the civil engineer needs to consider the possible effects on such features as dams. With large structures, such as dams, there is the need to consider the local magnification of displacements which

can occur on some configurations.

On an intermediate scale are the man-made surface waves which are produced by the vibration of large rotating machines, by rhythmic hammer blows or an explosion. These produce a problem of structural isolation for the civil engineer. These waves have wavelengths of the order of tens of metres and the isolation of a structure from, or the scattering of, the waves produced by a structure, is achieved by means of isolation trenches or sheet piling, which scatters locally produced Rayleigh waves; the results from experimental studies such as that by Woods (1968) are considered in Section 9.

In the field of surface acoustic wave devices there has been extensive practical measurement of the parameters which describe the propagation and isolation of Rayleigh waves, (White 1970) and these include studies of isolation of components on a single crystal and the study of groove profile. (Tuan 1975, Tuan & Parekh 1975) The majority of such surface acoustic wave device related studies are not of direct use to the understanding of the types of interactions of Rayleigh waves on the configurations of interest in the present study.

The final group of practical studies are those which consider the use of Rayleigh waves in the study of surface and near surface features in metals up to depths of about one and a half wavelengths. Surface waves have the potential to be used to study such surface features as surface cracks and near-surface voids and inclusions, as well as such surface features as roughness, pitting, corrosion and layer thickness. Work has been performed to apply Rayleigh and other surface waves to all these problems.

The first work using ultrasonic waves which can be called pulse-echo ultrasonic nondestructive testing, then known as ultrasonic reflectography, appears to have been performed by Firestone in the late 1930's and reported in a patent application of May 1940 (Firestone 1942). The first article to appear is that by Firestone (1945) in which he describes the use of short (1 microsecond) pulses of five megahertz body waves generated by a surface contact quartz crystal. In this paper Firestone applies the ultrasonic body waves to the measurement of wall thickness, lamination detection, grain size measurement and bond testing, in addition to defect detection and location.

He also notes the problems of defect sizing with features that have dimensions of the order of a wavelength or less.

The original suggestion for the use of Rayleigh waves in nondestructive testing, by the method then known as ultrasonic reflectography, appears to have been made by Firestone and Frederick (1946). However before the technique could be developed it required the improvement of transducers by the development of wedge transducers and the work of Benson (1950), Frank (1952), Minton (1954) and Cook and Valkenberg (1954). The principles and development of Rayleigh wave transducers are considered in Section 8.

Since the work in the 1950's and particularly since about 1960 the applications of Rayleigh waves in nondestructive testing have been numerous and have included studies to detect cracks in plates (Pohlmann 1963), the inspection of turbine blades (Vybornov & Ogurtsov 1962), the inspection of wires and the inspection of heat exchangers (Bridge 1976, Private communication) and the inspection of hot foundry products (Cole 1977).

In addition to these inspection studies there have been studies on specific problems such as surface roughness by Urazakov et al (1973) and Bridge and El-Dardiry (1976).

Rayleigh waves have now proved themselves as a useful inspection tool and this review now considers the specific problem of Rayleigh wave crack depth measurement.

2.5.1 Rayleigh wave crack depth measurement.

The location and sizing of cracks, particularly those due to fatigue, is of great importance to industry. The calculations of fracture mechanics now enable, at least in principle, the prediction of critical defect size and when this defect size is known it enables the establishment of reasonable nondestructive testing levels, for quality control and both preservice and product acceptance inspection. Engineering experience has shown the necessity for the establishment of both preservice and in-service inspection for crack detection from the extensive damage which can result from crack growth to failure in an item such as an aircraft, a pressure vessel or a pipeline. In relation to the significance of a defect, from both practical measurement and the fracture mechanics calculations, it is shown that a surface defect, of given length

is as significant as a buried defect of twice its length. (Young 1977)

It is therefore important not only to detect and locate a defect, but also to be able to establish accurately its dimensions and orientation. In the case of a surface breaking defect there is little problem in locating a crack by such methods as dye penetration; however even then depth/length measurement is a problem. The studies reported in this review are divided into two groups, firstly those which seek to determine the minimum size of defect detectable and secondly those which seek to size a defect which has previously been located either by an ultrasonic or some other method.

Three types of surface breaking feature are considered in this study and these are shown in Figure 2.9. These are the artificial defects, shown as Figure 2.9a, which are the V groove and the milled or cut slot; the fatigue crack, which often has a form as shown in Figure 2.9b, nearly normal to the free surface with near constant width of the order of 0.01 mm; and the stress corrosion crack, which often comes in groups and is shown in Figure 2.9c. The stress corrosion crack is a defect of which no two have the same form and hence it is difficult to establish characteristic dimensions.

a. Minimum detectable defects.

This group of studies includes much early work which gave limits for the detection of surface features. That by Brinczewski (1957) was able to detect V grooves 50μm deep using a pulse with a wavelength of 1.25 mm (2.25 MHz) on aluminium.

Studies have been performed on the monitoring of crack growth and those by Vybornov (1969) and Rasmussen (1962) found that fatigue cracks could be detected inaluminium at 40 % of the fatigue life, on samples with good surfaces, but only at higher percentages of their life if the testpiece had a poor surface.

For stress corrosion cracking Cordellos et al (1969) and Brummer et al (1969) showed that 70μm cracks are identifiable when working with aluminium blocks and pulses of 4 MHz frequency, this detection being achieved at only 18 % of the normal stress life.

In all practical work with Rayleigh waves the quality of the surface finish has been found to have a considerable influence on propagation characteristics. This is shown in the work by

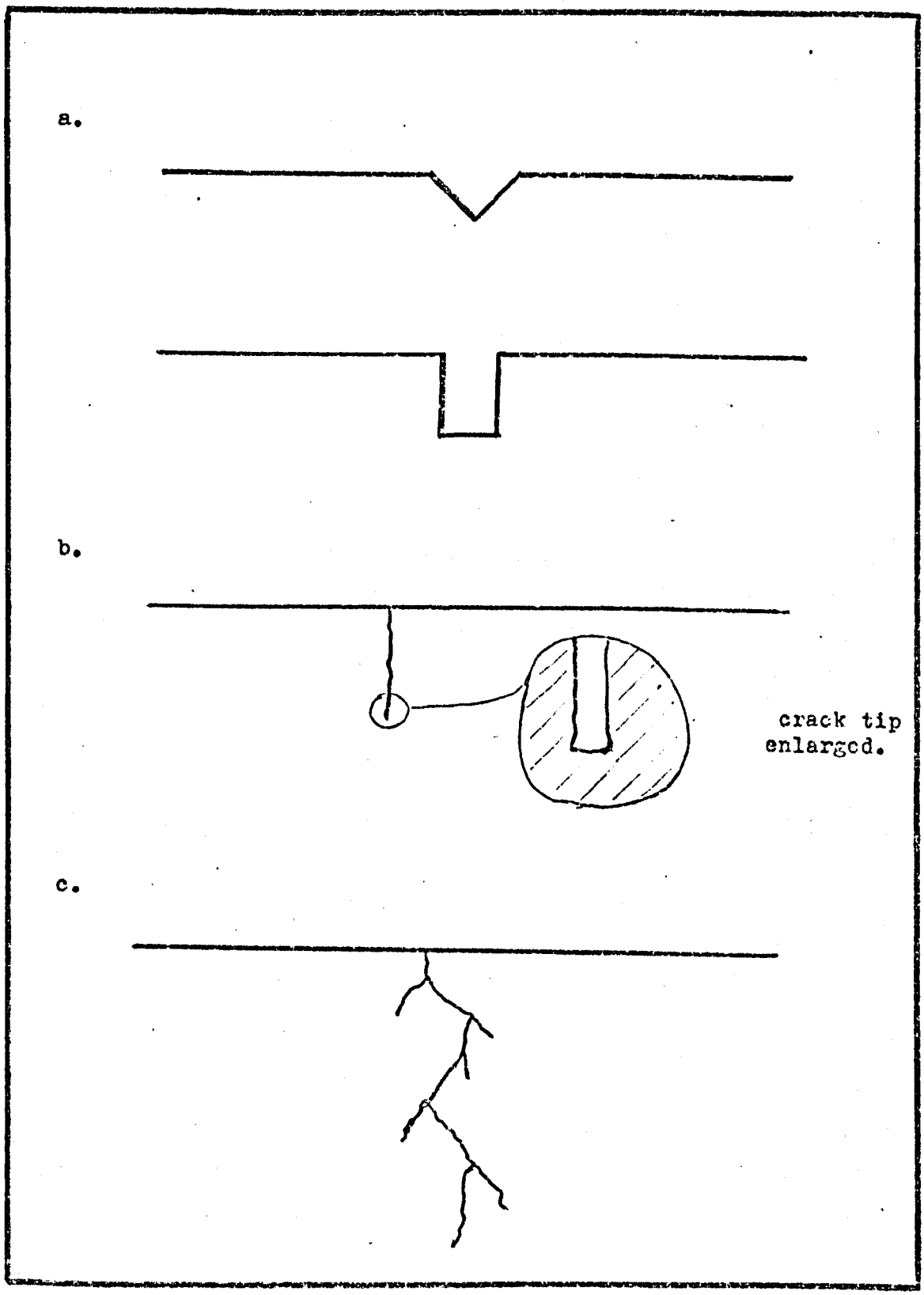

Three types of surface breaking feature; a. Artificial defects, b. Fatigue crack, c. Stress corrosion crack.

FIGURE 2.9.

Rasmussen (1962) with regard to the detection of a significant feature against a background of small scallerers Although the studies have at present considered body waves, work by Quentin (1975) has applied spectroscopic techniques to detect regular targets on damaged surfaces.

A further group of studies are those by Brinczewski (1957), Bykov (1960) and Bridge and El-Dardiry (1976) which show the attenuating effect of a rough surface.

Other studies have considered propagation on thin films, but those not considered in relation to layered systems in Section 2.4.5 or in relation to the coupling of transducers in the section on experimental work, Section 8, are outside the scope of the present study.

b. Crack sizing.

This second group of studies are those which consider crack location and sizing. As early as 1958 Böhme (1958) showed that for defect detection Rayleigh wave methods compare well with those using X-ray or eddy currents, and the performance of ultrasonic methods has improved, at least in the laboratory, over recent years. (Lloyd 1970,1975, Curtis 1975)

However crack depth measurement has proved to be undependable (Musil 1967) or at least give a large scatter in the results (Hudgell et al 1974) and this is attributed to the many obvious variables present which include crack type, depth, orientation and length, in addition to transducer variation and operation problems. There is also found to be variable reflectivity from different cracks of the same physical length. The coupling problems can be overcome by using noncontact transducers, as is done in the work of Frost et al (1975) and Cole (1977).

The variables which introduce scatter into Rayleigh wave measurements all work against automatic inspection, but the use of noncontact generation and detection has made possible such applications as hot billet inspection working between 25 and 33 kHz, a wavelength of about 10 centimetres, for surface and near-surface defect detection. (Cole 1977)

Measurements made by Morgan (1973) using Rayleigh waves on slots cut in aluminium alloy blocks have achieved an accuracy of about 20 % for defects less than a wavelength in length. In a more recent study by Lidington and Silk (1975), working at 2.5 MHz

on 16-28 mm (about 12 to 24 wavelengths) slots achieved about 1 % accuracy and achieved a similar level of accuracy to Morgan on a real crack. In a further study using a different technique, but still with Rayleigh waves, Silk (1976) working at up to 8 MHz has claimed accuracies of about 2.5% for cracks 20 to 30 mm (about 55 wavelengths or deeper at 8 MHz) deep, with reduced accuracy as feature depth reduces, so that for a depth of about 2 mm (about 5 wavelengths deep at 8 MHz) the accuracy is only a little better than that claimed for earlier studies. The general level of guaranteed accuracy being claimed by Silk (1976) is 15 %.

The time domain signals obtained experimentally using Rayleigh waves tend to indicate that the interactions at surface features and the resulting scattered pulses are more complex than a simple theory of reflection and transmission, with mode conversion losses at each corner, would produce. This is especially so for interactions with features that have dimensions of the order of a wavelength or less. This complexity not only arises from the variables present in the experimental system but also from the complex nature of the mode conversions that occur.

With the application of photoelastic visualization methods to Rayleigh waves, as in the work by Hall (1976), it is found that a wedge transducer does not just produce Rayleigh waves, but there are residual body waves which pass into the testpiece. Further consideration is given to unwanted body waves in testblocks in Section 8 where the experimental measurements made in the present study are reported.

Two reviews have been presented for the procedures for crack depth determination using Rayleigh waves and they are by Cook (1972) and Hudgell et al (1974). The methods described fall into two groups, those which use single probes and make pulse-echo measurements and those which use two probes. The basic pulses considered for slot depth measurement are shown in Figure 2.10. The details of the various methods of measurement as used in the present study are given in Section 6.

An additional wave pulse used for determining crack length, in the case of deep cracks, is the mode converted shear wave pulse and this has been considered by Silk (1976) who has presented the equations for pulse travel times, particularly for the tip converted shear wave. This is considered further in Section 9.

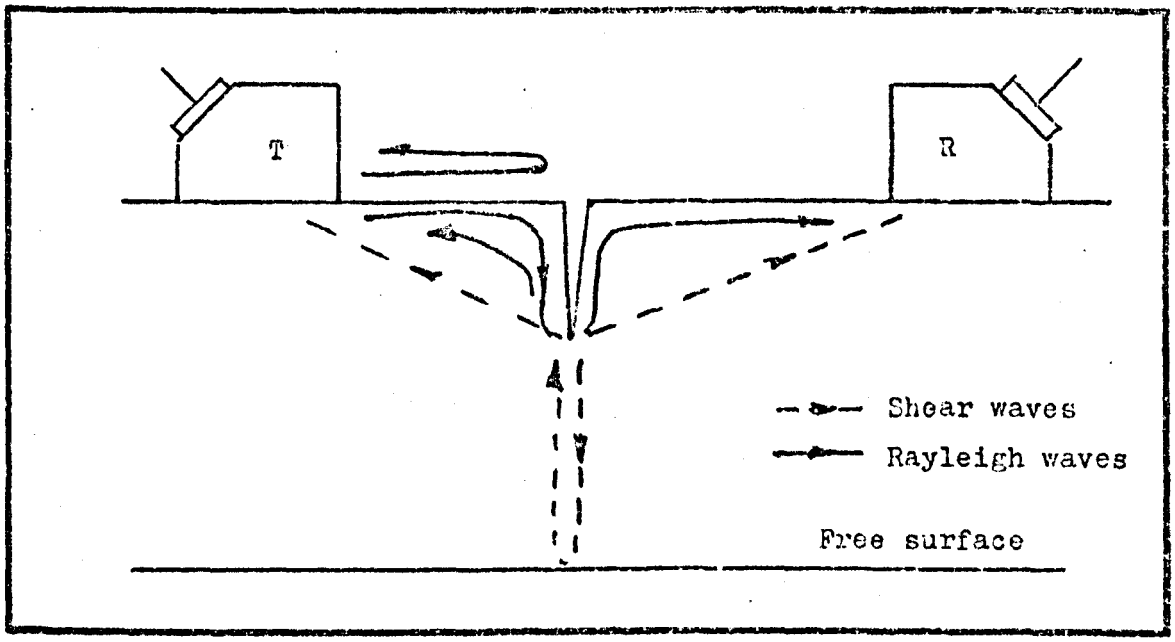

Pulses used in Rayleigh wave crack depth measurement.

FIGURE 2.10.

Rayleigh wave crack and defect location and measurement is now in routine use by a wide range of nondestructive testers, but much development work is still required to provide better transducers and experimental equipment at the practical end of work and basic analysis of the interactions and the resulting scattered pulses to aid in the understanding of the signals received in real experiments.

At present there is no full wave analytical theory for Rayleigh wave defect interactions and scattering and the limitations that this imposes on experimental measurements are considered in Section 8 with the experimental measurements and in Section 9 where all the results are considered.

2.6 Ultrasonic spectroscopy.

In ultrasonic nondestructive testing, methods which restrict consideration of the pulses to some form of time domain display and measurements, are made solely for some measure of amplitude and the position, the information in the signal which is present due to wavelength dependance is not given to the experimenter.

Ultrasonic spectroscopy is the analysis of the spectral content of an ultrasonic signal. This is obtained by passing the gated signal into a spectrum analyser, which performs the operation

electronically. This operation is equivalent to the application of a Fourier transform, and presents the amplitude of all frequencies swept by the system that are in the analysed signal.

The term ultrasonic spectroscopy seems to have first been applied to the analysis of short time domain ultrasonic signals, which have wide bandwidth, (which may be from 0.5 to 20 MHz or more) by Gericke (1963). Since this time the use of this method of analysis has increased, particularly with the increased availability of small wideband spectrum analysers and signal processing equipment, since about 1970.

The early work showed the diagnostic possibilities of spectroscopy for the study of such features as grain size, and with the introduction of ultrasonic techniques into medicine there has followed the introduction of spectroscopic techniques for such functions as tissue identification. The development of the techniques in both nondestructive testing and medicine has not resulted in two separate isolated groups of workers; the fields have much in common as was shown at a recent meeting at The City University. (Seville 1977)

In geophysics there has been increasing interest in both long and short period seismometers and as well as increasing the spectral range studied, there is increasing use of the spectral information in the signals. (Fuchs & Muller 1977) The spectral content of the signals is analysed in a variety of ways including cepstrum analysis in which the spectrum of the signal under investigation is normalised to, and compared with the spectrum of a reference signal and the difference between the signals taken. The difference signal is passed through a Fourier transform to bring the signal back to the time domain. This process has been applied to nondestructive testing configurations, open slots, by Morgan (1973).

There are two advantages in using short time domain signals both of which are of use in nondestructive testing. The first is the better time resolution which is possible and this has such applications as thickness measurement (Lloyd 1975). The second is the wide spectrum which is produced for broadband investigations. The production of broadband signals is considered in Section 8.

The scope of applications of frequency analysis in nondestructive testing has been considered by Dory (1973).

Further general material on ultrasonic spectroscopy can be found in the paper by Gericke (1971) and a recent introductory review which has been presented by Haines (1976). Longer articles, which include some of the applications of the technique, have been prepared by Brown (1973, 1976, 1978 to appear).

Spectral analysis applications have included studies of bonded structures (Rose & Mayer 1973), lap-joints (Lloyd 1974), the measurement of thin layers (Rose & Mayer 1974) and the characterisation of surface defects using pulsed ultrasonic Rayleigh waves, as performed by Morgan (1973).

The number of applications and potential applications is increasing all the time and the potential information given by spectral content will ensure its use in nondestructive testing. The technique is considered, as used in the present study, in Sections 5 and 8.

3. COMPARISON OF MATHEMATICAL METHODS.

3.1 Introduction.

Numerical methods, and particularly those for the solution of systems described by differential equations, are of increasing importance in many branches of physics and engineering, and the previous published work, both on numerical methods and their application to elastic wave propagation, has become extensive.

Using numerical methods coupled with recent advances in the speed and core capacity of large computer systems it is now possible to provide a full quantative understanding for many previously analytically intractable problems. It has become possible to model the time development of many systems and recently numerical methods have been sucessfully applied to hyperbolic or transient elastic wave problems; it is in this class that the type of pulsed wave problem to be considered in the present study falls.

The basic requirements for the numerical method to be applied in the present study are presented in Section 3.2 and a review of previous work and available methods is given in Section 3.3. The selection of finite difference methods is made for use in all model work in the present study and the details of the formulation are presented in Section 4, together with the supporting appendices.

3.2 Basic requirements for the numerical method.

The basic requirements for a numerical method are that it should provide a model of the propagation, interaction and scattering of pulses of broadband Rayleigh waves by features such as steps and slots, which form the basis for understanding the interaction and scattering of pulses by real surface features. There are a set of criteria against which the alternative methods used to model wave propagation must be considered, and these are;

1. The method must give nondispersive propagation of a pulse or pulses of wide bandwidth, on the surface of and in, a homogeneous medium.

2. The method must be able to handle the necessary boundary conditions, such as the stress free surface, 90° and 270° corners and material interfaces.

3. The method must, in addition to single pulse propagation, give the full wave solution, including mode conversion, for the interaction with surface features with dimensions of the order of a wavelength.

4. The method must be of such a form as to enable the required accuracy and stability to be achieved. (In terms of accuracy the variation from known analytical solutions must be minimal, there being for example no greater than say 5 % variation from analytically known displacements in the case of propagation on a half-space.)

5. The method should be such that a FORTRAN computer program can be written for use on a digital computer of either ICL 1905E or CDC 7600 type, at reasonable core size and run time. This condition is helped by the ability to restrict consideration to two spatial dimensions and time. Other workers, for example Munasinghe (1973) when using a machine comparable with the CDC 7600 have employed a dynamic core of about 100 (32 bit) words and used run times of up to 1500 sec.

The four numerical methods found in the literature search are now reviewed in Section 3.3.

3.3 Consideration of available numerical methods.

A detailed review of all the previous work on wave propagation and scattering, with details of the various mathematical methods is a mathematical study given in mathematical texts, which is beyond the scope of this thesis. In this section the particular papers mentioned to illustrate the various methods are given to serve as illustrations of applications of the particular technique, with no intention of being a complete bibliography. This is

especially so in the case of methods which have application to surface wave problems, but in the past have had only limited application to them.

Previous studies of wave problems can be grouped in several ways, and although the systems studied range from those considering earthquakes, to those for submillimetre waves on surface acoustic wave devices, the basic mathematical methods fall into four groups and it is according to these that the material in this section is presented. These methods are those which use ray-tracing, perturbation techniques, finite element approximation and finite difference approximation.

The four methods have all previously been applied successfully to solve particular problems. However all have their range of applicable problems together with their own strengths and weaknesses.

The four methods are now considered with reference to the solution of a system described by second order hyperbolic partial differential equations which is well posed and has Neumann type boundary conditions and particular reference is made to the conditions set out in Section 3.2.

3.3.1 Perturbation techniques.

The first technique considered is in fact a wide range of techniques, being those which use perturbation methods. These, as the name implies, perturb a system using some form of approximation. These come in many forms, however there are several common tools which include the use of the Born approximation, the use of sources to replace scatterers and the addition of a perturbation to a known function or equation. Perturbation techniques can and have been applied to a range of wave problems including those which consider surface waves. (Hudson 1977)

In general when these methods are applied to problems such as the scattering of a pulse by a step, they only work when the pulse or wave wavelength (ψ) is much larger or much smaller than the feature dimensions, often a maximum of a twentieth of ψ or greater than 1.5 ψ. These methods can be illustrated by the work of Sabina and Willis (1977) and Hudson (1970). However their application is restricted, in the case of surface waves, to

considering such features as surface roughness (Hudson 1970, Hudson et al 1973) or small localised irregularities, such as ridges. (Sabina & Willis 1977)

These types of methods do have application to problems where the principal interest is in features with dimensions much less than or larger than a wavelength, and an approximate form is acceptable for such items as mode conversion. This is not the case in the present study, so perturbation methods cannot be used in it.

3.3.2 Ray-tracing methods.

The second class of methods are the ray-tracing methods. These have formed a part of classical geophysics, with the work on pulse travel times and ray paths. The use of this method on geophysics is shown by the work of Gutenberg and Rickter (1939). These methods have now been computerised in several forms, such as shooting techniques, which are a form of iterative ray-tracing, as is shown by the work of Julian and Gubbins (1977).

In the case of ray theory for surface waves, there is the requirement for interfaces to be smooth curves; much of the work using these techniques is reviewed in a paper by Kennett (1974). Ray theory has been applied to give understanding in the case of a range of body wave problems, as illustrated by workers in both seismology (Julian & Gubbins 1977) and nondestructive testing (Lloyd 1975).

Although attractive in many ways, and in the past they have provided solutions to a range of problems, these methods rely on approximate formulations which can apply for reflection and refraction when surfaces and interfaces approximate to smooth curves and geometrical optics analogues can apply. Therefore singularities, like sharp corners, can only be included with difficulty. When ray-tracing models have been developed, as by Baborovsky et al (1973) empirical treatments of mode conversion and low energy waves have been necessary.

As the main interest, in the present study, is in time development of systems with scattering from corners and mode conversion, ray-tracing methods are not applicable.

3.3.3 Finite element methods.

The third class of methods are those which use finite element approximations in the model formulation. These are a recent addition to the numerical methods for the solution of problems described by differential equations and have provided solutions to a wide range of problems. (Zienkiewicz 1971)

Wave problems, including those with surface waves, have been studied extensively using finite element methods. However these have mainly been restricted to studies of elliptic or eigenvalue type problems, as in the surface wave studies by Lysmer (1970), Waas (1972) and Drake (1972) and much of the material by this group is covered in the paper by Lysmer and Drake (1972).

The finite element method has also been applied extensively to a range of body wave problems, with again much of the interest being from seismology, as in the work by Smith (1975).

These methods have two distinct strengths in that they can easily handle free surface, Neumann type, boundary conditions and they can be given higher grid densities where variables are expected to have rapid changes of value.

The majority of studies using finite elements considered either elliptic or parabolic problems, with extensions to systems that would be hyperbolic being achieved by reducing the problem to one that is pseudo-parabolic. This is done, in the case of a study by Alsop (1972), by using a semi-infinite wavetrain in the form of an harmonic driving force and not pulses of waves, and with the addition of a time dependent parameter at each node.

In addition in most finite element studies there is the requirement of a rigid boundary, as is used by Lysmer and Drake (1972). This is not possible for a study of a semi-infinite medium with a single free surface.

A recent extension of the application of finite element methods has been made in the work by Key (1975), who has produced a computer program system to consider wave problems including those of hyperbolic type similar to those considered by the TOODY finite difference programs of Bertholf and Benzley (1968).

Finite element and finite difference methods are generally considered to be completely different approaches for solving systems described by partial differential equations. However

Friedrichs and Keller (1966) have demonstrated that if triangular elements are set up so that the nodes are on a rectangular grid the two methods yield the same difference formulation for interior points. This however loses some of the advantages which finite element methods have over those which use finite difference approximations, but it does introduce a considerable simplification in the use of a finite element scheme on a digital computer.

A wide range of elliptic and parabolic problems have been sucessfully solved using finite element methods Zienkiewicz 1971) and others (Key 1975) have shown that they have application to specific types of hyperbolic problems. There are however restrictions on the size of grid (about 100 by 100 nodes) which can be used due to the problems in inversion of a large, albeit sparse matrix. In general these methods have yet to prove themselves for the solution of general hyperbolic partial differential equations. (Sykes 1976, private communication)

For these reasons finite element methods were not selected for use as the numerical method for the models in the present study.

3.3.4 Finite difference methods.

The fourth group of methods are those which use finite difference approximations in the solution of differential equations. These methods constitute an extensive group of mathematical methods and the detailed formulation can take several forms. (Richtmyer & Morton 1967) The basic method replaces the differential terms in the equations which describe a system under study with an incremental approximation. This method of equation solution was first discussed by Courant et al (1928) and since that time has provided the solution for many types of differential equations particularly since the development of fast digital computers.

For surface waves studies using finite difference methods have included work by Boore (1970) who has considered the propagation of a single component Love wave packet in a non-homogeneous material. There have been Rayleigh wave studies for semicontinuous waves on homogeneous quarter spaces by Alsop and Goodman (1972). Both Lamb and plate waves have also been studied by this method.

The largest body of literature on elastic wave propagation

using the finite difference methods is that due to the late Professor Alterman and her students and coworkers in mathematical geophysics, working from the mid-1960's until her death in 1974. Professor Alterman's life and work is to be commemorated in a special volume edited by Bolt (1978, to appear) which will include a bibliography of her work. Her group has studied a wide range of mainly body wave problems including waves on and in planes, in wedges, with propagating slots and also with both cylindrical and spherical geometries and co-ordinate systems. (Alterman & Loewenthal 1972), It is from this work that the work by Munasinghe (1973, 1976) follows. The Alterman work is being continued directly in that by Ilan and Loewenthal (1976), Ilan (1977a & b) and Ilan (1978, to appear).

The work by the Alterman group has been used in other geophysical groups including Stockl (1977) and Scherneck (1976). In the field of surface acoustic wave devices there has been an extensive study by Munasinghe (1973) and Munasinghe and Farnell (1973), which has considered Rayleigh wave propagation and this has been mentioned in the review in Section 2.4. This work by Munasinghe (1973) has been extended to consider anisotropic and further layered media configurations. (Munasinghe 1976) There has also been a recent study by Cuozzo et al (1977) who have modelled semicontinuous Rayleigh waves on a range of features on homogeneous media.

There is also work using a series of finite difference computer programs called TOODY due to Berthlof and Benzley (1968). The TOODY programs have been used extensively to study many types of systems and although originally produced to model seismological configurations the TOODY 11 program has been used by Rose and Meyer (1975), in what appears to be the only published application of the technique for ultrasonic wave problems, to test an analytical result in a nondestructive testing body wave field analysis study.

The finite difference methods give the full wave solution to wave scattering problems, including mode conversion, and they can be used with broadband pulses which have a smooth wave number spectrum. The upper limit on the frequency which will propagate is set by the internodal spacing, in nodes per wavelength. The necessary boundary conditions can be handled and in one form,

as used by Alterman and Loewenthal (1972), the formulation provides the displacements at each node, which can be used as data to undergo data processing without further computation.

Finite difference methods now constitute an extensive group of methods and their advance has been helped by the developments in large digital computers in both speed and core size. The advantages of these methods include, that they give the time development of the system, with the full wave solution including mode conversion; they have the ability to hand smooth pulses; they can be formulated to cover Neumann type boundary conditions and they are relatively easy to turn into a computer program. Also from the view of the potential user they have the advantage of a good history of sucessful applications to hyperbolic problems, as is shown by the work of the Alterman group.

It is for these reasons that finite difference methods have been selected and it is from the Alterman school of finite difference modelling that the methods used in the present study, which are described in Section 4, have been developed.

4. NUMERICAL MODEL FORMULATION.

4.1 Introduction.

Following the selection of finite difference approximation as the basis for the method to model the configurations of interest in the present study, it is necessary now to consider and develop full finite difference formulations for the range of nodes which are required. The basic method can be applied to give several formulations which differ in detail and two classes of these are considered, with full sets of equations being presented for the nodes used in this study.

The basic spatial coordinates and the finite difference computation star are presented as Figure 4.1a and b respectively. The basic formulation used for the body of the material, the body node formulation, is considered in Section 4.2. This is followed by a consideration of the boundary condition formulations in Section 4.3 and the supporting appendices. It is the boundary condition formulations which set the limits to the region of stability and also have the potential to reduce the accuracy for the whole scheme. In the course of the present study, two types of first order formulations and one second order formulation were used for the boundary conditions in the computer programs and the details of these, together with their derivations are given in Appendices E, F and C.

Following the presentation of the finite difference formulations used, are the initial conditions which are given in Section 4.4. These include the formulation of the Rayleigh wave pulse which is used.

The last part of this section, Section 4.5, presents a consideration of accuracy and stability.

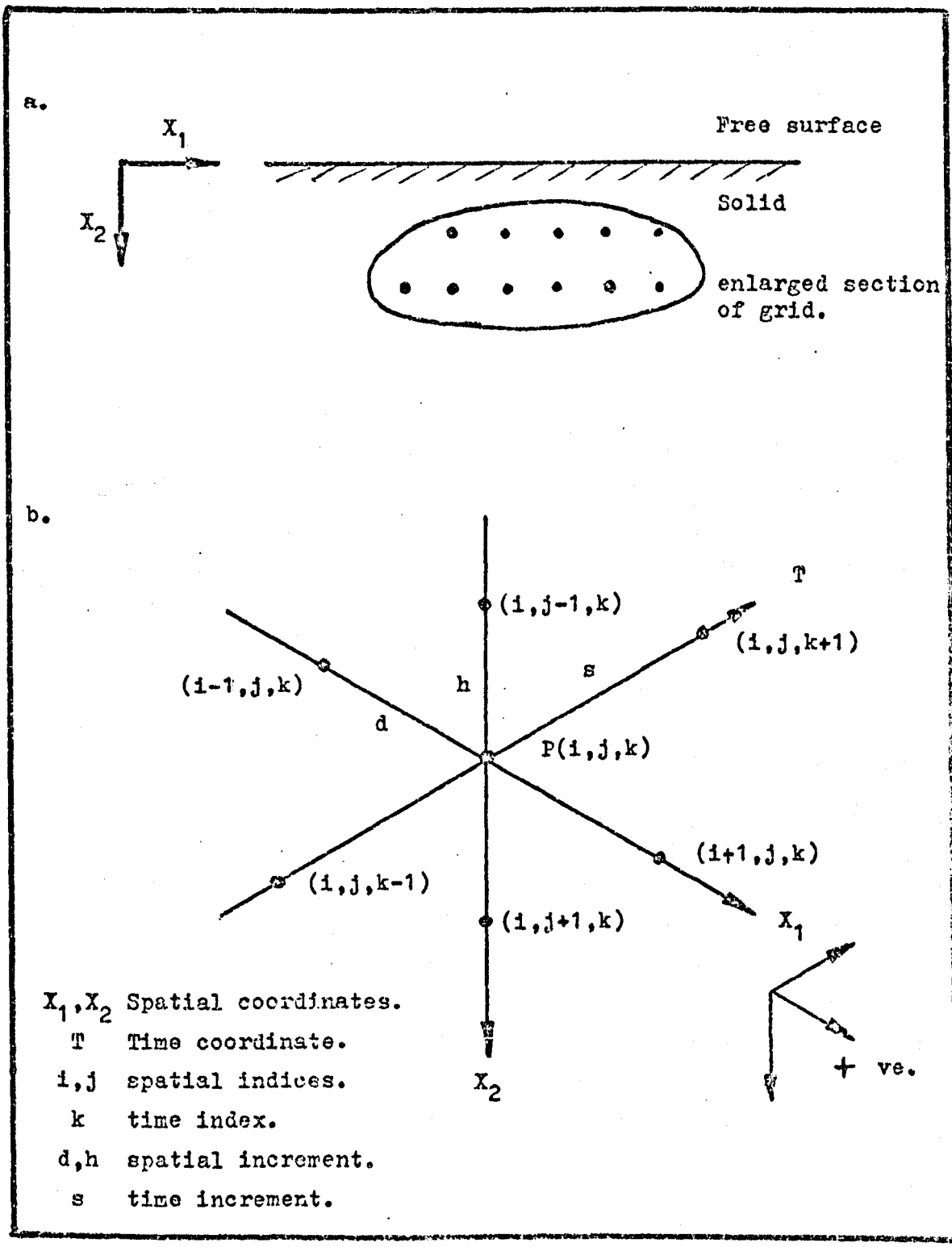

Coordinate system for finite difference schemes;
a. Basic spatial coordinates, b. Computation star.

FIGURE 4.1

4.2 Body node formulation.

The basic finite difference formulation used for body nodes in this work has been presented by many authors including Alterman and Loewenthal (1972). This basic body node formulation has been sucessfully applied to a range of wave propagation problems including that by Munasinghe (1973) which considers Rayleigh waves on half, quarter and three-quarter spaces, steps and layered wide slots and that by Ilan and Loewenthal (1976)which has considered compressional wave pulses. The results from both of these studies are considered in Sections 6 and 9.

The basic formulation for the body node is central to the finite difference scheme as it is this formulation which is used for the majority of nodes considered. It is also the body node formulation which sets the limits to increment step size and this is considered in Section 4.5.

The form of finite difference approximation used is second order centred differences. An outline of the derivation of the basic difference forms and the body node formulation, following a method given by Munasinghe (1973), is given as Appendix D. Also included in this appendix is an extension of the formulation to the case of a nonuniform grid, the spatial form of which has been used by Ilan (1977a, 1977b)

The final form of the finite difference formulation using centred differences for the body node, with a uniform grid which has been used in the majority of the work reported in this thesis, is given in Appendix D as equation D.8 and here as;

$$\underline{U}(i,j,k-1) = 2\times\underline{U}(i,j,k) - \underline{U}(i,j,k-1) + s^2\, Fp(\underline{U}) \qquad 4.2.1$$

where $\underline{U} = \begin{bmatrix} U_1 \\ U_2 \end{bmatrix}$ the components of the displacement vector.

$Fp(\underline{U})$ is an explicit expression of constants and displacements the form of which was given by Alterman and and which is given in Appendix D as equation D.9.

4.3 Boundary condition formulations.

The finite difference formulations for the boundary nodes are of much greater importance than those for the body node, as it is these which set the limits to the accuracy and stability in any scheme. The whole subject of accuracy and stability is considered in Section 4.5, with in this section, the presentation of the various alternative finite difference formulations for boundary nodes, together with their truncation errors.

Two classes of boundary conditions have been considered in detail and one main set of formulations has been used from each class. The two classes of boundary node difference formulations are defined according to whether first or second order derivatives are subjected to difference approximation.

In the first order formulations, which are produced to enable the application of the body node formulation to the boundary node, a line of imaginary nodes or pseudo-nodes is introduced outside the surface or along an interface and displacements for these are calculated. The details of schemes using pseudo-nodes are given in Sections 4.3.1 and 4.3.2 and Appendix E, which are developed from the boundary conditions given in Section 2.3.

By contrast, the second order formulation for the boundary node is produced by direct solution of the full set of equations of motion, subject to the boundary conditions, which results in a formulation which gives the time development of displacements at the boundary node as it does not use pseudo-nodes or require subsequent application of the body node formulation. The second order formulations are considered in Sections 4.3.3 and 4.3.4 and the supporting appendices, Appendices F and G.

The approximation in the pseudo-node schemes has a truncation error of the size of the spatial increment or increment squared, depending on the detail of the scheme used to approximate the first order spatial derivatives, whereas in the second order scheme the truncation error is normally of the order of the size of the increment squared. In general a second order scheme should be more accurate and should make it possible to achieve the same or better stability than a first order scheme.

4.3.1 First order formulations for free surface boundary conditions.

These are finite difference formulations which use pseudo-nodes to satisfy the boundary conditions, and they are obtained by a procedure in which the first order spatial derivatives in the boundary conditions, which are defined in Section 2.3 as specified components of the Cartesian stress tensor, are converted to difference form and the displacements at a line of pseudo-nodes outside the free surface are obtained, this allowing the application of the normal body node formulation to give the time development at the boundary node.

In the present study two sets of pseudo-node formulations were considered. The first of these, known as a Centred Difference Formulation, as the name implies is based on the use of centred differences and was developed by Alterman and Karal (1968). This type of boundary node formulation has been used by a number of workers including Munasinghe (1973), who used it with Rayleigh waves, and Ilan and Loewenthal (1976) and Ilan (1978, in press), who have tested it with compressional wave on the half and quarter spaces respectively.

This type of formulation is illustrated by the equation which is produced to enable application of the body node formulation at the horizontal free surface. The formulation to give the displacements at the pseudo-node P, shown in Figure 4.2, which is outside the free surface is given as;

$$U_1(i,j-1,k) = U_1(i,j+1,k) + \left\{U_2(i+1,j,k) - U_2(i-1,j,k)\right\} \qquad 4.3.1$$

$$U_2(i,j-1,k) = U_2(i,j+1,k) + \left[\frac{V_c^2 - 2\,V_s^2}{V_c^2}\right]\left\{U_1(i+1,j,k) - U_1(i-1,j,k)\right\}$$

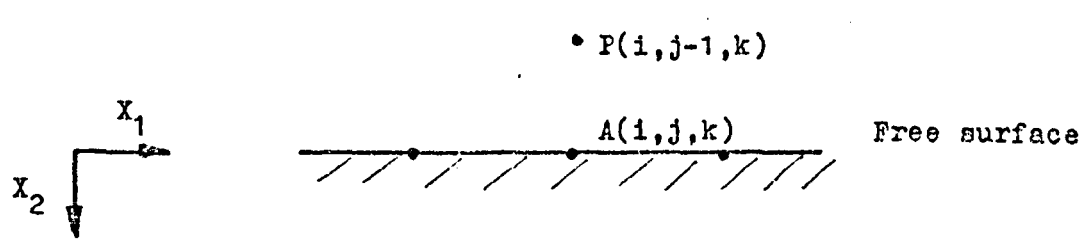

Nodes for free surface pseudo-node formulations.

FIGURE 4.2

For the first order Centred Difference scheme the truncation error is of the order of the spatial increment squared.

The second set of pseudo-node formulations, which are known as One Sided Formulations, are due to Alterman and Rotenberg (1969), and these are obtained in a similar mannar to the method used to derive equation 4.3.1, except that off-centred (one sided) difference forms are used and these have truncation errors of the order of the spatial increment.

The one-sided formulation is illustrated by the equation for the displacements at the pseudo-node P shown in Figure 4.2 outside the horizontal free surface which is given as;

$$U_1(i,j-1,k) = U_1(i,j,k) + \tfrac{1}{2}\left\{U_2(i+1,j,k) - U_2(i-1,j,k)\right\}$$

$$U_2(i,j-1,k) = U_2(i,j,k) + \left[\frac{V_c^2 - 2\,V_s^2}{2\,V_c^2}\right]\left\{U_1(i+1,j,k) - U_1(i-1,j,k)\right\} \qquad 4.3.2$$

In the present study in the majority of models which use a first order scheme for the boundary conditions, the Centred Difference scheme, as illustrated by equation 4.3.1 has been used. Following recent work by Ilan (1978, in press) on stability of the quarter space, the use of the One Sided formulation has been adopted in some models for the nodes adjacent to the 90° corner. This is considered further in Section 7 where the results of the models are presented. In general the Centred Difference scheme has been found to be the first order scheme with the larger range of stability. The topics of both accuracy and stability are considered in detail in Section 4.5.

The full set of nodes for which first order formulations are given in this thesis are shown in Figure 4.3. The full finite difference formulations, with the new derivations by the author, are given as Appendix E.

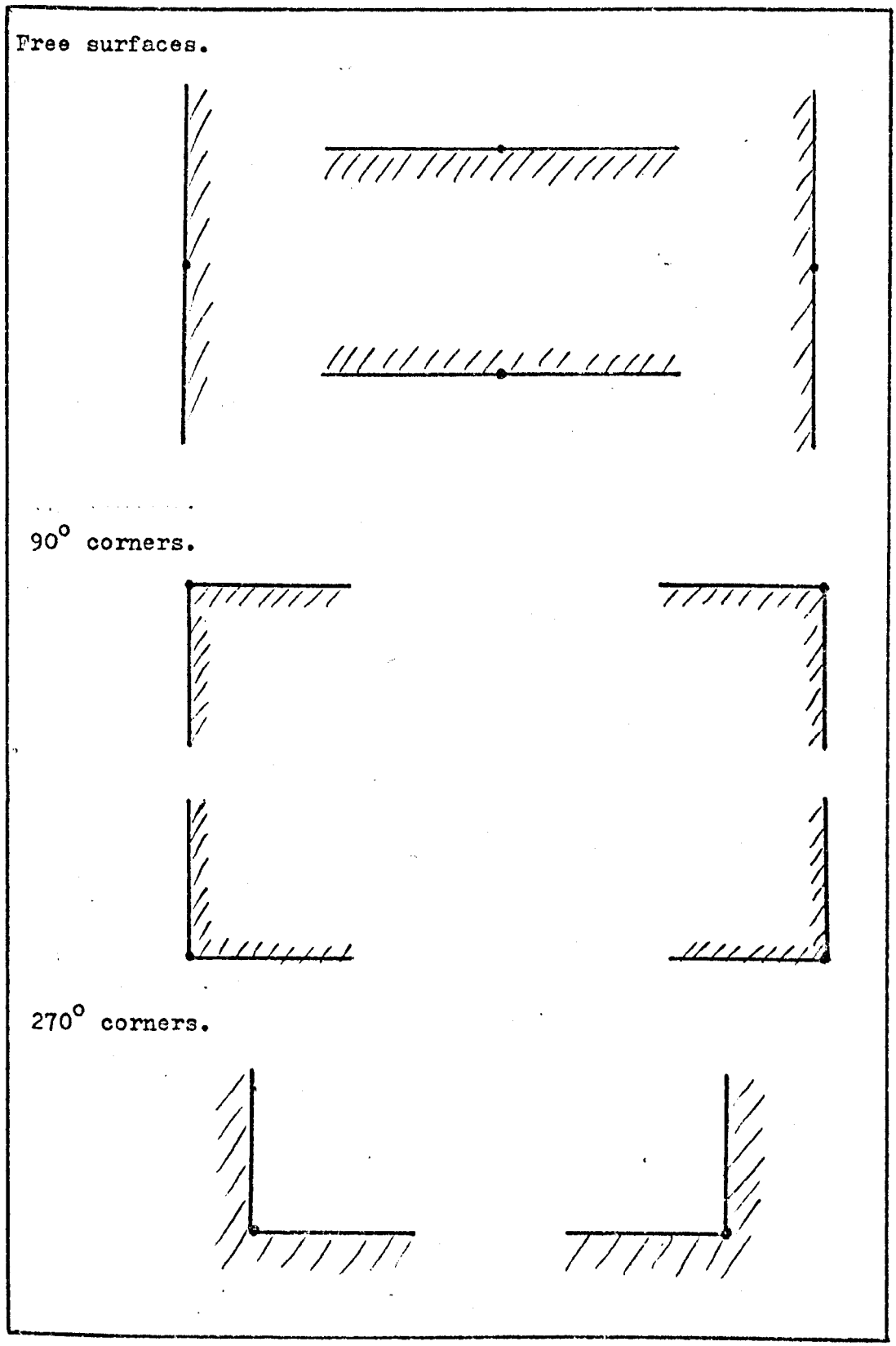

Nodes for which first order difference formulations are given.

FIGURE 4.3.

4.3.2 First order formulations for interface boundary conditions.

The use of pseudo-node formulations has been extended by Alterman and Karal (1968) to consider the interface between two media for use in body wave problems. This type of scheme has been applied to Rayleigh waves on layered media by Munasinghe (1973).

The boundary conditions for an interface between two solid media are that both stresses and displacements are continuous and these are given in Section 2.3.

The basic node arrangement used for the horizontal interface is shown in Figure 4.4. To evaluate the displacements at node C, the nodes A and B and A' and B' are given the same values and the pseudo-node C is given the parameters of the lower medium.

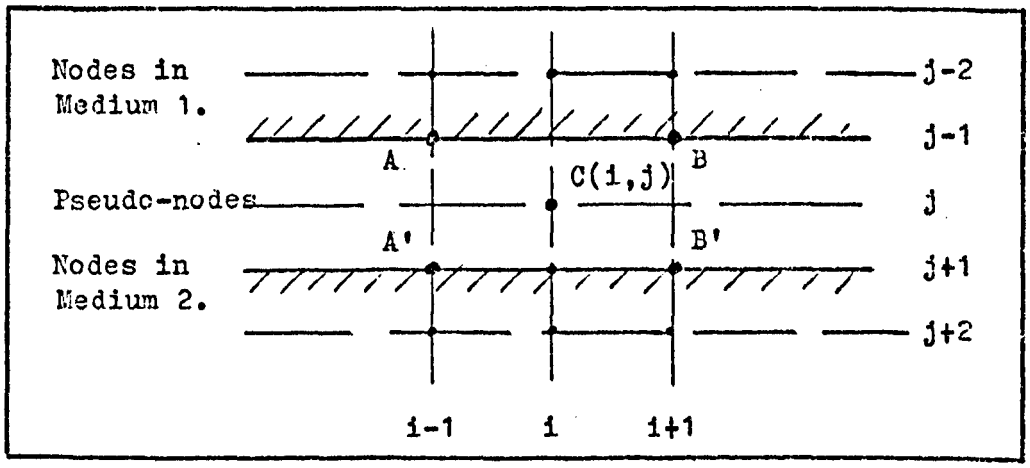

Nodes used for the pseudo-node formulation at an interface.

FIGURE 4.4.

The equation obtained from the boundary conditions which gives the displacements at node C, is given as;

$$\underline{U}(i,j,k) = \underline{U}(i,j+1,k) + \underline{H}_1\left[\underline{U}(i,j+2,k) - \underline{U}(i,j-1,k)\right]$$
$$+ \tfrac{1}{2}\Big\{\underline{H}_2\left[\underline{U}(i-1,j-i,k) + \underline{U}(i-1,j-2,k) - \underline{U}(i+1,j-1,k) - \underline{U}(i+1,j-2,k)\right]$$
$$+ 3\underline{H}_3\left[\underline{U}(i+1,j+1,k) - \underline{U}(i-1,j+1,k)\right] + \underline{H}_3\left[\underline{U}(i-1,j+2,k) - \underline{U}(i-1,j- \ ,k)\right]\Big\} \qquad 4.3.3$$

where

$$\underline{H}_1 = \begin{bmatrix} g_1 & 0 \\ 0 & g_2 \end{bmatrix}; \quad \underline{H}_2 = \begin{bmatrix} 0 & g_1 \\ g_3 & 0 \end{bmatrix}; \quad \underline{H}_3 = \begin{bmatrix} 0 & 1 \\ g_4 & 0 \end{bmatrix} \quad g_1 = \frac{(\rho V_s^2)_1}{(\rho V_s^2)_2}$$

$$g_2 = \frac{(\rho V_c^2)_1}{(\rho V_c^2)_2} \quad g_3 = \left[\frac{\rho(V_c^2 - 2V_s^2)}{(\rho V_c^2)_2}\right]_1 \quad g_4 = \left[\frac{V_c^2 - 2V_s^2}{V_c^2}\right]_2$$

The introduction of a line of pseudo-nodes between the media in a layered problem has been extended to the free surface/interface node, for welded quarter spaces, shown as node P in Figure 4.5. However the further extension of this type of scheme becomes increasingly complex and has not been considered by other workers. Any further extension of the scheme would involve complex node formulations and introduce additional lines of pseudo-nodes into the scheme, adding to the complexity of the resulting computer program.

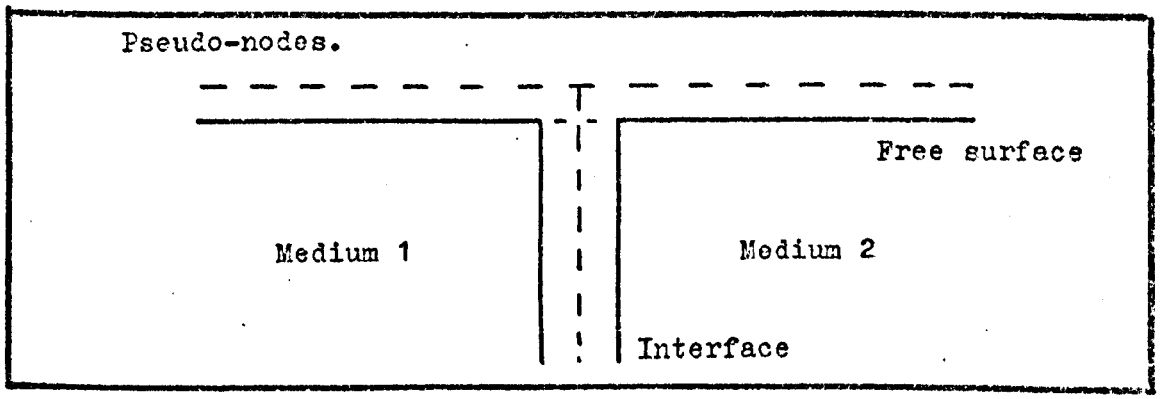

Pseudo-node arrangement used for welded quarter spaces.

FIGURE 4.5.

A finite difference scheme which considers interfaces without the use of pseudo-nodes would have considerable advantages and such a scheme has been developed for some nodes by Ilan et al (1975). The scheme has been extended by the author and it is considered in Section 4.3.4 and Appendix G.

4.3.3 Second order formulations for free surface boundary conditions.

The pseudo-node schemes, for free surface nodes, which are considered in Section 4.3.1 have several inherent weaknesses. These weaknesses are firstly, that they do not give the time development for the node in a single equation, but require the application of the body-node equation to the boundary nodes, following the pseudo-node calculations. Secondly the pseudo-node formulations are not as accurate as the body node formulation, and it is the boundary formulation which sets the limits to the accuracy and stability in a scheme.

In an attempt to improve on the pseudo-node formulation Ilan et al (1975), motivated by the work of Lax and Wendoff (1960),

produced a second order free surface boundary condition formulation, known as a Composed Approximation.

The Composed Approximation formulation is illustrated by the expression for the horizontal component of displacement at a horizontal free surface, which is given as;

$$U_1(i,j,k+1) = 2V_s^2(s/h)^2 U_1(i,j+1,k) - U_1(i,j,k-1)$$
$$+ 2V_s^2(s/h)^2 \left[(h/s)^2 \frac{1}{V_s^2} - 1 - (h/d)^2 \left[\frac{3V_c^2 - 2V_s^2}{V_c^2} \right] \right] U_1(i,j,k)$$
$$+ V_s^2(s/h)^2 \, h/d \left[U_2(i+1,j,k) - U_2(i-1,j,k) \right]$$
$$+ V_s^2(s/d)^2 \left[\frac{3V_c^2 - 2V_s^2}{V_c^2} \right] \left[U_1(i+1,j,k) - U_1(i-1,j,k) \right] \qquad 4.3.4$$

where parameters are as defined on Figure 4.1.

A similar expression is obtained for the vertical component of displacement and the details of the derivations of these equations are given in Appendix F. This scheme has a truncation error of the order of the increment squared.

It has been found by Ilan and Loewenthal(1976) that the region of stability for the Composed Approximation is not as good as that achieved by the pseudo-node schemes, so it can only be used to model media with a low Poisson's ratio (less than $\sigma \simeq 0.27$). The main weakness in the formulation is due to instability, resulting from a poor formulation for calculating the vertical component of displacement.

In an attempt to overcome this limitation on the use of second order formulations Ilan and Loewenthal (1976) have produced an improved formulation for the vertical component of displacement on a horizontal free surface.

In the present study, following the procedure used by Ilan and Loewenthal (1976), an equation has been derived which is applicable to the horizontal free surface node, in the coordinate system used in the present study, which is given as equation 4.3.5. The details of the derivation of this equation are given in Appendix F. In the present study the formulation used for the horizontal free surface was the components given as equations 4.3.4 and 4.3.5.

$$U_2(i,j,k+1) = 2\left[1 - (s/h)^2 V_c^2 - (s/h)^2 V_s^2\right] U_2(i,j,k)$$
$$+ 2(s/h)^2 V_c^2 U_2(i,j+1,k) - U_2(i,j,k-1)$$
$$+ V_s^2 (s/h)^2 \left[U_2(i+1,j,k) - U_2(i-1,j,k)\right]$$
$$+ \tfrac{1}{2}(s/h)^2 (V_c^2 - V_s^2) \left[U_1(i+1,j+1,k) - U_1(i-1,j+1,k)\right]$$
$$+ (s/h)^2 \left[\frac{V_c^2 - 3V_s^2}{2}\right] \left[U_1(i+1,j,k) - U_1(i-1,j,k)\right] \qquad 4.3.5$$

The second order scheme has been extended to cover the range of nodes shown in Figure 4.6, and the details of the formulations and their derivations are given in Appendix F.

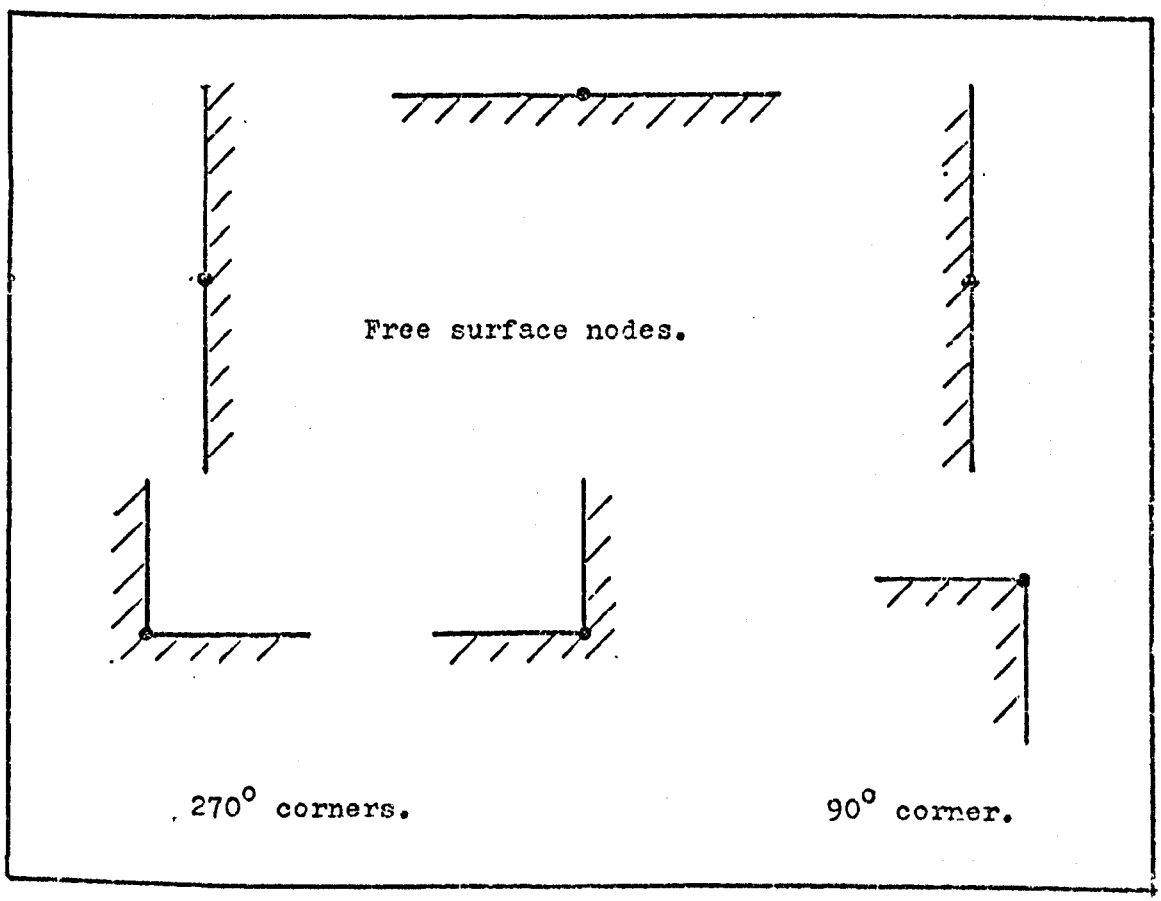

Free surface nodes for which second order formulations are given

FIGURE 4.6.

The treatment of 90° corners in second order schemes, for use with body waves, has been considered by Ilan (1978, to appear), and this work with the present limitations of second order schemes, as found in the present study, is considered further in Sections 7 & 9.

4.3.4 Second order formulations for interface boundary conditions.

The application of a pseudo-node scheme to multi-media problems presents practical difficulties, with the need to introduce a line of pseudo-nodes, and the range of nodes considered by other workers using this method is limited, as was shown in Section 4.3.2.

A limited set of second order interface nodal formulations have been developed by Ilan et al (1975) and extended by the author in the present study.

The second order interface formulations are illustrated by consideration of that for the horizontal interface, which is due to Ilan et al (1975). The equation for the vertical component of displacement at the horizontal interface, in the notation and coordinate system used in the present study, is given as;

$$U_2(i,j,k+1) = 2U_2(i,j,k) - U_2(i,j,k-1)$$

$$+ \frac{2}{\rho_1 - \rho_2}\left[\frac{s}{h}\right]^2 \Big[\rho_2 V_{c2}^2 U_2(i,j+1,k) - \rho_1 V_{s1}^2 U_2(i,j-1,k)$$

$$- (\rho_1 V_{c1}^2 + \rho_2 V_{c2}^2) U_2(i,j,k) + \tfrac{1}{2}\frac{d}{h}\Big[\big[\rho_2 V_{c2}^2 - 2\rho_2 V_{s2}^2\big] - \big[\rho_1 V_{c1}^2 - 2\rho_1 V_{s1}^2\big]\Big] Z \Big]$$

$$+ \left[\frac{\rho_1 V_{s1}^2 + \rho_2 V_{s2}^2}{\rho_1 + \rho_2}\right]\left[\frac{s}{d}\right]^2 \big[U_2(i-1,j,k) - 2U_2(i,j,k) - U_2(i-1,j,k)\big]$$

$$+ \frac{s^2}{\rho_1 + \rho_2} \cdot W \qquad 4.3.6$$

where $Z = U_1(i+1,j,k) - U_1(i-1,j,k)$; ρ = density.

W is an expression, the form of which was modified from that used by Ilan et al (1975) following the use of the original form by the author and subsequent discussions with Ilan (1977, private communication), the new form for which is presented in Appendix G.

The second order scheme was extended by Ilan et al (1975) to consider a quarter space set in a three quarter space and by the author to consider the free surface/interface node for welded quarter spaces.

The new formulation for the welded quarter spaces free surface/interface node is illustrated by the formulation for the horizontal component of displacement, which is given as;

$$U_1(i,j,k+1) = 2U_1(i,j,k) - U_1(i,j,k-1)$$
$$+\left[\frac{s^2}{\frac{1}{V_{s1}^2} + \frac{1}{V_{s2}^2}}\right]\left[\left[1 + \frac{\rho_2 V_{s2}^2}{\rho_1 V_{s1}^2}\right]\frac{2}{h^2}\left[U_1(i,j+1,k) - U_1(i,j,k) + \tfrac{1}{2}\left[U_2(i+1,j,k) - U_2(i-1,j,k)\right]\right]\right]$$
$$+\frac{(G_1 + G_2)}{2} \qquad 4.3.7$$

where G_1 and G_2 are functions, the form of which is given in Appendix G.

The range of nodes which now have second order formulations is shown in Figure 4.7, and the derivations are presented in Appendix G.

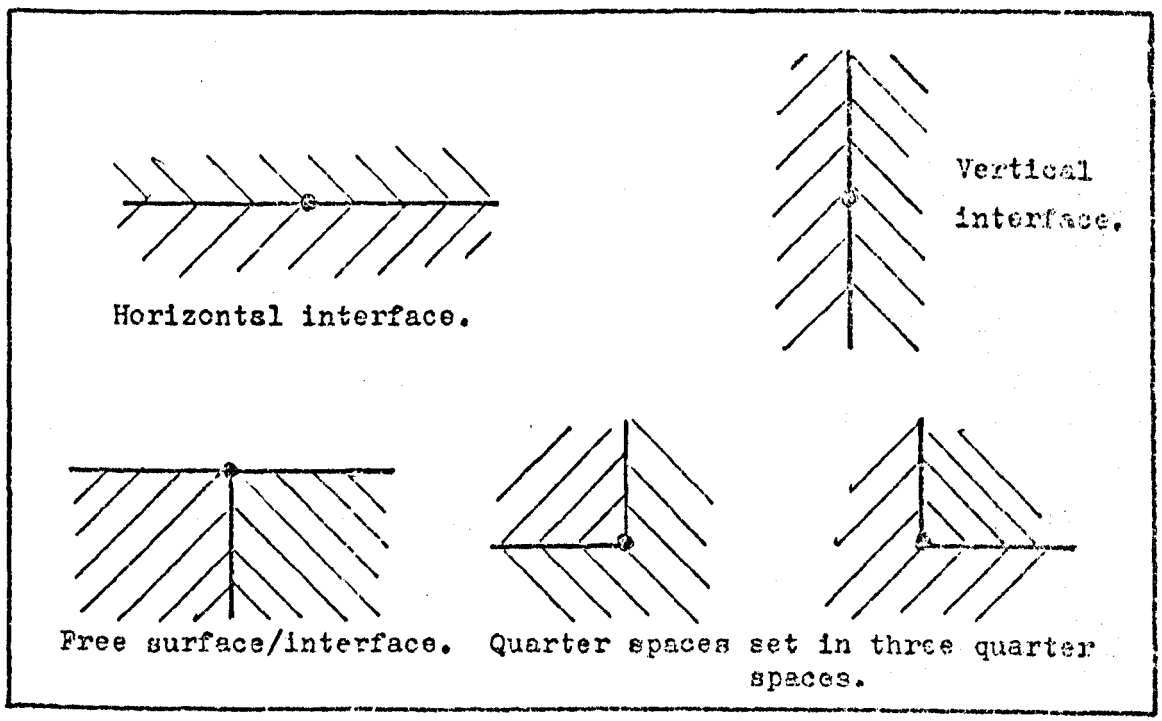

Interface nodes for which second order formulations are given.

FIGURE 4.7.

The formulations presented in this section, together with those in Sections 4.3.1 and 4.3.3, and the supporting appendices, are used in the computer programs described in Section 6, which produce the results given in Section 7.

4.4 Initial Conditions.

To produce a full model of Rayleigh wave propagation and scattering based on the finite difference forms presented in Sections 4.2 and 4.3 there are some additional basic requirements, including the basic material data, the specification of internal artificial boundaries and the specification of the basic pulse at two initial time levels.

The requirements for the basic material data are that enough data should be given to enable the calculation of a consistent set of parameters, such as elastic moduli..In the present study the material data which is required is the shear wave velocity, the compressional wave velocity and the density. All other necessary parameters are calculated using relationships based on those given in Section 2.3.

Calculations are also performed in accordance with the stability and accuracy limits, as set out in Section 4.5, to give the size of increments in both time and spatial domains.

Irrespective of the size of computer available it is not possible to model a semi-infinite medium, so artificial internal boundaries must be set at some distance from the region of special interest in the calculations. These boundaries can be considered in one of two ways, either by producing an absorbing nodal formulation, as is done in the finite element model by Lysmer and Drake (1972), or by keeping a larger iteration space((Alterman & Lowenthal 1972) and specifying that the internal boundaries have zero displacement, as is done by Munasinghe (1973). The second procedure is used in this study, and the scattered waves reflected by these artificial boundaries were found only to be significant if a small iteration space is used, the size of which is specified in Section 4.5, or if the model performs a large enough number of iterations to enable multiple reflections to bulid up.

The practical limits for grid size, accuracy and stability, as established in the present study are presented in Section 6.3.

The final requirement is the specification of the initial displacements at all nodes and it is this which determines the t type and extent of the wave which will propagate.

The initial disturbances on the grid, in the region where

the pulse is specified, are calculated at two time levels, t = 0 and t = s, where s is the time increment which is determined from stability criteria.

The present study requires that a pulse of Rayleigh waves, of limited spatial extent, be specified, which has a similar form to that observed for pulses used in nondestructive testing. For this study a form of pulse is used that was specified by Ricker (1945), and this has been used in a finite difference model of Love waves by Boore (1970) and a model of Rayleigh waves by Munasinghe (1973). A comparison between real experimental Rayleigh waves, and the numerical pulse, both on half-spaces, is shown in Figure 4.8. The details of how the experimental measurement was made are given in Section 8.

The use of the wave number form, or spectrum, as the form of the input pulse was selected as it is this form of display which is considered by Morgan (1973) in his experiments using ultrasonic spectroscopy. The use of the spectrum also provides the opportunity to produce a Rayleigh wave pulse in the numerical model based on the spectra of real signals.

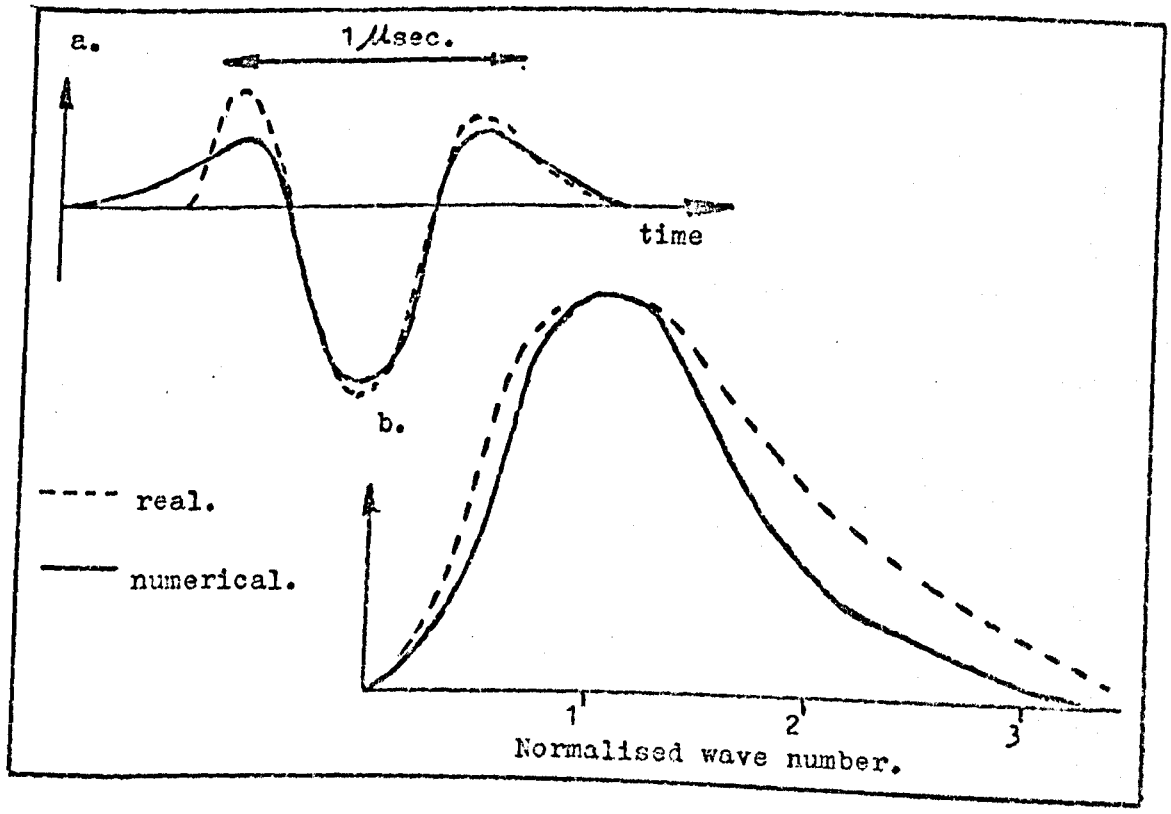

Comparison between real and numerical Rayleigh wave pulses on aluminium (σ =0.34) half-spaces; a. Time domain signals, b. Spectra.

FIGURE 4.8.

4.4.1 The input pulse.

The form of Rayleigh wave pulse used in the present study is that given in analytical form by Ricker (1945). One of the important features of this pulse, in addition to the similarity it has to real Rayleigh wave pulses, as shown in Figure 4.8, is that it is not too extensive in either the real space or the wavenumber space. The main features of the Ricker pulse, including its synthesis, are given in this section with an extended discussion, including the presentation of further information on the basic Rayleigh wave equations and both the analytical and incremental forms of the Ricker pulse, as given by Munasinghe (1973), set out as Appendix H.

The equation for the vertical component of displacement on a horizontal free surface for the pulse is given as;

$$R_2(X_1,0,0) = -\frac{\sqrt{\pi}}{\lambda_0}\left[\left(\frac{\pi X_1}{\lambda_0}\right)^2 - \frac{1}{2}\right]\exp\left[1 - \left(\frac{\pi X_1}{\lambda_0}\right)^2\right] \qquad 4.4.1$$

The corresponding wavenumber amplitude is given as;

$$S(K) = \left(\frac{K}{K_0}\right)^2 \exp\left[1 - \left(\frac{K}{K_0}\right)^2\right] \qquad 4.4.2$$

where K is the wave number,

K_0 is the primary wave number corresponding to the centre wavelength (λ_0).

The primary wave number in terms of wavelength is given as;

$$K_0 = \frac{2\pi}{\lambda_0} \qquad 4.4.3$$

In the production of the basic pulse for use in the numerical model, the initial disturbances for each depth and time level are obtained by performing the series of operations shown in Figure 4.9.

The procedure for obtaining the basic pulse starts from the digitised form of the pulse amplitude spectrum, (which is given as equation H.2.1 in Appendix H.) In the present study, in the wavenumber domain, a base set of 512 (i.e. 2^9) nodes has been used, (this is the range of the J components in equation H.2.1). The parameter of the number of nodes per wavelength is set for each

1. Calculation of S(K) spectum.

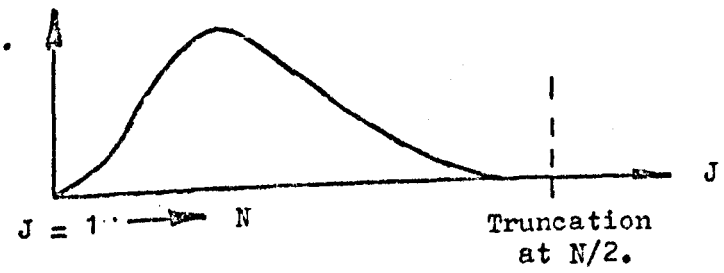

2. Reorder data for operation of F.F.T.

3. Operation of Fast Fourier Transform (F.F.T)

4. Data as output from F.F.T.

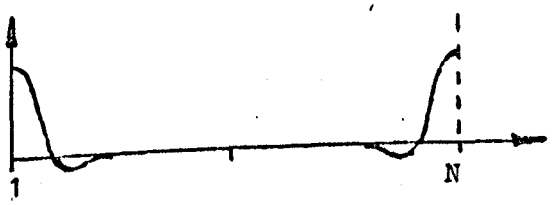

5. Displacements reordered and truncated to fit space where pulse is to propagate.

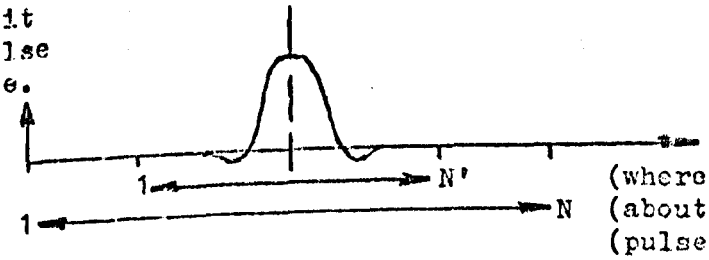

(where N' is (about three (pulse wave- (lengths.

Basic operations for the synthesis of the displacements for one component, for one row of nodes, at one time level, for a Ricker-type pulse of Rayleigh waves.

FIGURE 4.9

pulse synthesis and it is this parameter which determines the number of nodes in the amplitude spectrum which have significant amplitudes. The criteria by which the number of nodes per wavelength is set is considered in Section 4.5 in connection with considerations of accuracy and stability. In the present study calculations have been performed mainly at 16, 32 and 35 nodes per wavelength. The effect of different values for the number of nodes per wavelength is considered with the results of the computer programs in Section 7.

The transformation of the pulse data from the wavenumber to the spatial domain is performed by the application of a single-sided fast Fourier transform, which folds about the node (N/2 + 1) and requires the data length to be halved and the spectral information to be reordered.

The fast Fourier transform is then applied and following this operation the pulse data, which is now displacements in the spatial domain, is reordered and truncated to fit into a realistic computation space.

The series of operations shown in Figure 4.9 are repeated at the depth below the surface of each row of nodes, set by the number of nodes per wavelength in the case of a uniform grid, for the second component of displacement. The whole procedure is repeated to give the displacements at the second initial time level, except that in the case of calculations at times other than $t = 0$, a complex spectral component is introduced which requires the same basic data reordering and combines with the principal spectrum in the fast Fourier transform.

The procedure outlined above was performed for each of the two time levels, $t = 0$ and $t = s$, using polystyrene ($\sigma = 0.24$) data and 35 nodes per wavelength, the resulting spectra are shown in Figure 4.10.

The set of components of surface displacements corresponding to the spectra shown in Figure 4.10, at $t = 0$ with part of the set of horizontal displacements at $t = s$ are shown in Figure 4.11. Also shown in Figure 4.11 is part of the set of components for the vertical surface displacement on aluminum ($\sigma = 0.34$) at $t = 0$.

The displacements at the points of maximum surface displacement were calculated with aluminum data and increasing depth and plotted with the curve given by the analytic expression

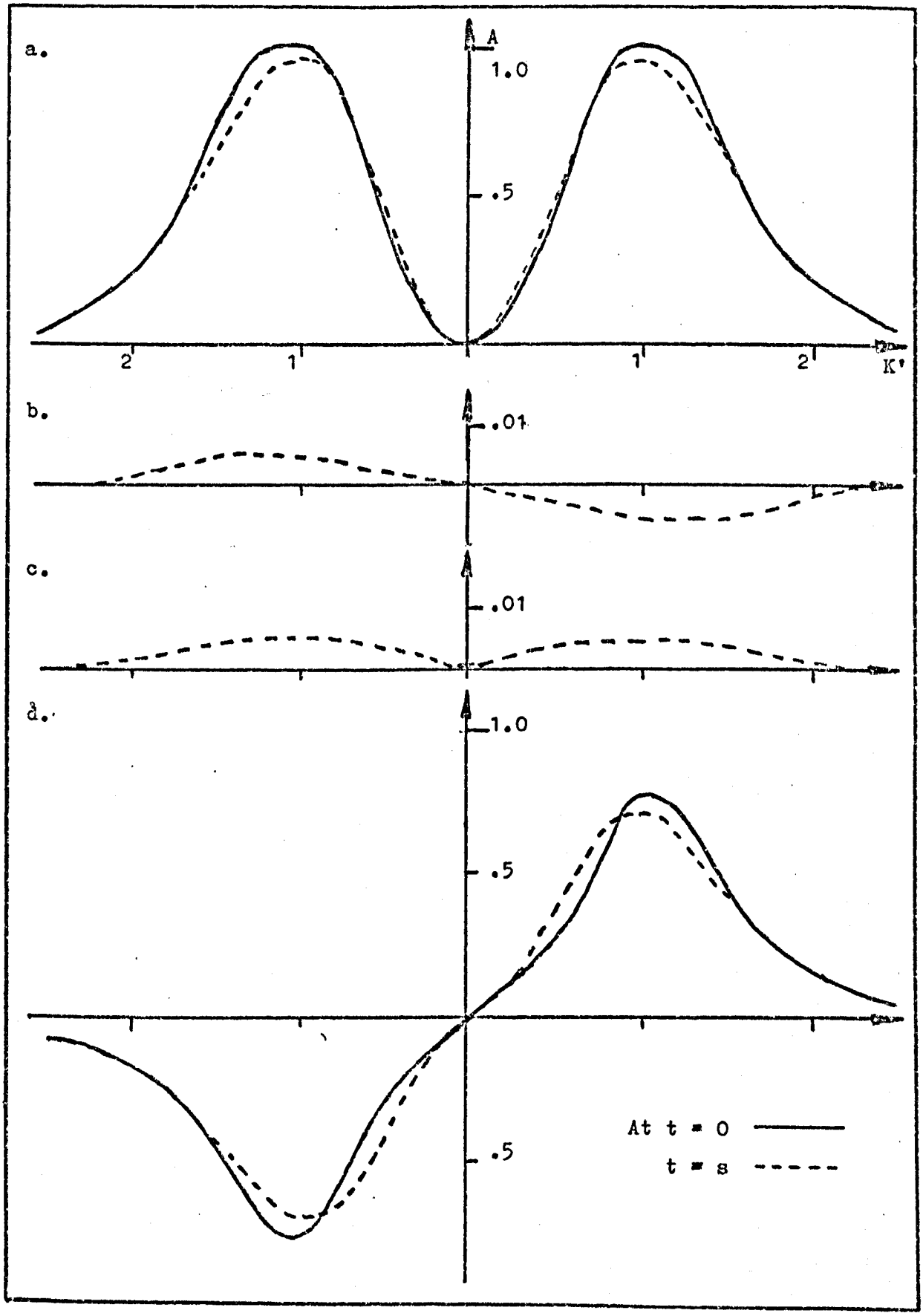

Ricker pulse spectra showing normalised amplitude (A) against normalised wave number (K'), calculated with polystyrene data at 35 nodes per wavelength; showing the real (a) and complex (b) components for the vertical component, and the real (c) and complex (d) components for the horizontal component.

FIGURE 4.10.

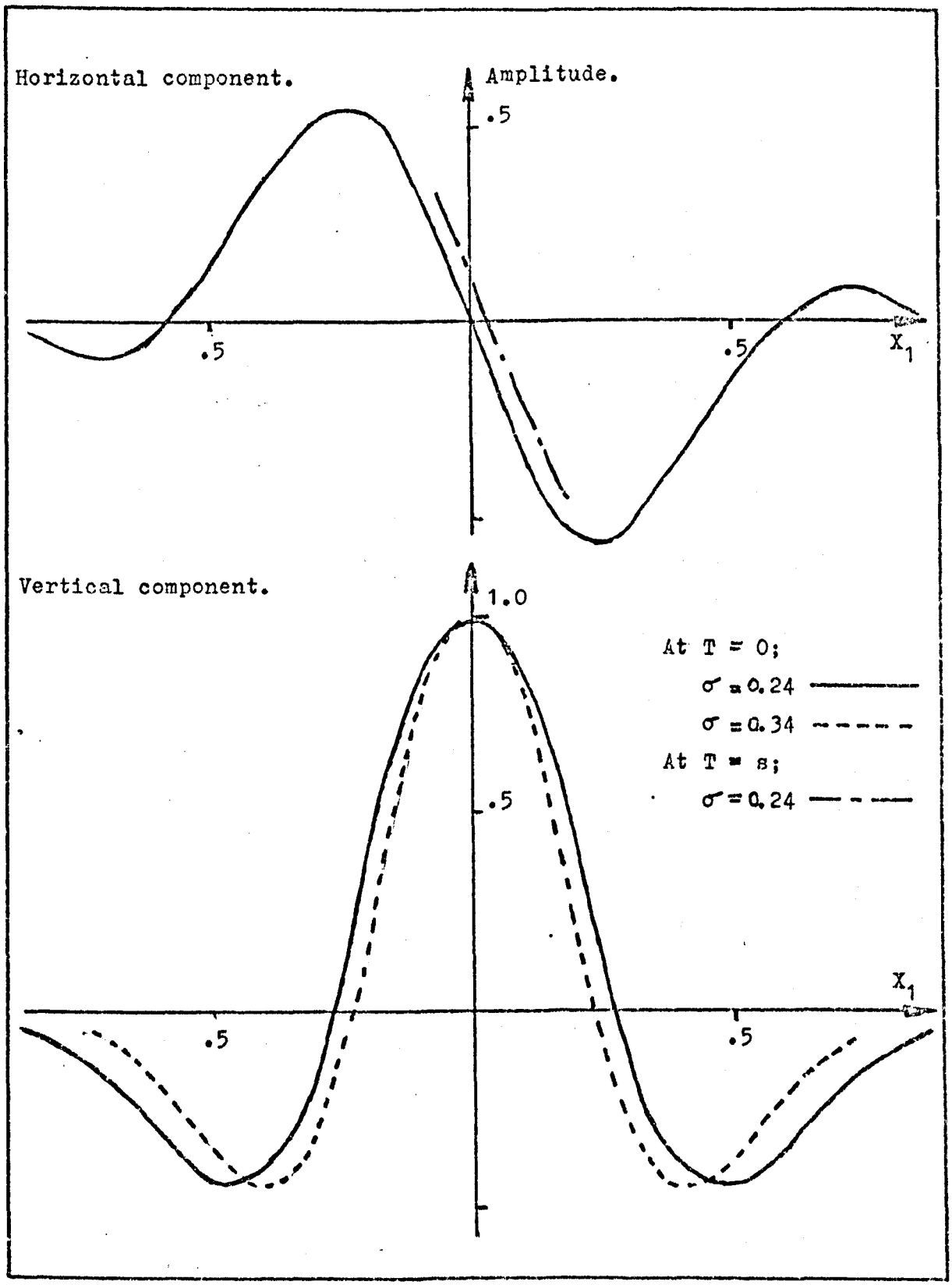

Surface displacements for a Ricker type pulse, at 35 nodes per wavelength; horizontal component of displacement calculated at t = 0 and t = s using polystyrene (σ=0.24) data, and vertical component of displacement calculated at t = o using polystyrene (σ=0.24) and aluminum (σ=0.34) data.

FIGURE 4.11.

for the corresponding harmonic Rayleigh wave as Figure 4.12.

With only a limited node space available in which to model the propagation, interaction and scattering of the Rayleigh wave pulse, due to the limits in the size of computer core, the basic arrays used to set up the pulse must truncate that given by the analytical form which is infinite in extent. It has been found that depending on how the pulse truncations, in both the wave-number and spatial domains,are performed there are changes in pulse shape which affect the accuracy with which the pulse will propagate using a particular finite difference formulation for the boundary conditions, at a particular number of nodes per wavelength.

The values of the surface displacements were measured at different numbers of nodes per wavelength, at different distances from the pulse centre, on different media and the results are shown in Table 3.

Material.	Nodes per wavelength.	Distance from pulse centre (in wavelengths)	
		1.0	1.25
Polystyrene	32	5.0	0.4
Polystyrene	16	0.15	-
Aluminum	35	0.1	-
Aluminum	32	0.2	-
Aluminum	16	0.27	-

Pulse surface displacement amplitudes, at distances from the centre of a Ricker pulse, as a percentage of maximun displacement.

TABLE 3.

The values of the displacements, measured at the points of maximum surface displacement were measured at a series of depths, for a pulse calculated with aluminium data at 35 nodes per wavelength and the results are shown in Table 4.

The effects of different numbers of nodes per wavelength and dimensions for the basic pulse of Rayleigh waves are considered, with the results of the computer models, in Section 7.

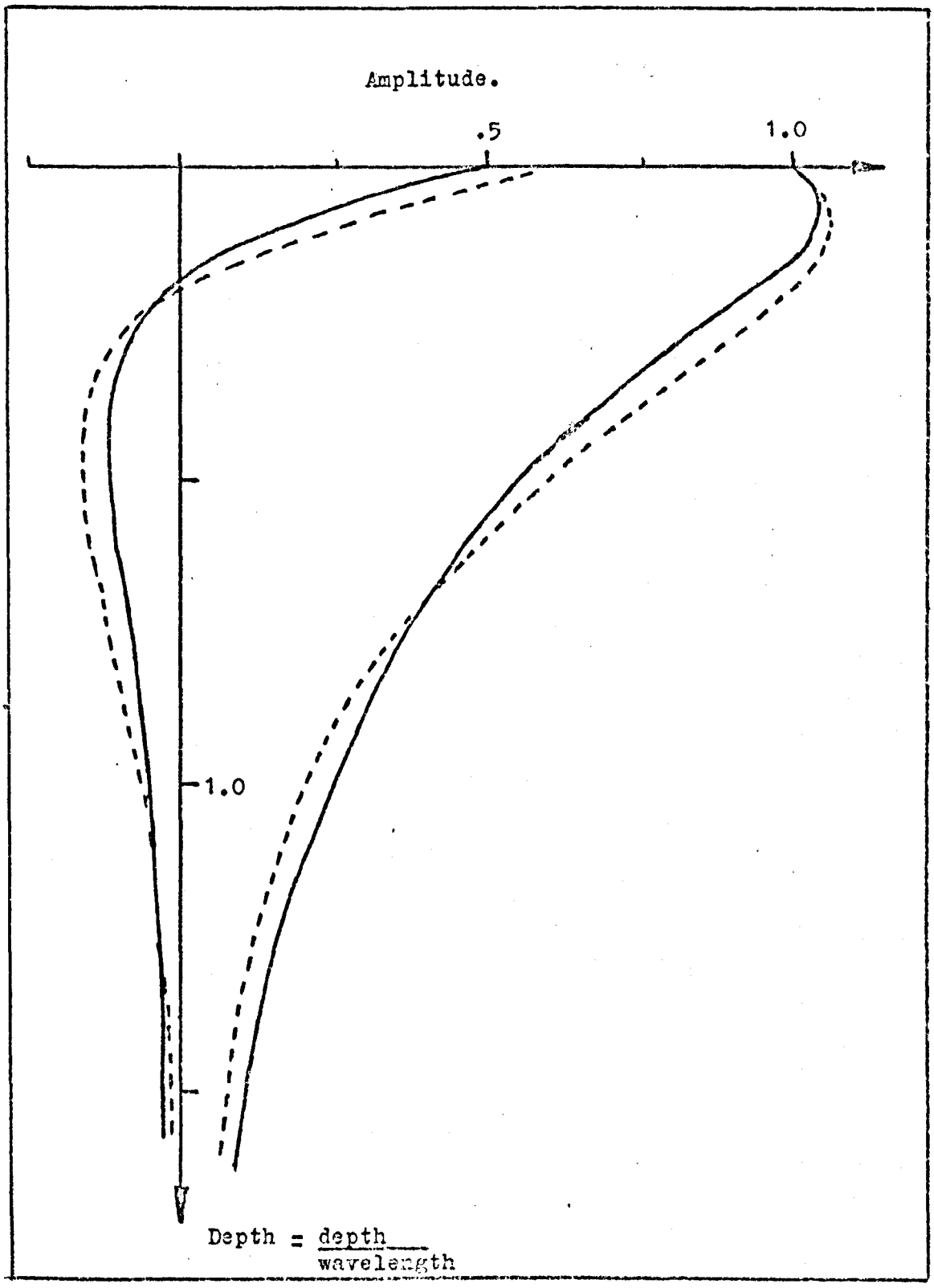

The decay with depth of the displacements of a Ricker type pulse, at 35 nodes per wavelength (solid line) and the corresponding harmonic Rayleigh wave for the pulse centre wavelength (dashed line), at the points of maximum surface displacement, calculated with aluminum data.

FIGURE 4.12

	Depth (in wavelengths)					
	1.0	1.5	2.0	2.5	3.0	3.5
Pulse displacement amplitudes.	29.	15.	7.	4.3	2.5	1.7

Pulse displacements as a percentage of maximum displacement, measured at points below that of maximum surface displacement, for a series of depths and calculated with aluminium data at 35 nodes per wavelength.

TABLE 4.

It has been found that pulse length is the more important dimension when scattering by shallow features, with dimensions up to the order of a quarter wavelength, is considered and that the pulse can be truncated at about two wavelengths depth. However with larger features a pulse depth of about three wavelengths is required.

For scattering of Rayleigh wave pulses by most features pulse truncation levels of 1.0 % of the maximum surface displacement were chosen and found to give solutions of acceptable accuracy. This level of truncation involves the use of an input pulse with dimensions of about three wavelengths wide and three wavelengths deep, which are similar values to those used by Munasinghe (1973). The full input pulse is shown, using numerical visualisation, as Figure 4.13.

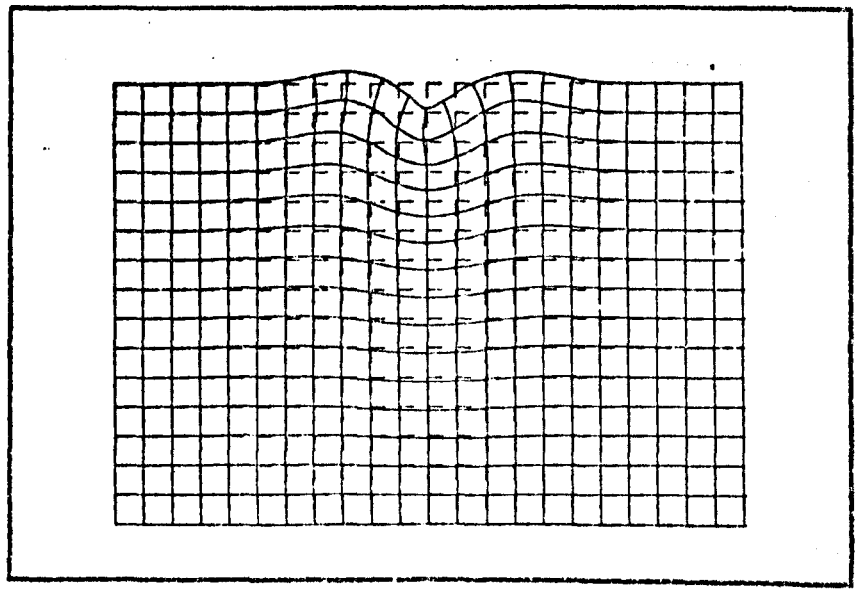

The Ricker type pulse, calculated at t = s, where s is time increment, withaluminium data at 32 nodes per wavelength.

FIGURE 4.13.

In addition to the effects of pulse spatial dimensions, a parameter which has been found to be of considerable importance, is the number of nodes per wavelength. It was found by Munasinghe (1973) that values of about 35 nodes per wavelength were required for the pulse to propagate without distortion, which is higher than might be expected from a preliminary treatment and in this study values between 16 and 35 were used for this parameter. The number of nodes per wavelength and their effect in the computer models are considered in Sections 4.5 and 7 respectively.

4.5 Accuracy and stability.

The consideration of accuracy and stability is fundamental in the development of any finite difference scheme and it is these considerations which often impose limitations on the range of configurations and materials which can be modelled, using a particular numerical scheme.

A finite difference scheme is said to be stable if the difference between the analytical and numerical solutions of the difference equations, remains bounded as time development proceeds, with fixed time step and grid dimensions.

For any numerical scheme there are a range of material and model parameters, outside which the scheme is subject to inaccuracy and instability, which is usually shown by uncontrolled growth in the calculated variables. The aim of accuracy and stability analysis is firstly to set the bounds within which a scheme can be said to be stable and secondly, to provide a measure of the accuracy of a particular solution.

In general the parameters which affect these conditions are the equations of motion, the boundary conditions, the finite difference formulations, the initial conditions and the material parameters.

The basic equations of motion and the boundary conditions together with the initial conditions are often part of the basic formulation of the system under study and set constraints within which the system must be solved.

For a numerical scheme the full analysis of the effects of all parameters which influence the solution of a scheme

is not possible for the scheme as a whole, but the measurement of the effects of various components can be made. The accuracy and stability of a given scheme are closely linked and each of these is now considered with reference to a scheme based on the finite difference formulations developed in Sections 4.2 and 4.3, and the supporting appendices, and the initial conditions set out in Section 4.4

4.5.1 Accuracy.

For any numerical scheme, which remains stable within the definition given in Section 4.5, it is necessary to produce results with a known accuracy that is as close as possible to any known analytical results. This section considers some of the basic truncation errors, and limits, to the parameter nodes per wavelength which affect the accuracy of the finite difference schemes.

The ultimate limit to accuracy is set by the number of digits used in the computer calculations. This is the level at which the computer truncates numbers and in the present study twelve significant figures are used. The resulting truncation errors are negligible when compared with other errors in the scheme.

The finite difference formulation truncation errors, which depend on the detailed approximations used, are of considerably more importance and make up one of the major errors in a scheme. The size of the truncation error, which consists of the sum of the disregarded terms in the series used in the derivation of the formulation, the largest of which is of the order of either the size of the increment or the increment squared that has a maximum value of about 0.1 % of the previous term.

A further limit is set by the accuracy with which the material parameters and other constants are given, or can be calculated, and this is to about 0.1 % of the parameter value, for material data.

As previously mentioned in Section 4.4.1, the parameter, the number of nodes per wavelength, has a considerable effect on the performance of a numerical scheme. The number of nodes

Per wavelength (γ) defines the grid internodal spacing as;

$$\Delta x = \gamma_o/N \qquad 4.5.1$$

where N is the number of nodes per wavelength.

The internodal spacing sets the high-frequency cut off and the minimum wavelength that will propagate as;

$$2\Delta x = \gamma_m \qquad 4.5.2$$

where γ_m is the minimum wavelength.

The condition, given as equation 4.5.2, has a corresponding equation which gives the cut off in the wavenumber spectrum, which is given as;

$$K_m = 2\pi/\gamma_m \qquad 4.5.3$$

where K_m is the wavenumber cut off.

It has been found experimentally by Alford et al (1974) that for a second order formulation, as used for the body nodes in this study, a minimum of ten nodes per wavelength is required at the upper half power point. From the power curve for the Ricker type pulse, as used in this study, shown as Figure 4.14, it is found that the upper half power point is at about 1.5 K/K_o (where K is wave number and K_o is the wavenumber at the pulse centre frequency) which gives a value of about 15 nodes per wavelength, at the centre frequency, for ten nodes per wavelength at the upper half power point. The value of 15 nodes for nodes per wavelength at the centre frequency, is about half the value found necessary by both Boore (1970) and Munasinghe (1973) to give nondispersive propagation. This apparent contradiction was investigated.

In the study by Munasinghe (1973) he defines a useful range of normalised wavenumbers as from 0.5 K/K_o to 2. K/K_o, in which measurements could be made to an accuracy of 2 %, and a critical range, defined as from 2. K/K_o to 3. K/K_o, in which the pulse will suffer severe distortion as the number of nodes per wavelength, defined at the centre frequency, is reduced.

A measure of the error in the digitised pulse spectrum is given by the relationship for the fractional error, which

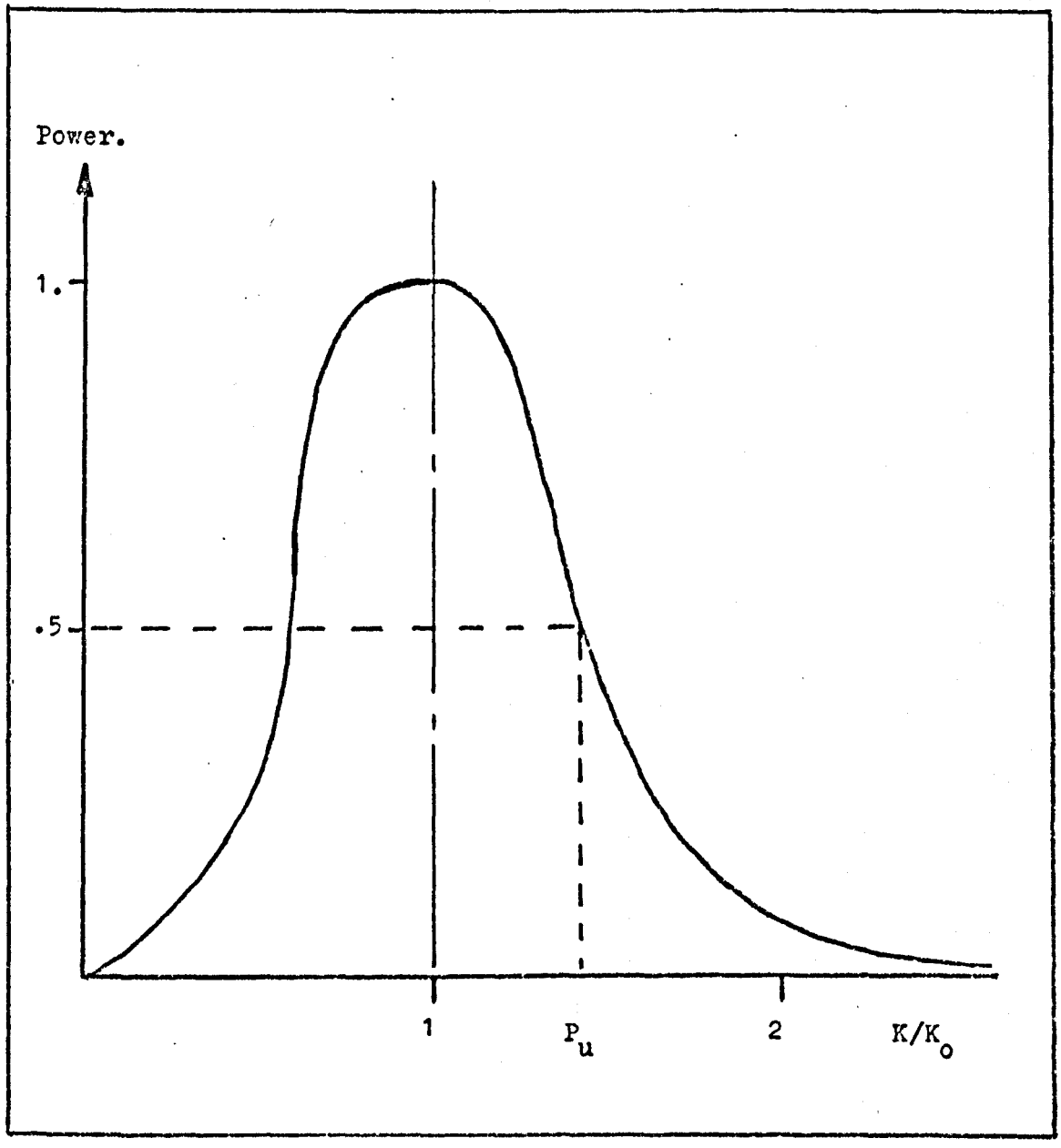

The power spectrum of the Ricker type pulse, calculated with aluminium data at 35 nodes per wavelength, showing the upper half power point (P_u)

FIGURE 4.14.

compares the exact form with second order derivatives and is given by Munasinghe (1973) as;

$$E(K) = \left(\frac{2\pi K}{N \; K_o} \right)^2 \Big/ 12 \qquad 4.5.4$$

when $K\Delta x$ is assumed to be less than one and only the first order error is considered.

Using the relation, given as equation 4.5.4, to give values for a range of N values at several values for K/K_o the results shown in Table 5 were obtained.

N	Values for K/K_o. 0.5	1	2	3
40	0.05	0.20	0.82	1.8
30	0.09	0.36	0.84	3.2
20	0.20	0.82	3.3	7.4
15	0.30	1.4	5.8	15.0

Fractional error, as a percentage, in a Ricker pulse spectrum.

TABLE 5.

It is seen from the results shown in Table 5 and the work by Munasinghe (1973), that if the spectrum is to be used to measure pulse shape with propagation, a restriction of about 30 nodes per wavelength must be imposed. However, in the present study it has been found that, when using the same boundary condition formulation as Munasinghe (1973), it is possible to measure pulse amplitudes to better than 5 % down to values of 16 nodes per wavelength.

In the studies by Boore (1970, 1972), where the Ricker pulse was applied to Love waves, spectral analysis was used down to values of 20 nodes per wavelength, with the majority of the measurements being made at 34 nodes per wavelength.

The effects of dispersion on phase and group velocities were investigated by Boore (1970) and these were found to become important only when 10 or less nodes per wavelength were used. The errors resulting from the use of a small number (less than 15) of nodes per wavelength to define a wave were also considered and

Boore found that to obtain a 95 % accuracy at least 7 nodes per wavelength are required.

4.5.2 Stability.

Having considered the basic accuracy of the various components of the finite difference scheme and the parameter of the number of nodes per wavelength, attention now turns to trying to provide a measure of the conditions which will give stability in relation to increment size and ranges of parameter values.

A practical limit that must always be observed is that information must be able to propagate across the grid faster than the highest wave velocity, i.e. in this study the compressional wave velocity, and this sets a bound for the scheme.

The stability of the scheme is not however guaranteed by the above bound. For an infinite domain, with only body nodes, by the application of harmonic stability analysis to the body node finite difference formulation, Alterman and Loewenthal (1970) have shown that the von Neumann criterion yields a stability condition which links the spatial increment for a uniform grid (h) to the size of the time step (s). This condition, the von Neumann limit, can be written as;

$$\frac{s}{h} \leqslant \sqrt{\frac{1}{V_s^2 + V_c^2}} \qquad 4.5.5$$

The number of nodes per wavelength which gives the value for h is set by the frequency content of the pulse subject to the conditions given in Section 4.5.1.

The inequality, equation 4.5.5, provides an accurate bound outside which the whole scheme has a tendancy to go unstable, and if this occurs it is termed gross instability. Using the inequality to set the limit to the s/h ratio, in this study and that by Ilan and Loewenthal (1976), values of 90 % of the limit value have been used, it is found that it is the boundary condition formulation which sets the limits within these limits for which the scheme will give accurate results.

Of particular importance is the effect of the corner approximations on the stability of the scheme, and the instability

that grows from a poor boundary condition formulation is known as local instability. Such instability may be reduced or removed by reformulation of the finite difference approximations used for a particular boundary node, and this has recently been considered for the 90° corner by Ilan (1978, in press), but it is never possible to produce a scheme for a boundary node that has a larger range of stability than given by the von Neumann limit for a body node.

The practical test for stability and accuracy of a scheme of difference forms for differential equations is provided by Lax's equivalence theorem which states that given a properly posed initial-value problem and a finite difference approximation to it that satisfies the consistency condition, stability is the necessary and sufficent condition for convergence, (Richtmyer & Morton 1967) in that a reduction of grid increment should cause the result for a stable scheme to converge to the correct result.

The procedure of reducing grid increments can become impractical for a large scheme as the number of nodes required to cover a given spatial area may use a greatly increased quantity of core and hence use much longer computer run times.

In seeking to measure the range of stability for a particular finite difference scheme, before computer runs are performed, Ilan and Loewenthal (1976) have developed a system known as local matrix analysis.

The basic idea of finite difference theory is to replace a differential problem by a set of linear algebraic equations. There is an operator which performs the solution of such a set of equations from one time step to another which can be represented in a matrix form. This matrix is the propagation matrix which must include the information as to whether the scheme is stable or not; however for the usual grid in a finite difference problem this matrix has huge dimensions and the analysis is therefore difficult if not practically impossible. The procedure of local matrix analysis considers a typical small grid to include such nodes of interest as the surface nodes, and this has been found to give accurate information about stability which can be applied to the whole scheme. (Ilan & Loewenthal 1976, Ilan 1978, in press)

Also using the propagation matrix, Ilan and Loewenthal (1976) have found that by investigation of the matrix eigenvalues for

a range of elastic parameters, principally the ratio V_s/V_c, plots known as Gershgorin's circles can be obtained. The centres of the circles are the diagonal elements of the eigenvalue matrix and the radii are the sums of the absolute values of the off-diagonal elements, (Richtmyer and Morton 1967, p76), and it is found that if the circles reduce in radius as V_s/V_c reduces, this indicates atability, but when the radius of the circles increases with reduced V_s/V_c values, this indicates the source of potential instability in a scheme.

Using Gershgorin's circles Ilan and Loewenthal (1976) were able to identify the source of instability in the composed formulation for the free surface node, as being in the vertical component formulation.

An alternative to considering explicit finite difference schemes that have been used in the present study, and those by Munasinghe (1973) and Ilan et al (1975), is to use an explicit scheme, the stability for which can be guaranteed unconditionally (Richtmeyer & Morton 1967), and which also allow the use of large time increments. However large time increments decrease accuracy and an implicit type of formulation results in the need to solve a system of coupled equations which describe all grid points. The solution of such a system of equations involves the inversion of a large, albeit sparse, matrix, which would limit the size of iteration space to about 100 by 100 nodes, which is smaller than the potential grid size possible using an explicit scheme which is limited only by the limits on computer program run time and computer core and store available.

A summary of the linked set of parameters for the finite difference schemes used in this study are set out in Table 6.

Pulse centre wavelength.	λ_o metre.
Material parameters, wave velocities and density.	ρ kg/m^3 V_s, V_c m/sec.
Nodes per wavelength.	N, minimum of 16
von Neumann limit.	s/h, eqn. 4.5.5
Percentage limit used.	90 %

Basic parameter set for finite difference schemes.

TABLE 6.

4.5.3 The range of stability.

Various semi-empirical methods have been used in previous studies to define regions of stability and recently new methods have been under development by Ilan and Loewenthal (1976) and Ilan (1978, in press) to make the procedure more empirical. However at the present time it is only possible to establish a set of basic guidelines based on previous studies, which can be improved with experience in the operation of a model for a particular type of wave propagation system.

Using four sets of boundary condition formulations, as considered in Section 4.3, Ilan and Loewenthal (1976) and Ilan (1978, in press), have determined bounds for these formulations when used in the half and quarter space configurations respectively using their body wave source. Their results are set out in Table 7.

Finite difference approximation.	Lower limit to range of stability, value for V_s/V_c ratio.	
	Half-space.	Quarter space
Centred.	0.3	0.3
One-sided.	0.35	0.35
Composed.	0.57	0.575
New composed.	0.28	0.00

The range of stability for half and quarter spaces using body waves with a range of boundary condition formulations.

TABLE 7.

However Alterman and Rotenberg (1969) and Ottaviarni (1971) have obtained the largest range of stability in their studies with first order formulations for the boundary conditions using off-centred (one-sided) difference schemes. This is explained by considering the truncation error of the approximations in the frequency domain where it is found that the error of the one-sided approximation is of the order of f^2 (where f is frequency), while in the cases of the centred and composed schemes it is found to be of the order of f^3. This explanation was proposed and tested by Ilan and Loewenthal (1976) using different source functions, with

different orders of smoothing, and as expected the apparent contradiction in the Alterman and Rotenberg (1969) and the Ottaviarni (1971) results, was found to be due to the source function used; in that for a low frequency source the expected order of the schemes is restored.

A graph of the V_s/V_c ratio against Poisson's ratio, obtained from equation 2.3.18, is given as Figure 4.14.

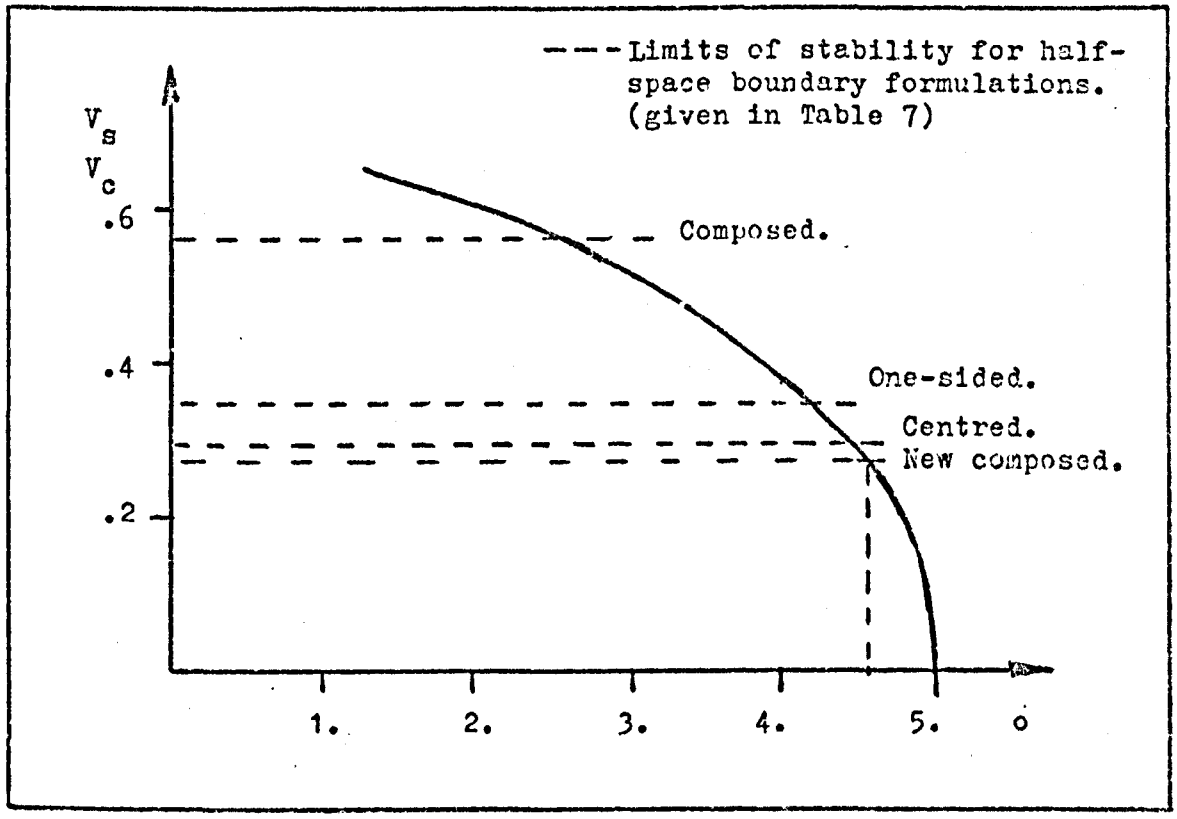

Graph to show the ratio V_s/V_c against Poisson's ratio, with the limits of stability for numerical schemes on half-spaces.

FIGURE 4.15.

Some of the media used in the present study are listed as Table 8, with their V_s/V_c ratio and Poisson's ratio values.

Material.	V_s/V_c ratio.	Poisson's ratio.
Polystyrene.	0.58	0.24
Steel (mild).	0.54	0.29
Aluminium.	0.48	0.34

List of media, with values of the V_s/V_c ratio and Poisson's ratio.

TABLE 8.

By comparison between Tables 7 and 8 it is seen that the composed approximation can be expected to be unstable for many common media. This is found to be the case with the computer models produced in the present study, so the new composed formulation was used.

It is seen from Figure 4.15 that as the value of Poisson's ratio approaches 0.5 the slope of the curve increases and it is found that for Poisson's ratio values over about 0.375 the results become increasingly inaccurate, with the introduction of a period of oscillation in the region behind the pulses so lengthening the pulses. This effect has also been observed in body wave studies by Ilan (1978, in press). Problems are also found in the propagation of pulses in media with low shear velocities, which are media having high Poisson's ratios.

It has also been found by Ilan and Loewenthal (1976) and Ilan (1978, in press), when using body wave sources, that there is a delay in the arrival of secondary pulses, when pseudo-node or the composed approximations are used and in both schemes the delay occurs to a larger degree in the vertical component, increasing as the V_s/V_c ratio is reduced. These findings with body wave have also been observed in the Rayleigh wave scattering considered in the present study and they are considered further in Sections 7 and 9.

A further complication is that, although Ilan and Lowenthal (1976) have found, as shown in Table 7, that with their form of body wave source function there is a limited region of stability for each scheme, Munasinghe (1973), using a Ricker type pulse and the centred difference form for the boundary formulation, has been able to achieve stability just outside the region defined in Table 7.

At present it therefore appears that there is no absolute test which can be applied to select boundary condition formulations which will give the best performance, that is independent of both material parameters and the pulse to be used in the study.

A set of practical bounds, which have been established in the course of the present study, are presented in Section 6, and the results obtained with the computer programs are presented in Section 7.

5. METHODS FOR ANALYSING SYSTEMS.

5.1 Introduction.

The primary aim of the present study is the characterisation of surface features using Rayleigh waves and to help in achieving this aim the series of computer models which are considered in Sections 6 and 7 have been developed, using the finite difference schemes set out in Section 4.

This section considers the different methods which are used to present information about systems in which a Rayleigh wave pulse propagates and interacts with some surface feature, producing a number of scattered waves. These are basically transmitted and reflected Rayleigh waves and some pulses of mode converted waves in the body of the medium. All features of the propagation, interaction and the resulting scattered pulses are of interest and the methods used to study the system are required to give information, which,if possible,can be tested by measurements on real test pieces.

The four groups of methods used in presenting information on the systems which are studied, are discussed in this section. The methods are given firstly, in terms of that used in the computer models and then followed by, where possible, the equivalent supporting measurements which are made in real experiments. The methods used are numerical visualisation, which is considered in Section 5.2, various forms of time domain display, which are considered in Section 5.3, spectral analysis, which is considered in Section 5.4 and analysis of power and energy, which is considered in Section 5.5.

5.2 Numerical Visualization.

This is a term which the author has applied to a form of data display for the computer model results, an example of which is shown as Figure 5.1; which is after Munasinghe((1973) and others. In these the displacements of a sampled set of nodes are plotted, as a displaced grid over a reference grid, the plotting being performed at selected times after propagation has started and the data from each time level being used to produce a single frame.

The particular value of this form of display is that as a full wave solution is given by the finite difference method, the resulting mass of data (up to 60,000 displacements, for one time level) is displayed in a compact visual form which enables a rapid visual study of the interaction, including the mode converted pulses, to be made.

An example of the information given by the final frame for scattering of Rayleigh waves on a quarter space is shown in Figure 5.1. The pulses indicated are identified by comparison with ray theory, the pulse velocities and the direction of the displacements in the pulses, compared with the direction of propagation of the pulse.

In the present study this form of data display has been used to follow the time development of all Rayleigh wave feature interactions and has provided the basis for the interpretation of these systems.

This form of display also presents the information about the waves in the system in a form which enables direct comparisons with the photographs which are produced by conventional visualizations techniques to be made. This is seen when the results for the quarter space, shown as Figure 5.1, are compared with those seen by Hall (1976) for Rayleigh waves scattered at the corner (boundary) of a glass block. (Hall, 1976)

Numerical visualisation is particularly attractive when, as in the present study, computer graphics facilities are available which give the graphics output plotted directly on either 35 mm or 16 mm sprocketed film. The 16mm facility has the particular attraction that it enables short sequences of cinematic film to be produced. Two frames from a sequence for a Rayleigh wave, Ricker type, pulse on an aluminium half space are shown as Figure 5.2.

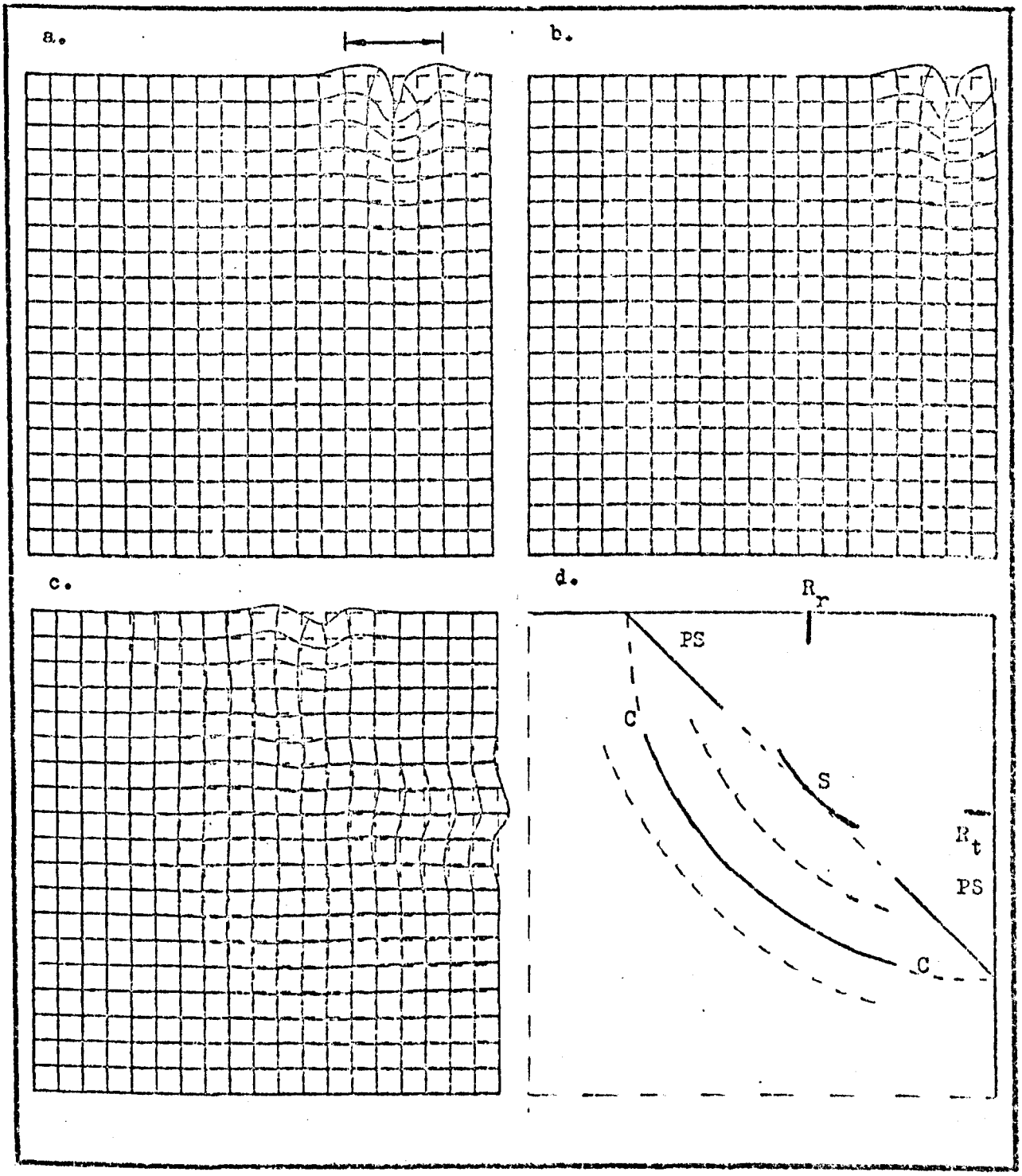

Numerical visualisation display for Rayleigh wave scattering on a quarter space, calculated with chromium data at 32 nodes per wavelength; a. Pulse of Rayleigh waves before scattering.
b. Pulse interacting with corner.
c. Pulses after scattering; R_r reflected Rayleigh wave.
R_t transmitted Rayleigh wave, S Shear wave,
C compressional wave, PS compressional wave mode converted at surface.

FIGURE 5.1.

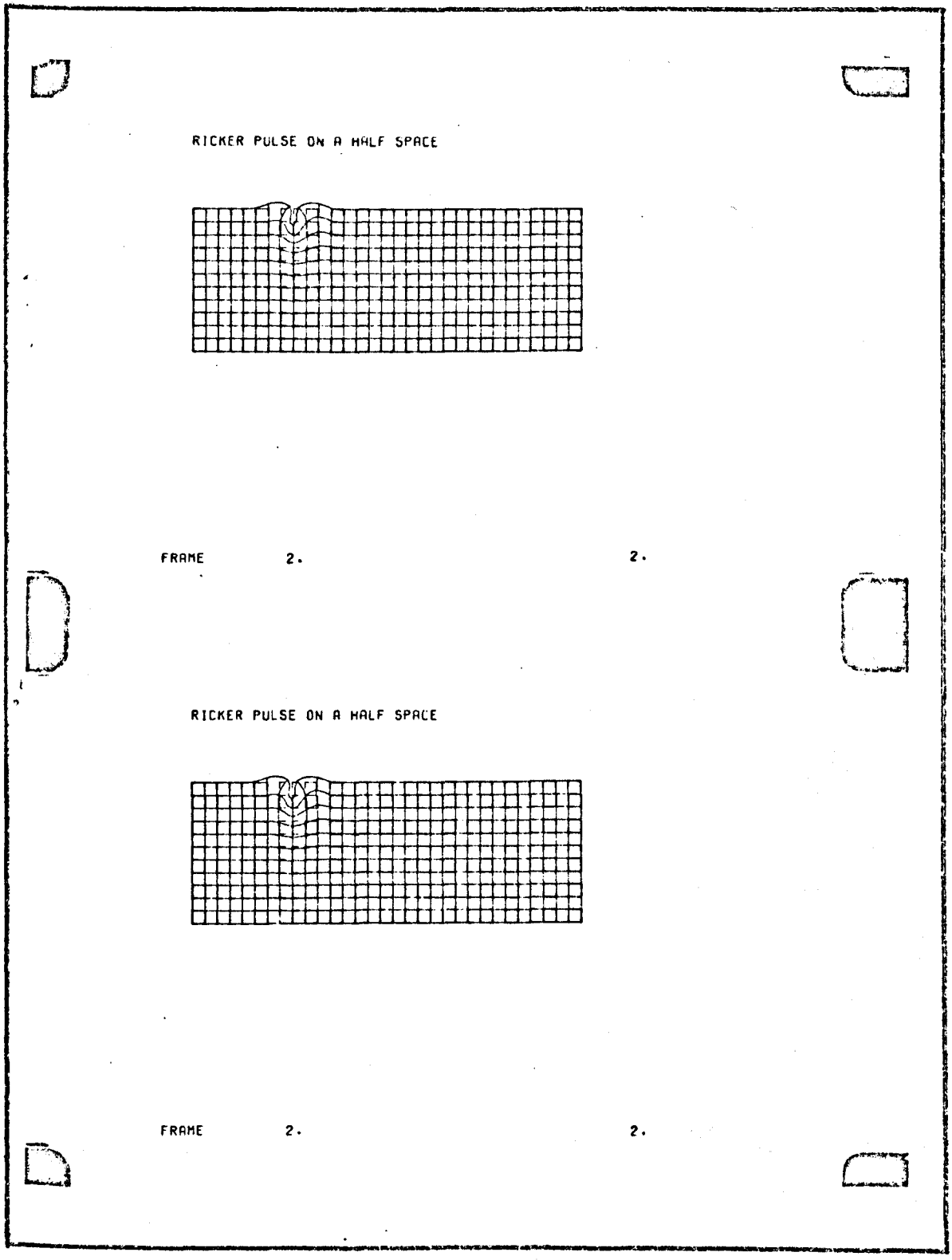

Ricker type pulse of Rayleigh waves, on a half-space with aluminium data, as shown in 16mm format.

FIGURE 5.2

5.3 Time domain displays.

This is a term which describes all the various forms of display which show the time development of displacements at a point and covers a wide range of displays which are used in both numerical model and experimental work.

In mathematical geophysics this form of display is known as seismometer analysis and the displacement data is used to plot synthetic seismograms. (Alterman & Loewenthal 1972)

In the present study displacement data from the computer model are used to plot synthetic time domain signals. An example of this form of output, plotted with the real time domain signal for a pulse on an aluminum block, is shown as Figure 5.3. The details of the experimental method to give the real signal are given in Section 8.

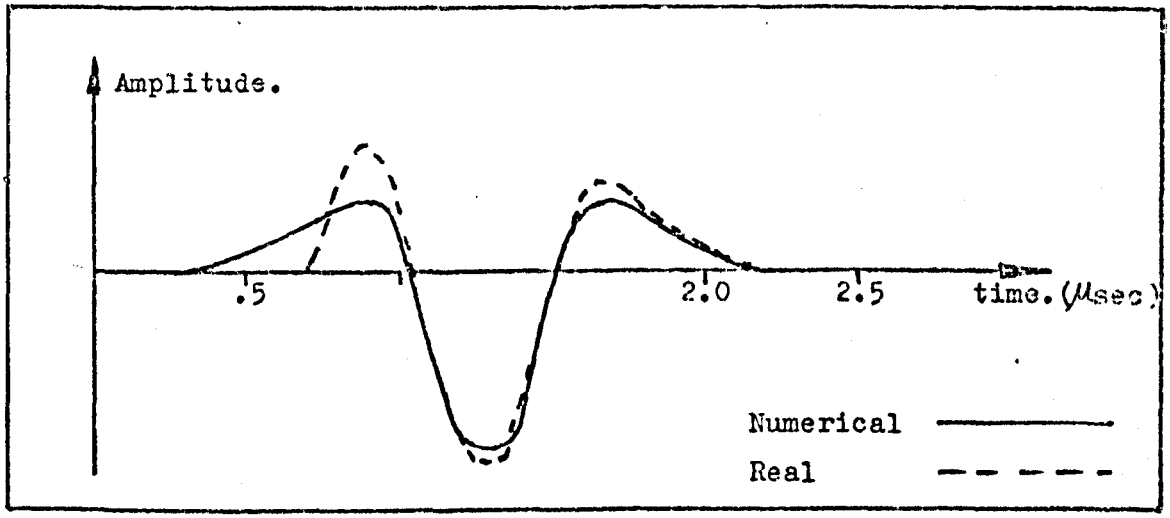

Numerical and real Rayleigh wave pulses on aluminium, the numerical pulse calculated using 32 nodes per wavelength.

Figure 5.3

An alternative way of producing a 'time domain' display is to use the computer model displacements along a particular row or column or direction across the grid so using data just from one time level. The advantage of this is that only displacement data from one time level is used, the data at each node has performed the same number of iterations, so that numerical errors linked with the number of iterations are the same for all points.

A further form of time domain plot is the particle path display, an example of which is shown as Figure 5.4, which shows

the displacements at a point on the free surface of a half-space with the numerical pulse shown in Figure 5.3 passing.

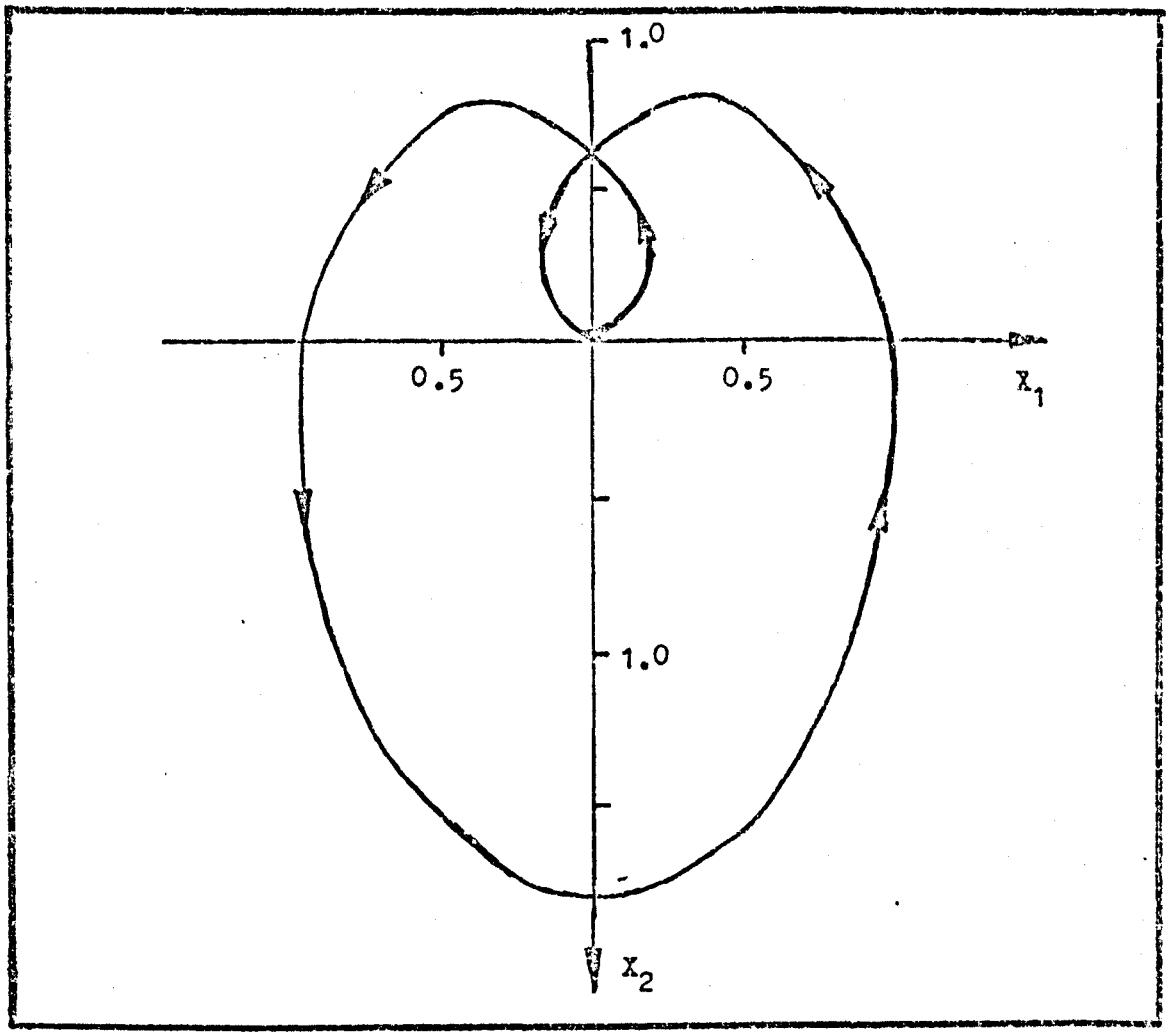

Particle path for a point on the free surface of an aluminium half-space, with the Ricker type pulse, shown in Figure 5.3, passing.

FIGURE 5.4.

The position of pulses was found by the use of synthetic time domain displays. Displays of the type shown in Figure 5.3 were used to study pulse shape changes compared with the shape of the input Ricker pulse.

5.4 Spectral analysis.

This is the study of the spectral content of broadband signals and a spectrum can be obtained from both numerical and experimental signals. This is illustrated by Figure 5.5 which gives the spectra for the two time domain signals, for pulses on half-spaces, shown in Figure 5.3.

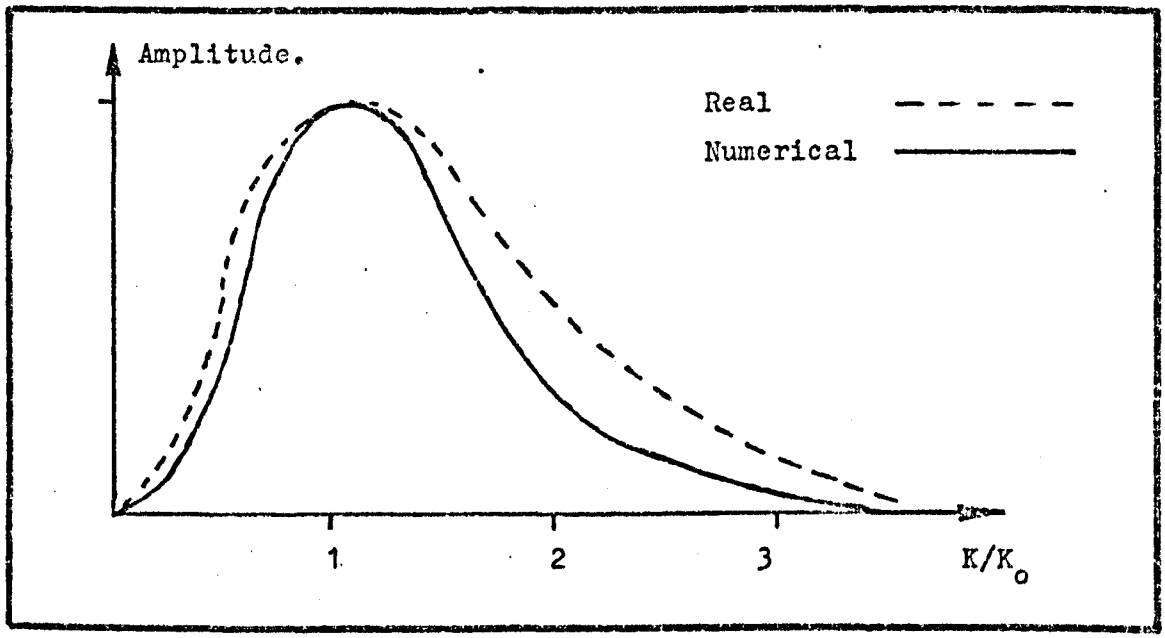

Normalised wavenumber spectra for the real and numerical pulses on aluminum half-spaces shown in Figure 5.3.

FIGURE 5.5.

In nondestructive testing the technique of studying spectra is called ultrasonic spectroscopy, which is considered in Section 2.6.

For the numerical model the procedure for spectral study involves the selection of the pulse to be examined, followed by the application of a fast Fourier transform, in a procedure which is the reverse of that used in setting up the pulse described in Section 4.4.1.

It is found with a broadband pulse that the numerical model is most accurate over a range of wavelengths near the pulse centre wavelength, this being due to the truncation which occurs in setting up the pulse and the digitised nature of the equations used. It has been found by Munasinghe (1973) that the useful range in the

normalised wavenumber spectrum, at about 30 nodes per wavelength, is from 0.5 to 2.0 It is also found that increasing errors are introduced into the results with some finite difference schemes, due to pulse shape changes and a lag in the higher frequency components, this is considered further in Section 7.

For real pulses, obtained experimentally, the equivelent procedure to the application of a Fourier transform is to use a gate to select the signal to be analysed which is then passed into a spectrum analyser which electronically gives an analogue wavenumber spectrum. The details of the experimental method are considered in Section 8.

The use of spectral analysis is of particular importance when changes occur in the shape of the pulse time domain signal which make the determination of accurate transmission and reflection coefficients difficult or, if they are measured, inaccurate. Pulse spectral analysis for experimental signals can provide a measurement of scattering coefficients across the full spectral range in one measurement. This is of particular use for detecting wavelength dependance in a pulse/feature interaction, which is considered further in Sections 8 and 9.

5.5 Power and energy.

The measurement or calculation from the pulse displacements and material parameters of the power flow and energy is of use in helping to follow the energy in a pulse feature interaction. One of the problems with visualisation methods is the limited information which is given about pulse energy so that this is an area where numerical studies can provide useful information.

The instantaneous vector power flow per unit area across a plane, mathematical rather than material, normal to the direction of flow at every point in a material is defined by Love (1934) and Auld (1969) and given as;

$$\underline{P} = -\underline{T}\left[\frac{\partial \underline{U}}{\partial t}\right] \qquad 5.1$$

where $\underline{P} = \begin{bmatrix} P_1 \\ P_2 \end{bmatrix}$ $\underline{T} = \begin{bmatrix} T_{11} & T_{12} \\ T_{21} & T_{22} \end{bmatrix}$ and T_{11} etc. are components of the stress tensor, equation 2.3.8

This has been considered further by Munasinghe (1973) who developed a difference form for calculation of the instantaneous power flow at a particular node and this is given as;

$$\begin{matrix} P_1(i,j,k) \\ P_2(i,j,k) \end{matrix} = -\frac{\rho}{4ds} \begin{bmatrix} V_c^2 D_{11} + (V_c^2 - 2V_s^2)D_{22} & V_s^2(D_{12} + D_{21}) \\ V_s^2(D_{11} + D_{12}) & (V_c^2 - 2V_s^2)D_{11} + V_c^2 D_{22} \end{bmatrix} \begin{bmatrix} D_{1t} \\ D_{2t} \end{bmatrix} \qquad 5.2$$

where, for a uniform spatial grid;

$$D_{m1} = \left[U_m(i+1,j,k) - U_m(i-1,j,k)\right]$$
$$D_{m2} = \left[U_m(i,j+1,k) - U_m(i,j-1,k)\right]$$
$$D_{mt} = \left[U_m(i,j,k+1) - U_m(i,j,k-1)\right]$$

From measurement of power flow the sum over time gives energy, and integral forms for this have been given by several authors including Munasinghe (1973).

In the present study the measurement of energy has been restricted to, for both experimental and numerical systems, the relation given as;

$$\text{Energy} \propto (\text{Pulse amplitude})^2 \qquad 5.3$$

This relation, equation 5.3, for a given medium, is used in both numerical and experimental systems to provide the data for calculation of scattering coefficients from the maximum pulse amplitudes. The details of the experimental measurements and the related calculations are considered in Section 8.

6. THE COMPUTER PROGRAMS.

6.1 Introduction.

This section presents the background computing information for the computer programs which have been produced using the finite difference formulations described in Section 4 and which implement the methods of analysis outlined in Section 5.

The system of Fortran computer programs for the propagation and scattering of pulsed Rayleigh waves has been developed to cover the range of geometries shown in Figure 6.1.

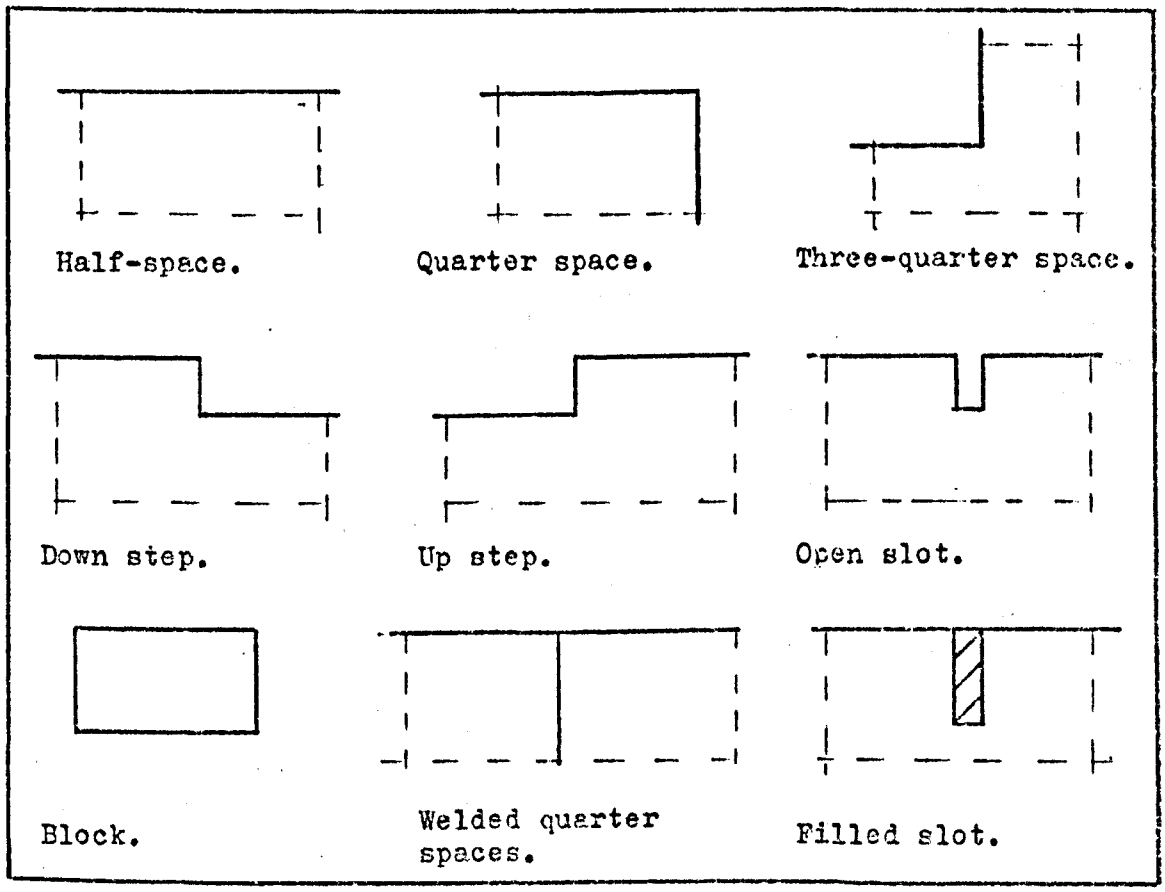

Geometries for which finite difference computer programs have been written.

FIGURE 6.1.

The types of finite difference formulations used for the boundary nodes in the computer programs for each configuration are shown in Table 9.

Model configuration.	Type of boundary conditions used.	
	1st Order.	2nd Order.
Half-space.	Program A	Program H
Quarter space.	Program B	Program I
Three-quarter space.	Program C	Program J
Down step.	Program D	----
Up step.	Program E	----
Open slot.	Program F	----
Block.	Program G	----
Welded quarter spaces.	----	Program K
Filled slot.	----	Program L

Configurations for which computer programs have been written and the type of boundary condition formulation used.

TABLE 9.

The material presented in this section is in two parts, the first, Section 6.2, presents basic computing information and an outline of the main sections of the computer programs and their operation. The second part, Section 6.3, considers the practical operation of the computer programs, including bounds to the range of material and scheme parameters, to give particular degrees of accuracy and stability.

6.2 Basic computer system and computer program information.

The computer programs used in this study have been written to make the maximum possible use of the computing facilities at the University of London Computer Centre (ULCC) which has as its main computer a CDC 7600, and this has resulted in a set of machine dependent computer programs.

The computer programs were written in Fortran and the basic nodal subroutine testing was performed on The City University (TCU) computers, two ICL 1905E's. The main programs were then developed to take advantage of the ULCC facilities and the programs were then placed in a program library at ULCC. Changes to the library programs were then performed using the TCU-ULCC Link and the library UPDATE system (Waddell 1974). Program operation was also performed using the link to send a small control deck of job control and data cards.

Two particular ULCC facilities are central features in the programs; the Random Access Mass Storage System (ULCC 1976) which provides the large data store required by the programs, and the Microfilm Plotting System (Gilbert 1976), providing plotting on either 35 or 16 mm film, which is both much faster than paper plotting and more convienent to store than conventional paper plots.

To produce a computer program for the finite difference schemes described in Section 4 requires the specification of two basic arrays which represent the sets of displacements for all the nodes in the scheme at two time levels. The basic programs were constructed around two large arrays held in the Mass Storage system which reduces the active core storage requirements for the programs. The basic file arrangement using Mass Storage is shown as Figure 6.2.

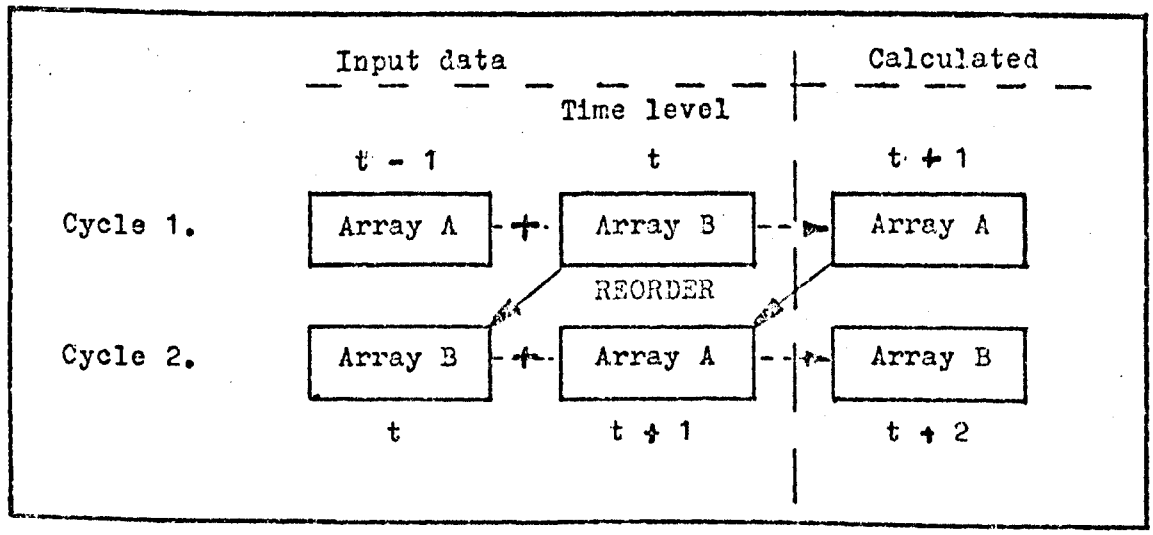

Basic file control using Random Access Mass Storage System.

FIGURE 6.2.

The main array manipulation is built into the arrangement of the main operations of the computer programs ans it is found that the calls to mass store represent a major component in the total job run time. The exact way in which the data is arranged and called can cause up to about 30 % differences in total program run time.

The main operations of the computer programs are shown in Figure 6.3. For each program the master segment reads and writes the basic material data and control parameters, performs the main control functions, including data manipulation using the mass storage system, and calls the necessary supporting and nodal calculation subroutines. The supporting subroutines perform such operations as plotting and calculation of spectra.

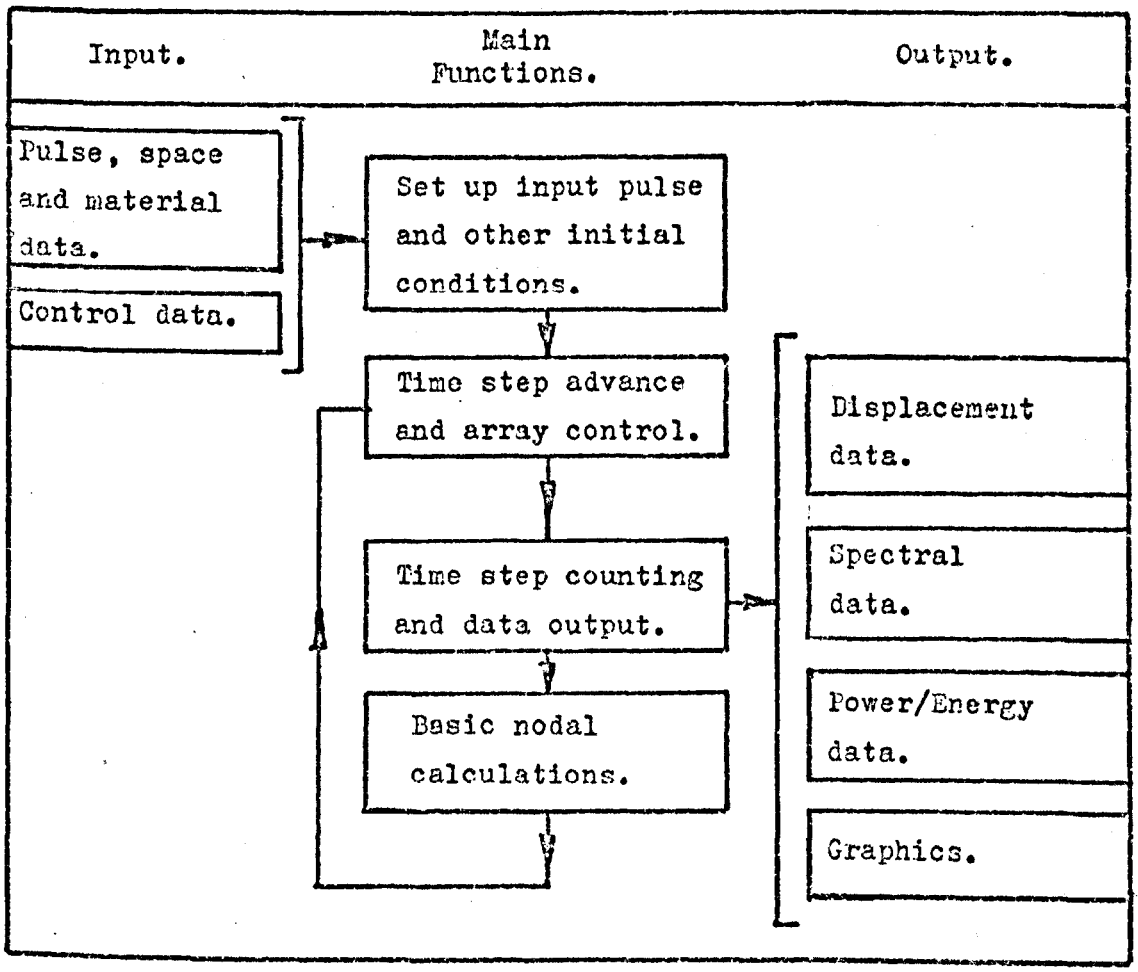

Basic arrangement of main operations in the computer programs.

FIGURE 6.3.

In the detailed writing of the computer programs there are several factors which must be considered. It is important to design efficient subroutines for the nodal calculations, as for example the body node subroutine may be called up to 9,000,000 times in a single program run. It is also important to ensure the optimum arrangement of DO loops, including the ordering of the array subscripts, with the innermost loop calling the first array subscript. In all operations it is important to use the most efficient types and ordering of Fortran statements, for example the use of IF statements which are faster than two or more branched computed 'GO TO' statements and the statements for branching to be arranged so as to minimise the number of tests and subroutine calls.

In a set of complex computer programs of the type developed in this study, each of which may be required to perform 300 sets of nodal calculations for up to about 30,000 nodes, it is found that the compiler used has a considerable influence on job run time. In this study the ULCC compiler OPT - 2, which optimises for rapid execution was used. A typical set of computer program job parameters are given as Table 10.

Program geometry.	Welded quarter spaces.
Space dimensions.	160 by 100 nodes.
Nodes per wavelength.	16.
Number of cycles.	260
Job requirements.	
Small core.	10,072 KWS
Large core.	10,173 KWS
Mill time.	177 sec.
Job run time.	400 sec.
Plotting output.	15 frames 35 mm film.
Lines output.	2,000.

Job parameters and requirements for finite difference model of of Rayleigh wave propagation on welded quarter spaces.

TABLE 10.

6.3 Computer program operation.

This section considers the practical operation of the set of computer programs which model Rayleigh wave propagation and scattering, including the limits for material parameters and grid increments.

It is seen from the job parameters given in Table 10 that the computer programs in the present study are large; they require large quantities of core and have long run times. It is therefore vital that the computer programs are run in as efficient way as possible. This can be achieved by the correct combination of a range of factors including those in the construction of the program, which are considered in Section 6.2, and the parameters used in the operation of the program for both the material data and grid increments.

There are two particular aims in the operation of the individual computer programs which use finite difference schemes and these are the minimisation of core requirements and run time, and the improvement of the accuracy of the results. The steps necessary to achieve either of these two aims often result in a conflict; as the increasing of grid increments, which results in reduced core and run time, tends to reduce accuracy while conversely the reduction of grid increments and the increasing of the number of nodes per wavelength, which results in improved accuracy, increases both run time and core requirements. This results in the need to reach a compromise between high levels of accuracy (better than 1 %), on small grids and less accurate results (about 5 %), on much larger grids, when grid size is measured in wavelengths.

The parameter of the number of nodes per wavelength is therefore of considerable importance, as it is this which sets the limits to the size of region, measured in wavelengths, which can be modelled with a given number of nodes. This parameter is set by the criteria given in Section 4.5.

It is seen in the work with Ricker pulses by both Boore (1970) and Munasinghe (1973) that about 30 nodes per wavelength were used, which results in the requirement for a model of Rayleigh wave propagation on a quarter space of a total of about 25,600 nodes, to avoid unwanted reflections from the

artificial internal boundaries.

The ability to reduce the number of nodes per wavelength to 15, by the use of a different boundary condition formulation or by performing measurements on the scheme in a different way, would reduce the number of nodes required to model the same size of space, in wavelengths, to 6,400 nodes. The resulting savings in core and run time are substantial. Such a reduction would also make possible the modelling in core of many configurations and greatly increase the range of geometries which can be studied using the additional store in the mass storage system. The use of different numbers of nodes per wavelength was investigated and the results are presented in Section 7.

A practical set of limits for parameter values and grid sizes have been established in the course of the present study and these are now presented. The starting point for the guidelines is provided by the accuracy,and stability is not possible,it is only by the use of the computer programs that practical guidelines are established.

The information presented in this section is presented with the aim of providing general guidance and not rigid laws. The values given are those found when using a Ricker type pulse of Rayleigh waves as the imput pulse. In general a system which models body waves is more accurate and stable than one which considers mainly surface waves, as the latter are continually interacting with the least accurate and least stable part of the whole scheme, the boundary nodes.

The aim of the present study was to produce a model with at least 10% accuracy. It has been found that in experimental measurements of the depth of such features as a two wavelength deep crack, an accuracy of about 15% is achieved. (Silk 1976) In the present study accuracies for the model of accuracy well within the 10 % limit have been achieved and the model results and bounds used are given in Section 7.

In this section the set of criteria which follow form bounds within which the present study was performed.

a) For pulse spectrum calculations the base set of data points used was 512 (i.e.2^9)nodes.

b) The minimum extent of the spatial pulse in propagation and interaction studies was about three wavelengths in each dimension. For system testing pulses as small as two wavelengths in each dimension were used. (32 by 32 nodes at 16 nodes per wavelength.)

c) The minimum number of nodes per wavelength at the centre wavelength was 16, corresponding to about 11 nodes per wavelength at the upper half power point.

d) For the time step increment up to 90 % of the von Neumann limit was used (given as equation 4.5.5.).

e) The minimum grid dimensions and limits to number of iterations were set by the first arrival of unwanted reflections from artificial boundaries in a region where measurements were made. This size was determined from the data velocity (i.e. one grid point per iteration). Typical grids were five wavelengths square for the quarter space, and six wavelengths deep and 18 wavelengths long for shallow steps and slots. In practice, smaller grids were used to test the model formulations.

f) In practice for pseudo-node schemes a limiting value for the Vs/Vc ratio was found to be 0.35 (corresponding to $\sigma = 0.42$) below which artificial oscillations introduced large errors and the pulse was spread spatially as propagation proceeded.

g) It was also found that the accuracy of models using the pseudo-node 90° corner formulation reduced as the number of nodes per wavelength was reduced, which set a limit of about 20 nodes per wavelength on configurations such as the quarter space.

The results obtained with the set of computer programs which support the establishment of the guidelines set out in this section are now given in Section 7.

7. COMPUTER MODEL RESULTS.

7.1 Introduction.

This section presents the details of the computer model results obtained with the computer programs outlined in Section 6, which model the configurations listed in Table 9 and shown in Figure 6.1.

The numerical model results presented in this section are divided into two groups according to the type of formulation used for the boundary conditions in the computer programs. The results are presented in two sections, firstly, in Section 7.2, those from the computer programs which use first order formulations for the boundary conditions, and secondly, in Section 7.3, those from the computer programs which use second order formulations for the boundary conditions.

The computer programs use the finite difference schemes defined in Sections 4.2 and 4.3 with the Ricker type pulse of Rayleigh waves which is described in Section 4.4. In all the programs the value of the ratio of the spatial to time increments was set at 90 % of the von Neumann limit, as defined in Section 4.5.

The media for which material data was used in the programs considered in this section are listed as Table 11, with the basic data used . An extended list of material data is presented as Appendix C.

A full comparison between the two sets of numerical model results, the experimental results, which are presented in Section 8 and previous results, is given in Section 9.

Material	Poisson's ratio. σ	Density kg/m^3	Wave velocities in m/sec. V_s	V_c	V_r
Quartz	0.169	2200	3765	5976	3412
Chromium	0.20	7160	4005	6608	3655
Polystyrene	0.24	1080	1180	2030	1084
Perspex	-	1220	1370	2360	1280
Steel(mild)	0.29	7850	3235	5960	2996
Aluminium	0.34	2700	3110	6422	2906
Titanium	0.36	4510	3182	6130	2958

List of media used in models with basic material data.

TABLE 11.

7.2 Programs with first order formulations for boundary conditions.

This section presents the computer model parameters,with the model results, for pulses of Rayleigh waves on homogeneous, isotropic, single media configurations shown in Figure 7.1. The models use the centred difference pseudo-node formulations for the boundary conditions which are presented in Section 4.3.1 and Appendix E.

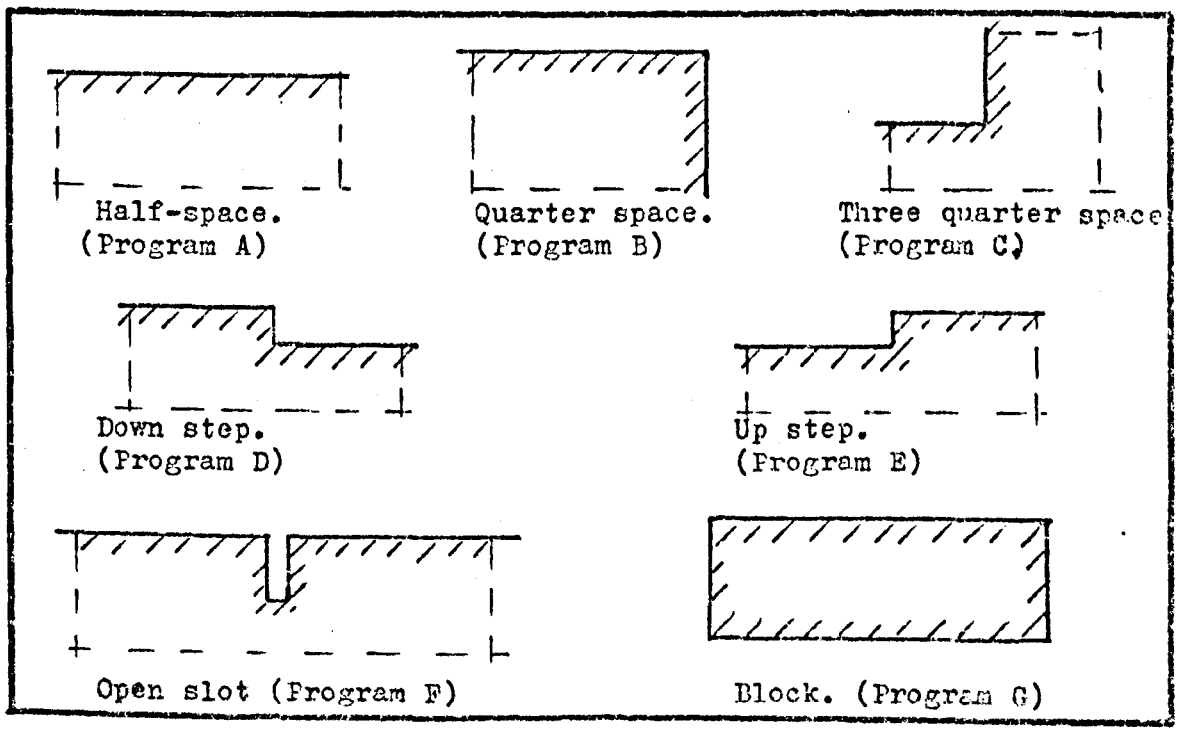

Configurations studied using pseudo-node formulations for the boundary conditions in computer programs.

FIGURE 7.1.

7.2.1 Rayleigh waves on half-spaces.

The ability to produce a computer model which gives the nondispersive propagation of a Rayleigh wave pulse on a half-space, as indicated by the analytical theory which is presented in Section 2.3, is a prerequisite to the development of a model for the interaction and scattering of Rayleigh waves by more complex features.

The basic model node arrangement for the computer program, Program A, which models a Rayleigh wave pulse on a half-space, is shown as Figure 7.2.

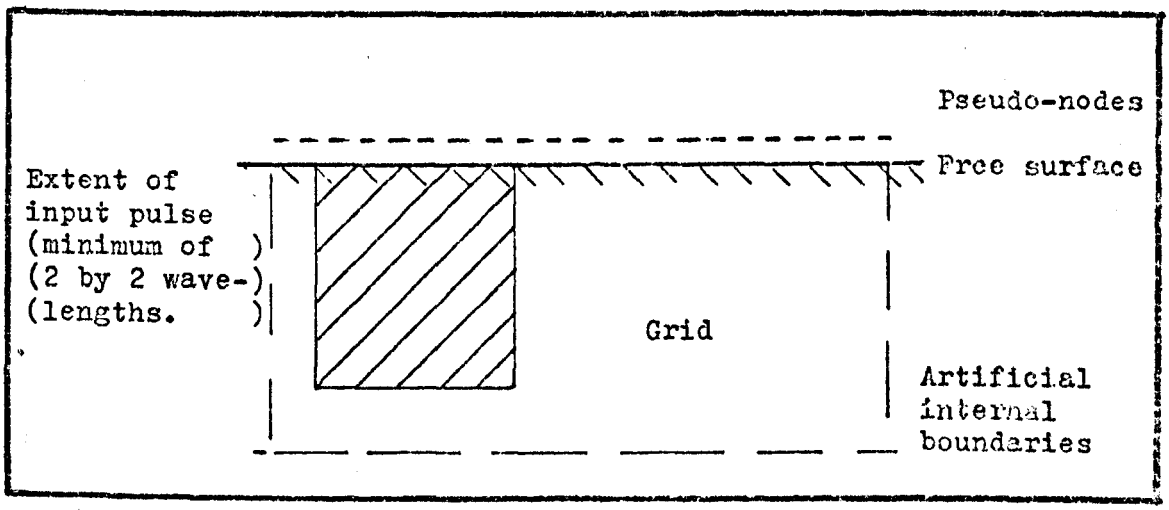

Node arrangement for first order finite difference model of Ricker type pulse of Rayleigh waves on a half-space.

FIGURE 7.2.

The propagation of the Ricker type pulse of Rayleigh waves on a half-space was investigated for two values for each of the two parameters, the material data for the half-space (polystyrene $\sigma = 0.24$ and aluminium $\sigma = 0.34$) and the number of nodes per wavelength (16 and 32 nodes). The value for the pulse wavelength, in metres, was that for 1 MHz. The media data used in the program is that given in Table 11.

The maximum spatial extent of the half-space was 12.5 wavelengths long and 6.25 wavelengths deep, which corresponds to grid dimensions of 200 by 100 nodes, at 16 nodes per wavelength.

a. Distance travelled by pulse.

The propagation of Ricker pulses on half-spaces, at 16 nodes per wavelength, is shown by numerical visualisation for the case of polystyrene data as Figure 7.3 and that using aluminium data as Figure 7.4.

For the two cases shown in Figures 7.3 and 7.4 the numerical model for the half-space, Program A, was tested for the accuracy of wave propagation velocity. The distance travelled by the pulse, as observed in the numerical visualisation and the free surface displacement data was measured and this was compared with the distance the pulse should travel, as given by the wave velocity and the time; the number of iterations multiplied by the time increment. The results obtained for the two cases, shown in Figures 7.3 and 7.4 are presented as Table 12.

	On polystyrene.			On aluminium.		
Distance travelled given by calculation.	0.516	2.59	5.70	0.457	2.28	5.03
Distance travelled given by finite difference scheme.	0.498	2.52	5.58	0.436	2.18	4.87
Percentage difference, when distance as given by F.D. is compared with that given by calculation.	- 4	- 3	- 2	- 5	- 5	- 4

Comparison of distance travelled by Rayleigh wave pulses on half-spaces, as given by pseudo-node finite difference model with that given by calculation using the wave velocity, for polystyrene and aluminium.

TABLE 12.

It is shown by the values for distance travelled given in Table 12 that there is a systematic lag in the position of the centre of the pulse which is larger than the maximum position error due to grid spacing of ± 0.04 which gives a percentage error of 0.8 % at .5 wavelengths on polystyrene. The errors are also seen to be larger for the higher Poisson's ratio material, aluminium.

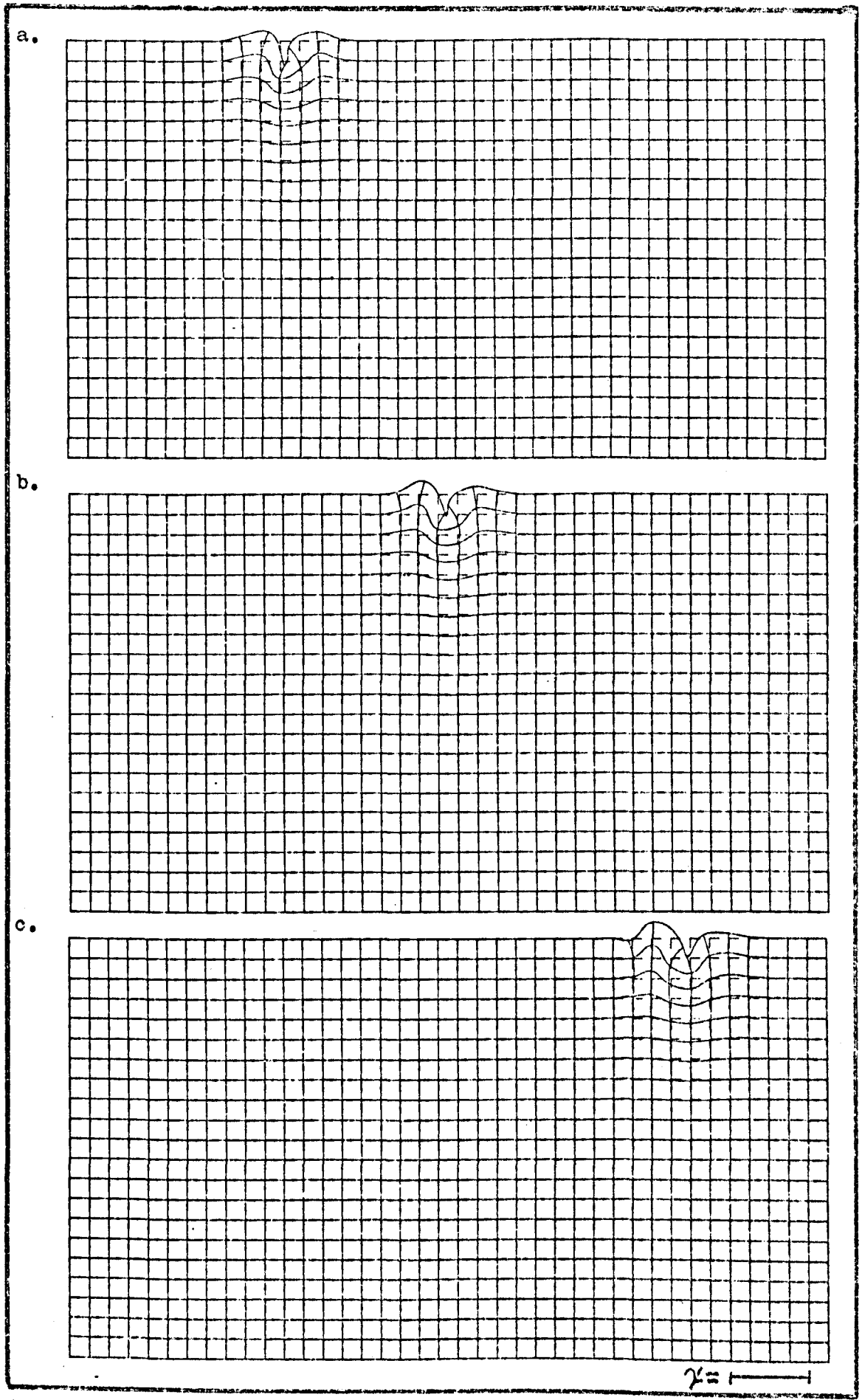

Ricker pulse on a polystyrene ½ space, using 16 nodes per wavelength, after a. 20, b. 100, c. 220 iterations. λ= one wavelength.

FIGURE 7.3

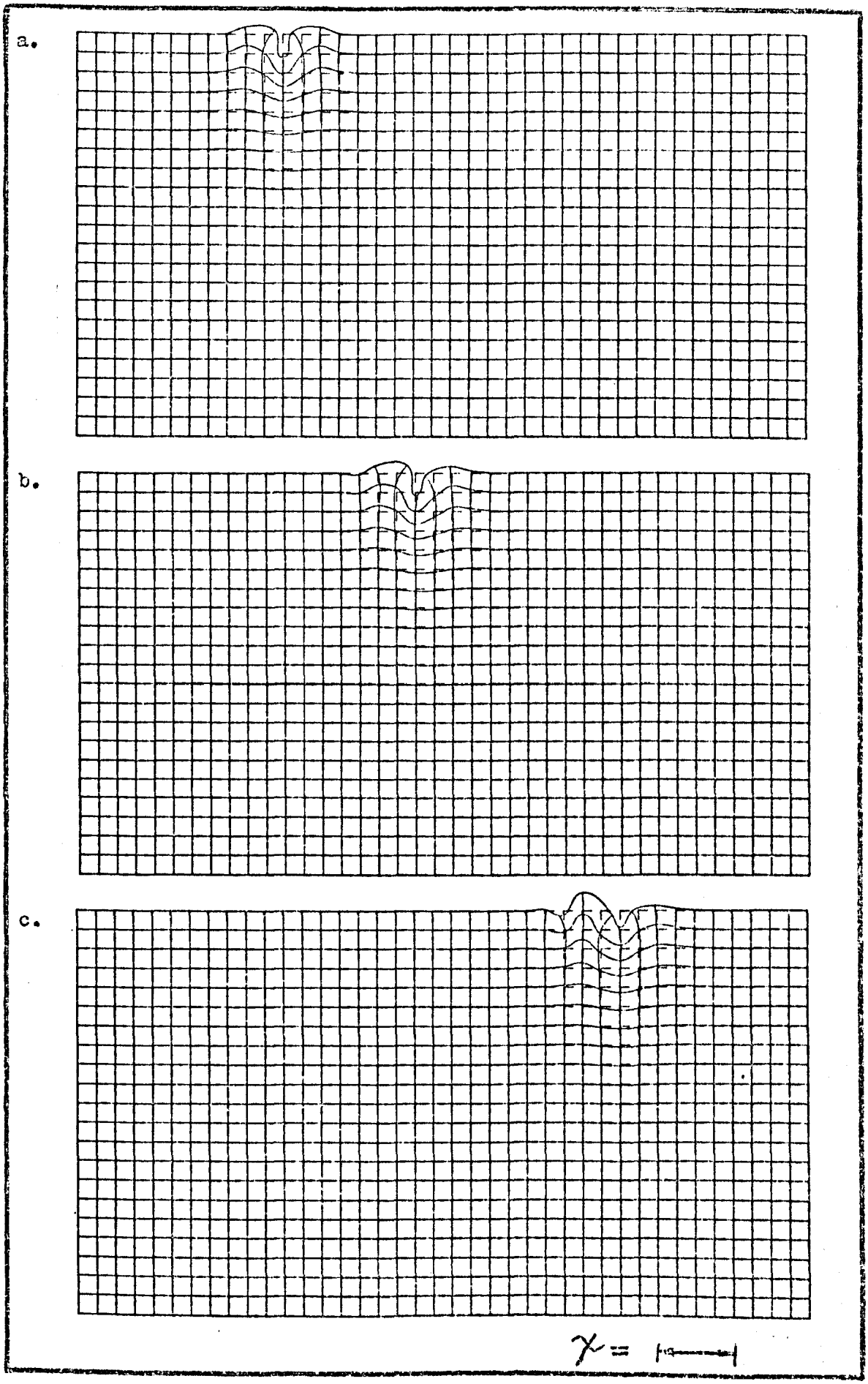

Ricker pulse on a aluminium half-space, using 16 nodes per wavelength, after a. 20, b. 100, c. 220 iterations. λ = one wavelength.

FIGURE 7.4.

b. Pulse shape changes.

The change of pulse shape with distance travelled was investigated for the model using both polystyrene and aluminium data and with different numbers of nodes per wavelength. The pulse as given by the model, for calculations at 16 nodes per wavelength, for the two media, after different numbers of iterations are shown in Figures 7.3 and 7.4.

It is shown in the figures that about up to 100 iterations the pulse shape change, measured as a percentage change in amplitude of the pulse compared with the corresponding point in the input pulse, when measured, was less than 10 %, but after this number of iterations distortion rapidly increased.

When 32 nodes per wavelength were used in the model it was found that the number of iterations before 10 % changes in amplitude occured increased to about 200, but the distance travelled in wavelengths, because of the corresponding reduction in the time increment, was almost the same and the calculations required the number of nodes to be quadrupled to give the same dimensions of space in wavelengths.

The pulse displacement decay with depth curve is shown as Figure 4.12. It is necessary to truncate the pulse at some depth, as was considered in Section 4.4.1, and it is found that to give a pulse which will propagate without introducing additional errors the depth truncation must be made at three wavelengths at least.

c. Spectral measurements.

The Ricker pulse used in the present study is constructed by calculations which start from the wavenumber spectra. The spectra for a pulse, calculated with polystyrene data using 35 nodes per wavelength, are shown as Figure 4.10.

In spectral analysis measurements the pulse spectra are obtained using a procedure which is the reverse of that set out in Section 4.4.1 for pulse synthesis.

After pulse propagation has started the major problem is the synchronising the position for the application of the pulse analysis subroutine with the pulse centre positioned on or very close to a node. It is found, even at 32 nodes per wavelength, that changes of the order of 5 % occur in the maximum amplitude of the wave number spectra as the pulse moves from one node to the next.

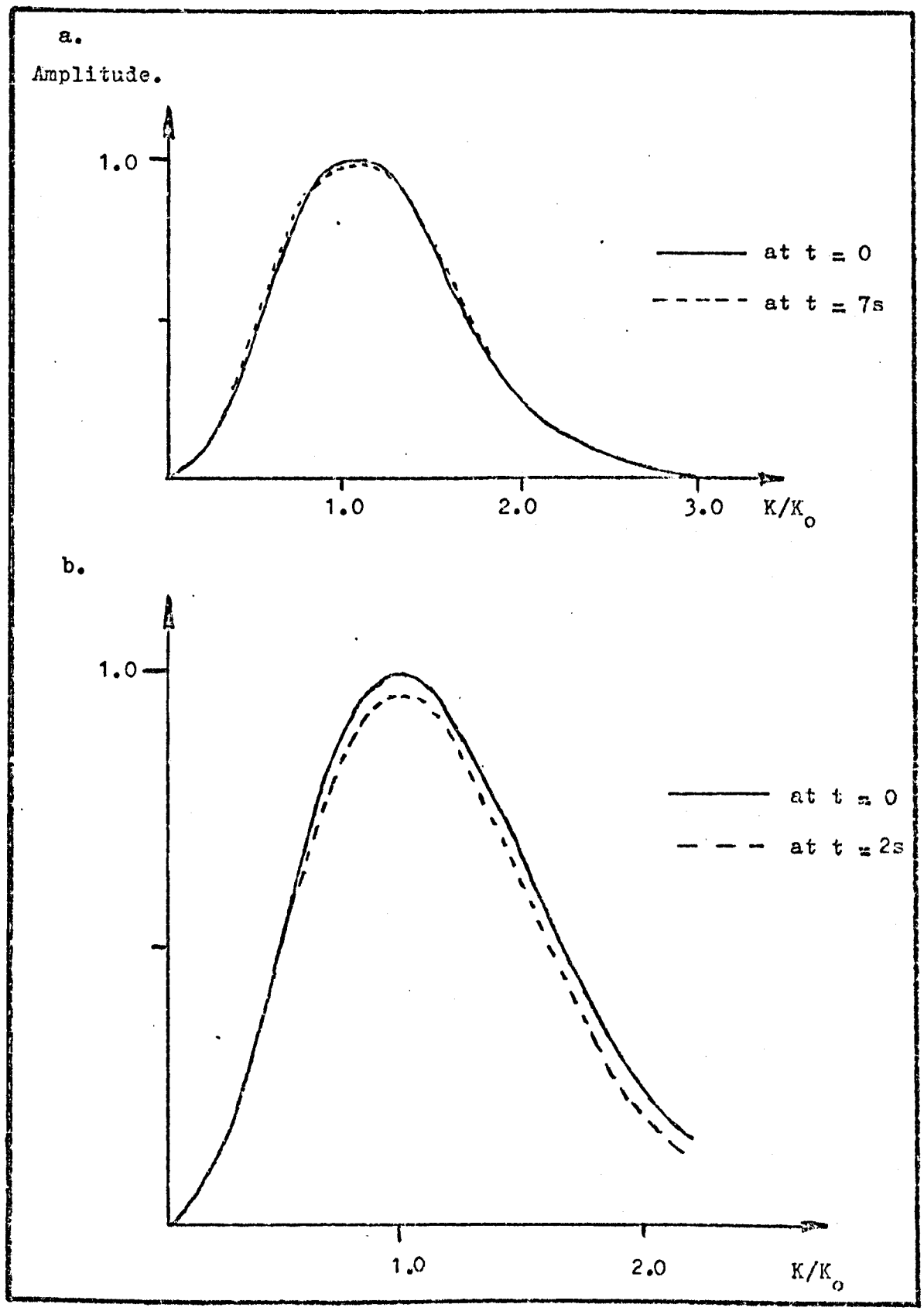

Spectra of Ricker pulses on half-spaces; a.Spectra calculated with polystyrene data using 35 nodes per wavelength at t = 0 and after 7 iterations. b. Spectra calculated with polystyrene data using 16 nodes per wavelength at t = 0 and after 2 iterations.

FIGURE 7.5.

As propagation proceeds errors were found to increase, especially at the high frequency end of the spectra.

In the present study, measurements of the spectra were made using 16 and 32 nodes per wavelength and the resulting spectra for the vertical component of displacement are shown as Figure 7.5. For the case of spectra calculated at32 nodes per wavelength, shown as Figure 7.5a, it is seen that repeatable spectra are obtained. However in the case of the calculations at 16 nodes per wavelength, shown as Figure 7.5b, large percentage errors are found to have been introduced after only two iterations. The percentage errors observed are given as Table 13.

Wave number, (normalised)	0.5	1.0	1.5	2.0
Percentage difference c.f. t = 0 spectra.	- 3.	- 4.	- 7.	-15.

Percentage change found in wavenumber spectrum for 16 nodes per wavelength curve in Figure 7.5b.

TABLE 13.

The values given in Table 13 are found to be in general agreement with those for the Fractional error term given in Table 5.

The results presented in this section are compared with those from a model using a second order formulation, which are presented in Section 7.3.1, experimental measurements and the results of previous studies, in Section 9.2.

7.2.2 Rayleigh waves on quarter spaces.

The quarter space is a single corner configuration, with a 90° corner at the intersection of two free surfaces. From the basic Rayleigh wave theory, as there is no characteristic dimension in the corner, there should be no wavelength dependance in the scattering of the Rayleigh wave pulse by it. This should enable wavelength independant scattering coefficients to be established.

The basic node arrangement for the computer program, Program B, which models a Ricker type pulse of Rayleigh waves on a quarter space is shown as Figure 7.6.

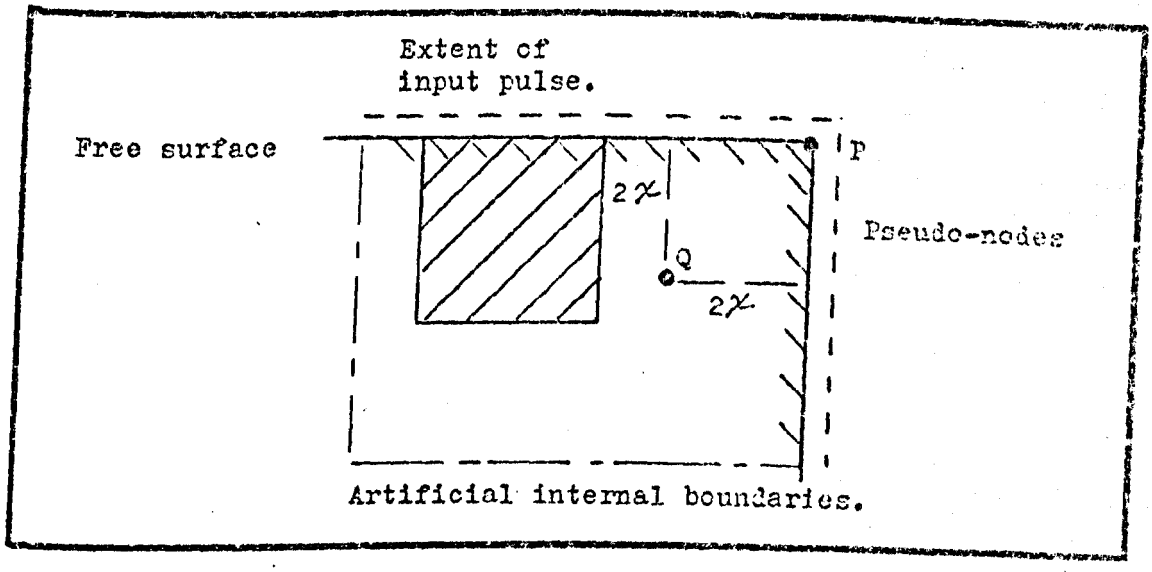

Node arrangement for first order finite difference model of Ricker type pulse of Rayleigh waves on a quarter space.

FIGURE 7.6.

The propagation of the Ricker type pulse of Rayleigh waves on a quarter space was investigated using the node arrangement shown in Figure 7.6 with the data for a range of different media which have Poisson's ratios in the range from .2 to .36, using pulses of different sizes and a centre wavelength corresponding to a frequency of 1 MHz.

a. Basic pulse analysis.

The propagation and scattering of the Ricker pulse was investigated and for each model run, at regular intervals (usually every 20 iterations), sets of displacements were recorded and numerical visualization type displays plotted, an example of which was shown in Section 5.2 as Figure 5.1, is shown here as

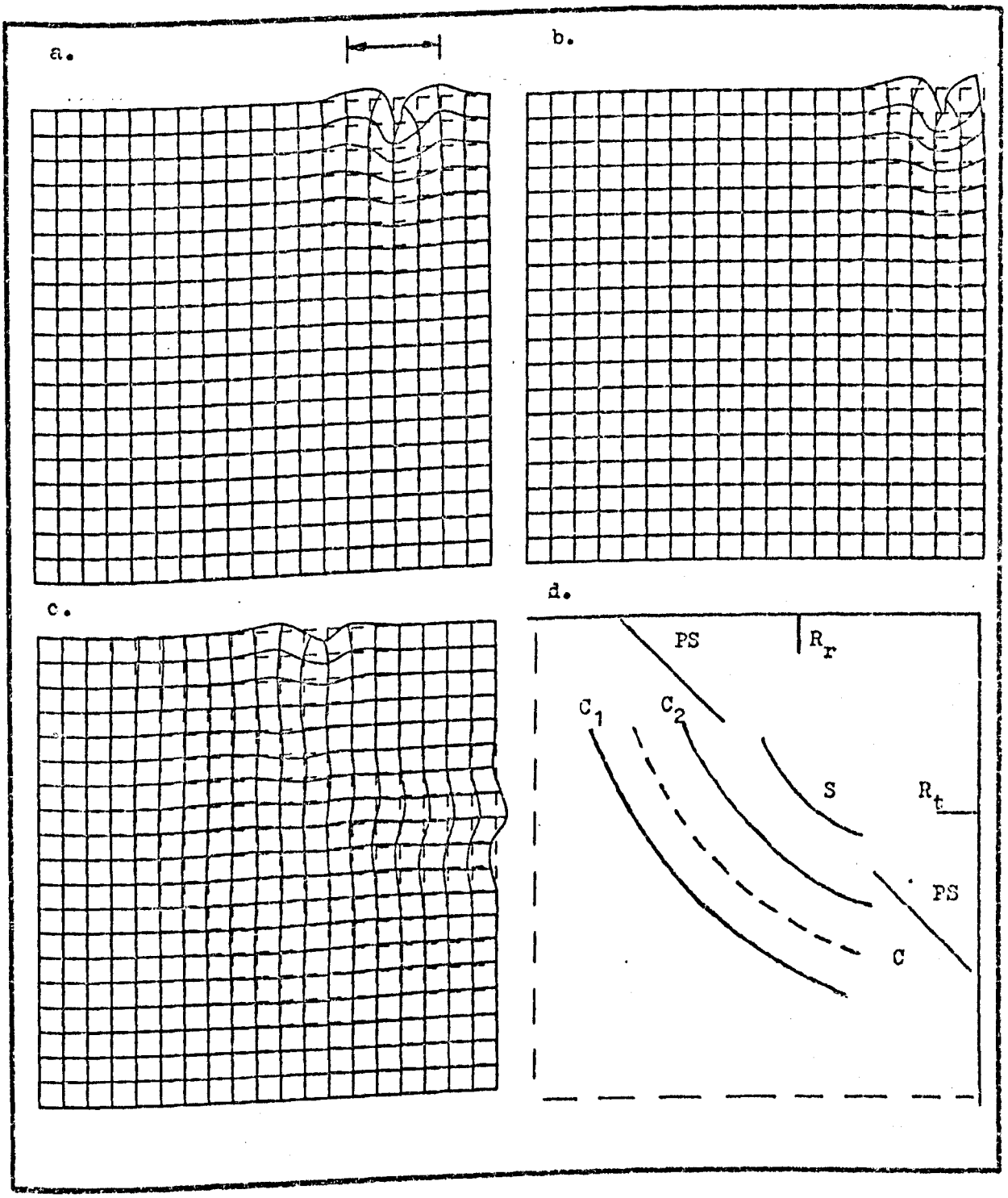

Ricker pulse on a quarter space, using chromium data and 32 nodes per wavelength, after a. 20 ,b. 60, c.180 iterations.
d. Main pulse identification;
R_r Reflected Rayleigh wave.
C Compressional wave.
C_1 Compression.
C_2 Rarefaction.
R_t Transmitted Rayleigh wave.
S Shear wave.
PS compressional wave mode converted at surfaces.

FIGURE 7.7.

Figure 7.7. In the frames given as Figure 7.7 the time development of the system, including mode conversion, can be seen.

The scattered pulses generated at the corner by the model are identified by observing the direction of displacements in the pulses in relation to the respective direction of propagation for each pulse and by measurement of the wave velocities as given by the finite difference scheme, which can be compared with those from the material data. Typical values for the velocities of the scattered pulses obtained using aluminium data and 16 nodes per wavelength are presented in Table 14 together with the corresponding values for the wave velocities given in the data presented as Table 11.

	Rayleigh wave vel. m/sec.	Compressional wave vel. m/sec.	Shear wave vel. m/sec.
Data from Table 11.	2906.	6422.	3110.
From F.D. model.	2773. ±100	6141. ±100	2972. ±100
Percentage difference between F.D and data.	- 5	- 4	- 4

Wave velocities for scattered pulses on an aluminium quarter space as given by finite difference first order scheme compared with material data values.

TABLE 14.

A further form of analysis, which assists in following the time development of the system at specific nodes, and helps to identify pulses, is seismometer analysis, which gives particle displacements with time. Examples of this type of display, for the two nodes P and Q, shown in Figure 7.6, are given as Figure 7.8.

The main scattered pulses identified on the quarter space are, firstly a compressional wave with a pulse wavelength which corresponds to the centre frequency of the Ricker pulse. Secondly a shear wave pulse, which is only identifiable in the final frame, shown as Figure 7.7c; this wave has a velocity of only 7 % more than the Rayleigh wave pulses; and thirdly a pair of PS pulses, so called in geophysics, which occur where the expanding compressional wave front meets the surface and mode converts. The

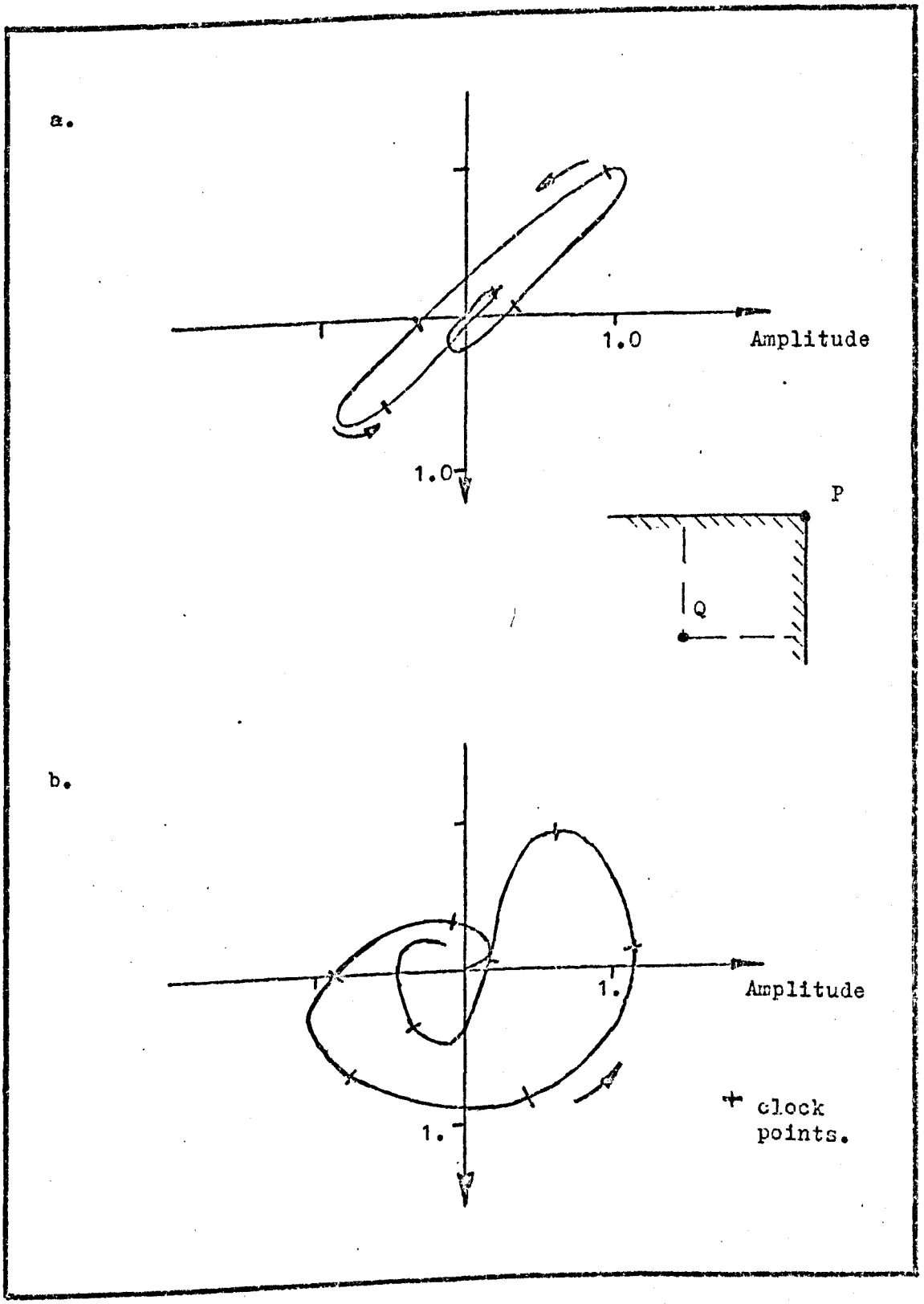

Particle displacements at nodes P and Q on a quarter space, with polystyrene data using 35 nodes per wavelength.
a. For node P, at corner. b. For node Q, 2 wavelengths from corner along each surface.

FIGURE 7.8.

PS wave has a straight wavefront which forms a tangent to the shear wave.

b. Transmission and reflection coefficients on quarter spaces.

Following from the identification of the basic pulses which result from the scattering of a Rayleigh wave pulse on a quarter space, measurements were made, based on the amplitude data, to establish transmission and reflection coefficients and estimate the loss in energy from Rayleigh waves, due to mode conversion.

A series of model runs were performed for a range of different media, with different combinations of pulse length and depth at different numbers of nodes per wavelength. Some of the results obtained are presented as Table 15.

Pulse size (in nodes)		Nodes per λ	Material	Poisson's ratio	Ref. coef.	Trans coef.	Mode conv. loss (%).
Width	Depth						
50	50	16	Aluminium	0.34	0.51 ±.06	0.54 ±.08	45
64	74	16	Aluminium	0.34	0.45 ±.05	0.51 ±.05	64
100	90	35	Aluminium	0.34	0.49 ±.05	0.64 ±.05	35
100	90	35	Polystyrene	0.24	0.39	0.65	43
100	90	35	Steel(mild)	0.29	0.56	0.47	47
100	90	35	Chromium	0.21	0.52	0.54	44
100	90	35	Titanium	0.36	0.56	0.51	40

List of transmission and reflection coefficients for Ricker pulses on quarter spaces, for a range of values for both pulse and material data, with a space with dimensions of 156 by 156 nodes.

TABLE 15.

It is shown by the results given as Table 15 that there are several factors which influence the values for the scattering coefficients on a quarter space. These factors are identified and considered further in relation to these results, those from an alternative numerical model, reported in Section 7.3.2, experimental measurements and those of other workers in Section 9.3.

7.2.3 Rayleigh waves on three-quarter spaces.

The three-quarter space is a single corner configuration, with a single 270° corner at the intersection of two free surfaces. This configuration, like the 90° corner or quarter space, has no characteristic dimension so it should have wavelength independent scattering coefficients.

The basic model node arrangement for the computer program, Program C, which models a Rayleigh wave pulse on a three-quarter space is as shown in Figure 7.9.

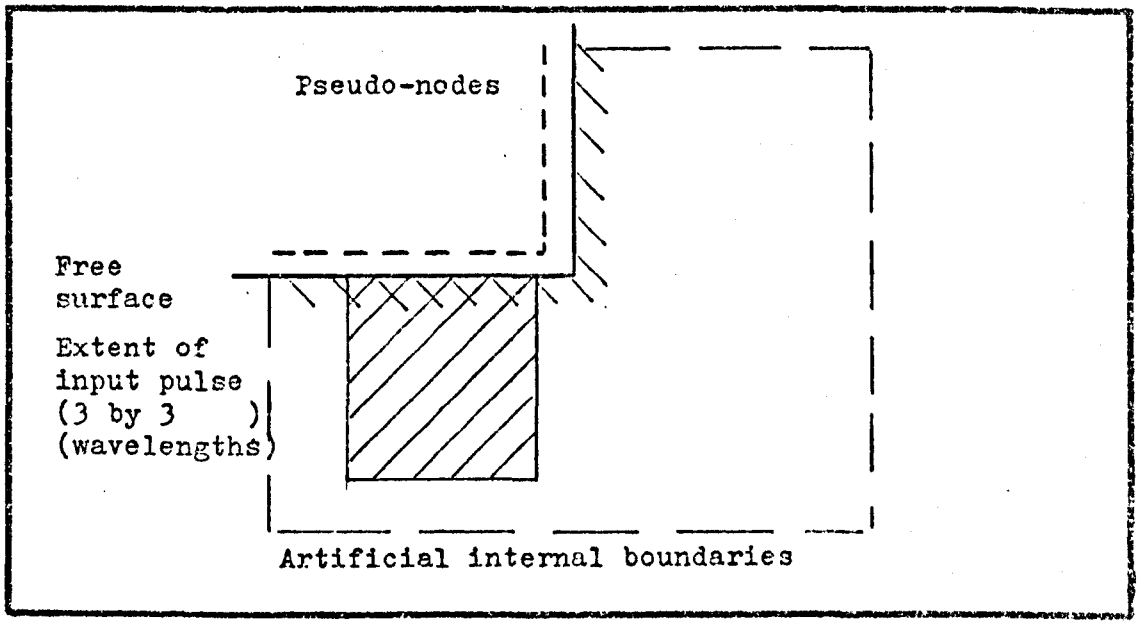

Node arrangement for first order finite difference model of a Ricker type pulse of Rayleigh waves on a three-quarter space.

FIGURE 7.9.

The propagation of a Ricker type pulse of Rayleigh waves on a three-quarter space was investigated using the node arrangement shown in Figure 7.9, using both polystyrene ($\sigma = 0.24$) and aluminium ($\sigma = 0.34$) data from Table 11 and 16 nodes per wavelength with the pulse centre wavelength corresponding to a frequency of 1 MHz.

a. Basic pulse analysis.

The propagation and scattering of a Ricker pulse was investigated and for each model run a series of sets of displacements were recorded at regular intervals and numerical visualisation type displays were plotted, an example of which is shown as Figure 7.10.

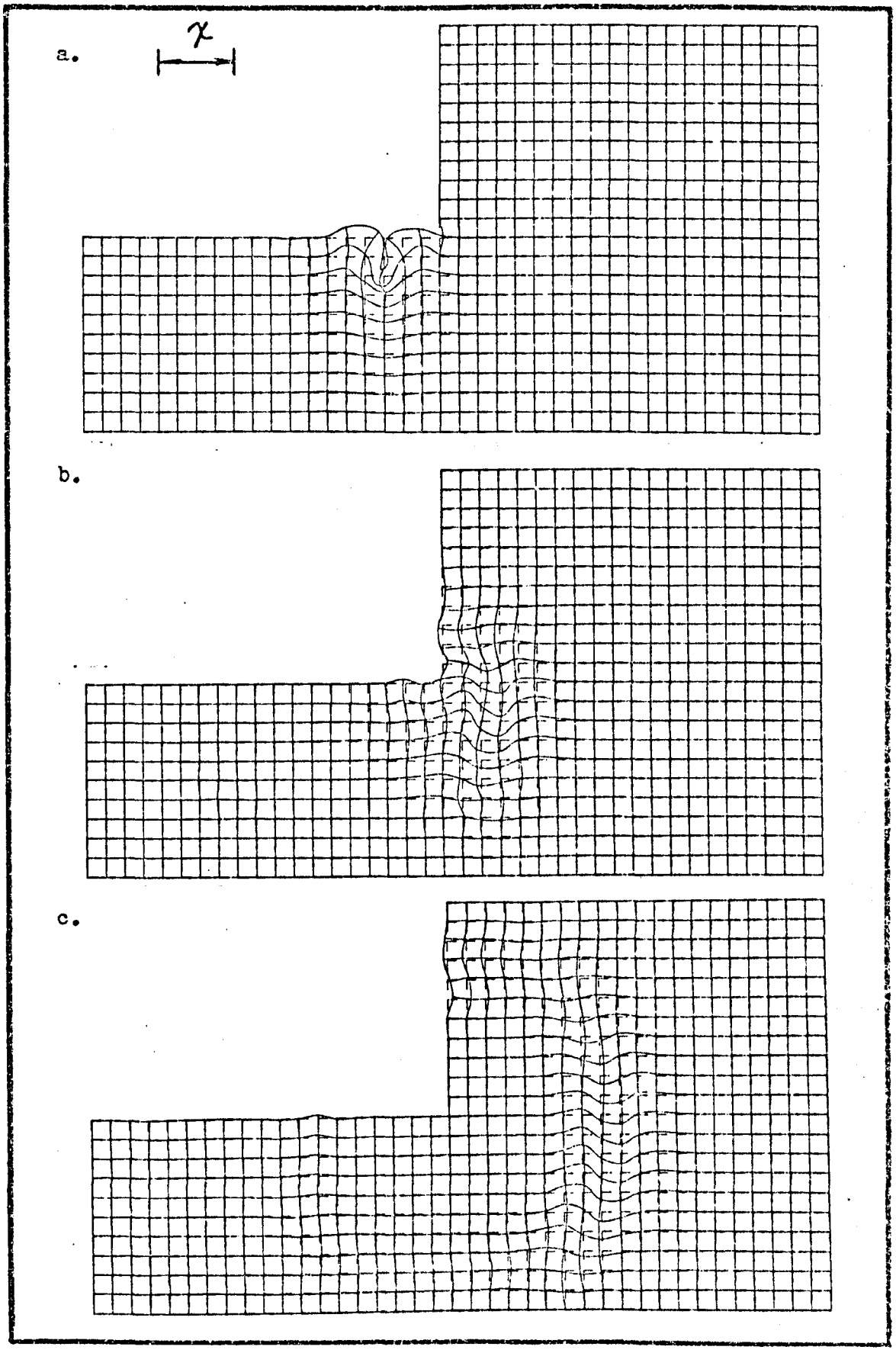

Ricker pulse on a three-quarter space, using polystyrene ($\sigma = 0.24$) and 16 nodes per wavelength. a. 20, b. 60, c. 160 iterations.

FIGURE 7.10.

The time development of the system is shown and the main mode converted pulse is a near circular shear wave centred at the corner, the majority of the energy in which is in the arc 45° about the direction of propagation of the Ricker pulse on the free surface before the interaction at the corner. There was very little energy mode converted into compressional waves.

The wave velocities of the scattered Rayleigh and shear wave pulses were measured on the model and they were found tc be in the same range of wave velocities as those shown in Table 14.

b. Transmission and reflection coefficients on three-quarter spaces.

Following the identification of the basic scattered pulses for Rayleigh wave scattering on three-quarter spaces, measurements were made, based on pulse amplitude data, to establish transmission and reflection coefficients and to establish the mode conversion energy loss from Rayleigh waves.

Model runs were performed using the data for two media, polystyrene ($\sigma = 0.24$), which is shown in Figure 7.10, and aluminium ($\sigma = 0.34$), both using 16 nodes per wavelength. The results obtained for values of scattering coefficients are presented in Table 16.

Material	Poisson's ratio.	Reflection coefficient.	Transmission coefficient.	% mode conversion loss.
Polystyrene	0.24	0.09 ±.03	0.24 ±.03	93
Aluminium	0.34	0.10 ±.03	0.22 ±.03	94

List of transmission and reflection coefficients for Ricker pulses on polystyrene and aluminium three-quarter spaces, using 16 nodes per wavelength.

TABLE 16.

The results for the three-quarter space are considered further, together with those an alternative numerical model reported in Section 7.3.3, experimental measurements and the previous work of other workers, in Section 9.4.

7.2.4 Rayleigh waves at down steps.

The down step, with a 90° and a 270° corner separated by a vertical distance (h), and when the step height (h) is less than two wavelengths it forms the simplest configuration for which the scattering coefficients are wavelength dependant. So it can be expected that the values of the transmission and reflection coefficients for scattering with pulsed Rayleigh waves will vary with the step height (h) to wavelength (λ) ratio.

The basic node arrangement for the computer program, Program D, which models a Rayleigh wave pulse at a down step is shown as Figure 7.11.

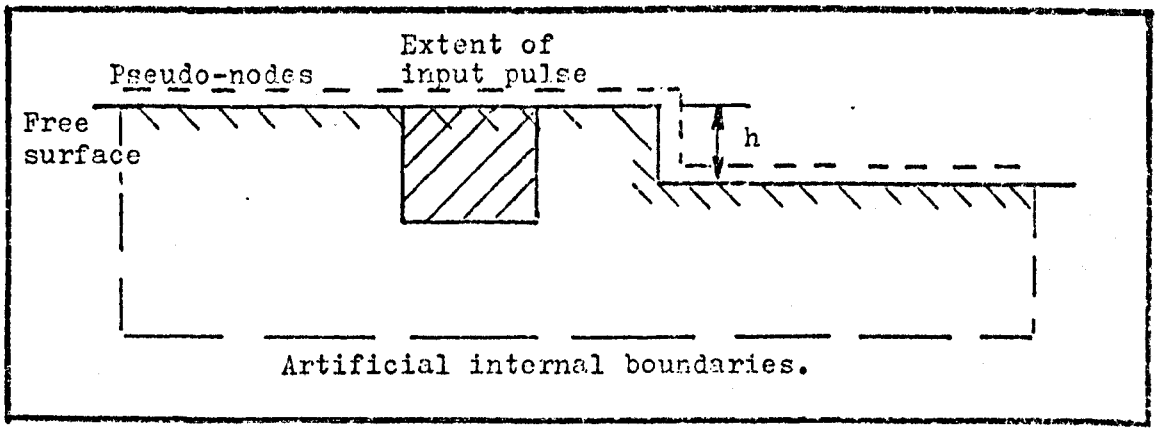

Node arrangement for first order finite difference model of a Ricker type pulse of Rayleigh waves at a down step.

FIGURE 7.11.

The propagation of a Ricker type pulse of Rayleigh waves and their interaction and scattering at a down step was investigated using the node arrangement shown as Figure 7.11. The model was used with data for three media, polystyrene, aluminium and quartz, the parameters used being given in Table 11, with a range of step heights, using 35 nodes per wavelength and the pulse centre wavelength corresponding to a frequency of 1 MHz.

The computer runs were all performed using a grid with dimensions of 300 by 100 nodes. The large space, in nodes was used because of the experience gained with half-space and quarter space models and also to permit the modelling of a range of different step heights in the main range of interest, step height to wavelength ratio values from about 0.1 to 1.0.

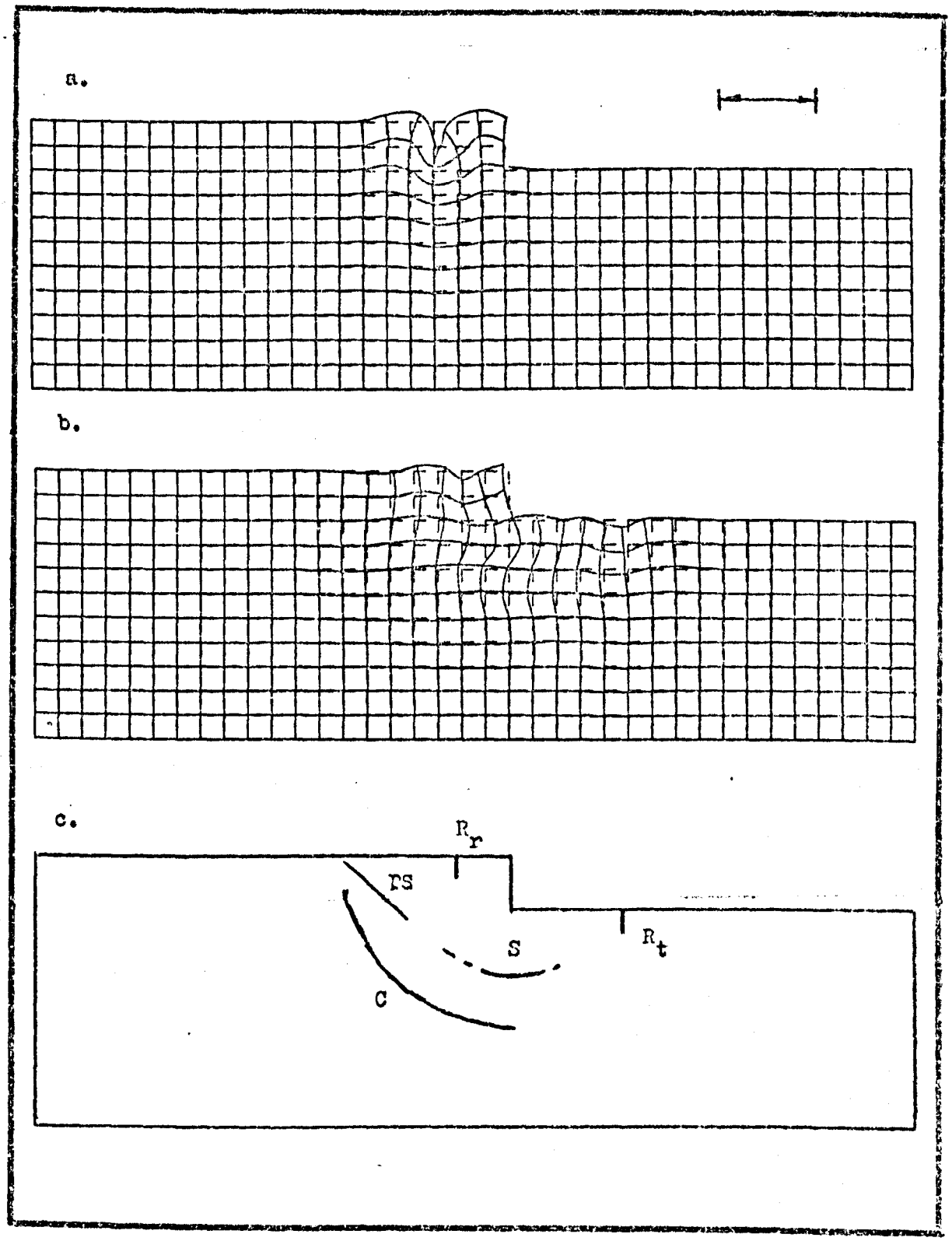

Ricker pulse at a half wavelength deep down step, using aluminium data and 35 nodes per wavelength. System after, a. 20, and b. 120 iterations. c. Main pulse identification;

R_r Reflected Rayleigh wave — R_t Transmitted Rayleigh wave
C Compressional wave — S Shear wave.
PS Compressional wave mode converted at surface.

FIGURE 7.12.

a. Basic pulse analysis.

The propagation and scattering of Ricker pulses by a range of different height steps, on different media, was investigated and for each model run a series of sets of displacements were recorded at regular intervals and numerical visualization type displays were plotted. Numerical visualization type displays for a half-wavelength deep down step, before and after scattering are shown as Figure 7.12. The main scattered pulses in the system are identified in Figure 7.12c. The compressional pulse radiates from a point near the 90° corner and the shear wave from the 270° corner. The energy in each mode is found to vary with step height.

b. Transmission and reflection coefficients at down steps.

Following the identification of the basic pulses in the pattern of scattered pulses at a down step, measurements were made, based on amplitude data, to establish transmission and reflection coefficients and to establish the mode conversion energy loss from Rayleigh waves. Some of the results obtained are set out in Table 17.

Material.	Step height.	Transmission coefficient.	Reflection coefficient.	% Energy mode converted
Polystyrene	0.228	0.65 ±.05	0.25 ±.05	52
Polystyrene	0.456	0.30 ±.05	0.40 ±.05	75
Polystyrene	0.694	0.30 ±.05	-	-
Aluminium	0.228	0.63 ±.05	0.24 ±.05	55
Aluminium	0.456	0.45 ±.05	0.49 ±.05	56
Aluminium	0.57	0.32 ±.05	0.48 ±.05	67
Aluminium	0.69	0.29 ±.05	-	-
Aluminium	0.912	0.18 ±.05	-	-
Quartz	0.456	0.34 ±.05	0.42 ±.05	71

Transmission and reflection coefficients for Ricker pulses at down steps, using 35 nodes per wavelength.

TABLE 17.

The gaps in the values for reflection coefficients, shown as Table 17, are due to the presence of oscillations in the region near the 90° corner which make amplitude based measurements inaccurate. The values for the scattering coefficients of the down step are considered further in Section 9.5.

7.2.5 Rayleigh waves at up steps.

The up step is similar to the down step except that pulse starts on the lower surface and is scattered first at the 270° corner. This configuration is of importance as it, when combined with the down step, enables an open slot to be constructed.

The basic node arrangement for the computer program, Program E, which models a Rayleigh wave pulse at an up step is shown in Figure 7.13.

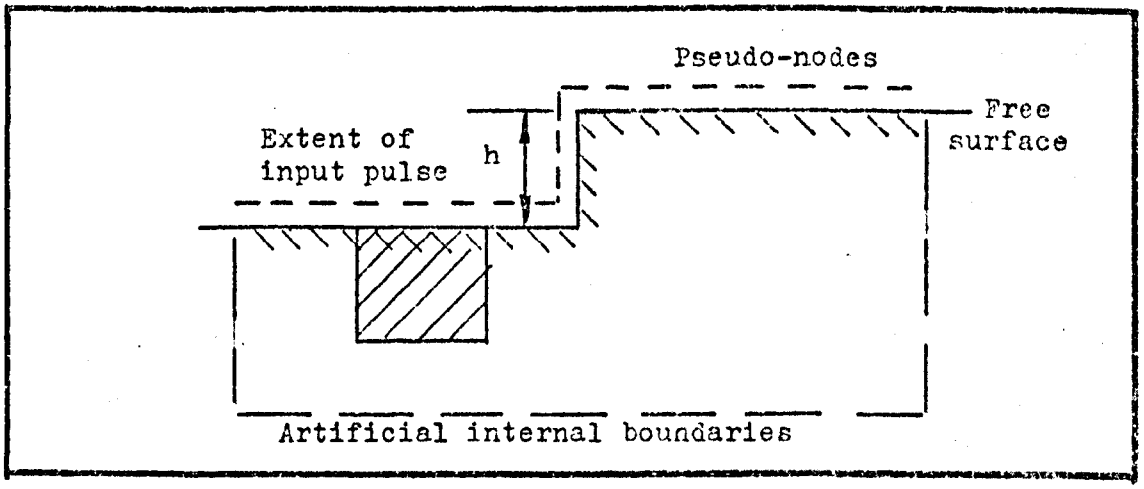

Node arrangement for first order finite difference model of a Ricker type pulse of Rayleigh waves at an up step.

FIGURE 7.13.

The propagation and scattering of a Ricker type pulse of Rayleigh waves was investigated for a range of different height steps using aluminium data with the node arrangement shown as Figure 7.13. The computer runs were performed using a grid with outside dimensions of 160 by 100 nodes and 32 nodes per wavelength, with the wavelength for the pulse centre frequency of 1 MHz.

a. Basic pulse analysis.

For each model run a series of sets of displacements were recorded at regular intervals and numerical visualization type displays were plotted. Numerical visulization type displays for pulses with half wavelength and 1.4 wavelength steps are shown as Figures 7.14 and 7.15 and Figures 7.16 and 7.17 respectively.

It is seen in all the figures that a strong pulse of mode converted shear waves radiates a nearly complete circular arc from the 270° corner which interacts with the upper surface but not the 90° corner. In the case of the deep step, secondary mode

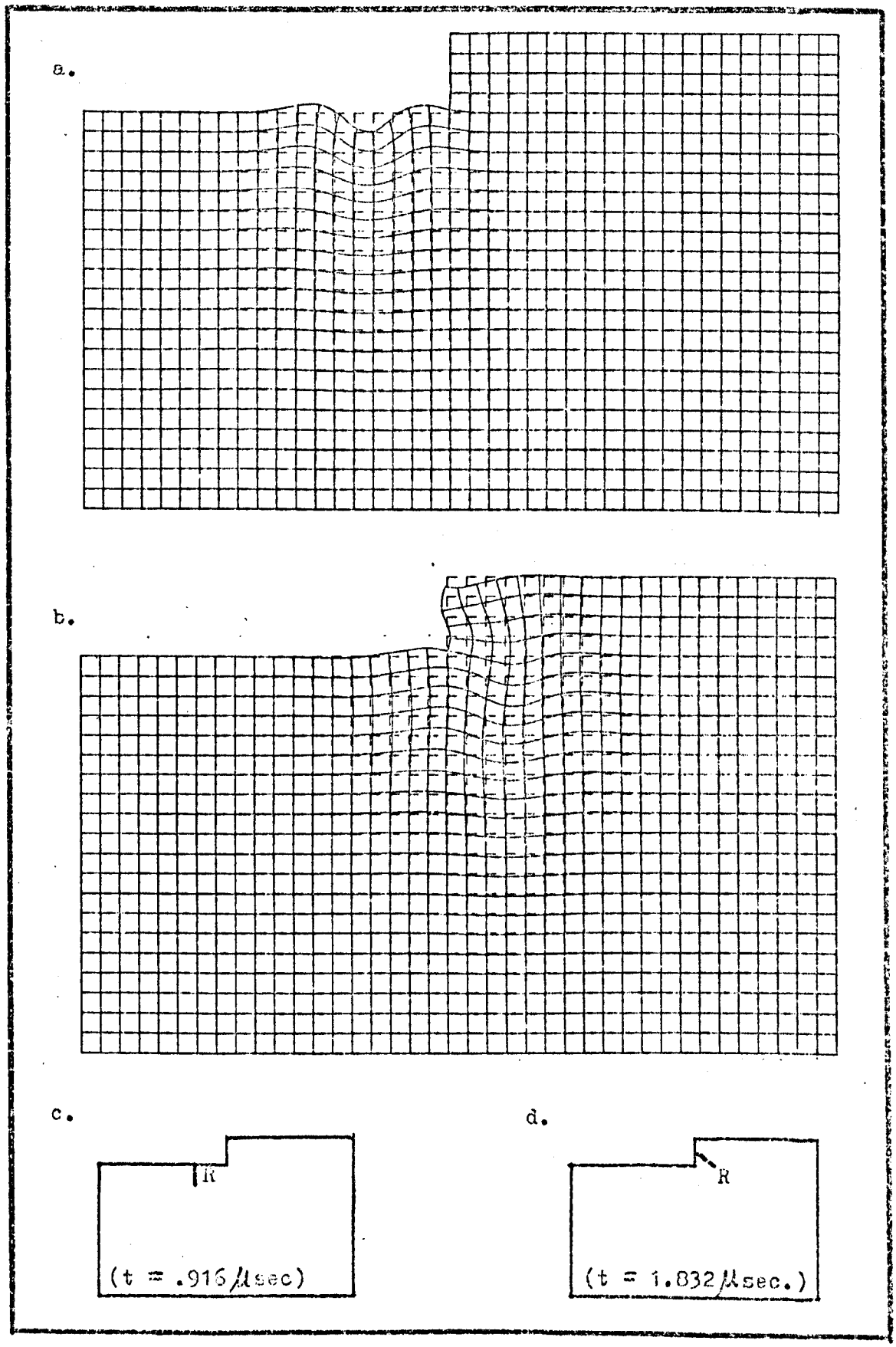

Ricker pulse at a half wavelength up step, using aluminium data and 32 nodes per wavelength. System after, a. 80, and b. 160 iterations. c and d indicate position of Ricker pulse (R).

FIGURE 7.14.

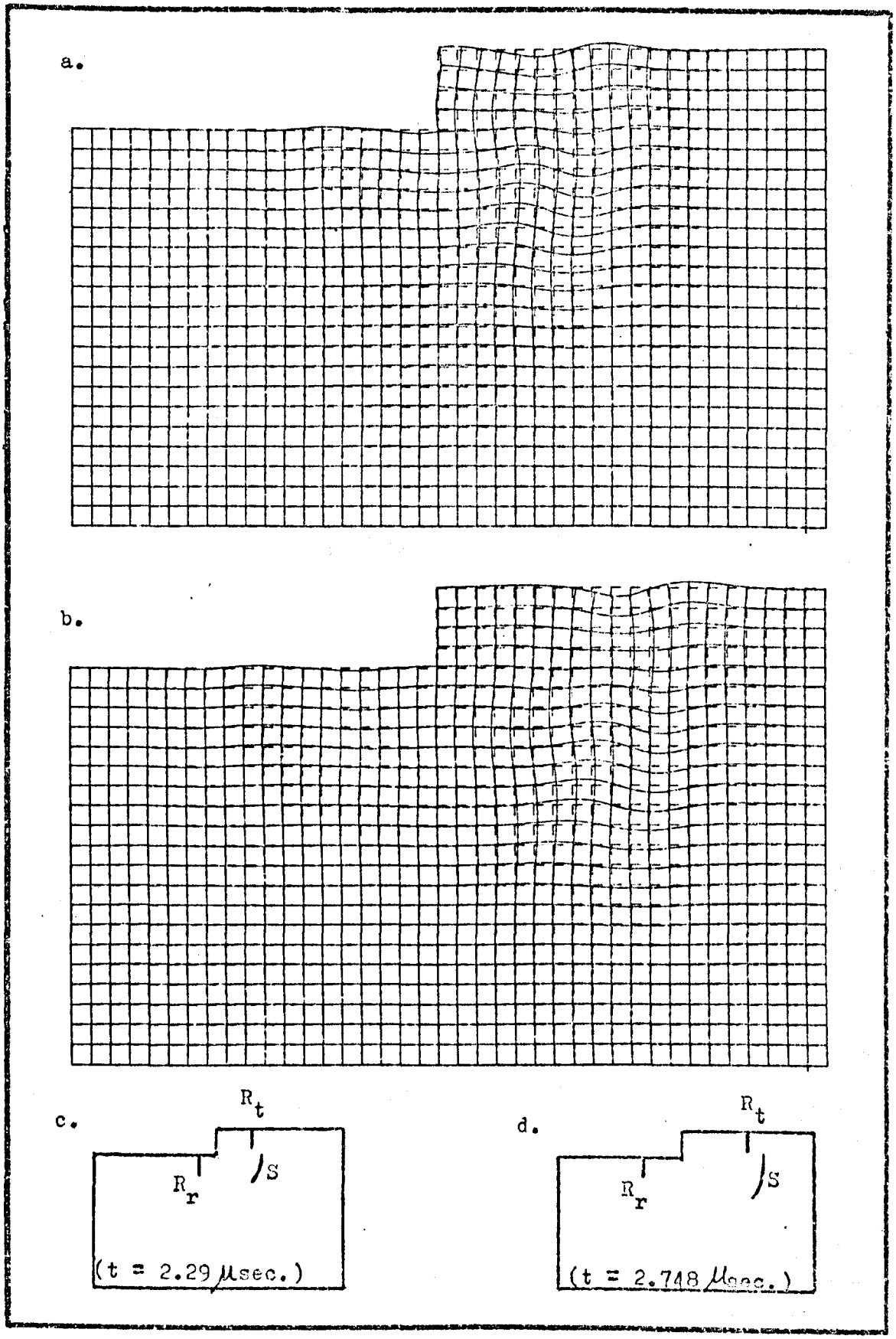

Ricker pulse at a half wavelength up step, using aluminium data and 32 nodes per wavelength. System after, a. 200, and b. 240 iterations. Main pulse identification; For a and b in c and d respectively. R_t Transmitted Rayleigh wave, R_r Reflected Rayleigh wave, S shear wave.

FIGURE 7.15.

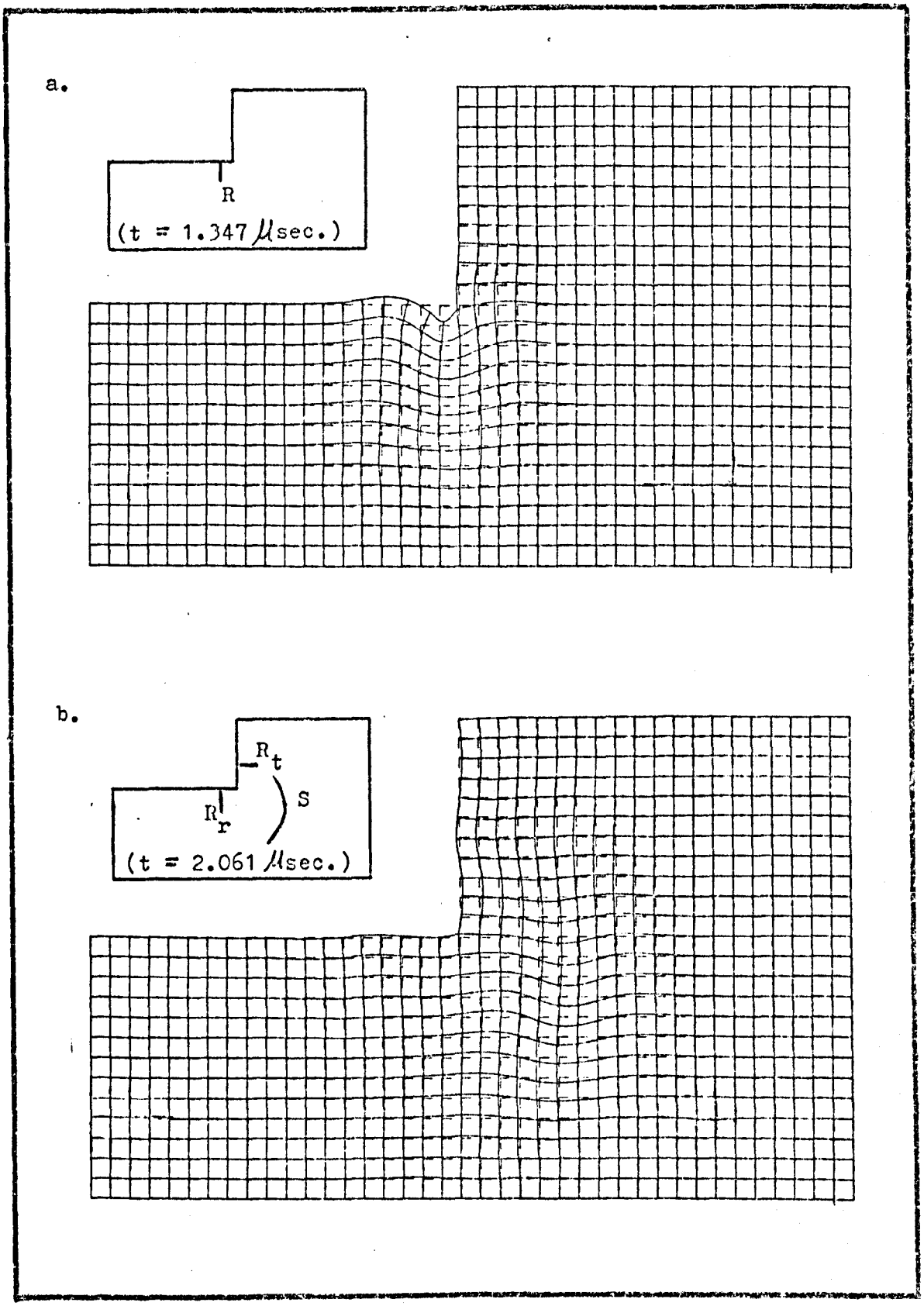

Ricker pulse at a 1.4 wavelength up step, using aluminium data and 32 nodes per wavelength. System after, a. 120 and b. 180 iterations. Main pulse identification. R Rayleigh wave input pulse. S Shear wave, R_r Reflected Rayleigh wave, R_t Transmitted Rayleigh wave.

FIGURE 7.16.

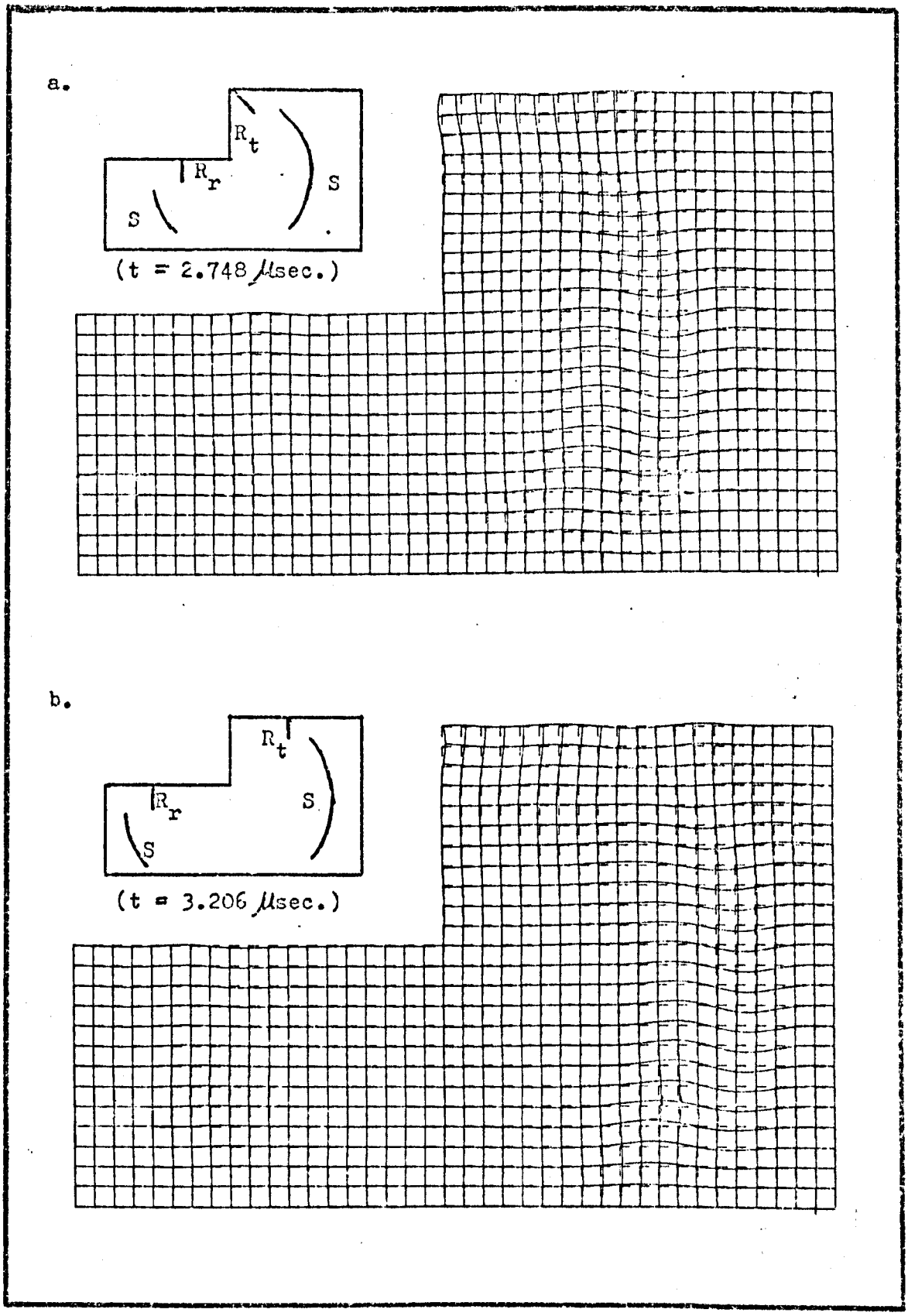

Ricker pulse at a 1.4 wavelength up step, using aluminium data and 32 nodes per wavelength. System after, a. 240 and b. 280 iterations. Main pulse identification, as for Figure 7.16.

FIGURE 7.17.

converted pulses are produced, as shown in Figure 7.17, when the Rayleigh wave transmitted past the 270° corner is scattered at the 90° corner.

In the case of the system shown in Figure 7.17, the surface wave pulse reflected at the 90° corner was also detected and measured on the vertical free surface, before it reached the 270° corner, where it was scattered, with most of its energy being mode converted into a shear wave pulse. The secondary scattered pulses are not identified in the figure, but they can be seen collectivly in the region behind the main pulses.

It was observed, in Figure 7.17, that the amplitude of the displacements in the pulse on the top surface increased as the pulse moved away from the 90° corner. This was investigated experimentally and the practical measurements and results are reported in Section 8.

b. Transmission and reflection coefficients at up steps.

Following the identification of the basic scattered waves, in the the pattern of scattered energy at an up step, measurements were made, based on amplitude data, to establish transmission and reflection coefficients and to estimate the mode conversion loss from Rayleigh waves. Some of the results obtained with up steps on aluminium are shown as Table 18.

Material	Step height.	Transmission coefficient.	Reflection coefficient.	% Energy mode converted.
Aluminium	0.5	0.5 ±.05	0.11 ±.05	74
Aluminium	0.75	0.4 ±.05	0.10 ±.05	83
Aluminium	1.375	0.16±.05	0.11 ±.05	96

Transmission and reflection coefficients for Ricker pulses at up steps on aluminium, using 32 nodes per wavelength.

TABLE 18.

From the results presented in Table 18 it is seen that reflected pulse from an up step is of the same amplitude as that from a three-quarter space, using aluminium data, and that there are increasing mode conversion energy losses from Rayleigh waves as the step depth is increased. The values for the scattering coefficients at up steps and the mode converted waves are considered further in Section 9.6

7.2.6 Rayleigh waves at open slots.

The open slot normal to the free surface is an idealised crack configuration, and it is modelled by combining the formulations used for the down and the up steps. The interaction and scattering of pulsed Rayleigh waves has been found to be wavelength dependant for slot depths up to about 1.5 wavelengths.

The basic node arrangement used in the computer program, Program F, which models a Rayleigh wave pulse at an open slot in a half-space is shown as Figure 7.18.

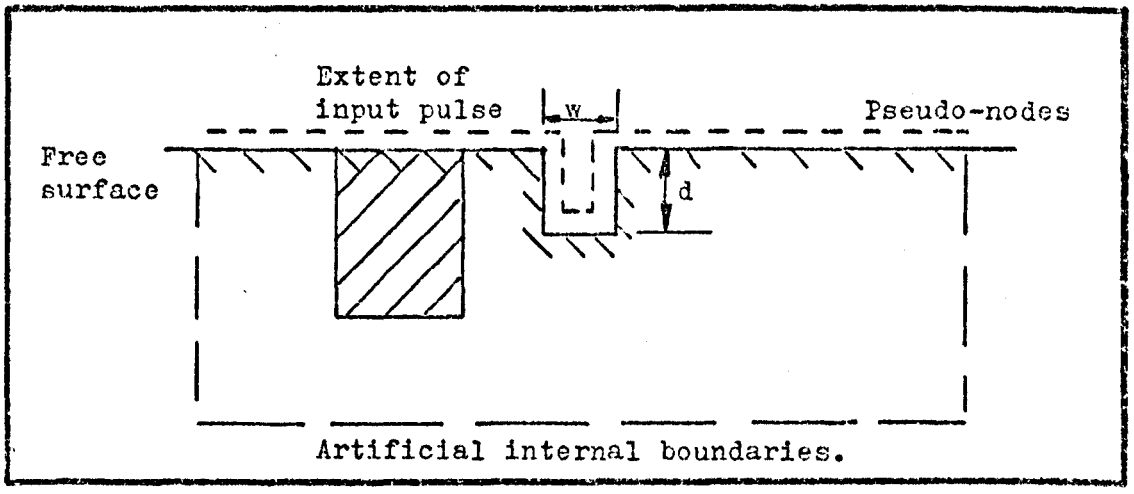

Node arrangement for first order finite difference model of a Ricker type pulse of Rayleigh waves at an open slot.

FIGURE 7.18.

The node arrangement shown in Figure 7.18 was used to investigate the propagation and scattering of a Ricker type pulse of Rayleigh waves at a range of open slots in an aluminium half-space. The computer model runs were performed on a half-space with node dimensions of up to 200 by 100 nodes, using 32 nodes per wavelength and the wavelength corresponding to a pulse centre frequency of 1 MHz.

a. Basic pulse analysis.

The propagation and scattering of Ricker type pulses by a range of slots was investigated and for each model run a series of sets of displacements were recorded and numerical visualization type displays plotted at regular intervals, normally every twenty iterations.

Selected frames from two series of numerical visualization type displays, for pulses at quarter and half wavelength deep (d)

and one eigth of a wavelength wide (w) open slots, are shown as Figures 7.19 and 20 and 7.21 and 22 respectively.

The main scattered pulses are, in both cases, reflected and transmitted Rayleigh waves, a shear wave, radiating from the bottom of the slot, a compressional wave, radiating from near the 90° corner and a PS wave where the compressional wave mode converts at the free surface.

The wave velocities of the various scattered pulses were measured and they were found to have values in the same range as those given in Table 14 (in Section 7.2.2).

It is found for wide slots, those with a width greater than about half a wavelength, that the pattern of "reflected" pulses is almost identical to that for the corresponding depth of down step.

b. Transmission and reflection coefficients at open slots.

Following the identification of the main pulses in the pattern of scattered waves at the open slot, a series of model runs were performed with $\frac{1}{8}$ wavelength wide slots of different depths to determine transmission and reflection coefficients, based on amplitude data. The results obtained for a range of different depth slots on aluminium are presented as Table 19.

Material	Slot depth.	Reflection coefficient.	Transmission coefficient.	% Energy mode converted.
Aluminium	0.125	0.12 ±.05	0.83 ±.05	30
Aluminium	0.25	0.20 ±.05	0.37 ±.05	82
Aluminium	0.5	0.42 ±.05	0.25 ±.05	77
Aluminium	0.875	-	0.07 ±.05	-
Aluminium	1.00	0.45 ±.05	0.06 ±.05	79

Transmission and reflection coefficients for Ricker pulses at open slots in aluminium, using 32 nodes per wavelength.

TABLE 19.

The results presented in Table 19 are considered further, together with those from experimental measurements, reported in Section 8, and the results of other workers, in Section 9.7.

a. (t = .229 μsec.)

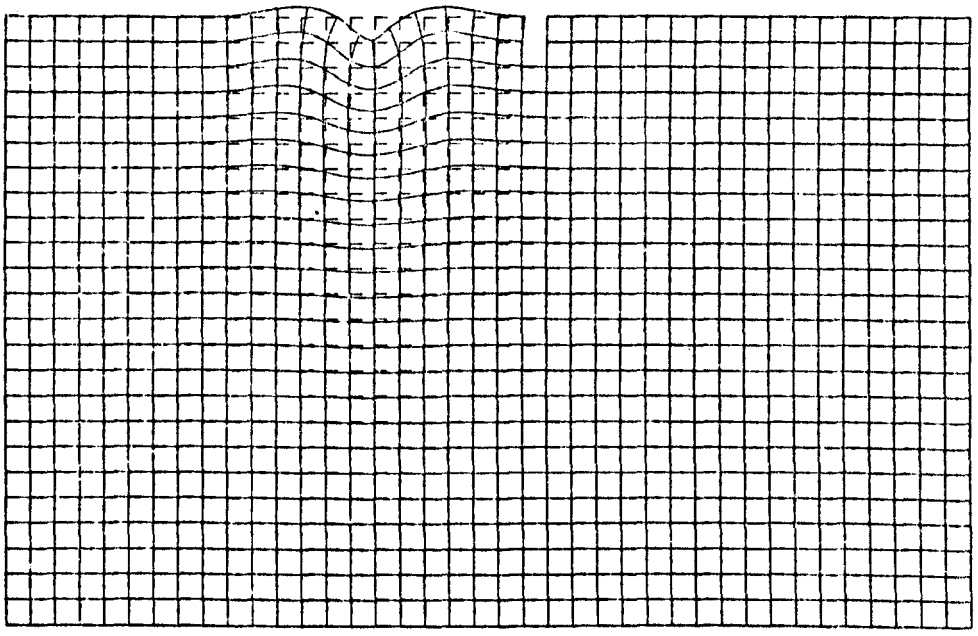

b. (t = .916 μsec.)

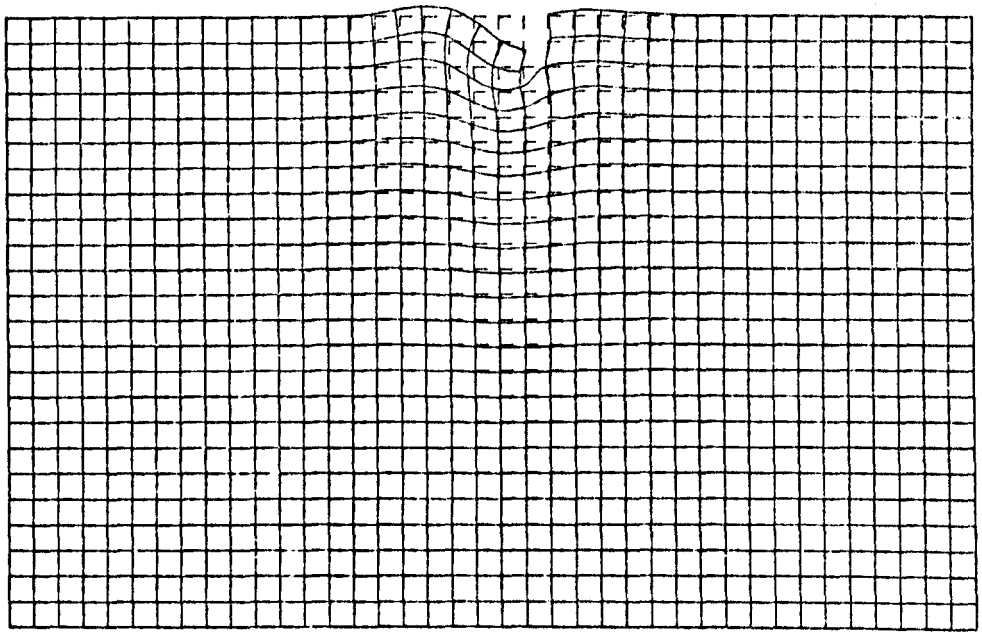

Ricker pulse at a 0.25 wavelength deep and 0.125 wavelength wide open slot, using aluminium data and 32 nodes per wavelength.
System after; a. 20 and b. 80 iterations.

FIGURE 7.19.

a. (t = 1.603 μsec.)

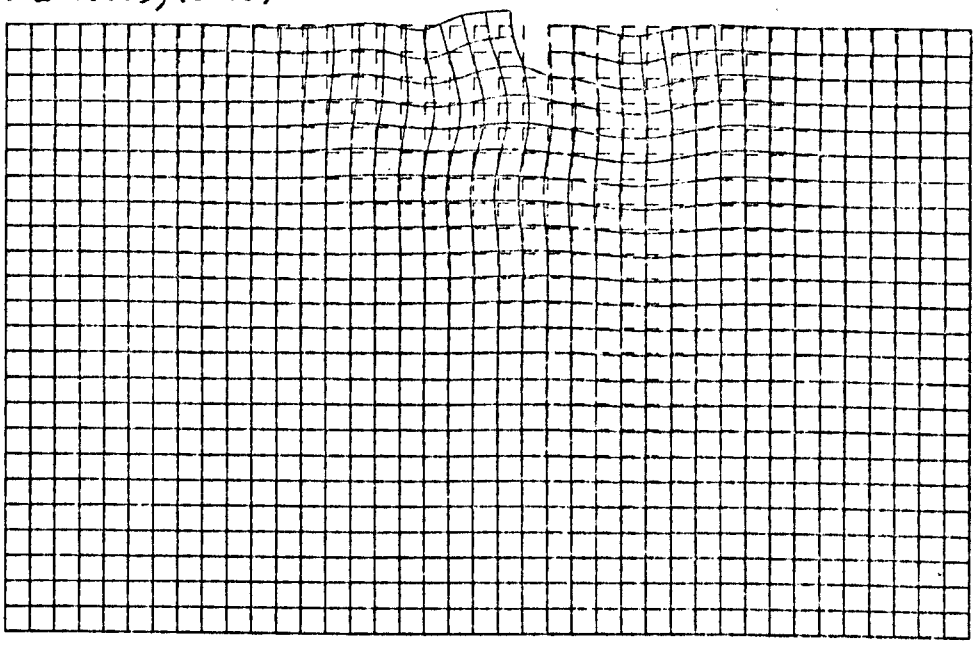

b. (t = 2.29 μsec.)

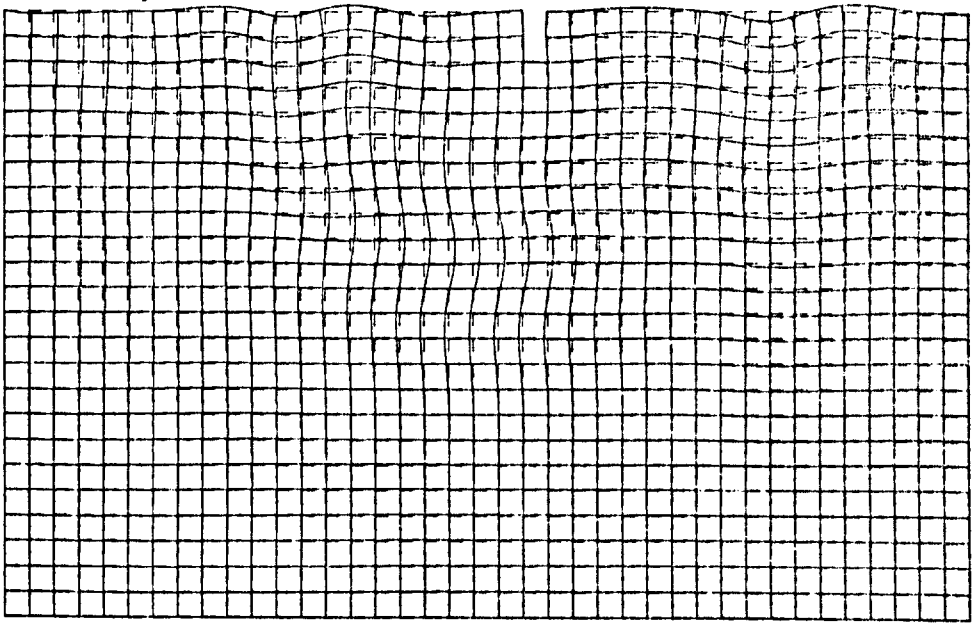

c.

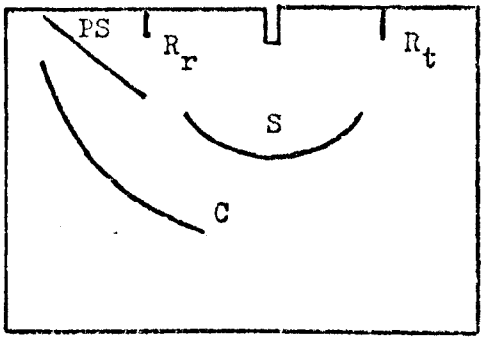

Ricker pulse at a 0.25 wavelength deep and 0.125 wavelength wide open slot, using aluminium data and 32 nodes per wavelength. System after; a. 140 and b. 200 iterations. c. Main pulse identification, as for Figure 7.12.

FIGURE 7.20.

a. (t = .229 μsec.)

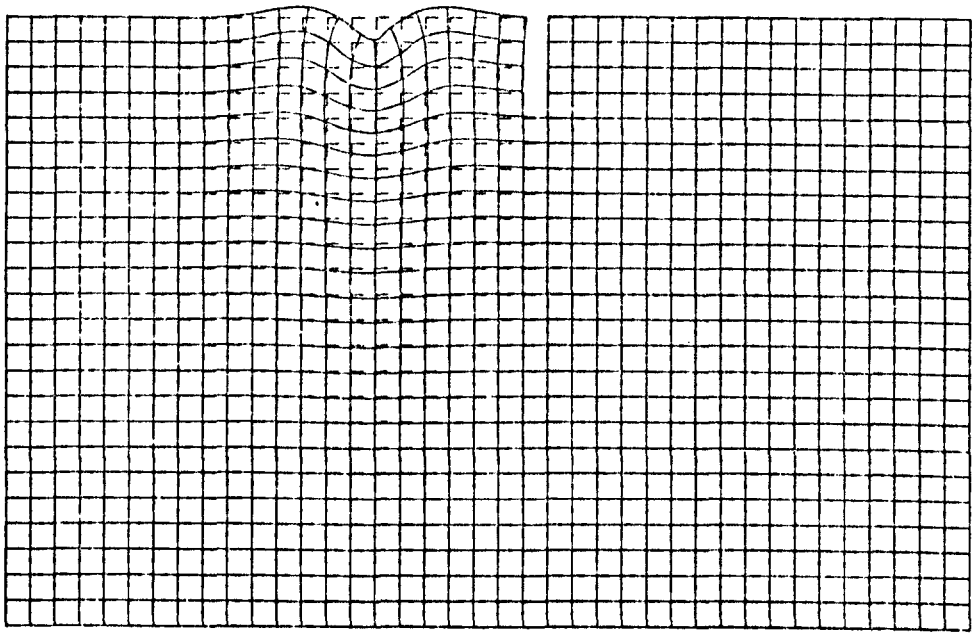

b. (t = .916 μsec.)

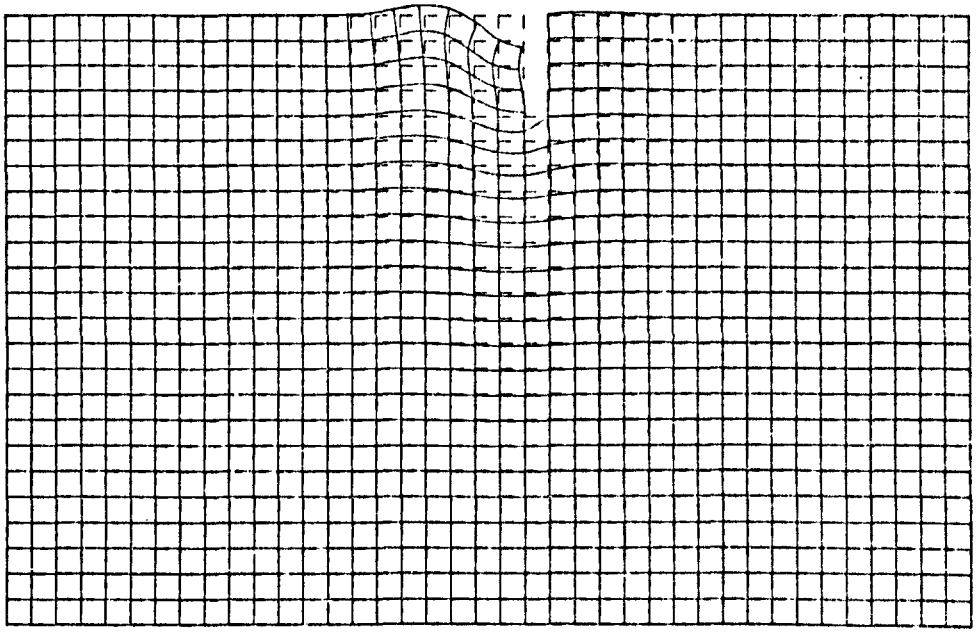

Ricker pulse at a 0.5 wavelength deep and 0.125 wavelength wide open slot, using aluminium data and 32 nodes per wavelength.
System after; a. 20, and b. 80, iterations.

FIGURE 7.21.

a. (t = 1.603 μsec.)

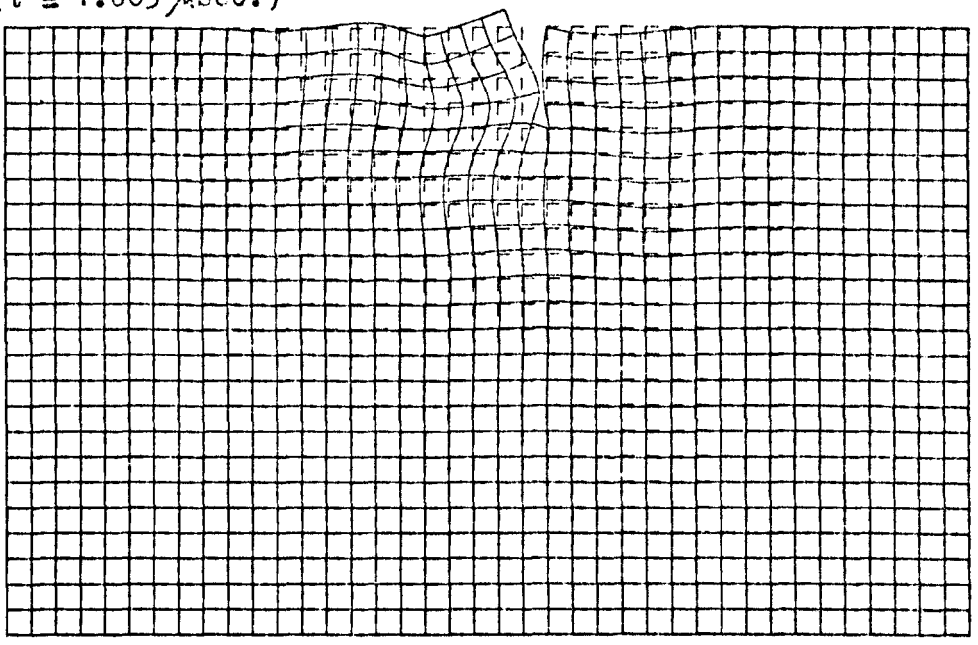

b. (t = 2.29 μsec.)

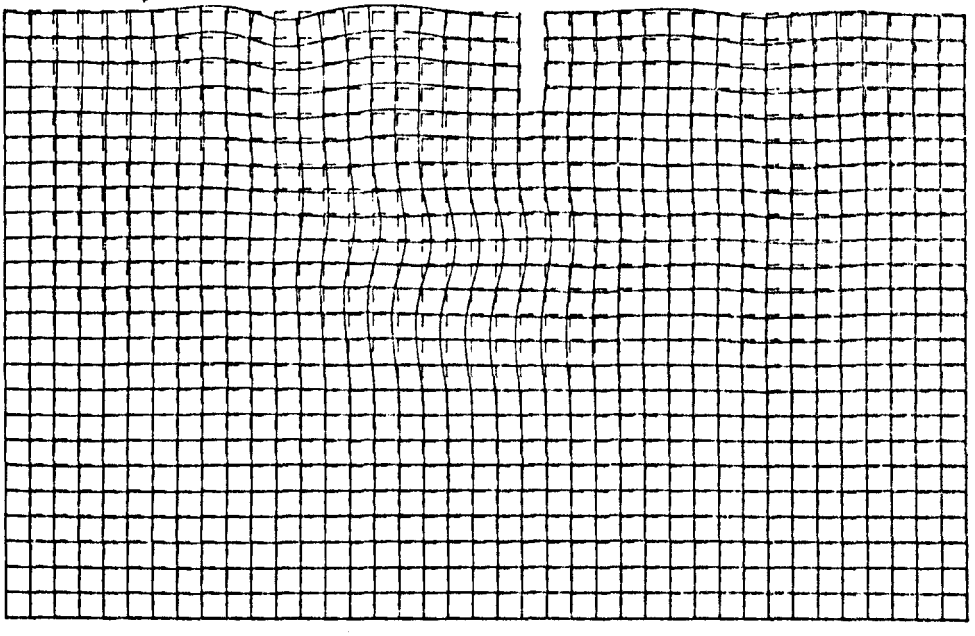

c.

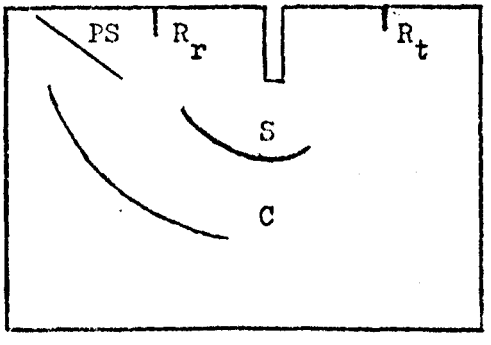

Ricker pulse at a 0.5 wavelength deep and 0.125 wavelength wide open slot, using aluminium data and 32 nodes per wavelength.
System after; a. 140, and b. 200 iterations.
c. Main pulse identification at t = 2.29, pulses as for Figure 7.12.

FIGURE 7.22.

7.2.7 Rayleigh waves on a block.

This section reports on the extension of the model to consider the propagation of Rayleigh waves on a block, a piece of material of limited spatial extent, as opposed to a semi-infinite medium with a step or a slot on the free surface. It provides a model of a real experimental configuration.

The block, a rectangular piece of material with four free surfaces and four 90° corners, is modelled using a pseudo-node scheme to satisfy the free surface boundary conditions which is extended from that used for the quarter space program, considered in Section 7.2.2, and presented in Appendix E.

The basic node arrangement used in the computer program, Program G, to model the Ricker type pulse of Rayleigh waves on a block is shown as Figure 7.23.

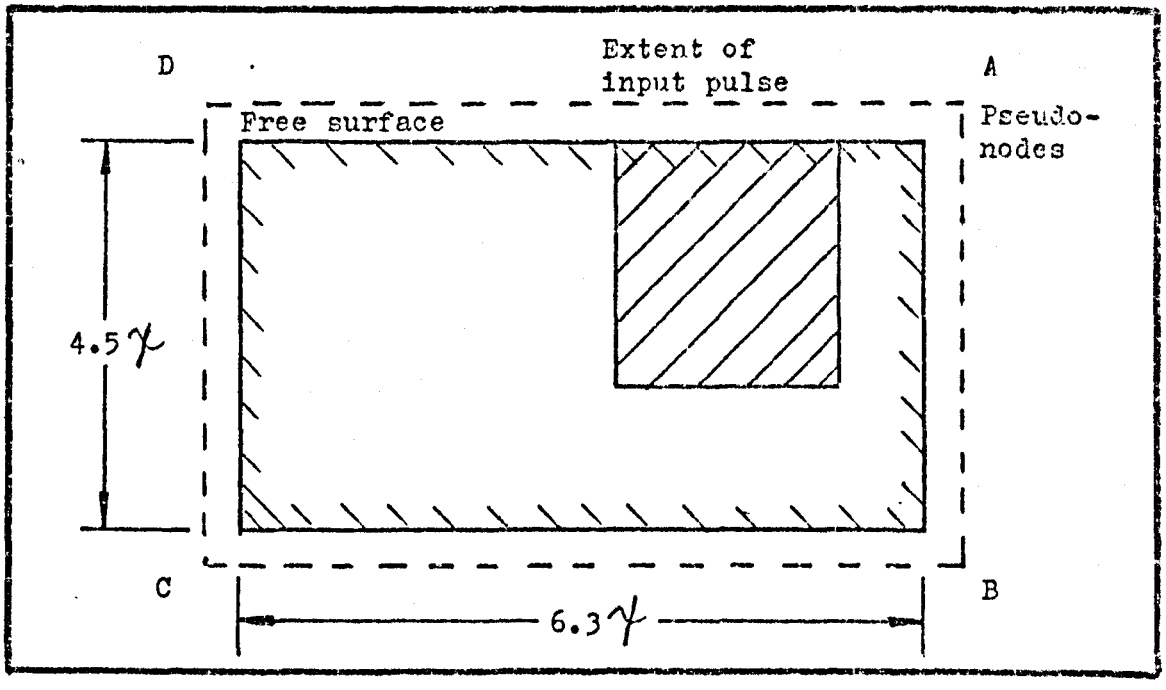

Node arrangement for first order finite difference model of a Ricker type pulse of Rayleigh waves on a block.

FIGURE 7.23.

The model arrangement as shown in Figure 7.23 was used to follow the propagation and scattering of a Ricker type pulse of Rayleigh waves on a block using aluminium ($\sigma = 0.34$) data, given in Table 11, at 16 nodes per wavelength. The size of grid used in the model was equivalent to a real block with dimensions of

18 by 13 mm for a pulse with a centre frequency of 1 MHz.

a. Basic pulse analysis.

For the model, sets of displacements were plotted at each of a series of time steps to give the numerical visualisation type of display. For each time time level for which a numerical visualisation plot was produced the numerical values at selected nodes, principally those at the free surfaces, were recorded for additional analysis.

The time development of the pulses on and in a block is presented as Figures 7.24, 7.25 and 7.26. The initial system was as indicated in Figure 7.23, with the corners identified by the letters A, B, C and D and the sides identified by the letter combinations AB etc.

The three frames, shown as Figure 7.24, follow the system development after the initial interaction of the Ricker pulse with the 90° corner A. The compression (C_1) and rarefaction (C_2) of a mode converted compressional wave (C) are seen to radiate across the block from corner A. The compression (C_1) is seen to be reflected at the surface BC, introducing the pulse (C_3). The PS and shear modes are identifiable in Figure 7.24c.

The three frames, shown as Figure 7.25, follow the system development in the time following that shown as Figure 7.24, from model time t = 4.58 to t = 5.496 μsec. The compressional wave (C) is seen to move along the surface generating the reflected compressional wave (C_rC) which radiates away from BC at the same angle as the incident pulse. It is also seen that in Figure 7.25b that the compression (C_1) reaches the surface CD causing it to bulge. In the frame for t = 5.496, shown as Figure 7.25c, it is seen that the surface mode conversion of the compressional wave (C), the PS waves have moved past the corners B and D. The compressional wave (C_rC) is crossing the bulk of the medium going towards the surface DA. The shear wave (S) is moving in the bulk of the medium and in the region near corner C a complex series of interactions between the compressional waves (C) and (C_rC) are occuring giving rise to further mode converted pulses.

The final state of the system at t = 5.95 μsec is shown as Figure 7.26. This is the system after 260 iterations after which the results become less accurate due to the limited size of grid

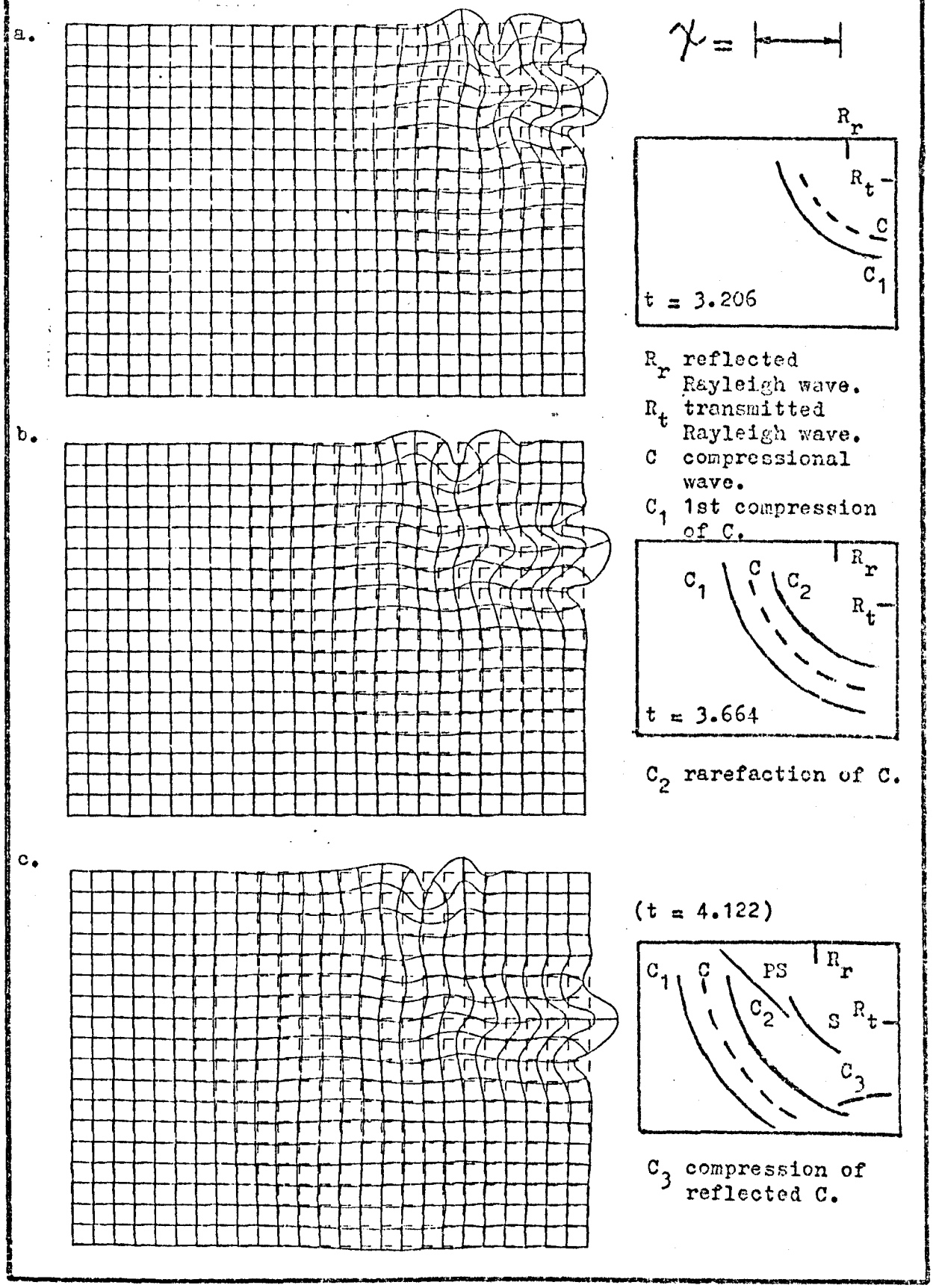

Pulse propagation on a block at times between t = 3.2 and 4.2 μsec.

FIGURE 7.21.

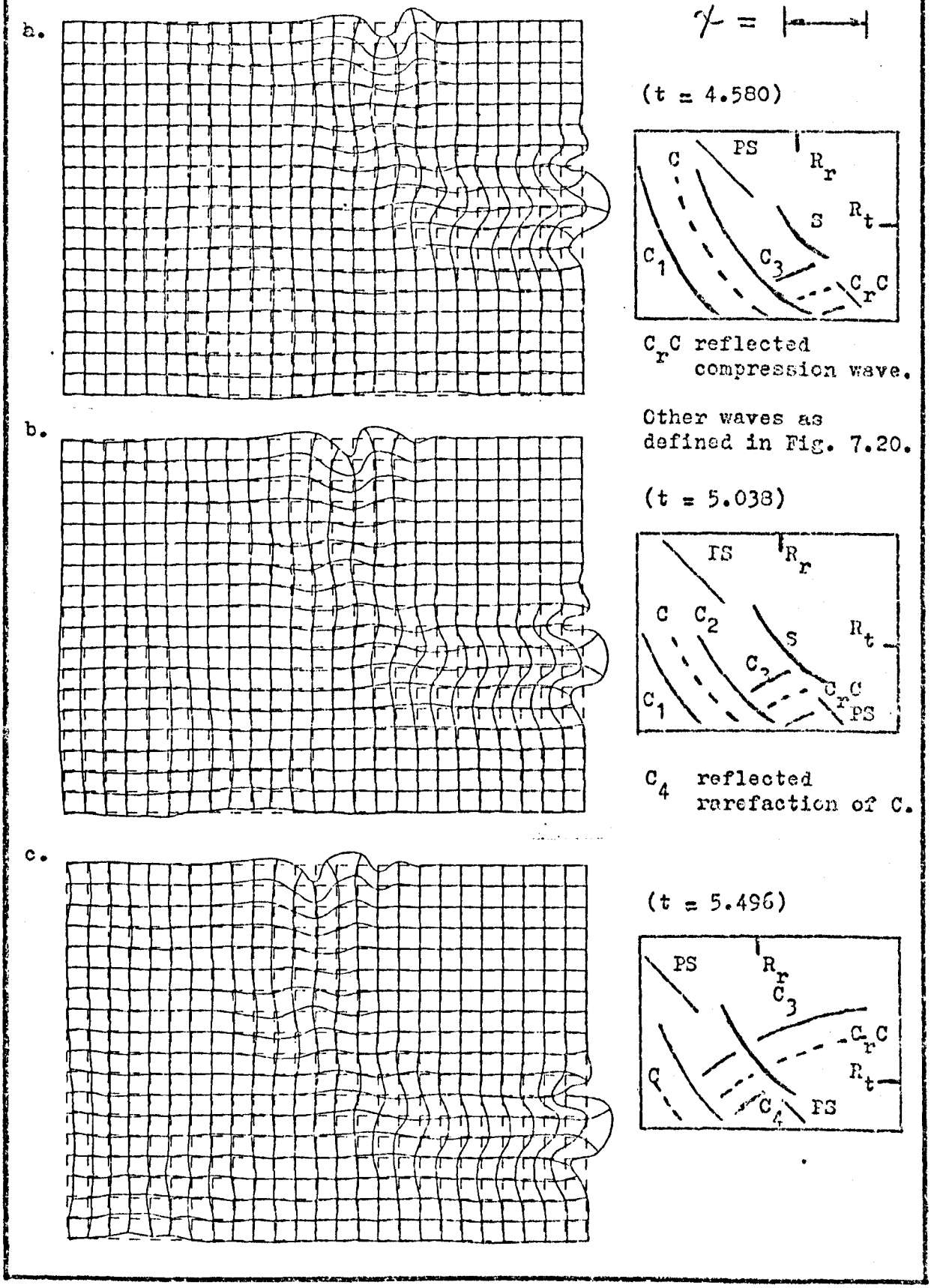

Pulse propagation on a block at times between t = 4.5 and 5.5 μsec.

FIGURE 7.25.

used. The main pulses identified in this frame are the reflected (R_r) and transmitted (R_t) Rayleigh wave pulses, the primary mode converted compressional wave (C) and the reflected compression compressional wave (C_rC), the primary mode converted shear wave (S) and the mode conversion of the compressional wave (C) at the free surfaces, the PS waves.

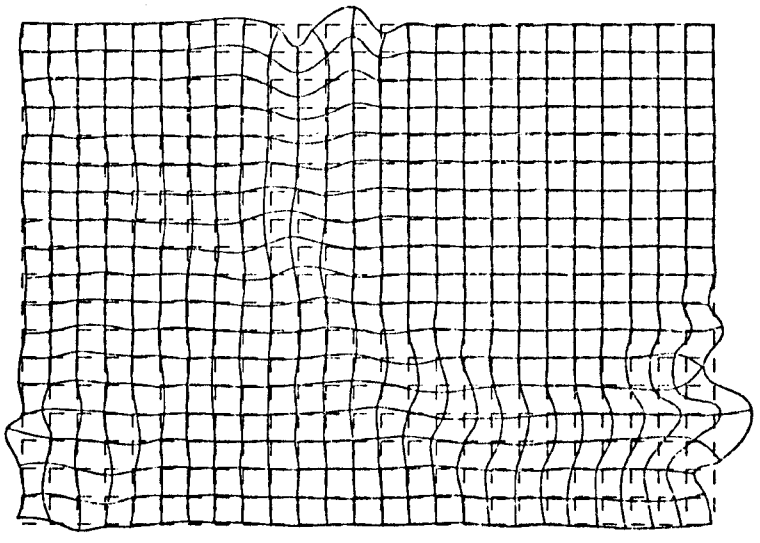

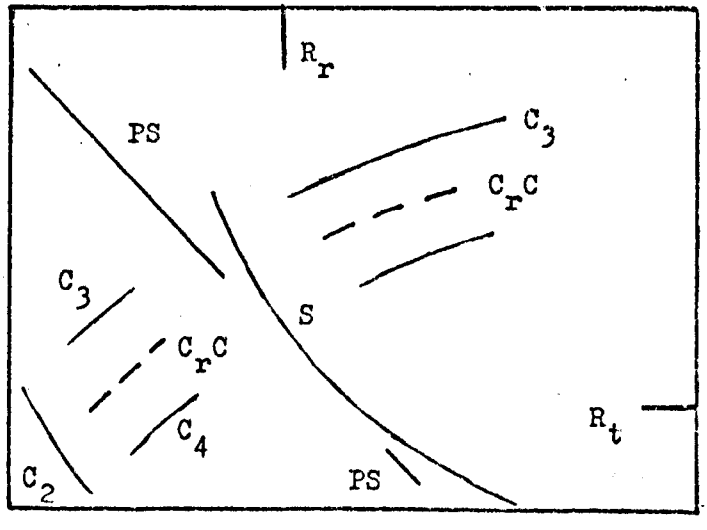

Pulses as defined on Figures 7.20 and 7.21.

Pulse system on a block at model time t = 5.954 μsec., (after 260 iterations), showing main pulses in system.

FIGURE 7.26.

7.3 Programs with second order formulations for the boundary conditions.

This section presents the computer model parameters, with the results, for pulsed Rayleigh waves on the range of single media and two media configurations shown in Figure 7.27.

The single medium models reported in this section were produced with the aim of improving on the results obtained with the models reported in Section 7.2, which use pseudo-node formulations for the boundary conditions. The two media configurations were considered with the aim of providing an understanding of the interaction of Rayleigh waves with a filled slot. The two media configuration models use the new formulation for the free surface/interface node, derived by the author, and presented in Section 4.3.4 and Appendix G.

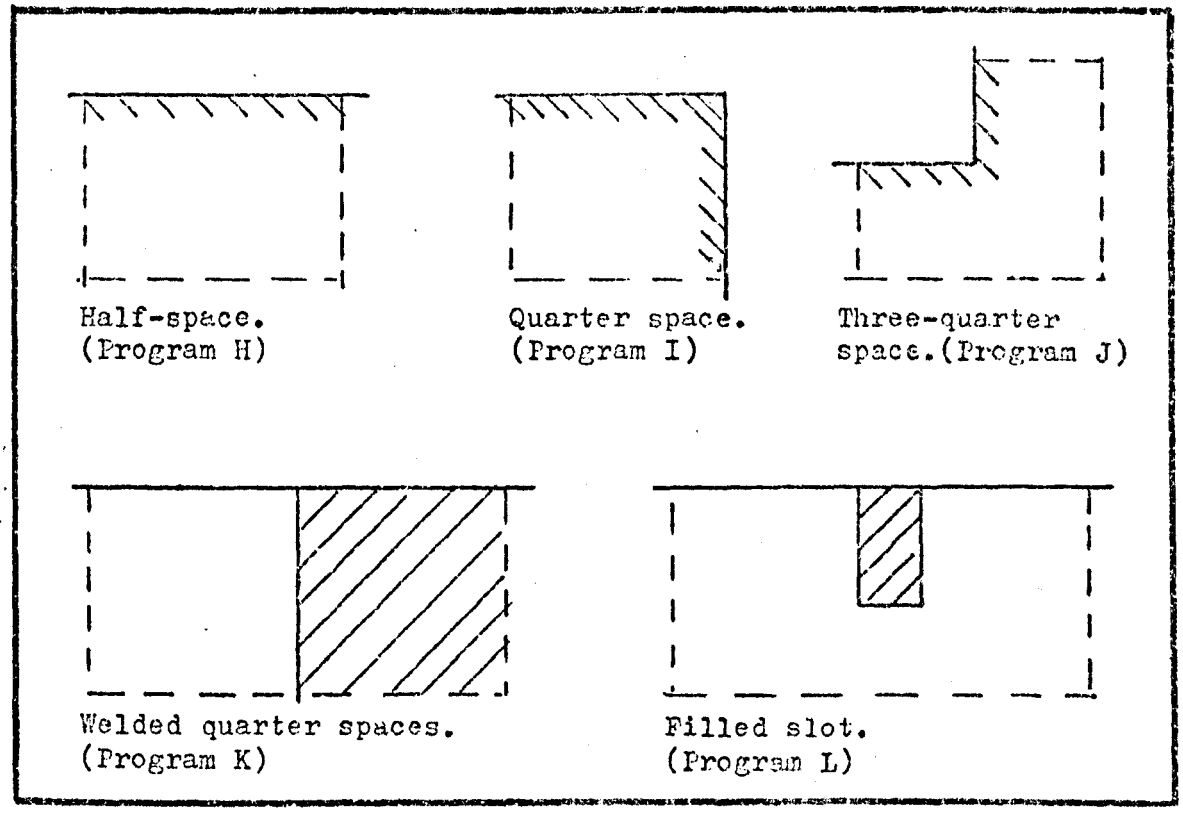

Configurations studied using second order formulations for the boundary nodes in the computer programs.

FIGURE 7.27.

The results presented in this section are considered further and compared,in Section 9, with those given by the models described in Section 7.2, the experimental results, presented in Section 8, and the results of other workers.

7.3.1 Rayleigh waves on half-spaces.

The ability to produce a computer model which gives the nondispersive propagation of a Rayleigh wave pulse is a prerequisite for the accurate modelling of more complex configurations.

The basic nodal arrangement used in the computer program, Program H, which models Ricker type pulses of Rayleigh waves on a half-space is shown as Figure 7.28.

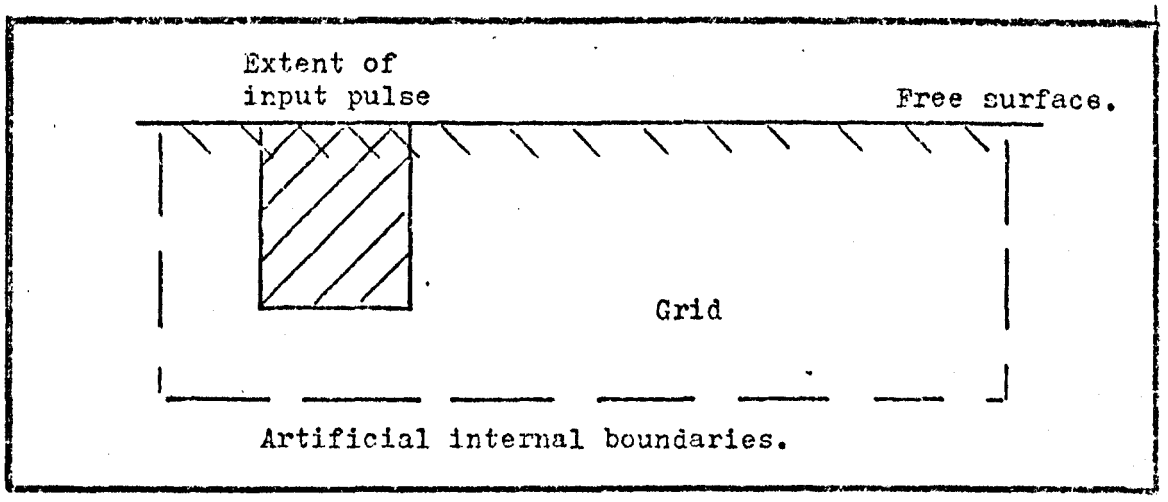

Node arrangement for second order finite difference model of a Ricker type pulse of Rayleigh waves on a half-space.

FIGURE 7.28.

A model was produced using the node arrangement shown in Figure 7.28 and using the second order composed formulation for the free surface nodes. However the program was found to have a limited range of stability, with the vertical component of displacement going unstable after only a few iterations when material data with a V_s/V_c ratio value below about .5 was used. This problem has been reported previously by Ilan and Lowenthal (1976) and their new composed formulation, which is presented in Section 4.3.4 and which has a larger range of stability, was adopted for use as the horizontal free surface formulation in the second order programs in the present study.

Using the new composed formulation, the propagation of Ricker type pulses of Rayleigh waves on half spaces was investigated using both polystyrene and aluminium data, presented in Table 11, and different numbers of nodes per wavelength with the wavelength corresponding to a pulse centre frequency of 1 MHz.

a. Distance travelled by pulse.

For each model run, a series of sets of displacements were recorded and numerical visualization type displays were plotted at regular intervals. Using the numerical visualization displays, the propagation of Ricker type pulses of Rayleigh waves on a half-space was investigated with both polystyrene and aluminium data using 16 nodes per wavelength. Selected frames of the output for the case of a pulse on an aluminium half-space are shown as Figure 7.29.

The distance travelled by the pulse, as given by the finite difference model using a four wavelength square pulse, was compared with that given by calculation with the wave velocity from the material data and the results using aluminium data are shown as Table 20.

	Number of iterations. 20	100	140	200
Distance travelled, given by calculation	0.458	2.291	3.207	4.583
Distance travelled, given by F.D. model	0.456 ±.05	2.278 ±.05	3.217 ±.05	4.590 ±.05
% difference between F.D. and calculated.	- 0.6	- 0.5	+ 0.4	+ 0.2
% error due to measuring pulse position to nearest ½ node.	-	-	-	1.0

Comparison of the distance travelled by a Rayleigh wave on an aluminium half-space as given by second order finite difference model, with that given by calculation from the wave velocity.

TABLE 20.

From the results presented in Table 20 it is seen that the errors found in the pulse distance travelled, as given by the finite difference scheme, are less than the limits to accuracy set by the measurement of the pulse position to the nearest node. From the results in Table 20 there is therefore no indication of any systematic error in pulse position up to 200 iterations. Similar accuracy was found in the results for a pulse when using polystyrene data.

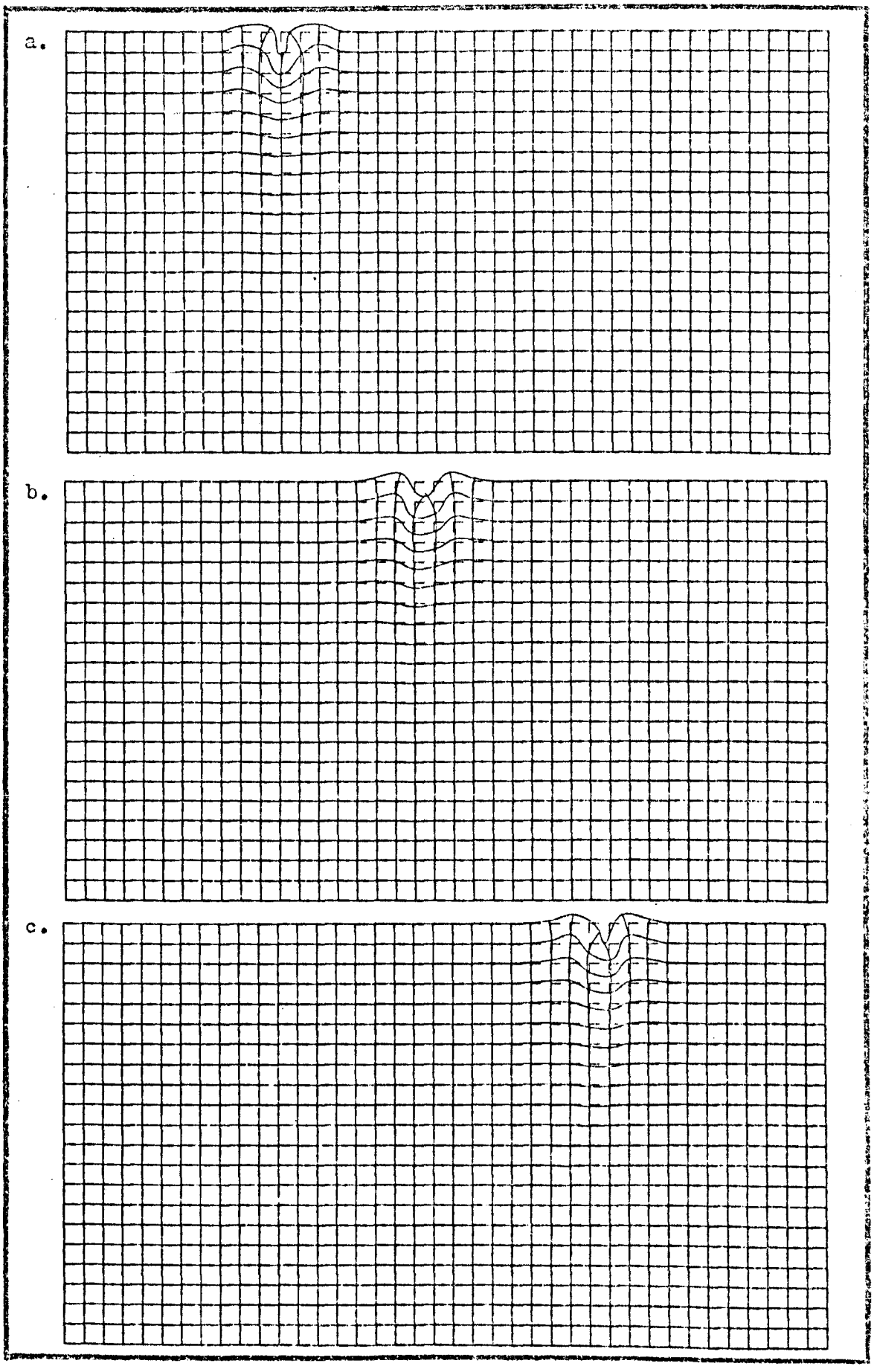

Ricker pulse on an aluminium ½ space, using 16 nodes per wavelength, System after; a, 20, b. 100, and c. 200 iterations.

FIGURE 7.29.

b. Pulse shape changes.

Following the measurement of pulse distance travelled, the change of pulse shape with distance, was investigated for the model using aluminium data and both 32 and 16 nodes per wavelength.

For the model, when using 32 nodes per wavelength, for measurements of pulse shape made up to 50 iterations there was no change of shape. Measurements were then made using 16 nodes per wavelength and the shapes of the vertical component of displacement at t = 0 and after 200 iterations, in which the pulse moved about 4.5 wavelengths, are shown as Figure 7.30.

c. Spectral measurements.

Because of the very good, almost nondispersive, pulse propagation achieved using the new composed formulation for the free surface nodes, when using only 16 nodes per wavelength, this scheme was adopted for use in all second order models. However, due to the inherent errors in spectral measurements at this number of nodes per wavelength they have not been used with the second order models. The use of16 nodes per wavelength gives, of course, considerable savings in the number of nodes required to model a given size of feature, when measured in wavelengths.

The model results presented in this section are compared with those which use the pseudo-node scheme, which were reported in Section 7.2.1, experimental measurements and the results of previous studies in Section 9.2.

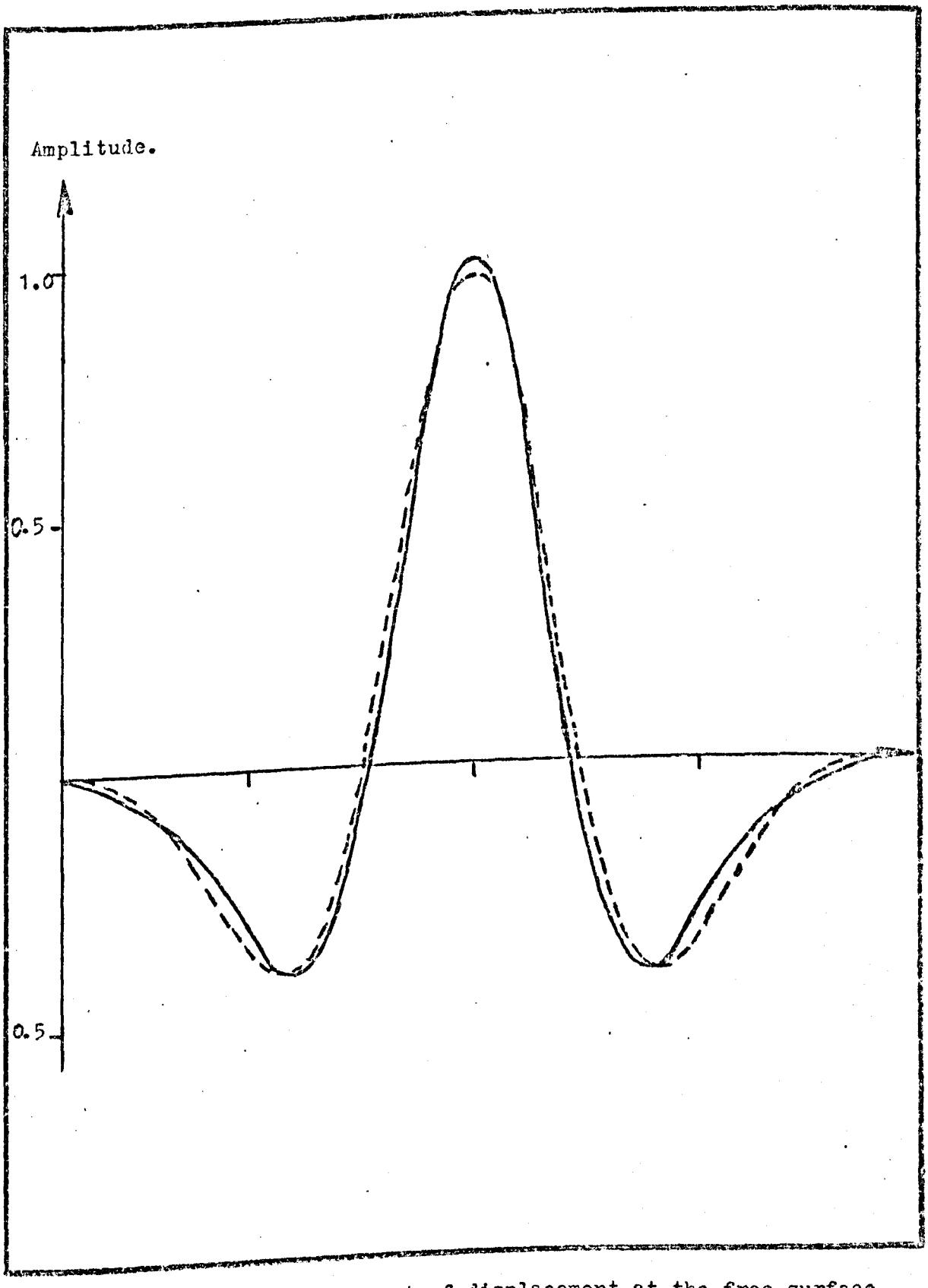

Ricker pulse vertical component of displacement at the free surface of a half-space, using a second order scheme with aluminium data and 15 nodes per wavelength, at t = 0 and after 200 (dashedline) iterations.

FIGURE 7.30.

7.3.2 Rayleigh waves on quarter spaces.

The quarter space is a configuration with a single 90° corner at the intersection of two free surfaces, the scattering at which should be characterised by wavelength independent transmission and reflection coefficients.

The basic nodal arrangement used in the computer program, Program I, which models Ricker type pulses of Rayleigh waves on a quarter space is shown as Figure 7.31.

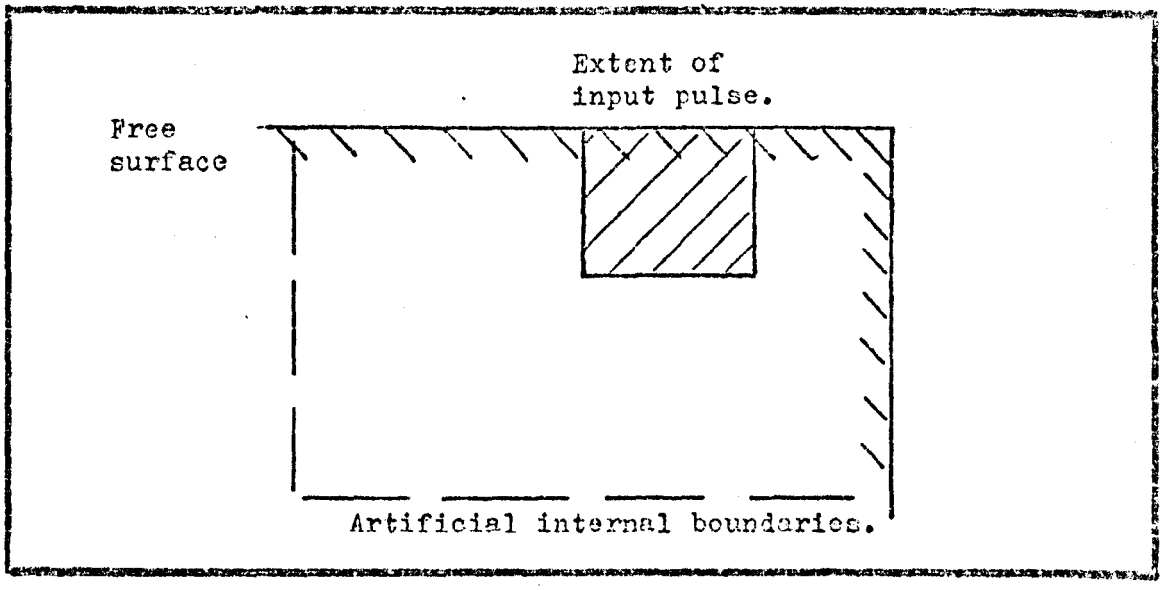

Node arrangement for second order finite difference model of a Ricker type pulse of Rayleigh waves on a quarter space.

FIGURE 7.31.

The propagation of the Ricker type pulse of Rayleigh waves on a quarter space was investigated using both polystyrene ($\sigma = 0.24$) and aluminium ($\sigma = 0.34$) data, presented in Table 11, and 16 nodes per wavelength, with the wavelength corresponding to the pulse centre frequency of 1 MHz.

a. Basic pulse analysis.

The propagation and scattering of the Ricker type pulse of Rayleigh waves was investigated and for each model run, a series of sets of displacements were recorded and numerical visualisation type displays were plotted at regular intervals. An example of selected frames from a numerical visualisation series are shown as Figure 7.32.

The scattered pulses generated by the corner can be clearly seen and are a compressional wave, a shear wave and reflected and

a.

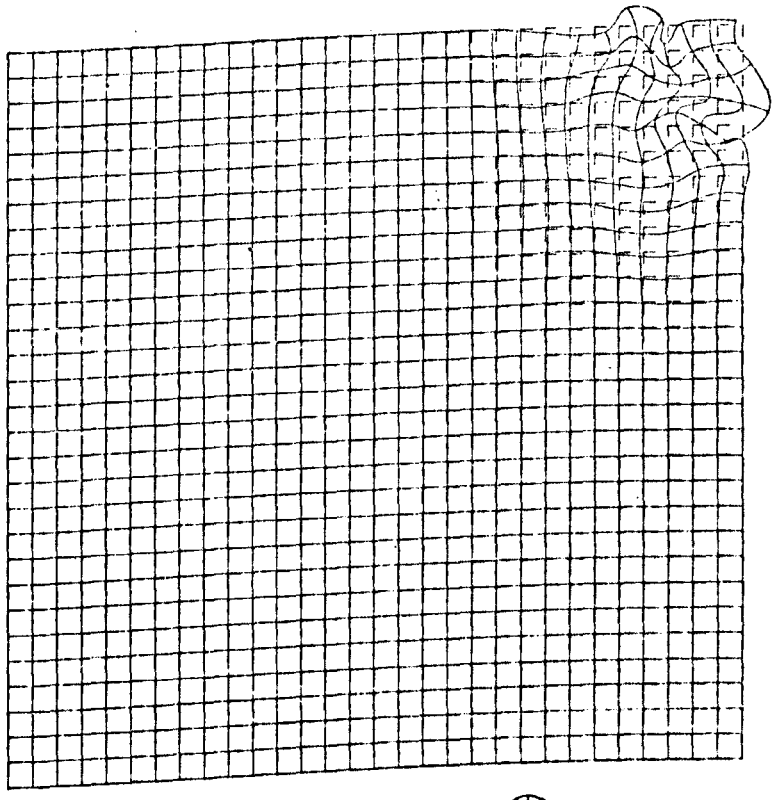

b.

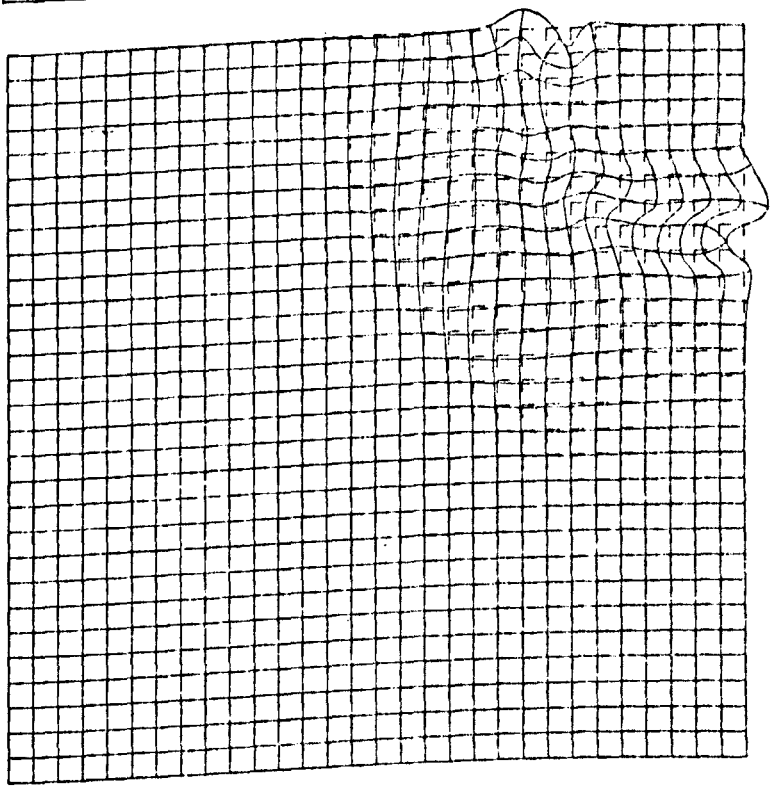

Ricker pulse on a quarter space using polystyrene data and 16 nodes per wavelength; System after a. 80 and b. 120. iterations.

FIGURE 7.32.

c.

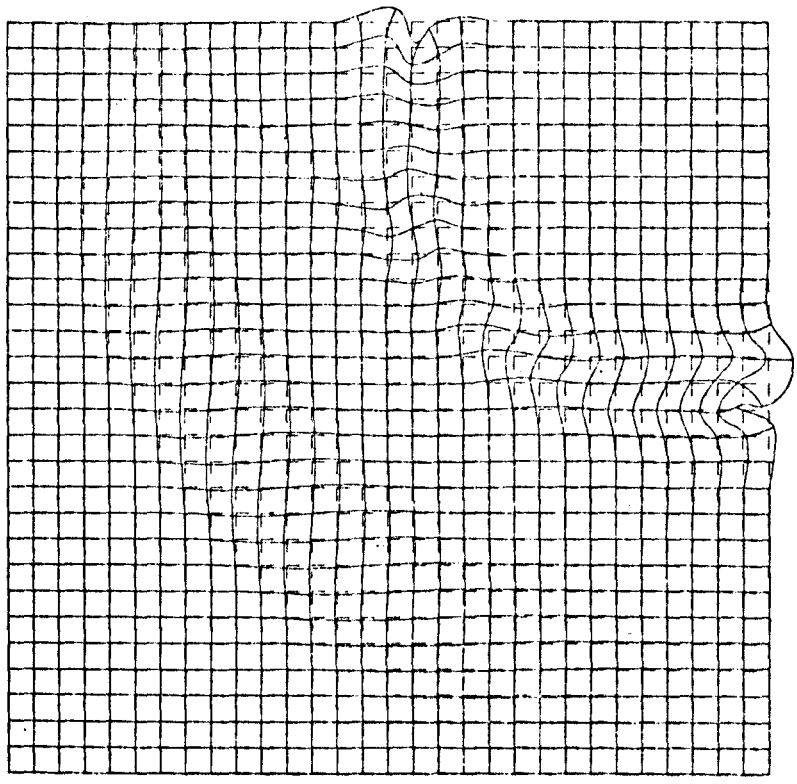

d.

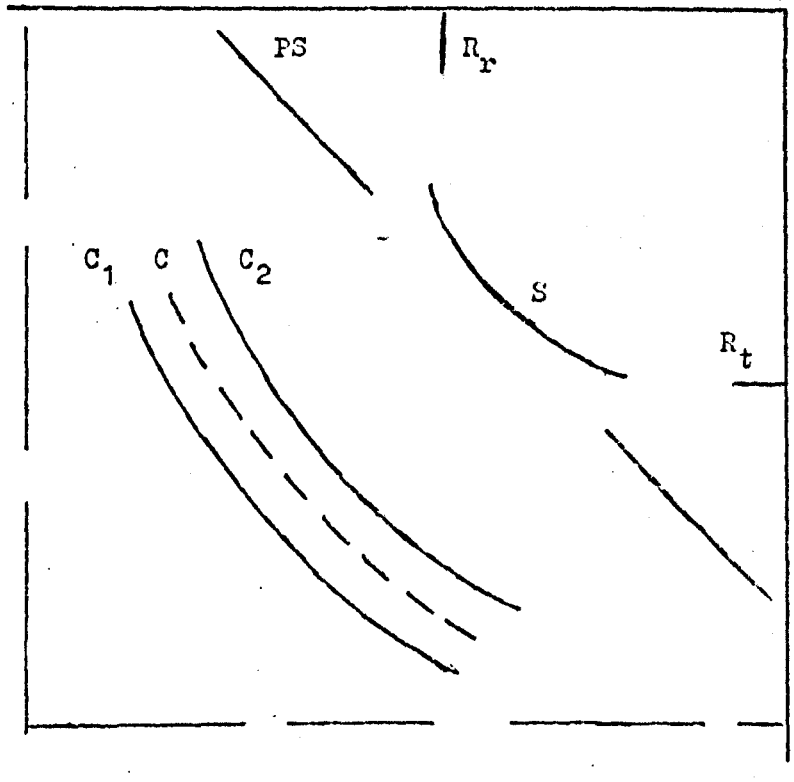

Ricker pulse on a quarter space, using polystyrene data and 16 nodes per wavelength. System after 180 iterations.
(d) Main pulse identification, pulses as shown in Figure 7.7.

FIGURE 7.32.

transmitted pulses of Rayleigh waves.

It is seen from Figure 7.32c, that there is a difference in the distance from the corner for the reflected and transmitted Rayleigh wave pulses, with the distance travelled by the reflected pulse being about 10 % less than that moved by the transmitted pulse.

The pulse velocities for the scattered pulses were measured for the model using aluminium data at 16 nodes per wavelength and these are presented in Table 21 together with the corresponding values for the wave velocities given in the data presented as Table 11.

	Rayleigh wave vel. m/sec.	Compressional wave vel. m/sec.	Shear wave vel. m/sec.
Data from Table 11	2906.	6422.	3110.
From F.D. model.	2873. ±100.	6539. ± 100.	3070. ± 100.
Percentage difference between F.D. and data.	- 1.2	+ 1.8	- 1.3

Wave velocities for scattered pulses on an aluminium quarter space as given by finite dfference second order scheme, compared with material data.

TABLE 21.

b. Transmission and reflection coefficients.

Following the identification of the basic pulses which result from the scattering of a Rayleigh wave pulse on a quarter space, measurements were made, based on amplitude data, to establish transmission and reflection coefficients and estimate the energy loss from Rayleigh waves, due to mode conversion.

Model runs were performed with polystyrene and aluminium data and the values for the transmission and reflection coefficients are shown in Table 22.

Pulse size (in nodes)		Nodes per	Material	Poisson's ratio.	Ref. coef.	Trans. coef.	Mode conv loss (%).
Width	Depth	λ_p					
48	48	16	Aluminium	0.34	0.47±.05	0.59±.05	44
48	48	16	Polystyrene	0.24	0.43±.05	0.57±.05	50

List of transmission and reflection coefficients for Ricker pulses on quarter spaces, with second order nodal formulations, with space dimensions of 122 by 122 nodes.

TABLE 22.

The results obtained with this scheme are considered further and compared with the results of the first order model, which are presented in Section 7.2, the experimental results, which are presented in Section 8.4, and those of other workers, in Section 9.3.

7.3.3 Rayleigh waves on three-quarter spaces.

The three-quarter space is a single corner configuration, with a single 270° corner at the intersection of two free surfaces, the scattering of Rayleigh waves at which, should provide wavelength independent transmission and reflection coefficients.

The basic model node arrangement for the computer program, Program J, which models a Rayleigh wave pulse on a three-quarter space is shown as Figure 7.33.

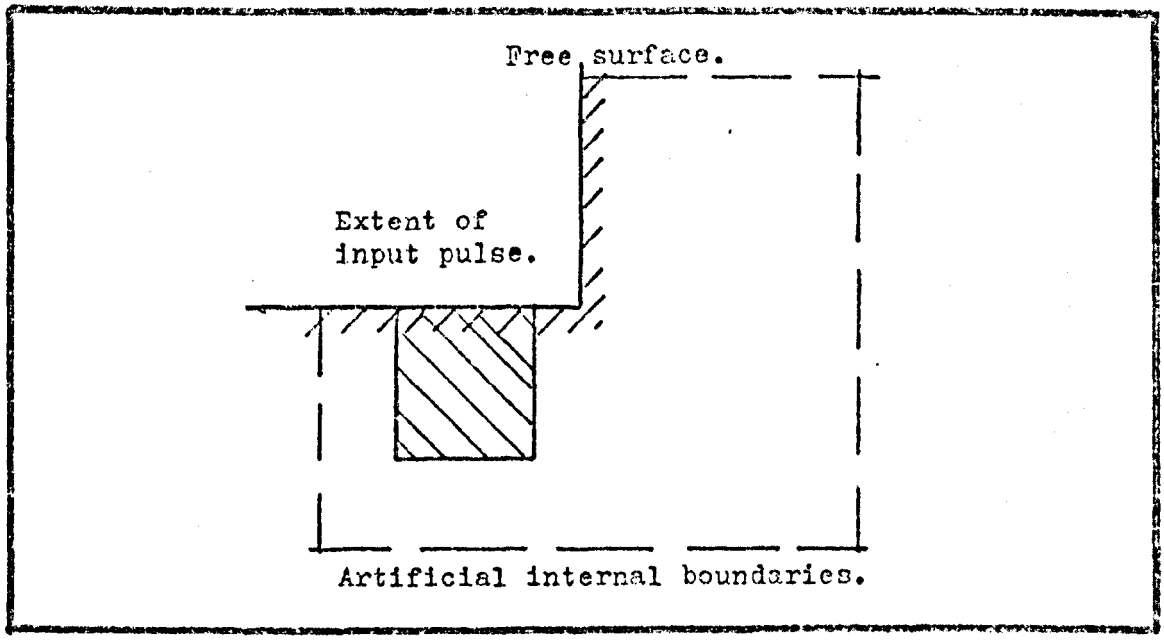

Node arrangement for second order finite difference model of a Ricker type pulse of Rayleigh waves on a three-quarter space.

FIGURE 7.33.

The propagation of a Ricker type pulse of Rayleigh waves on a three-quarter space was investigated using polystyrene data with the node arrangement shown in Figure 7.33 and 16 nodes per wavelength, with the pulse centre wavelength corresponding to a frequency of 1 MHz.

a. Basic pulse analysis.

The propagation of a Ricker type pulse was investigated and for each model run, a series of sets of displacements were recorded at regular intervals and numerical visualisation type displays were plotted, an example of which is shown as Figure 7.34.

The time development of the system is shown for a pulse using

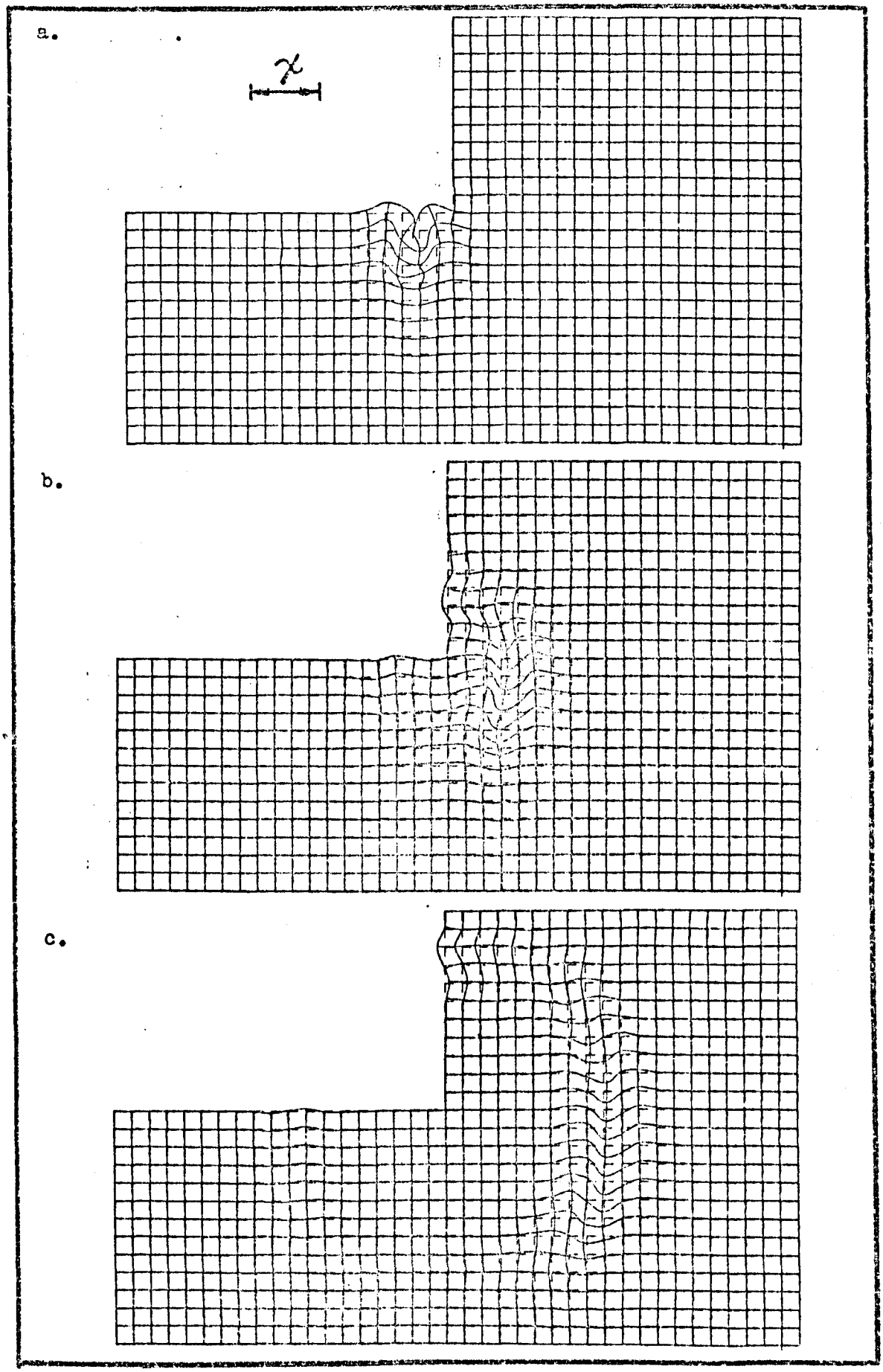

Ricker pulse on a three-quarter space, using aluminium ($\sigma = 0.34$) data and 16 nodes per wavelength. After a. 20, b.60, and c. 140 iterations.

FIGURE 7.34.

aluminium data and in Figure 7.34c is is shown that the main mode converted pulse is a shear wave that radiated on a near circular arc from the 270° with the majority of the energy in the arc ±45°.

b. Transmission and reflection coefficients.

Following the identification of the basic pulses in the system of mode converted waves, computer runs were performed using both aluminium and polystyrene data at 16 nodes per wavelength and measurements were made, based on amplitude data to establish transmission and reflection coefficients. The values of the transmission and reflection coefficients are given as Table 23.

Pulse size (in nodes)		Nodes per	Material	Reflection coefficient	Transmission coefficient.	% mode conv. Energy loss.
Width	Depth					
64	48	16	Aluminium	0.11 ±.03	0.23 ±.03	94
64	48	16	Polystyrene	0.09 ±.03	0.22 ±.03	95

Transmission and reflection coefficients on three-quarter spaces using second order boundary condition formulation, with polystyrene data and aluminium data, both at 16 nodes per wavelength.

TABLE 23.

The results obtained with this scheme are considered further and compared with the results of the first order model, which are presented in Section 7.2, the experimental results, which are presented in Section 8.4, and those of other workers, in Section 9.4.

7.3.4 Rayleigh waves on welded quarter spaces.

The configuration of welded quarter spaces, two quarter spaces of media welded along an interface, is one of the simplest two media configurations. It does not have a characteristic dimension and the scattering is dependant on the material parameters, such as the density and wave velocities in the two media.

The basic node arrangement in the computer program, Program K, which models Rayleigh wave pulses on welded quarter spaces, is shown as Figure 7.35. The nodal formulation used for the free surface/ interface node (P) is a new second order formulation derived by the author and presented in Appendix G.

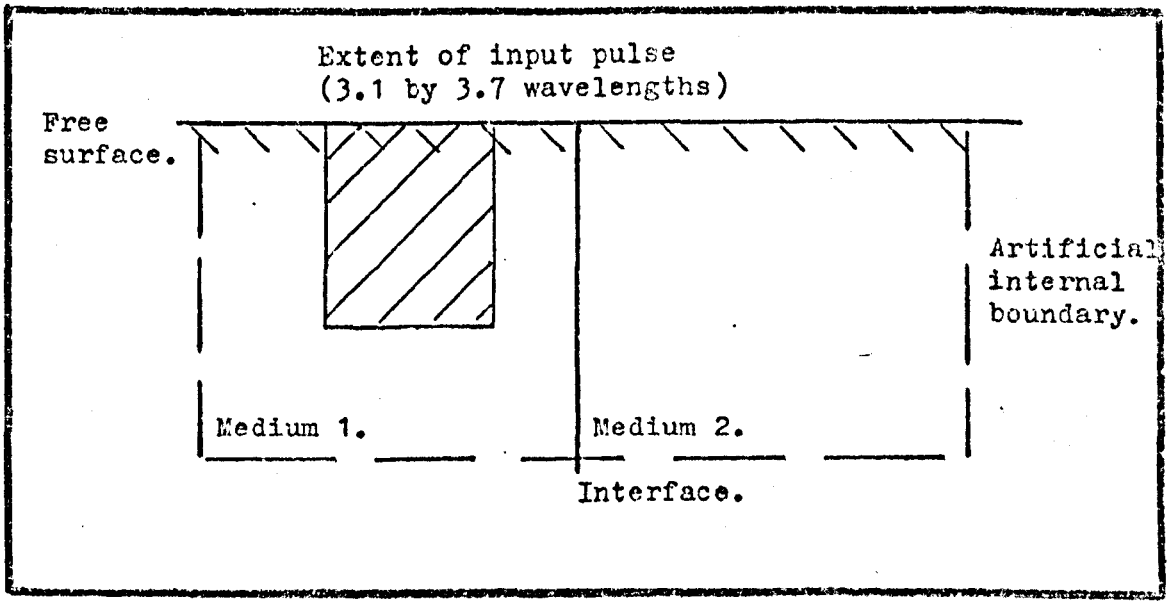

Node arrangement for second order finite difference model of a Ricker type pulse of Rayleigh waves on welded quarter spaces.

FIGURE 7.35.

The propagation and scattering of a Ricker type pulse of Rayleigh waves on welded quarter spaces was investigated using the node arrangement shown in Figure 7.35 with 16 nodes per wavelength, where the wavelength is that corresponding to a pulse centre frequency of 1 MHz in medium 1.

The basic nodal scheme was tested by using both polystyrene and aluminium data with 16 nodes per wavelength and the same data was used for both media. The scheme, including the new free surface/ interface node formulation, was found to give the nondispersive propagation of the Ricker pulse to the same level of accuracy as the second order scheme reported in Section 7.3.1 for propagation on

a half-space.

The scheme was then used with media data for the two quarter spaces that were different. The two media used in the present study were the same as those used by McGarr and Alsop (1967) and by Munasinghe (1973). These were polystyrene and perspex and the material data used is shown in Table 11.

a. Basic pulse analysis.

The propagation of a Ricker type pulse was investigated with the pulse moving fron polystyrene to perspex and vice versa and the time development of the systems was followed by the use of numerical visualisation type displays. The two combinations of perspex and polystyrene are shown in the visualizations shown as Figures 7.36 and 7.37.

The basic system of waves are transmitted and reflected pulses of Rayleigh waves and some low energy mode converted body and interface waves.

b. Transmission and reflection coefficients.

In the previous studies on this configuration by McGarr and Alsop (1967) and Munasinghe (1973) the transmitted and reflected pulses are measured in terms of coefficients which are the ratios of the incident and transmitted pulse amplitudes and the incident and the reflected pulse amplitudes respectively. The same procedure is used in the present study and the results for waves on the two combinations of polystyrene and perspex are given as Table 24.

Pulse travelling from 1 to 2.		Reflected / Incident	Transmitted / Incident
Medium 1	Medium 2		
Polystyrene	Perspex	0.08 ±.03	0.90 ±.03
Perspex	Polystyrene	0.07 ±.03	1.12 ±.03

Pulse amplitude ratios for the vertical components of displacement of the reflected and transmitted pulses of Rayleigh waves on welded quarter spaces.

TABLE 24.

The results presented in Table 24 are compared with those of previous studies in Section 9.9.

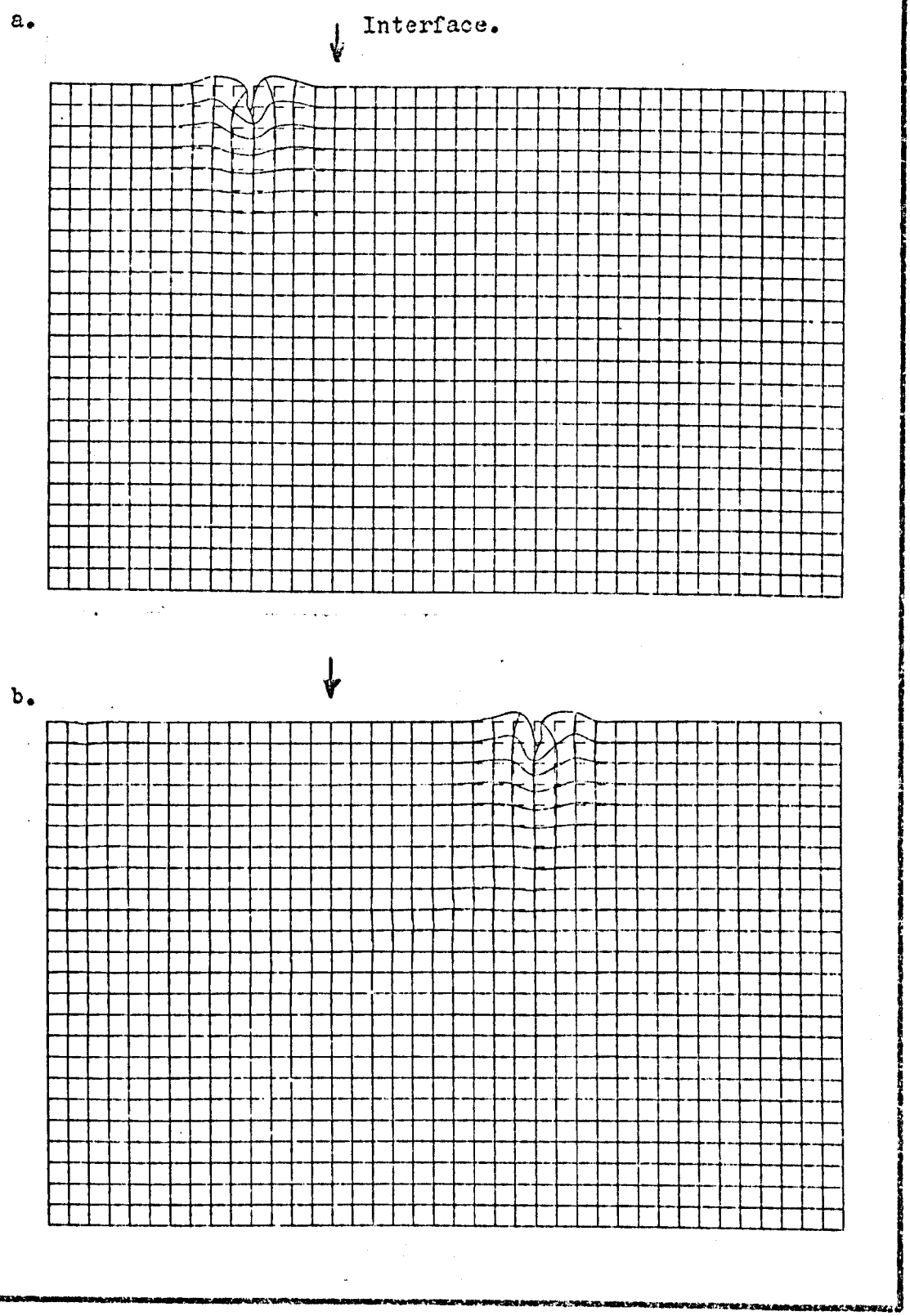

Ricker type pulse of Rayleigh waves on welded perspex and polystyrene quarter spaces, with the pulse moving from perspex to polystyrene. System after a. 20, and b. 160 iterations.

FIGURE 7.36.

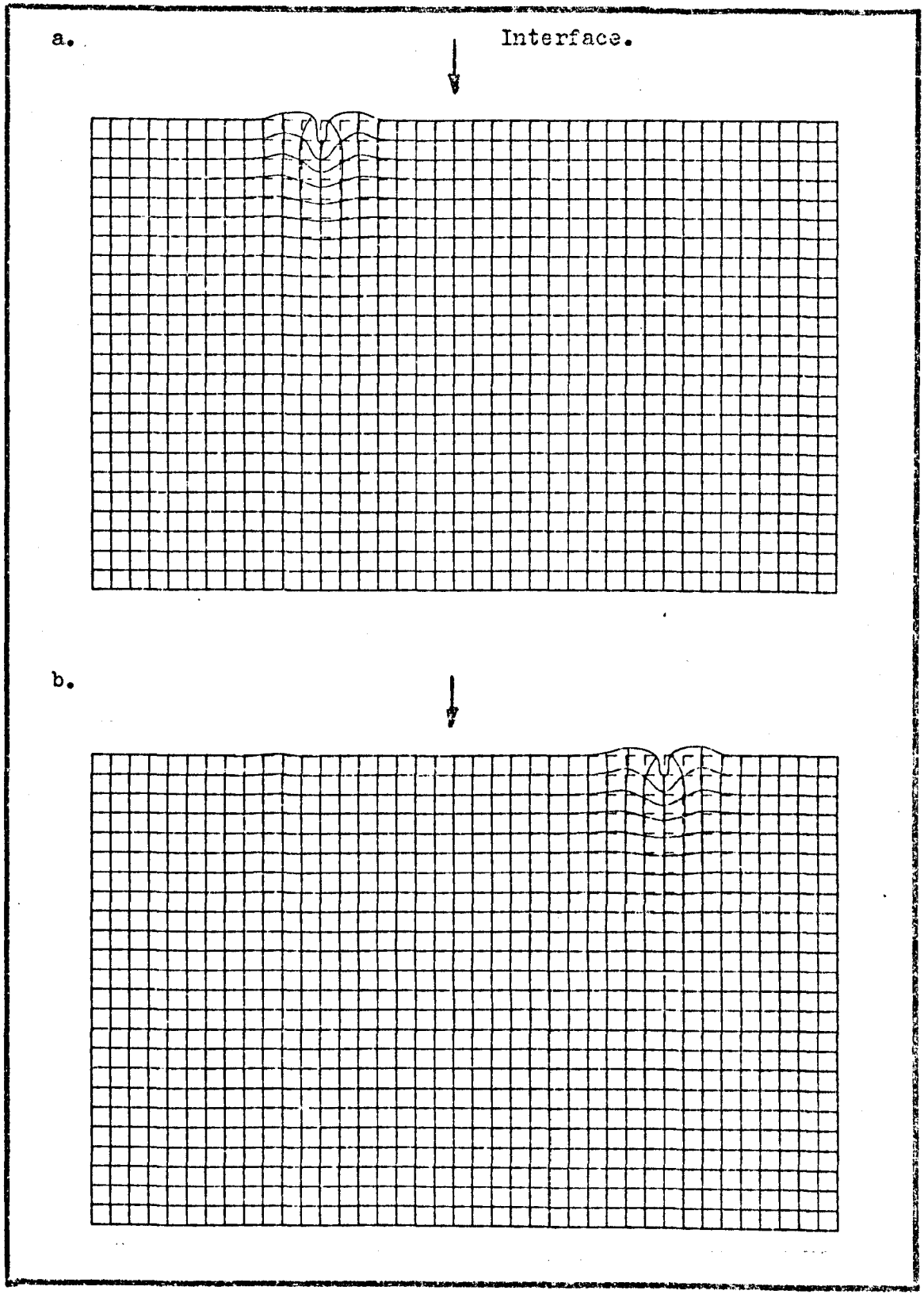

Ricker type pulse of Rayleigh waves on welded polystyrene and perspex quarter spaces, with the pulse moving from polystyrene to perspex. System after a. 20, and b. 180 iterations.

FIGURE 7.37.

7.3.5 Rayleigh waves at filled slots.

The configuration of a filled slot considered in the present study was for a rectangular section of one isotropic homogeneous medium set into and at, the surface of a half-space of a second isotropic homogeneous medium.

The basic nodal arrangement used in the computer program, Program L, which models a Rayleigh wave pulse at a filled slot is shown as Figure 7.38.

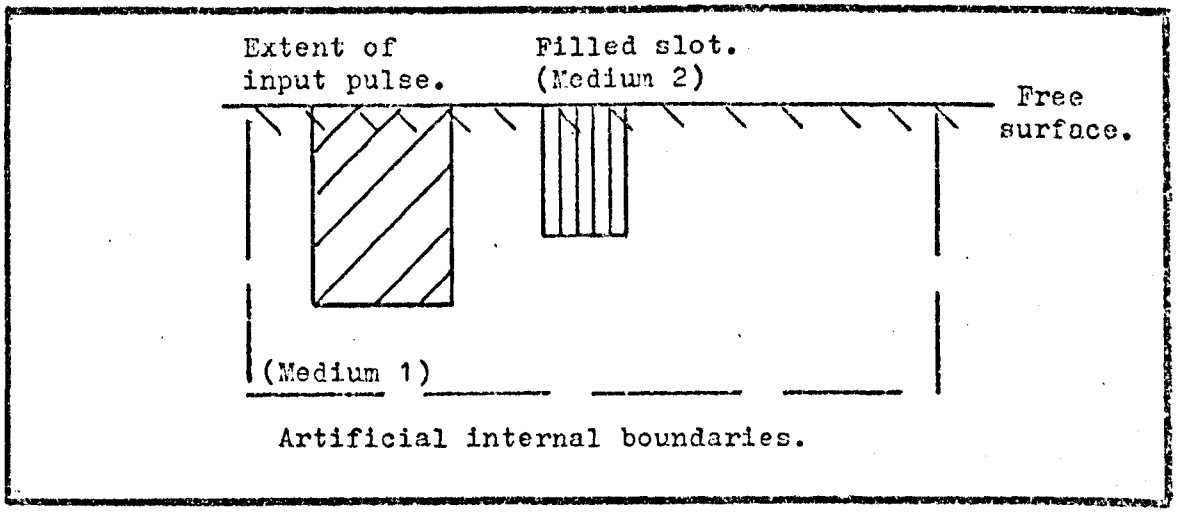

Node arrangement for second order finite difference model of a Ricker type pulse of Rayleigh waves at a filled slot.

FIGURE 7.38.

The model for the filled slot was a direct extension of the welded quarter spaces model and the media selected for use in this model were those used for the quarter spaces and described in Section7.3.4, as there are no previous results for this configuration. The node arrangement shown in Figure 7.38 was used to investigate the propagation and scattering of a Ricker type pulse of Rayleigh waves at a slot in a block of polystyrene filled with perspex and vice versa, using the material data shown in Table 11.

The model was used with 16 nodes per wavelength where the wavelength corresponded to a pulse centre frequency of 1 MHz in the medium used for the block.

a. Basic pulse analysis.

The propagation and scattering of a Ricker type pulse of Rayleigh waves was investigated for several model runs and for each a series of sets of displacements were recorded and numerical

visualisation type displays were plotted at regular intervals. An example of selected frames from a numerical visualisation series of a pulse at a wide deep slot are shown as Figures 7.39 and 7.40.

The largest pulse in the system is found to be the transmitted one which has about 90 % of the input pulse energy in it, in the cases of combinations of perspex and polystyrene. There are also reflected pulses at each interface and mode converted body wave and interface waves which have low energies.

The energy in each pulse was found to be dependent on the material parameters of the media considered and both the slot width and depth.

b. Transmission and reflection coefficients.

Following the identification of the main pulses in the system computer runs were performed using polystyrene and perspex data and 16 nodes per wavelength to give amplitude based measurements and establish transmission and reflection coefficients. The values of the transmission coefficient and the reflection coefficients for the pulses reflected at each interface for slots filled with polystyrene set in perspex half-spaces or vice versa are given as Table 25.

½ space material	slot material	slot size width (in nodes)	depth	Trans. coef.	1st ref. coef.	2nd ref coef.	% E loss.
polystyrene	perspex	20	70	0.92	0.1	0.08	14
perspex	polystyrene	20	70	0.96	0.08	0.06	7

Transmission and reflection coefficients at filled slots.
(all coefficients are given with error bands of ±.03)

TABLE 25.

The results obtained with this model are considered further in Section 9.10.

a.

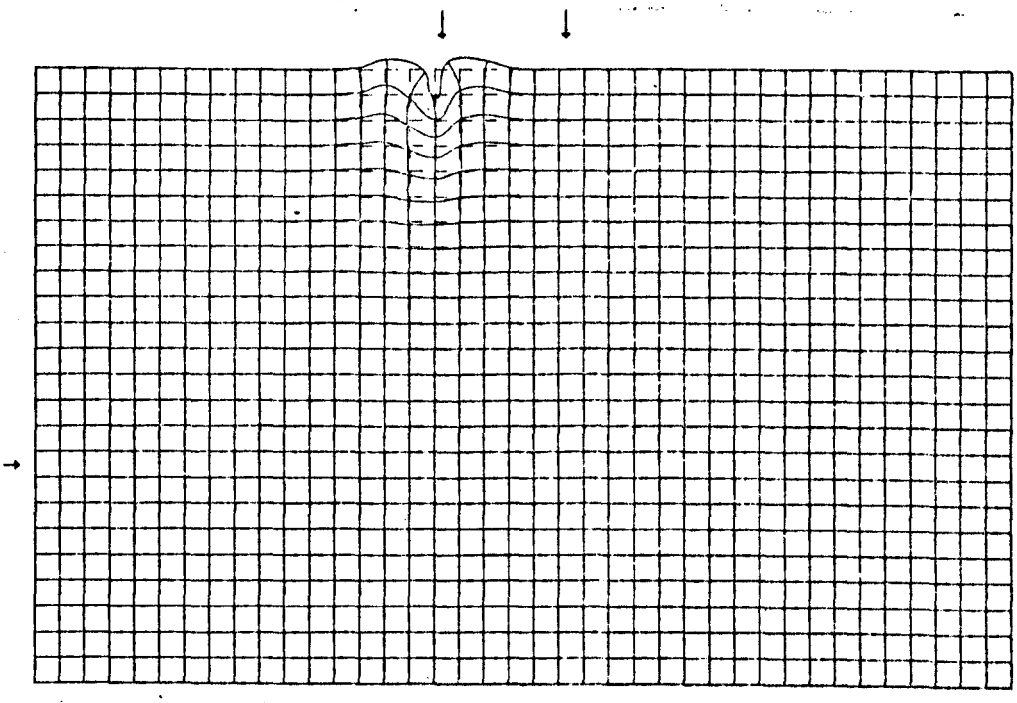

b.

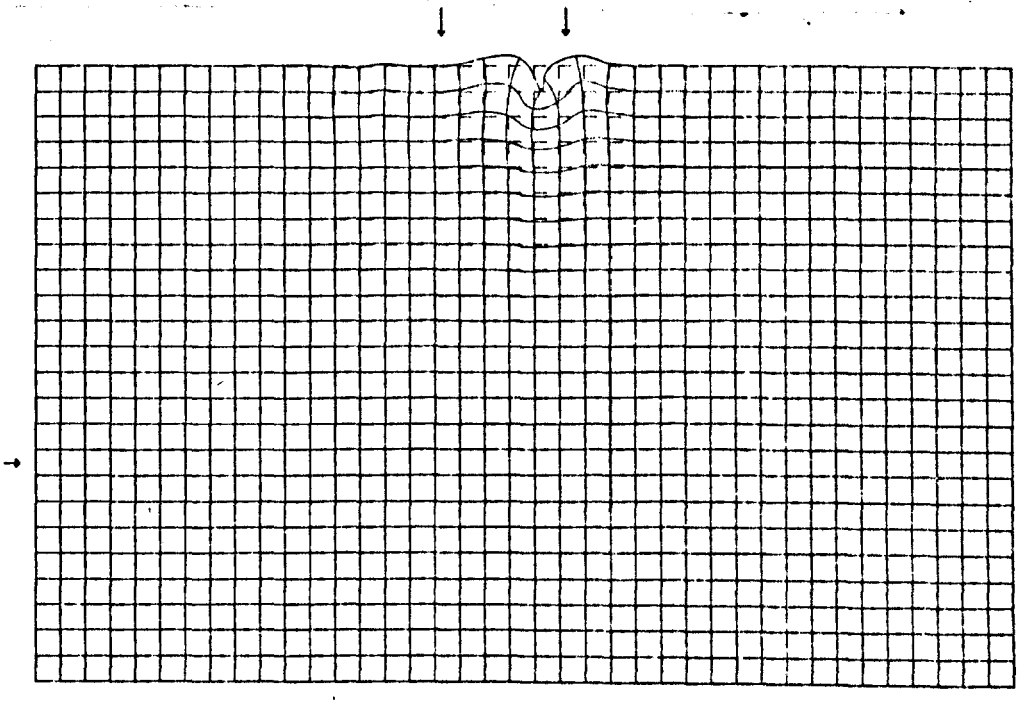

Ricker pulse at a filled slot, a perspex half-space with a slot filled with polystyrene. System after a. 80 and b. 120 iterations.

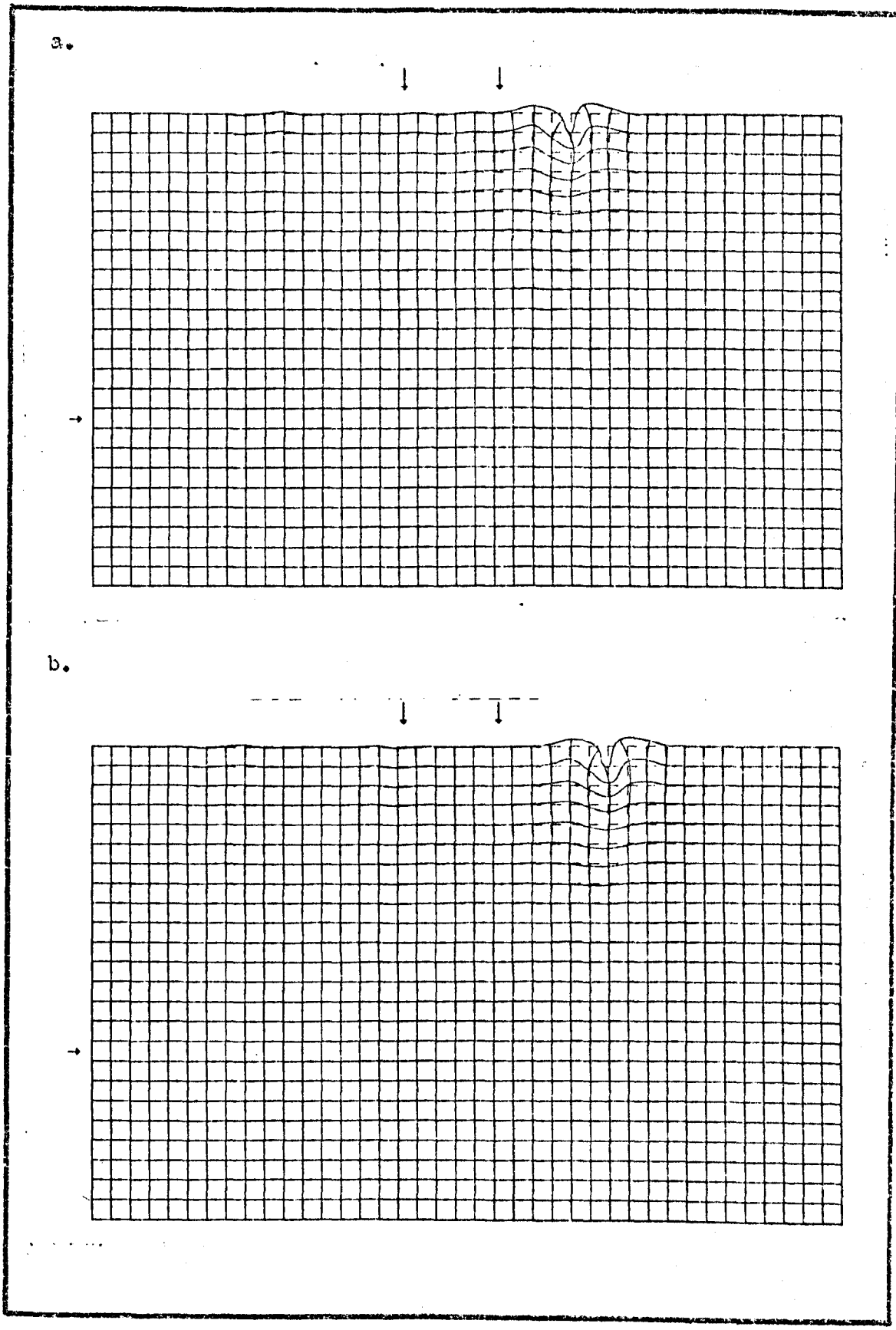

Ricker pulse at a filled slot, a perspex half-space with a slot filled with polystyrene. System after a. 160 and b. 180 iterations.

FIGURE 7.40.

8. EXPERIMENTAL WORK.

8.1 Introduction.

This section presents the experimental work which has been performed with broadband Rayleigh wave pulses, of 1MHz centre frequency, to test the results of the numerical models which are presented in Section 7.

As stated previously, the present study was started as a direct result of the work by Morgan (1973) at T.C.U., and the basic experimental equipment used in this study, with the exception of the transducers, was the same, or an updated version of the equipment which he used.

A full description of the basic analogue equipment, transducer drive unit, broadband receiver and spectrum analyser is given by Morgan (1973) and Weight (1975), who built much of the equipment. This equipment, together with supporting oscilloscopes, plotter and digital equipment forms the Central Ultrasonics Test equipment for the Research Group in Ultrasonics of the City University, and it is shown in Figure 8.1.

The main aim of the experiments was to provide time domain signals, spectra and reflection and transmission coefficients, as information for direct comparison with the results of the numerical model. Measurements were performed on a series of both aluminium and steel test blocks using the methods outlined in Section 5 and considered in detail in this section.

This section considers the production of Rayleigh waves in Section 8.2, which includes a more detailed consideration of the transducers used in the present study in Section 8.2.1.

The experimental measurements made in the present study are presented in two groups, firstly, a series of introductory measurements using one probe in pulse-echo mode are reported in Section 8.3, and secondly the main series of experiments using two probes on a range of geometries are reported in Section 8.4.

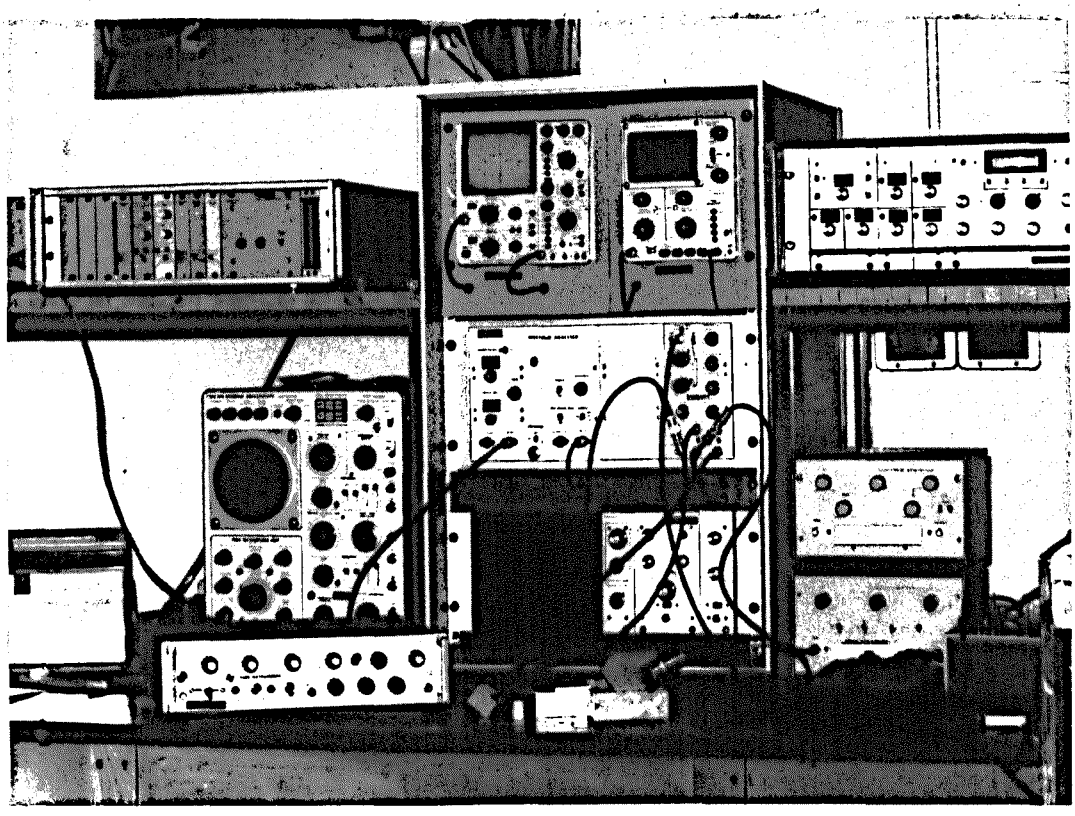

The Central Ultrasonics Test Equipment of the Research Group in Ultrasonics of The City University.

FIGURE 8.1.

For each of the series of experiments presented in Section 8.4, following the discussion of the method used, the basic results are given. A comparison of the experimental results with those given by the numerical models, and reported in Section 7, is given in Section 9 which includes discussion of the results of previous workers.

8.2 Rayleigh wave transducers.

This section presents a brief review of the alternative methods which have been used in previous studies to generate and receive Rayleigh waves. It includes Section 8.2.1 which gives a more detailed consideration of the transducers used in the present study.

Five basic methods have been used in previous studies for Rayleigh wave production and detection and the different types

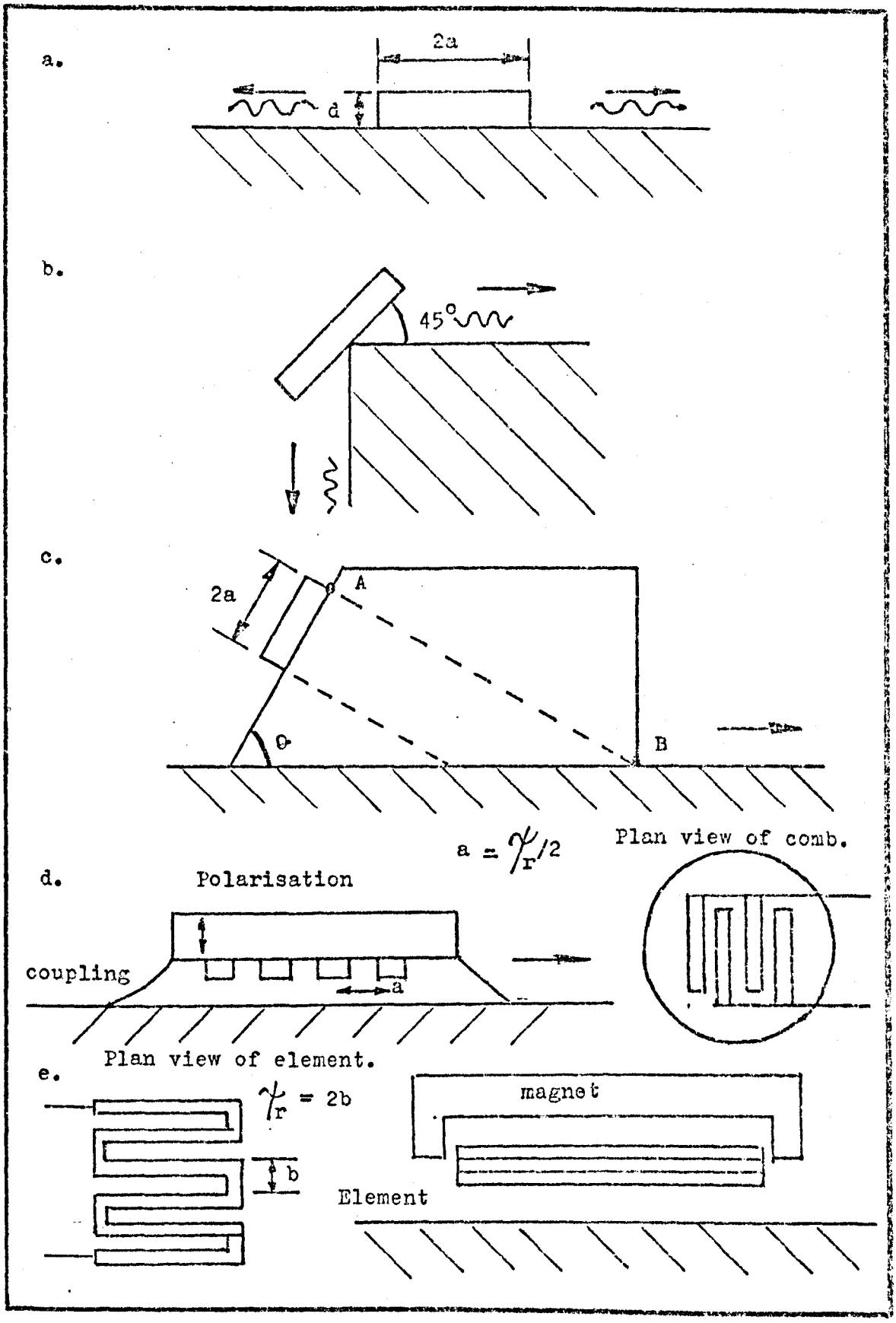

Rayleigh wave transducers using:- a. Contact disc, b. Corner disc, c. Wedge, d. Comb, e. Electromagnetic induction.

FIGURE 8.2.

of transducers are shown in Figure 8.2.

The first method of Rayleigh wave excitation is that used by Firestone and Frederick (1946), which is shown as Figure 8.2a., and uses a Y-cut quartz plate coupled to the surface of a solid by a thin oil film. Two Rayleigh waves are produced with equal amplitudes and the maximum energy conversion into these waves is achieved with the plate width (2a) to thickness (d) ratio of 7 ; 1. A piezo-electric disc can be used to produce Rayleigh waves in a similar manner.

The second method of Rayleigh wave production is that used by Minton (1954), which is shown as Figure 8.2b., and this uses an X-cut quartz crystal plate resting on an elastic wedge. Two weak Rayleigh waves are excited and the optimum conversion is achieved when the plate is set at 45°, with respect to the wedge faces.

The third method of Rayleigh wave production uses mode conversion at interfaces and is shown in Figure 8.2c. Plastic wedges with piezoelectric plates set on the sloping surface were used by Minton (1954) and Cook and Valkenberg (1954) to generate longitudinal (compressional) waves, at the disc resonant frequency, in the wedge, which with the correct wedge angle mode convert to give Rayleigh waves along the free surface.

The wedge angle required to give optimum Rayleigh wave production for a particular wedge material/test block material combination is given by the equation which is given as;

$$\sin \Theta = V_c/V_r \qquad 8.2.1$$

where V_c is the compressional wave velocity in the wedge,

V_r is the Rayleigh wave velocity in the test block.

The optimum energy conversion to Rayleigh waves is achieved, for a particular wedge angle and ignoring coupling problems, when the leading edge of the disc (A) projects to the front of the wedge at the point (B), as shown in Figure 8.2c. Bulk waves are also produced by a wedge transducer at a level of between 20 and 30 dB down on the Rayleigh waves.

An alternative to the use of a plastic wedge is to use one made of a metal such as copper or brass as this reduces coupling problems. However to do this the wave generated by the disc on the wedge is required to be a shear (transverse) wave, the velocity for which is used in equation 8.2.1 in place of the compressional

wave velocity to calculate the required wedge angle. The shear wave has a lower initial energy but with the coupling advantages this combination is sometimes preferable. (Shraiber 1959)

Using Rayleigh waves produced by shear waves in a copper wedge and photoelastic visualization, Hall (1976) has shown the complex nature of the waves generated in the test block, including the presence of several body wave pulses.

The fourth method of Rayleigh wave production is the use of an interdigital comblike structure produced on the lower surface of a disc of X-cut quartz, as shown in Figure 8.2d. (Sokolinski 1958) This type of transducer was developed by Morgan (1970) and used in his crack depth measurement studies. (Morgan 1973) However, he found it difficult to get high energy Rayleigh wave pulses with a short period. The fabrication of this type of transducer is quite complex as it involves either the deposition of the comb through a mask or the photo-etching of a layer of conductor previously deposited on the quartz or piezo-electric disc.

The fifth method is the use of the recently developed non-contact transducers which use eddy currents in the material under the transducer in which a Rayleigh wave is to be generated to give vibrations which result in the production of elastic waves. A transducer of this type due to Frost et al (1975) is shown as Figure 8.2e. This type of transducer has been developed for use as a tool to inspect hot metal blocks by Cole (1977).

8.2.1 Rayleigh wave transducers used in this study.

The experimental measurements made in the present study were performed to determine the 'surface displacements' in the Rayleigh wave pulses and not just the time domain signals given by wedge transducers with the supporting electronics and displayed on an oscilloscope.

In the present study, two types of Rayleigh wave transducers were used. These are the longitudinal (compressional) wave wedge type and a new broadband probe, which was invented by Professor Harnik while working with the author at The City University. This Harnik probe has subsequently been developed by the author in the course of the fabrication and use of the probes in the present study.

a. The wedge transducers.

The wedge transducers used in this study were based on a Panametrics special short pulse probe, used on wedges made to match the material of the test block. The compressional wave probe generated a 1 μsec pulse when driven by a Thyristor Pulse Generator which was found to have a 0 to 6 MHz spectrum. When the compressional wave probe was used with a wedge matched to aluminium the pulse-echo signal and spectrum obtained were as shown in Figure 8,3.

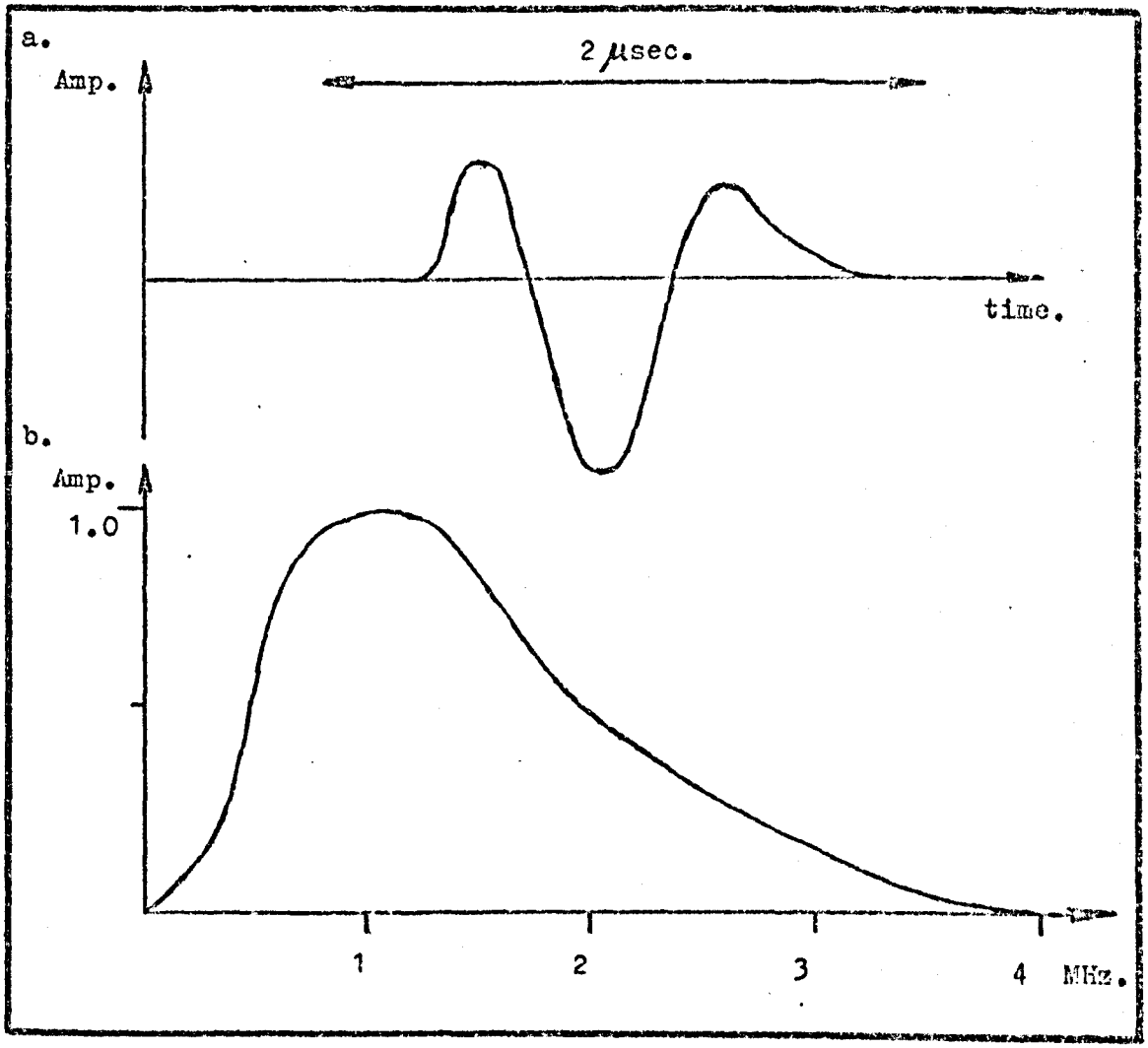

Rayleigh wave pulse on an aluminium quarter space, measured with a wedge type transducer in pulse-echo mode;
a. Time domain signal. b. Spectrum.

FIGURE 8.3.

In the present study the same compressional probe was used on wedges to match it with either the aluminium alloy or the steel of the test blocks. The wedge angles used are shown in Table 26.

Material.	Wedge angle.
Aluminium alloy.	68°
Steel (mild).	64°

Wedge angles required by Rayleigh wave wedge transducers.

TABLE 26.

b. Harnik type probes.

The Harnik probe was invented with the aim of determining the vertical component of the free surface displacements, because the time domain wave form given by a wedge transducer is for a mode converted wave which has passed through the wedge before reaching the piezoelectric crystal, where the electrical signal is produced.

The probe is described by Harnik (1977), both for construction and operation, and Figure 8.4, which shows the pulse construction, is after Figure 1 in that article. Following the production of the prototype transducer by Weight, for Professor Harnik, the author fabricated a series of probes using 10 MHz thickness discs. The discs for use in the Harnik probe are required to be thin when compared with the wavelengths of the pulses which they are to receive if they are to give the true wave form.

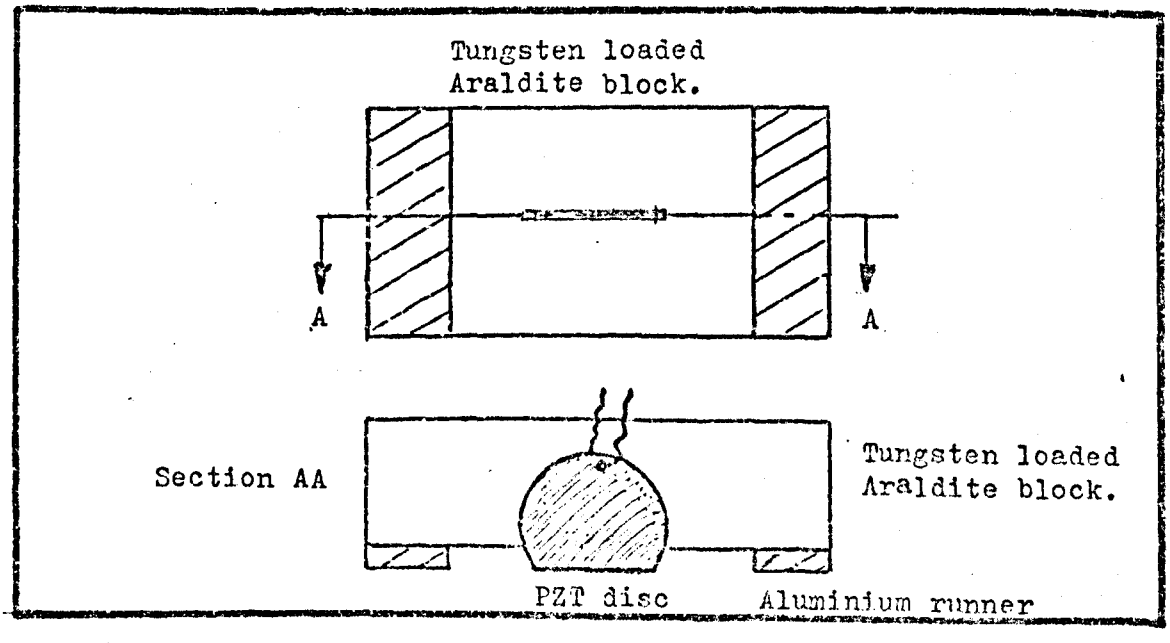

The construction of a Harnik type surface wave probe.

FIGURE 8.4.

In the construction of the prototype Harnik probes, tungsten powder was used to 'load' the Araldite so as to provide acoustic damping for resonant modes. In the later probes, constructed by the author, it was found that the main function of the Adaldite block was to provide mass and to prevent flexing of the plate, which gives rise to radial mode resonance. When 10 MHz resonant thickness discs are used to receive pulses of 1 MHz waves, the disc resonant thickness modes are not excited.

c. Test measurements with Harnik type probes.

A series of experiments were performed by the author to evaluate and if possible improve on the performance of the original Harnik probe. In these experiments Rayleigh waves were generated by a wedge transducer and the Harnik probes were used as receivers.

The Harnik probe is a line pickup and it is therefore unidirectional and requires accurate alignment normal to the wave train under investigation. To reduce the directionality of the probe, the author modified the design and used a complete disc in the probe which, after being set in the Araldite, was made to have a square contact area.

Using a square contact area, point-contact probe, the time domain signals with waves incident on the disc with angles from 0^{o} to 90^{o} were measured and the signals with waves at normal and parallel incidence are shown as Figure 8.5. A ten percent reduction in the pulse peak-to-peak amplitude was measured.

A series of measurements were made to compare the probes of Harnik type constructed by the author with the prototype and wedge probes.

A wedge probe was placed on an aluminium quarter space and the receiving probes were placed in the position shown in Figure 8.6. Measurements were then made on the same pulse, the pulse reflected from the 90^{o} corner, using the wedge probe in pulse echo mode, using a line receiver, Harnik type, probe constructed by the author and the prototype Harnik probe. The three time domain signals are shown in Figure 8.6.

It is seen from Figure 8.6 that the three transducers produce different shape time domain signals and this was investigated. The wedge and Harnik type probes cannot be expected

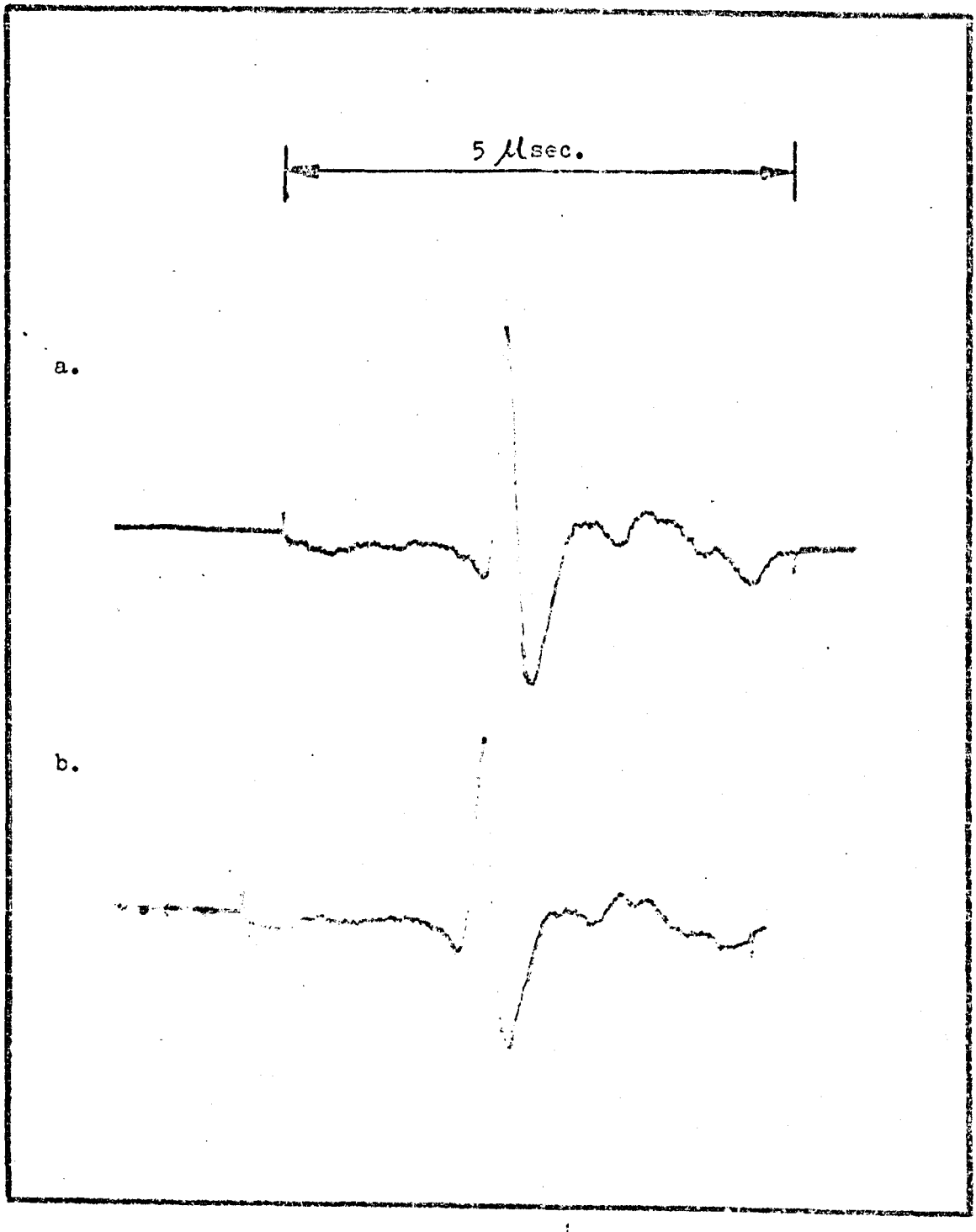

Time domain signals for square contact area Harnik-type probes;
a. Pulse at normal incidence, b. Pulse parallel to disc
for a broadband Rayleigh wave pulse with centre frequency of 1 MHz.

FIGURE 8.5.

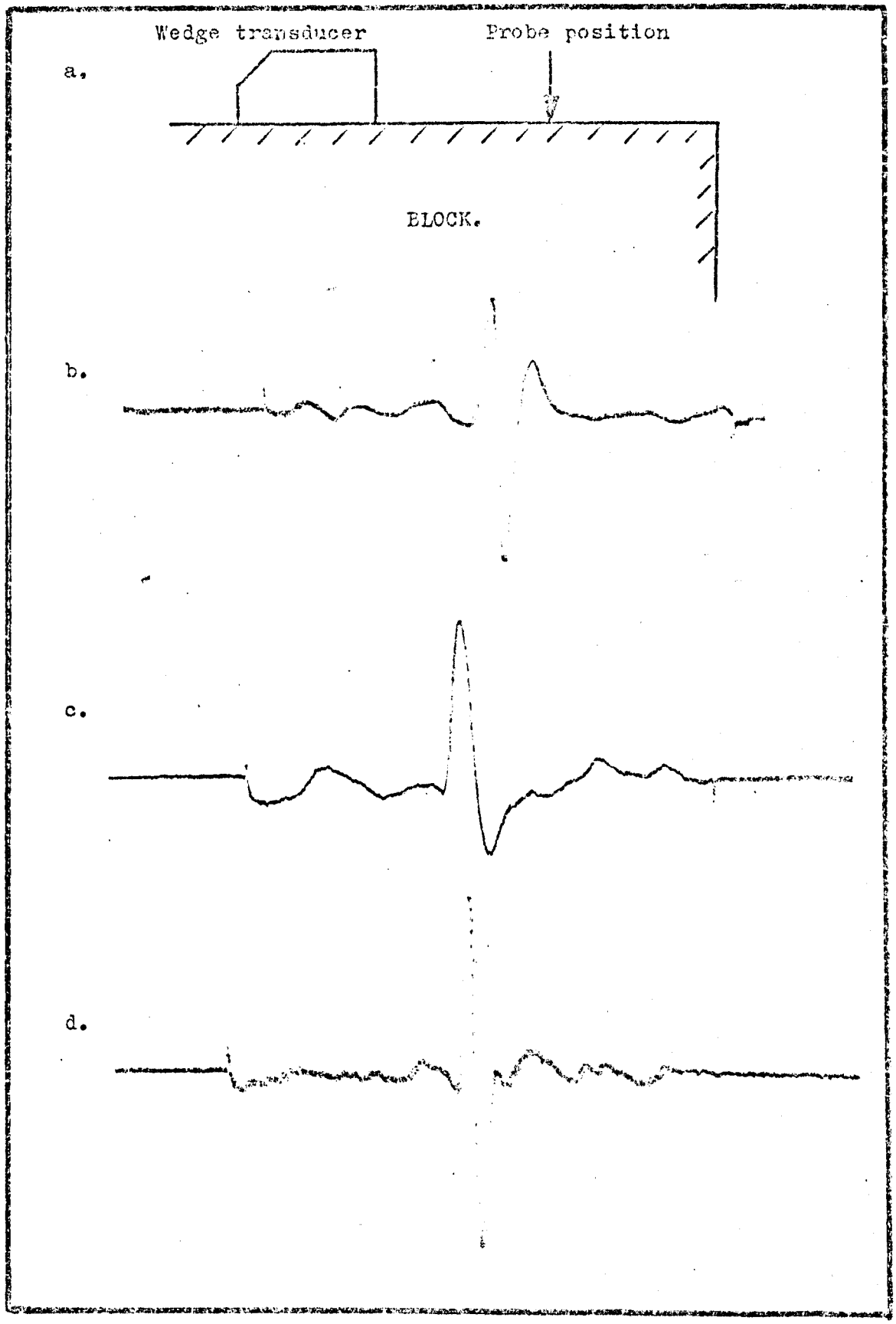

Time domain signals for Rayleigh wave pulses on an aluminum block, a. Transducer positions. Pulse reflected from corner as given by; b. Wedge transducer (pulse-echo mode), c. Harnik-type probe, made by author, d. Prototype Harnik probe.

FIGURE 8.6.

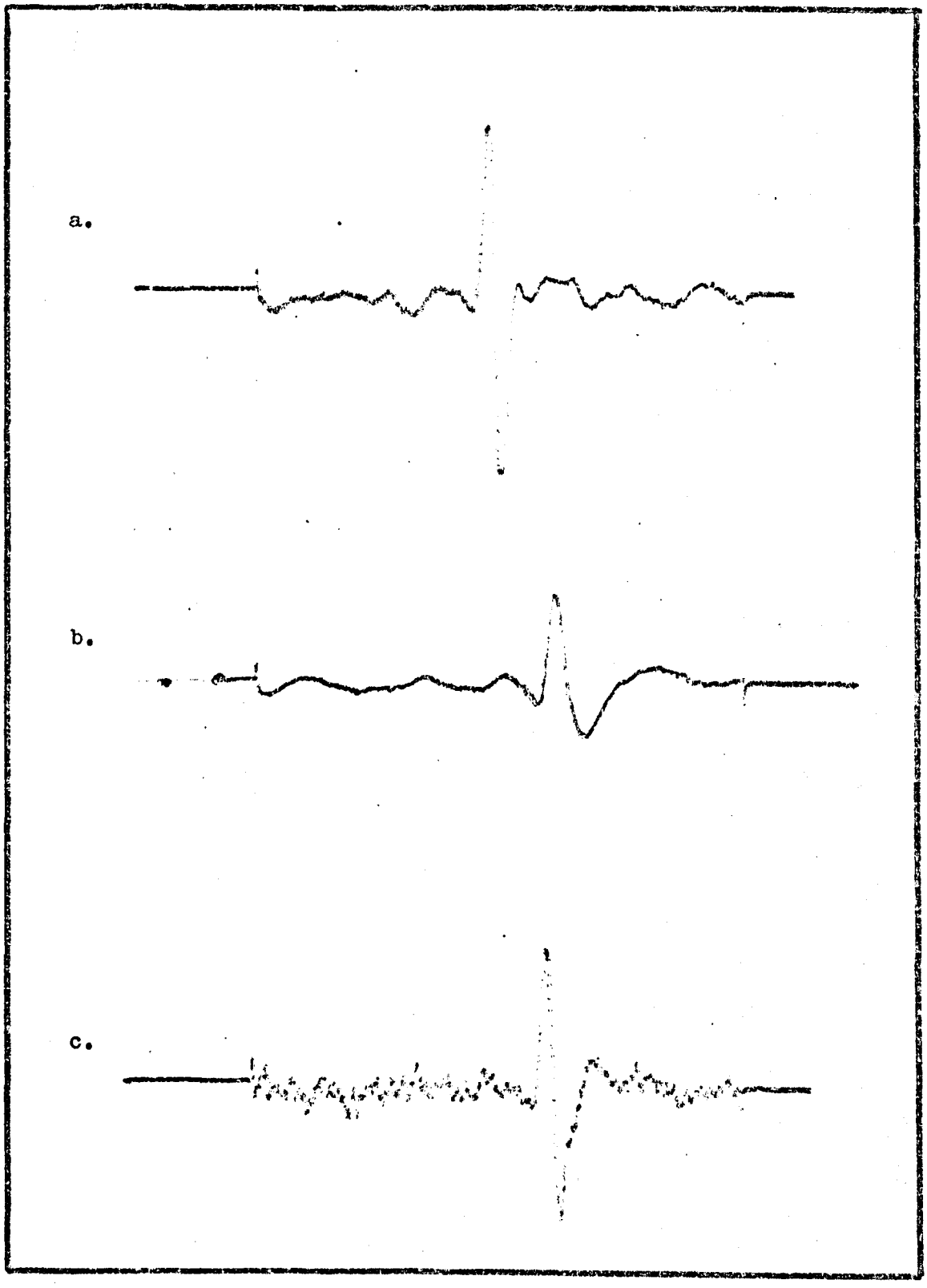

Time domain signals for the same Rayleigh wave pulse on an aluminium block in the same position as given by;
a.Prototype Harnik transducer, b. Harnik-type transducer built by the author, c. Harnik type transducer, built by author and used with an 8 ohm. resistance in parallel with the disc.

FIGURE 8.7.

to have the same time domain signals, as the wedge transducer measures a pulse that has been mode converted and passed through the wedge. However two Harnik-type probes could be hoped to give similar signals.

The D.C. resistance across the transducer leads of the two Harnik probes was measured and in the case of the prototype probe a resistance of 12 ohms was measured and in the case of the author's probe, a resistance of over 20,000 ohms was measured. The only difference between the two probes was in the quantity of tungsten powder used. The resistance across the prototype probe block was then measured and found to be similar to that across the leads. It was therefore concluded that the block was conducting and acting as a resistance in parallel with the disc.

This idea was tested using an 8 ohm. resistance in parallel with the disc in the author's probe. The resulting time domain signals from these measurements are shown as Figure 8.7. It is therefore concluded that when the original probe was made the concentration of tungsten powder used was such as to give a conducting backing block of low resistance, which caused the pulse shape in effect to be differentiated.

8.3 Introductory Rayleigh wave experiments.

This section describes the series of experiments which were performed using a wedge probe in pulse-echo mode, prior to the main experiments which test the results of the numerical models, given in Section 7, and these are described in Section 8.4.

a. Wedge transducer in pulse-echo mode on a quarter space.

A wedge probe on an aluminium block is shown as Figure 8.8, and the basic arrangement of the experimental system is shown in the diagram given as Figure 8.9, which includes the time domain signal with its spectrum for the configuration shown in Figure 8.8.

The quarter space is the simplest configuration for which pulse-echo measurements can be made. However, when only a single transducer is used, a reference signal can only be provided by that reflected on a configuration such as the quarter space. Some of the possible problems associated with the use of a reference reflected signal are now considered.

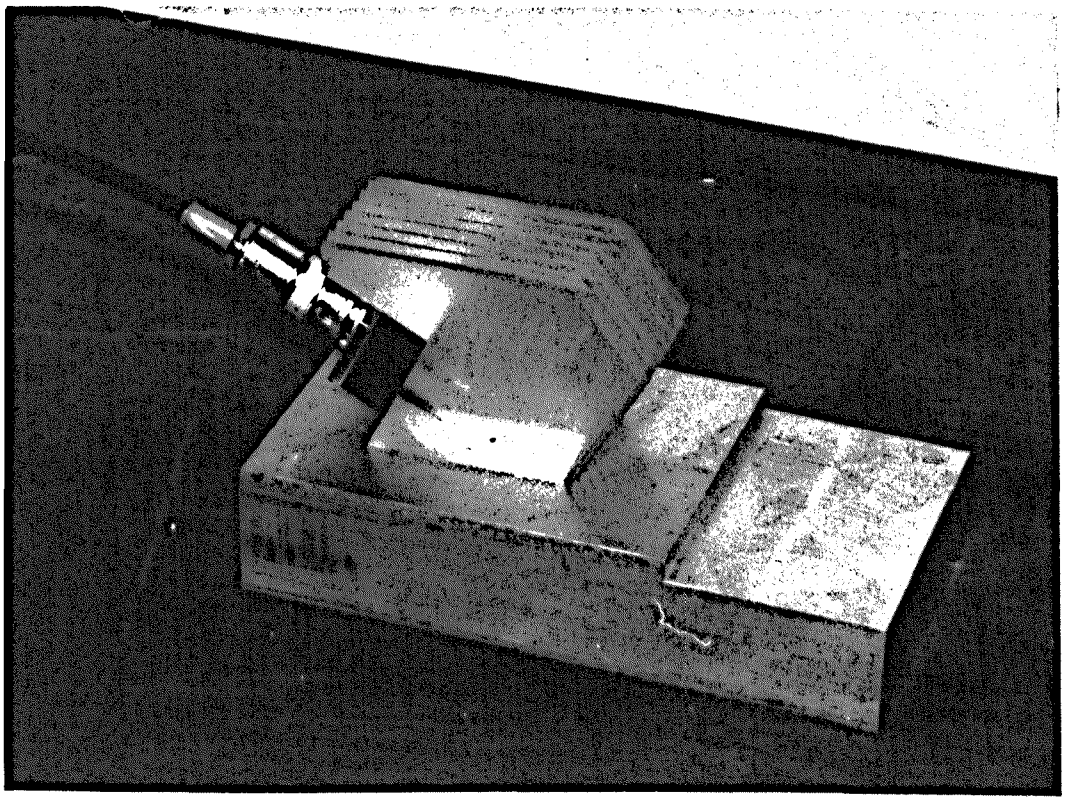

A wedge transducer on an aluminium block with a down step, in pulse-echo mode.

FIGURE 8.8.

To investigate the effect of transducer alignment with a corner, a series of measurements were made on a quarter space with angles of incidence from 80° to 100° and the time domain signals were plotted every 2½°, and these are shown in Figure 8.10. It is seen from the signals in Figure 8.10 that that there is a region of about 2½° which gives a uniform response for measurements made at a distance of 30 mm.

In all experimental ultrasonic measurements, where the reflected time domain signal is to receive further analysis, amplification or to be digitally recorded, a time gate is used to select the section of signal of interest. However, in the case of the application of spectral analysis the correct position and length of the gate is important as a gate position or length error will distort the resulting spectrum. If the gate is too narrow the end of the signal can be lost or if it is too wide, background noise is introduced which distorts the spectrum.

The effect of the gate applied to the time domain signal is

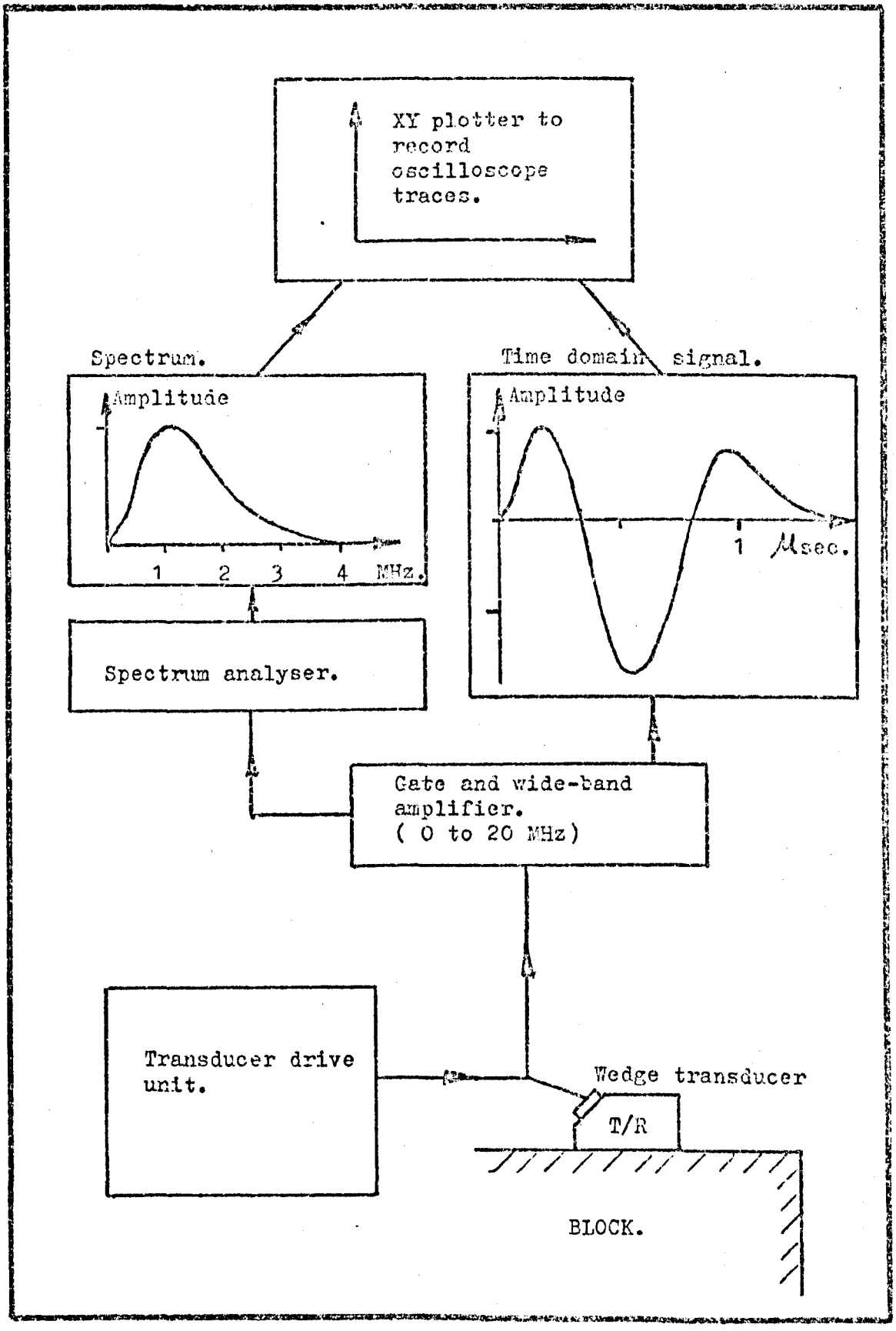

Experimental system for pulse-echo measurements using a wedge transducer, showing time domain signal and spectrum for reflected pulse on an aluminium quarter space.

FIGURE 8.9.

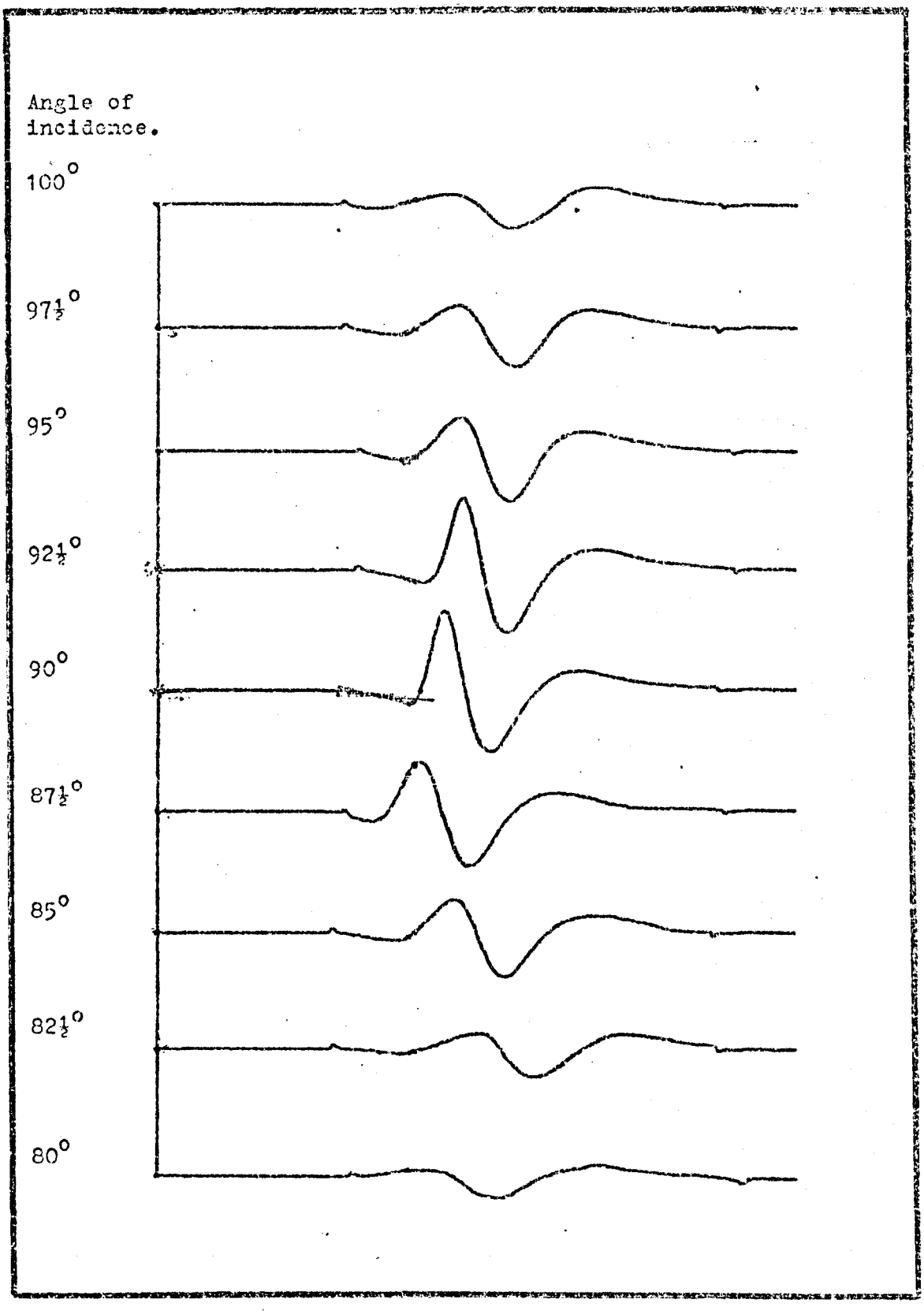

Time domain signals for a wedge transducer on aluminium for pulses reflected at a 90° corner, for angles of incidence from 80° to 100°.

FIGURE 8.10.

illustrated by the time domain signals and spectra for pulses on a quarter space with a wide and with a narrow gate, as shown in Figure 8.11. The optimum setting for the gate width and position can only be established by the operator making a series of measurements.

A further variable parameter in practical measurements is that of couplant thickness. It is important that enough couplant is used to give good signal transfer but that the layer is kept thin. It is also important, in the case of single probe transducer measurements, that a constant couplant thickness can be achieved if measurements are to be made on several test blocks and pulse amplitudes are to be compared.

There are therefore several problems which limit the use of simgle probe pulse echo measurements, some of which can be overcome by the use of a guide on the test block to give transducer alignment, making a series of measurements to set the gate width and position and the use of a clamp to give a constant loading and couplant layer for the transducer.

b. Two transducer methods on the quarter space.

The problem of the lack of a referance signal which is experienced in single transducer measurements can be overcome by the use of a receiving transducer placed between the transmitter and the corner of target. The receiving probe then measures the transmitted signal as it passes before interaction and the reflected signal after scattering.

The effect on the signals on a quarter space, by the introduction of a Harnik type probe was investigated. The pulse-echo signal of a wedge transducer was measured and it was then measured when a Harnik type transducer had been put in position. The resulting time domain signals are shown as Figure 8.12. The time domain signals on a quarter space as given by a wedge transducer and Harnik type probes are shown in Figure 8.6.

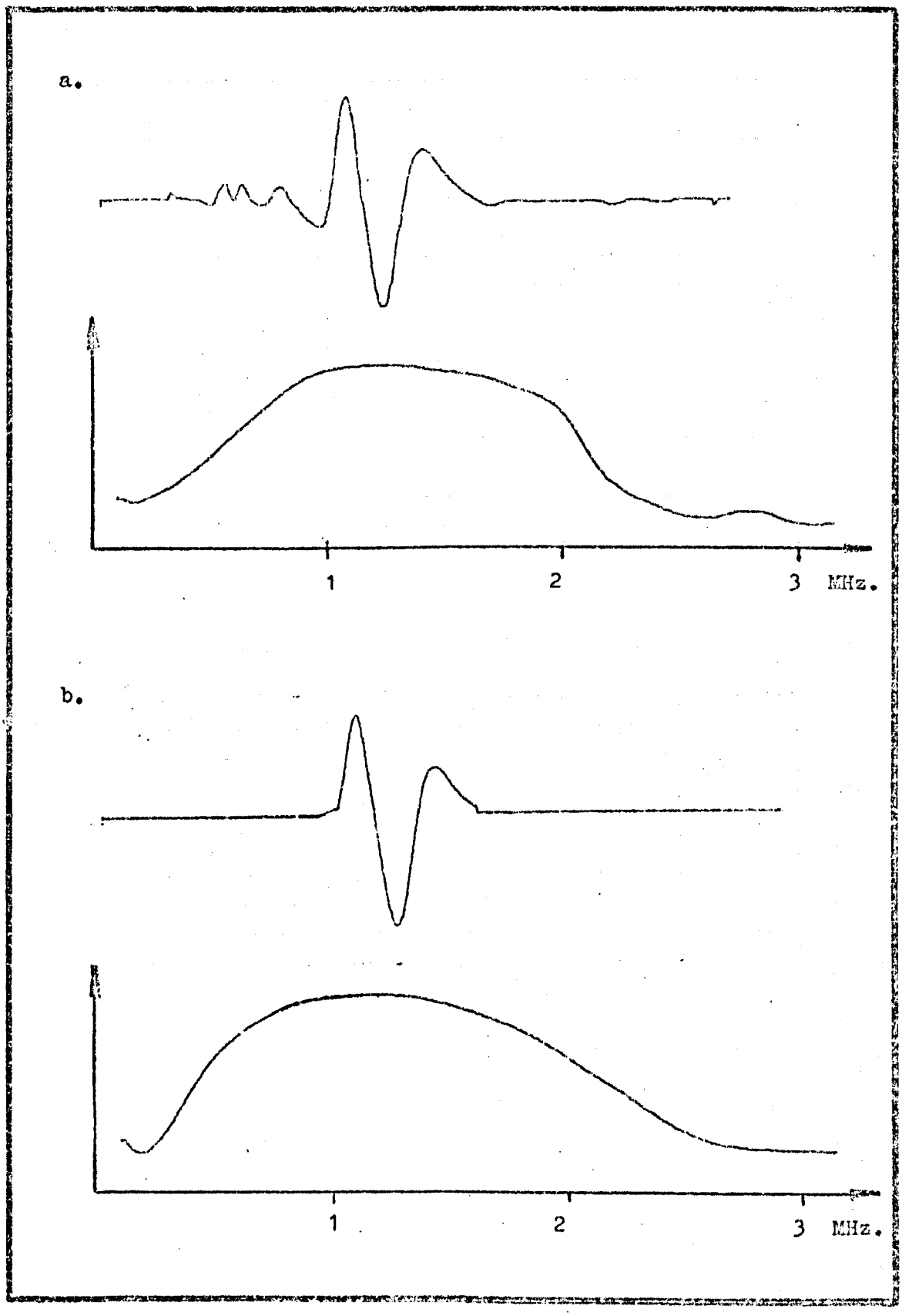

Time domain signals and spectra for pulses on an aluminium quarter space; a. when using a wide gate (about 5 μsec.)
b. when using a narrow gate (about 1.2 μsec.)

FIGURE 8.11.

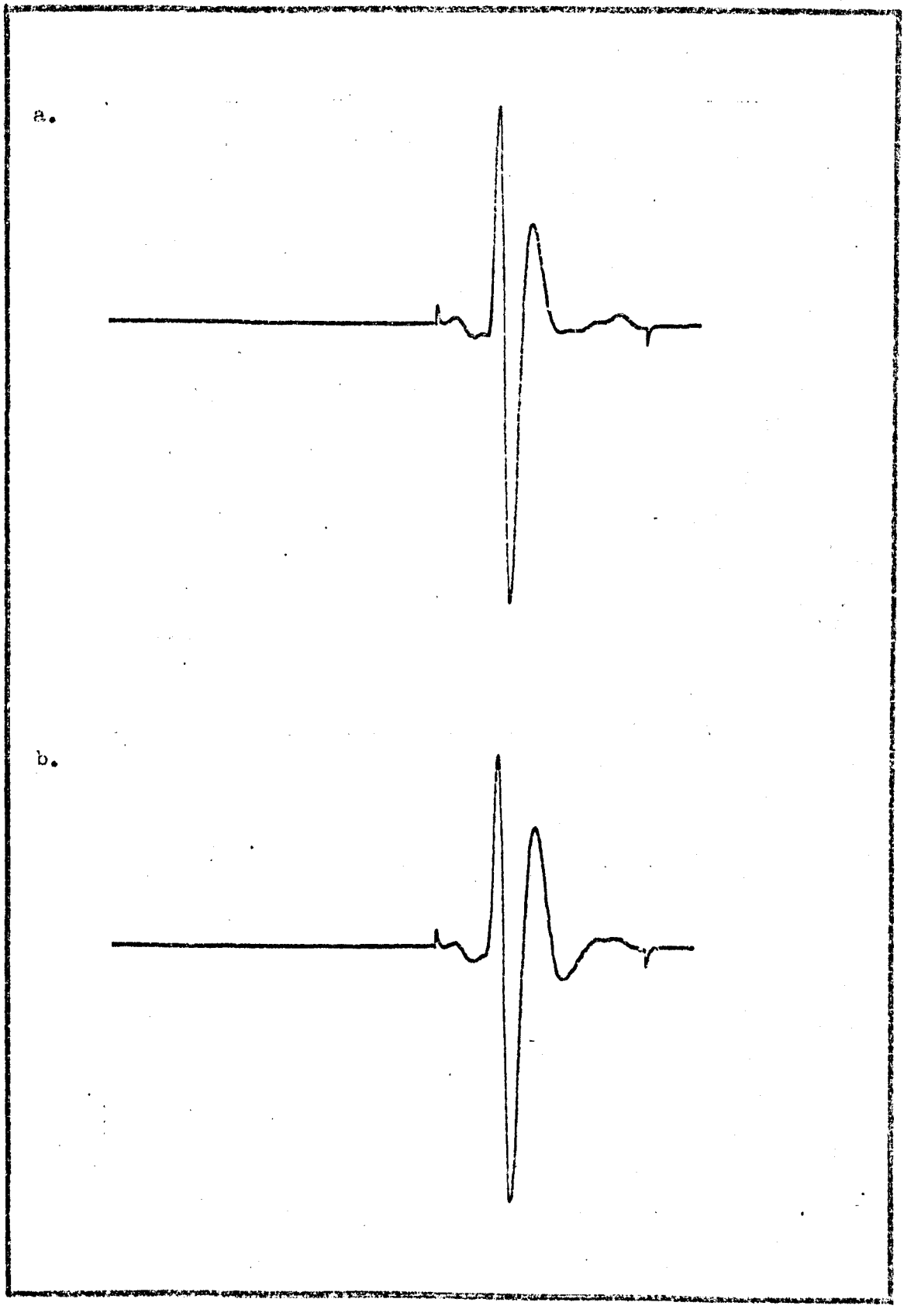

Time domain signals for pulses on a quarter space, as given by a a wedge transducer in pulse-echo mode; a. in normal pulse-echo. b. when an Harnik-type transducer is placed in position for use in two probe mode.

FIGURE 8.12.

8.4 Experimental measurements with Rayleigh waves.

This section describes the main series of experiments that were performed using two probes, a wedge transducer as transmitter and a Harnik type probe as receiver, and to provide experimental results to test those given by the numerical models and presented in Section 7.

The basic method used in the experiments is described in Section 8.4.1. The configuration upon which measurements were made are shown inFigure 8.13, and each is considered in Sections 8.4.2 to 8.4.7. The range of experimental blocks available in the present study included some of those used by Morgan (1973).

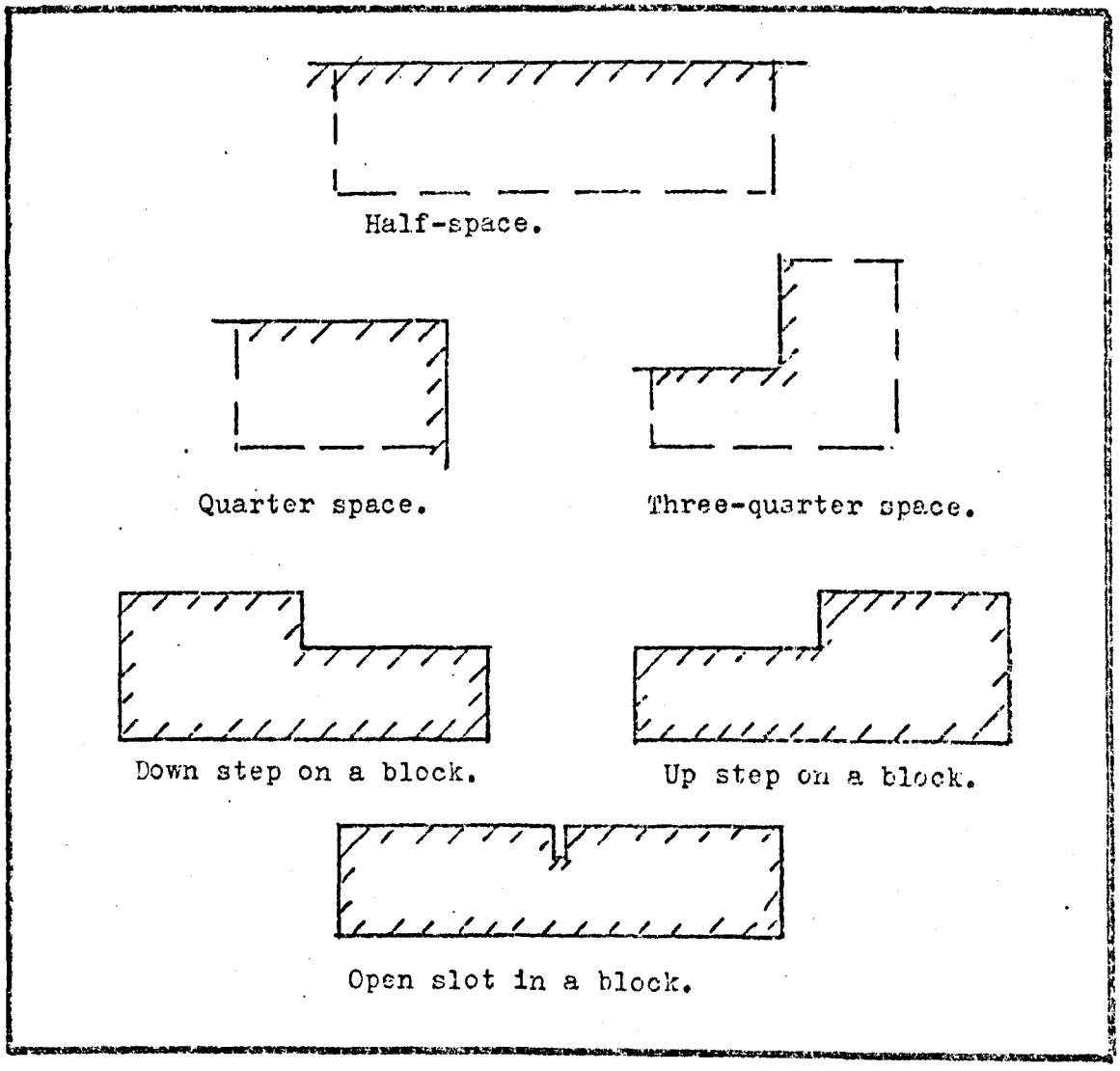

Geometries on which experimental measurements were made using Rayleigh wave pulses with 1 MHz centre frequency.

FIGURE 8.13.

8.4.1 Basic two probe experimental method.

The experiments described in Sections 8.4.2 to 8.4.7 all use the basic two probe methods with a wedge transducer as the transmitter and a Harnik type probe as the receiver, in either a reflection or a through-transmission mode. The basic transducer arrangements and the experimental system used are shown in Figure 8.14. The pulse generator, wideband gate, amplifier, spectrum analyser, the oscilloscopes and plotter are all part of the Central Ultrasonics Test Equipment of the Research Group in Ultrasonics and they have been described by Morgan (1973) and Weight (1975) and they are shown in the photograph shown as Figure 8.1.

The thyristor pulse generator is adjusted to give short time domain pulses, of length about 1 μsec, using a voltage of up to about 1,000 volts, with a pulse rate of about 750 per second. The transmitting, wedge type, transducer and the receiving probe, of Harnik type, are placed on the test block in either the reflection mode, which is shown as Figure 8.14a, or the through transmission mode, which is shown as Figure 8.14b. The received signals are then passed through the system shown as Figure 8.14. In the present study the wedge transducer had a pulse centre frequency of 1 MHz and the thickness of the disc in the Harnik probes was for a 10 MHz resonant frequency.

In the reflection mode the probe detects both the input and the reflected pulses so direct comparisons can be made. However in the through transmission mode only transmitted signals are detected so the system requires to be calibrated by measuring the input pulse and then moving the receiving probe to the through transmission position to measure the transmitted pulses.

The basic time domain signals, which are proportional to the free surface displacements, are displayed on an oscilloscope. The basic signal can be plotted on paper and or used to give a spectrum with the spectrum analyser, which can also be plotted.

The system shown in Figure 8.14 can be used in several ways to provide data to test the numerical models and this can be based on measurements in either the spatial or frequency domains. The available methods are illustrated by considering their application to study pulses on a quarter space.

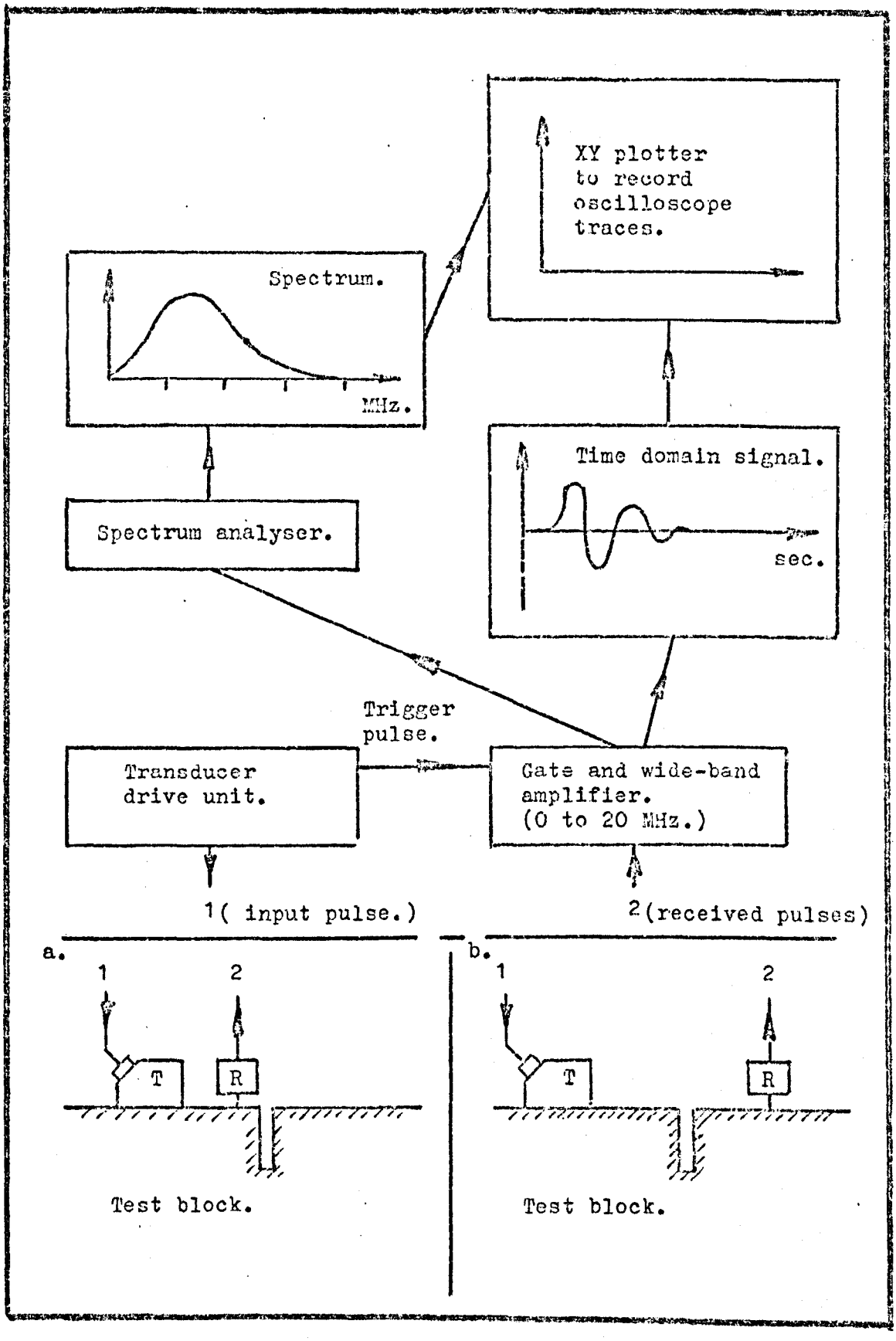

Experimental system for two probe measurements; With system transducers in a. Reflection mode, b. Through-transmission mode.

FIGURE 8.14.

a. Time domain measurements.

The reflected pulse on a quarter space can be measured by using the system in the arrangement shown as Figure 8.14a and using the wideband amplifier to give a constant maximum peak to peak signal for both the input pulse and the reflected signal.

The gate is used to select the input pulse and the amplifier setting is adjusted to give a convenient peak to peak amplitude on the oscilloscope. The amplifier setting, which is calibrated in decibels, is noted (I dB).

The gate is then moved to select the reflected pulse and the amplifier setting is again adjusted to give the same pulse peak to peak amplitude as for the input pulse. The amplifier setting is again noted (R dB). The amplifier settings are then used to calculate a reflection coefficient.

The transmitted pulse on a quarter space can be measured by using the system in the arrangement shown as Figure 8.14b, with the receiving probe on the other surface to the wedge transducer.

In transmission measurements, the input pulse is first measured with the receiving probe in the same position as for the reflected signal. The amplifier is adjusted, as for the reflection measurements, and the amplifier setting (I dB) is noted.

The probe is then moved to the second surface and reclamped with the same pressure to give the same couplant thickness. The gate is then adjusted to select the transmitted pulse and the amplifier setting is adjusted to give the same peak-to-peak amplitude for the pulse as the input pulse, and the amplifier setting (T dB) is noted. The amplifier settings are then used to calculate a transmission coefficient.

b. Spectral measurements.

The method used to give scattering coefficients based on time domain signals has one very large weakness in that it is difficult to compare two signals when they have different shapes. If however the spectra are obtained comparison is made much easier.

The procedure used to measure signals, so that scattering coefficients can be calculated from the spectra, is similar to that used for time domain measurements except that the amplifier

is adjusted with reference to the spectral amplitude at one frequency in the spectrum for each measurement. A range of measurements can therefore be made at different frequencies with the transducers in the same positions.

From the values for the amplifier settings, reflection and transmission coefficients can be calculated.

c. The calculation of transmission and reflection coefficients.

The data required for the calculation of transmission and reflection coefficients are the amplifier settings, which are given by the methods set out as a. and b. above.

The amplifier settings give a measure of the pulses on a logarithmic decibel (dB) scale so that the scattering coefficients are not just simple ratios.

The reflection coefficient is calculated from the amplifier settings of I d' and R d' for the input and reflected pulses respectively.

$$R - I = (-)X \text{ dB} \qquad 8.4.1$$

where X is the drop in signal level, measured in dB

The reflection coefficient (R_c) is given by;

$$R_c = \text{antilog}\left[\frac{-X}{I}\right] = \text{antilog}\left[-Y\right] \qquad 8.4.2$$

where $Y = X/I$,

and hence;

$$R_c = \text{antilog}\left(\overline{1} + (1 - Y)\right) \qquad 8.4.3$$

A similar procedure is used to calculate the transmission coefficient (T_c), with T replacing R in equations 8.4.1 to 8.4.3.

d. Background noise.

In the practical measurements on test blocks it has been found that there is a lot of background noise which is recorded in the time domain signals. These pulses are due to resonance and body waves in both the wedge transducer and the test block.

The noise level in the time domain signals can be reduced by between 5 and 10 dB by the use of a damping material, such as plasticine, on the top and front surfaces of the wedge and on all the test block faces which are not used for measurements.

8.4.2 Rayleigh waves on half-spaces.

The propagation of Rayleigh waves on a smooth surface was investigated and both the pulse amplitude and shape were recorded. A wedge transducer was clamped to an aluminium bar with a smooth surface. The bar had a cross section of 30 by 100 mm and was 300 mm long, which when used with pulses of 1 MHz Rayleigh waves which have a wavelength of about 2.9 mm gives a good approximation to a semi-infinite half-space.

A guide rail was set beside the wedge transducer and a Harnik type probe was moved along the rail to give measurements of the pulse shape and amplitude with distance.

It was found that for distances up to about 100 mm (about 34 wavelengths) the pulse shape remained constant with the amplitude varying within ½ dB The largest errors in the system were those due to coupling the receiving probe and then moving it and recoupling.

8.4.3 Rayleigh waves on quarter spaces.

The quarter space is the simplest configuration for which reflection measurements can be made and it is one of the configurations used to give reference signals in pulse-echo mode.

The pulses on a quarter space were investigated by a series of measurements which were made with a 1 MHz short-pulse wedge transducer as the pulse transmitter and in the two probe measurements, Harnik-type probes as the receivers. The transducers used are considered in detail in Section 8.2.1.

a. Preliminary measurements.

A wedge transducer was placed in pulse-echo mode, using the system as shown in Figure 8.9, on an aluminium block with a new 90° corner. The reflected pulse time domain signals were then measured at several points along the edge and the signals measured at four points are shown as Figure 8.15a.

A series of measurements were then made on three different aluminium blocks with corners that were a. sharp, b. slightly rounded and c. with a corner that had a radius of about 2½ mm. The resulting spectra were plotted and are shown as Figure 8.15b. It is seen from the spectra, shown as Figure 8.15b, that as the

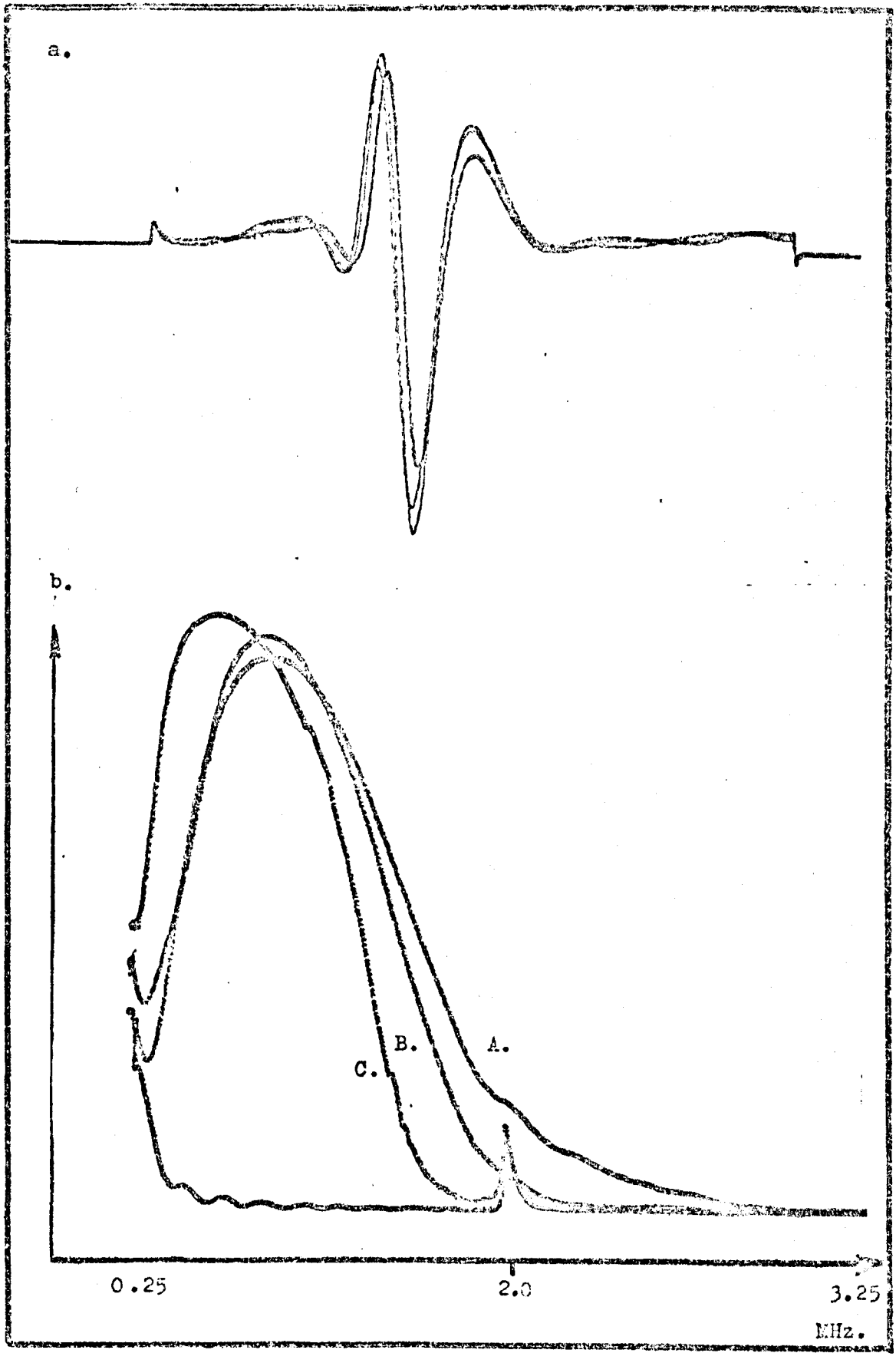

Time domain signals and spectra for pulses measured on aluminium quarter spaces in pulse-echo mode; a. Signals at four positions along a sharp edge with a 5 μsec gate. b. Spectra on spaces with A. Sharp, B. Slightly rounded, C. 2½ mm radius corners.

FIGURE 8.15.

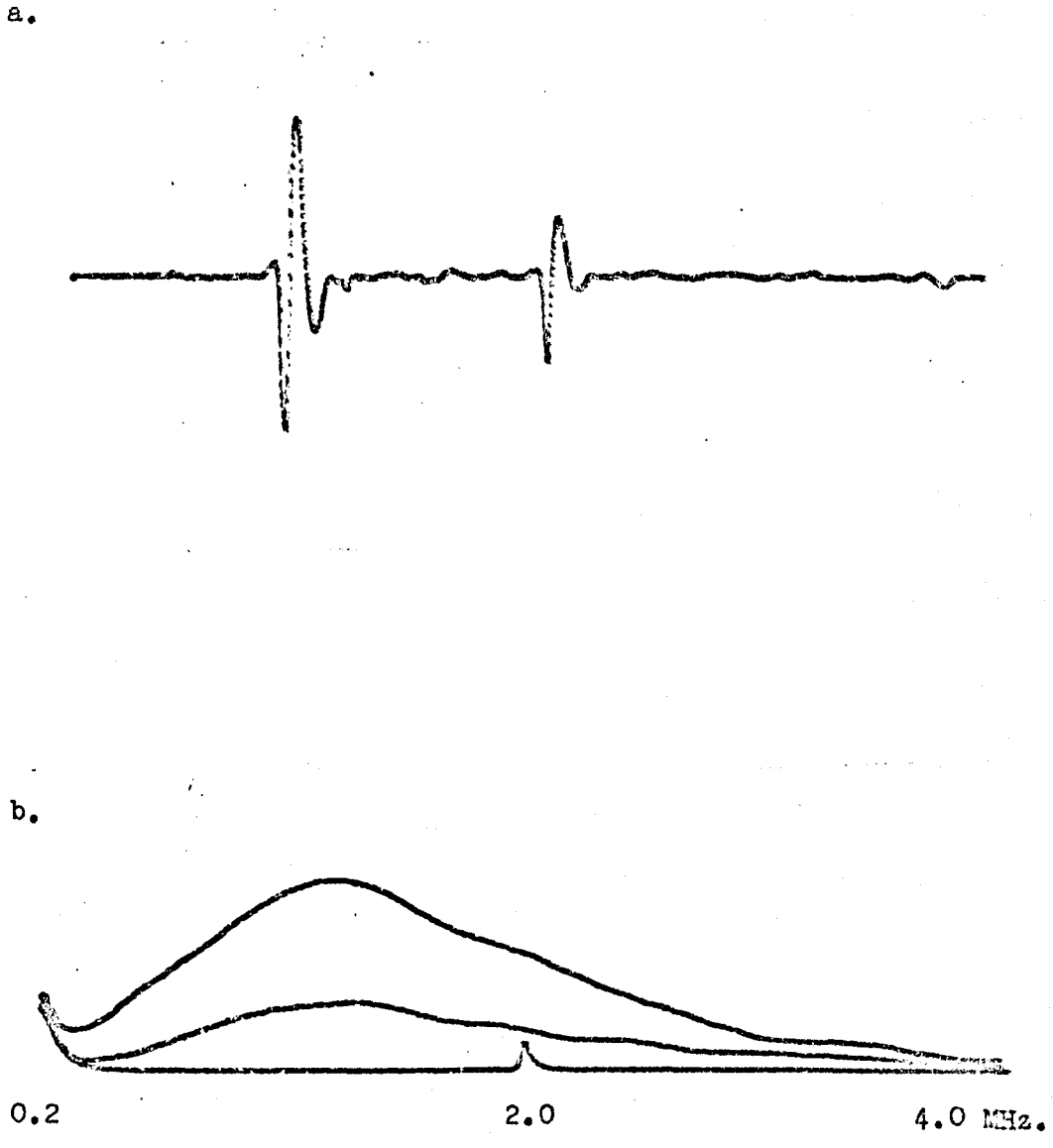

Time domain signal (a) and spectra (b) for input pulse and reflected pulse on an aluminium quarter space.

FIGURE 8.16.

radius of the corner is increased, the high frequency components, with wavelengths greater than about twice the radius of the corner are not reflected.

b. Transmission and reflection coefficients on quarter spaces.

Following the preliminary pulse-echo measurements, a series of sets of readings based on both amplitude and spectral signals were made to determine the transmission and reflection coefficients.

The basic method used was that set out in Section 8.4.1 with the system being used in both reflection and transmission mode, as shown in Figure 8.14. In the case of measurements in reflection mode the time domain signals and spectra for an aluminium block are shown as Figure 8.16.

The reflected pulses were measured on both aluminium and steel blocks and used to calculate the coefficients shown in Table 27. The transmitted pulses were also measured on both aluminium and steel blocks, but in the case of the measurements on steel the pulses suffered considerable distortion and attenuation due to surface roughness so only the aluminium results were used to calculate a transmission coefficient and this is shown in Table 27.

Material.	Reflection coefficient.	Transmission coefficient.
Aluminium	0.37±.05	0.60±.1
Steel.	0.43±.05	-

Transmission and reflection coefficients for pulsed Rayleigh waves at 1 MHz on steel and aluminium.

TABLE 27.

The larger errors were given for the transmission coefficient because the probe, when used to measure these signals, has been moved and recoupled after the measurement of the input pulse.

The experimental results are considered further and compared with those of the numerical models, which are presented in Section 7, and those of previous workers, in Section 9.3.

8.4.4 Rayleigh waves on three-quarter spaces.

Measurements were made on aluminium blocks to determine transmission and reflection coefficients for a three-quarter space, which is a 270° corner at the intersection of two free surfaces.

The scattering of Rayleigh waves, on three-quarter spaces, was investigated using the two transducer reflection and transmission methods, which are shown as Figure 8.14, and which are described for a quarter space in Section 8.4.3.

The measurements on three quarter spaces were restricted to blocks with sharp 270° corners as it was found that there was no reflected signal and there was less mode conversion to shear waves on blocks with even slight rounding at the corner.

The transmission and reflection coeffocients were calculated from the pulse amplitude data for time domain signals and spectra for waves on aluminium blocks and average values are given as Table 28.

Reflection coefficient	Transmission coefficient
$< 0.10 \pm .03$	$0.20 \pm .05$

Reflection and transmission coefficients for aluminium three-quarter spaces, measured with pulses with 1 MHz centre frequency.

TABLE 28.

The experimental results, presented as Table 28, are considered further and compared with those for the numerical models, which are presented in Section 7, and those of previous workers, in Section 9.4.

8.4.5 Rayleigh waves at down steps.

The down step is the simplest configuration which has a characteristic dimension and measurements were made to investigate the reflected and transmitted pulses.

A set of steps in aluminium blocks were made with depths up to 18 mm. The depths were measured with a travelling microscope and they were found to have depths along the step that were constant to $\pm .005$ mm.

a. Preliminary measurements.

A wedge transducer with a 1 MHz (3mm wavelength) centre frequency was placed on an aluminium block with a down step, of about 1.5 mm, in pulse-echo mode, at a range of 30 mm from the top of the step. The resulting reflected time domain signal is shown as Figure 8.17 together with the reflected signal for a quarter space measured with the same transducer at the same range. In Figure 8.17 the quarter space signal is shown with the time axis X2 compared with the down step signal.

It is shown in Figure 8.17 that the down step reflected pulse is more complex than that for a quarter space but the signals from the 90° and the 270° corners cannot be resolved in the time domain. It is found for steps with depths up to about 1.75 wavelengths, even with short pulses, that the reflected pulse is a mixture due to the interactions at the 90° corner, on the vertical free surface, and at the 270° corner.

b. Transmission and reflection coefficients.

Measurements were made in the two probe reflection and through transmission modes, shown in Figure 8.14, for a series of down steps to cover a range of step height to wavelength ratios up to 2. The details of the experimental methods are presented in Section 8.4.1.

It was found that when amplitude data was used to calculate reflection and transmission coefficients there were large variations at a given step height to pulse centre wavelength ratio. However this scatter in the results could be reduced by using spectral amplitude data at a series of frequencies for each step. Measurements were made in the range of frequencies from 0.75 to 2.0 MHz for a range of steps and the resulting transmission and reflection coefficients are shown as Figure 8.18.

From the experimental points plotted in Figure 8.18 it is seen that for the reflection coefficient plotted against step height, in wavelengths, there is an indication of a peak in the region about 0.6 h/λ and a trough in the region near 0.9 h/λ. The general shape of the relationship is shown by the dashed line. It is also seen in Figure 8.18 that there is significant scatter in the results for values of h/λ above about 0.65.

For the case of the results for the transmission coefficients which are also shown in Figure 8.18, it is seen that the values of

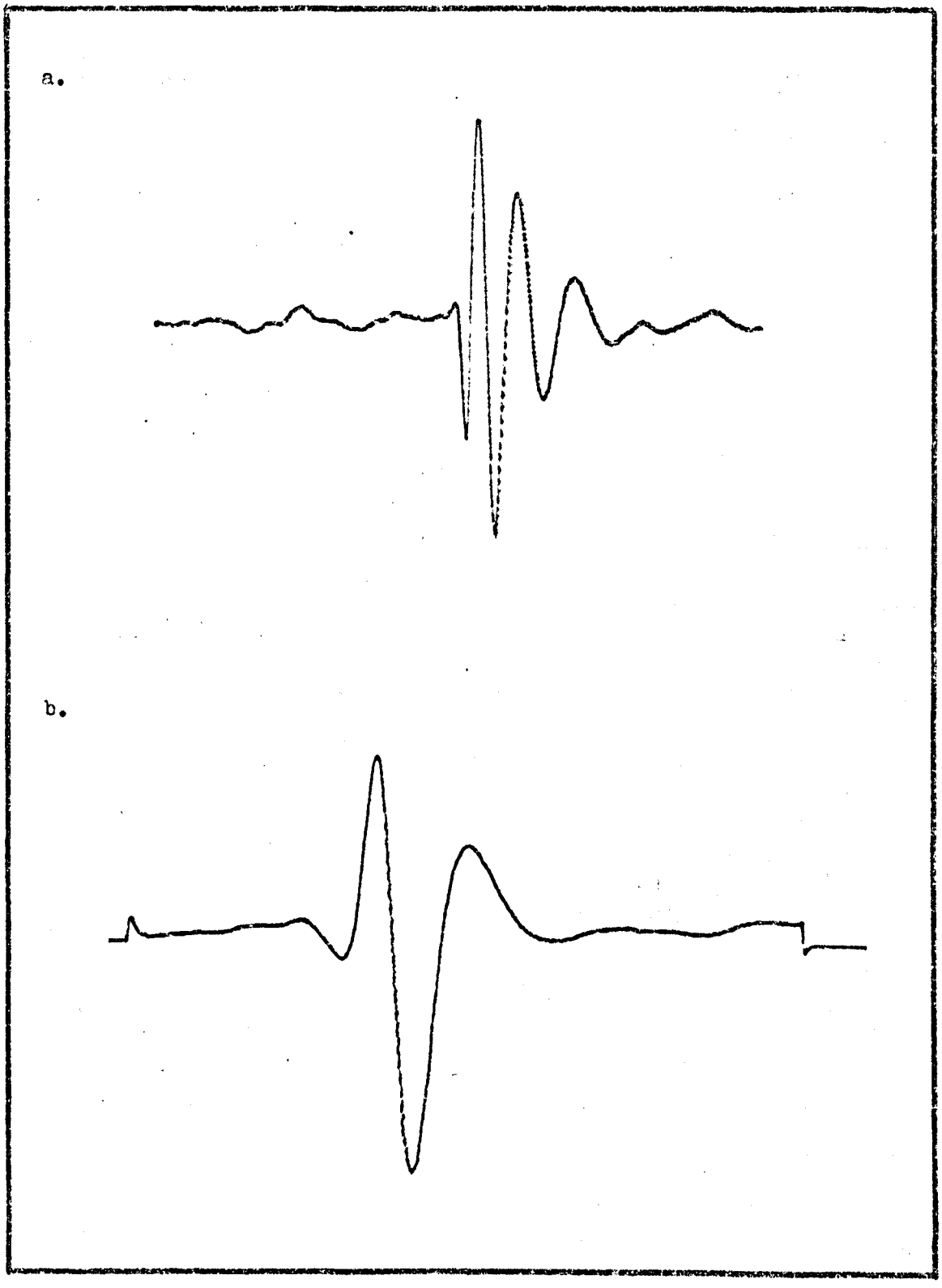

Time domain signals for the same Rayleigh wave pulse, reflected from;
a. a half wavelength down step (1.5 mm deep)
b. a 90^{o} corner. (For trace b. the time axis is expanded X2)

FIGURE 8.17.

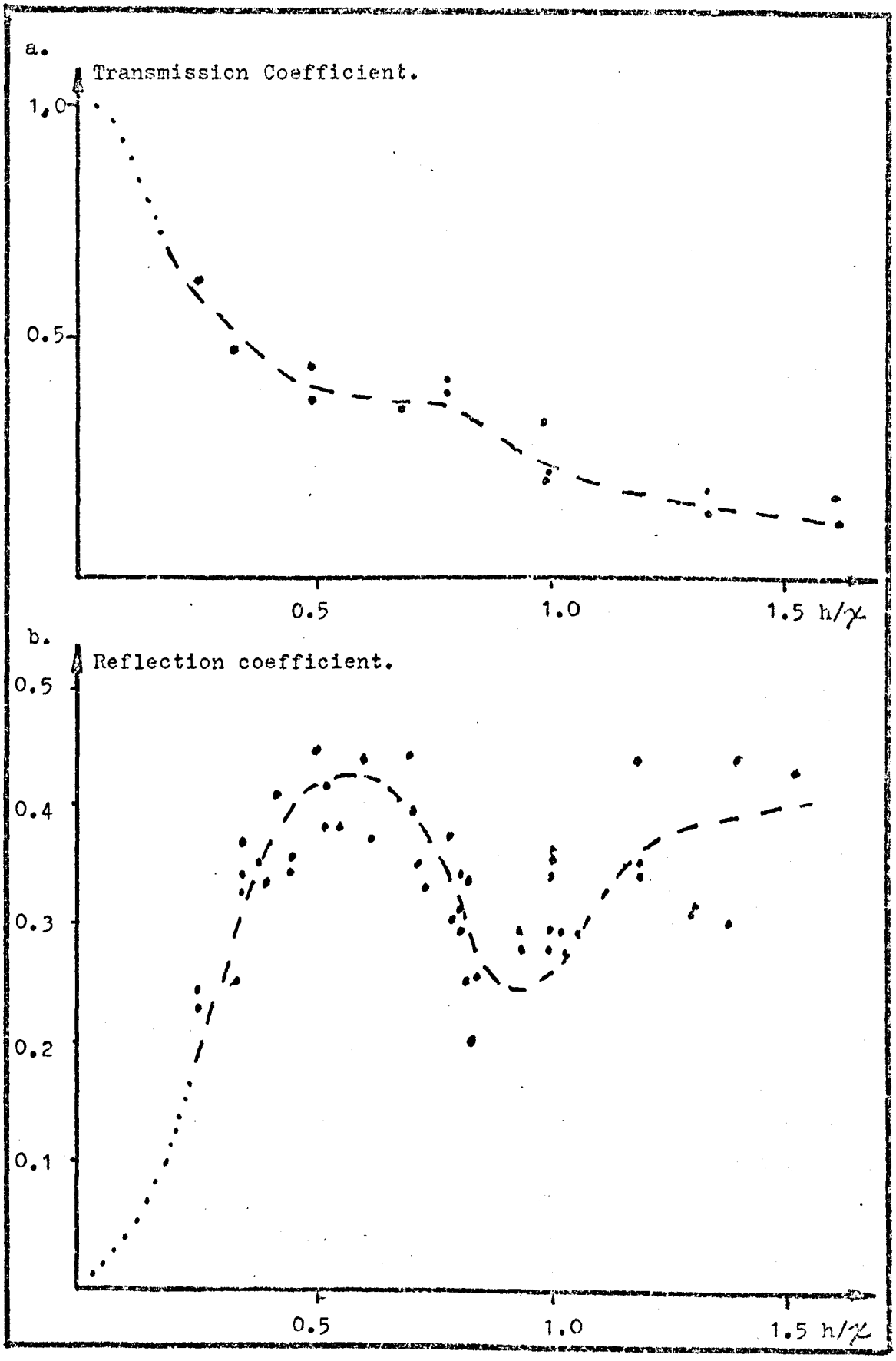

Experimental transmission and reflection coefficients for down steps on aluminium blocks, plotted against the step height to wavelength ratio, measured in two probe reflection mode with input pulses of 1 MHz centre frequency

FIGURE 8.18.

the coefficient reduce as the step height to wavelength ratio value increases, with a small hump in the general trend, which is shown as a dashed line, in the region of .75 h/λ.

The results shown as Figure 8.18 are considered further and compared with the numerical results and those of previous studies in Section 9.5.

8.4.6 Rayleigh waves at up steps.

The up step is a vertical rise, which when combined with a down step forms an open slot. Therefore the study of the waves at an up step should provide an understanding of those which occur at the up side of a wide slot.

a. Reflection measurements.

The two probe method that was used for the three-quarter space, which is described in Section 8.4.4, was used to measure the reflected and input pulses for a series of different height up steps and the resulting reflection coefficients were the same as that for an aluminium three-quarter space, which is given in Table 28.

b. Transmission measurements.

The transmitted pulses at up steps were investigated using the probe arrangement shown in Figure 8.19a, and the system in the configuration shown in Figure 8.14.

The time domain signals given by the Harnik-type probe at a series of positions on the upper surface at several shallow up-steps. It was found that at the top of the step there was a pulse with a complex time domain shape and that the energy in this pulse increased at the probe was moved away from the corner. The path by wich the energy was reaching the upper surface was investigated by placing damping material on the surface of the test block at the corner to remove the Rayleigh wave component. Energy was still detected on the upper surface and a pulse was found to grow as the probe moved away from the corner.

To test the idea that energy was reaching the upper surface after mode-converting into a shear wave and passing through the bulk material and then remode-converting at the upper surface, measurements were made on a 6mm (2 wavelengths at 1MHz) up-step.

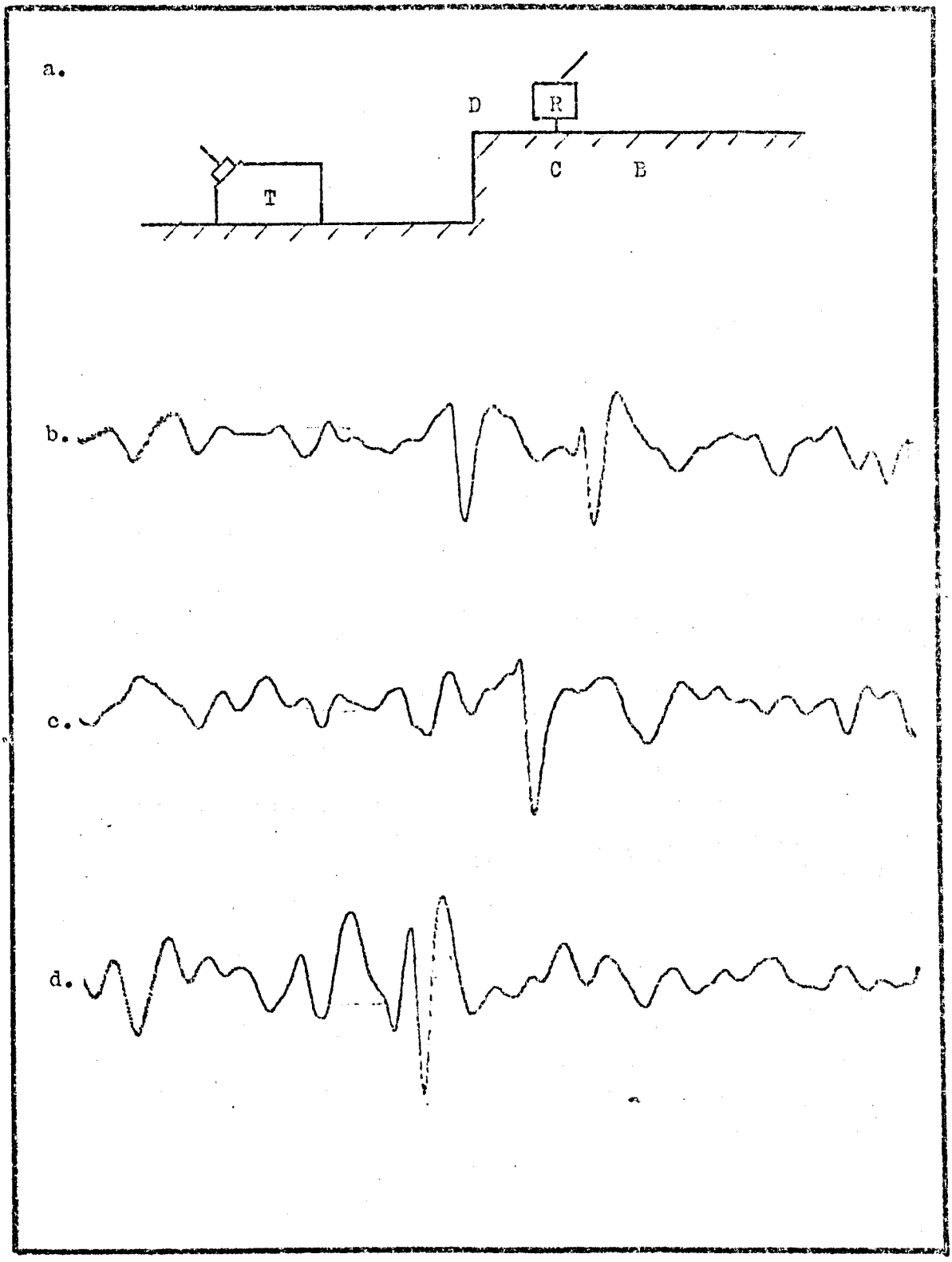

Experimental Rayleigh wave pulses at up steps. a. Basic transducer arrangement. Time domain signals for transmitted pulses at 6 mm steps on aluminium blocks, for pulses with a 1 MHz centre frequency. b. For R at point B, 10 mm from corner. c. for R at point C, 5 mm from corner. d. For R at top of corner.

FIGURE 8.19.

With the probe arrangement shown in Figure 8.19a the time domain signals received by the Harnik-type probe in positions B,C,and D were plotted and they are shown as Figure 8.19 b,c, & d. At the point B two pulses of Rayleigh waves are detected. When damping material was placed at the 90° corner the pulse R was removed from the signal recorded at point B. At the point C, which was a distance of about 5 mm from the corner, the body wave, which reconverts to a Rayleigh wave, was lost from the recorded time-domain signal. At the point D a complex signal is recorded.

The point where the mode-converted signal was detected, measured from the top of the step, was detected for pulses on blocks with deep steps and the resulting distances along the top surface, with the step height are shown as Table 29.

Step in mm.	Point where mode converted pulse detected.
6	5 mm
12	9 mm
18	15 mm

Distance from top of step where mode converted pulse pulse was detected on upper surface, using a pulse with 1 MHz centre frequency on aluminium blocks.

TABLE 29.

The results for pulses of Rayleigh waves at up steps are considered further and compared with those of the numerical models and previous studies, in Section 9.6.

8.4.7 Rayleigh waves at open slots.

The open slot is an idealised crack configuration and so the results from its study should provide a base for the understanding of the scattering of Rayleigh waves by real features.

a. Preliminary measurements.

A wedge transducer with a 1 MHz centre frequency was used in pulse-echo mode, with the experimental system shown in Figure 8.9,

to give the time domain signals for the pulses reflected at 90° corners and a 1.01 mm deep and .85 mm wide open slot. The resulting time domain signals are shown as Figure 8.20. For slots with depths up to about 1.5 wavelengths, even with short pulses, it is not possible to resolve the scattering centres in the time-domain signals and because of the pulse-shape changes on reflection, there is considerable scatter in reflection coefficients based on amplitude data.

b. Slot depth measurement.

The depth of a slot normal to a free surface can, at least in principle, be determined by measurements of the reflected and transmitted pulses. However in practice amplitude based measurements are subject to large experimental errors (up to about 20 %).

A method of depth measurement which is not subject to amplitude errors is to measure the travel time of the mode-converted shear wave from the slot tip. (after Silk 1976) A further method is to detect the pulse on the upper surface and measure the distance from the corner where the shear pulse vanishes. This is using the results of the up step measurements, given in Table 29 to calibrate the depth of the feature. The distance from the top of a slot where the shear wave mode conversion was detected was used to measure the depth of a known 5 mm deep and 1 mm wide slot. The results are presented as Table 30.

Actual slot depth.	Shear wave detected, distance from slot.	Depth from up step results.
5 mm	4.5 mm	5.4 mm ±.5

Depth of a slot measured using mode conversion point of a shear wave from slot tip, with up-step calibration.

TABLE 30.

The results for open slots are considered further, together with those from the numerical models and previous studies, in Section 9.7.

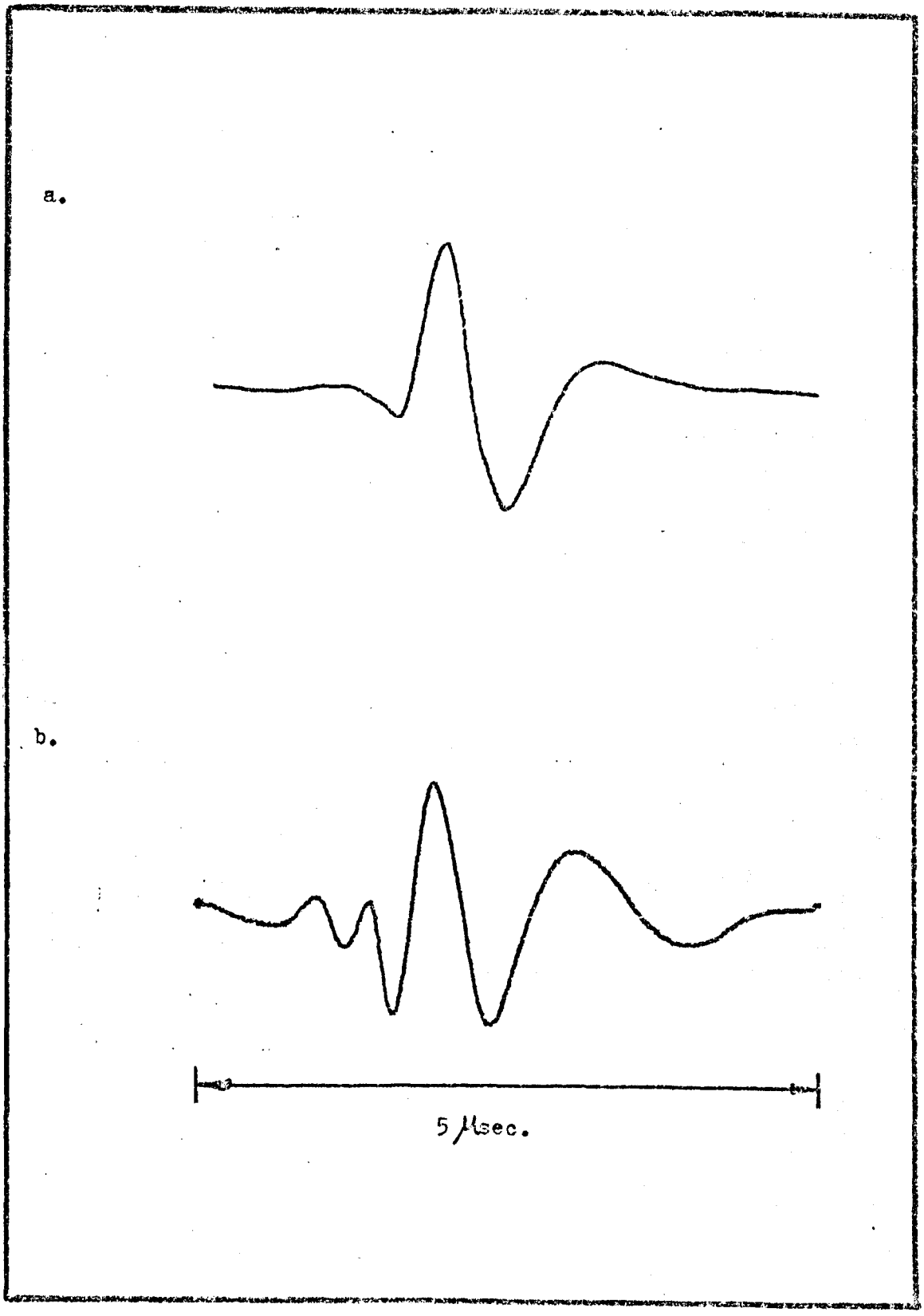

Experimental pulses of Rayleigh waves measured on aluminium blocks in pulse-echo mode with a wedge transducer of 1 MHz centre frequency; For the reflected pulse on, a. a quarter space. b. from a 1.01 mm deep and 0.85 mm wide open slot.

FIGURE 8.20.

9. COMPARISON AND ANALYSIS OF RESULTS.

9.1 Introduction.

This section reviews both the numerical model results, which are presented in Section 7, and the experimental measurements, which are presented in Section 8, made in the present study and compares the results with those of previous studies, where they exist.

The configurations considered in this section are shown in Figure 9.1, which also indicates the section in which they are considered.

Based on the experience gained with Rayleigh waves in the present study the author proposes, in Section 9.11, a development of the methods for defect characterisation using Rayleigh waves which makes use of the new transducer invented by Harnik (1977) and used by the author in the present study.

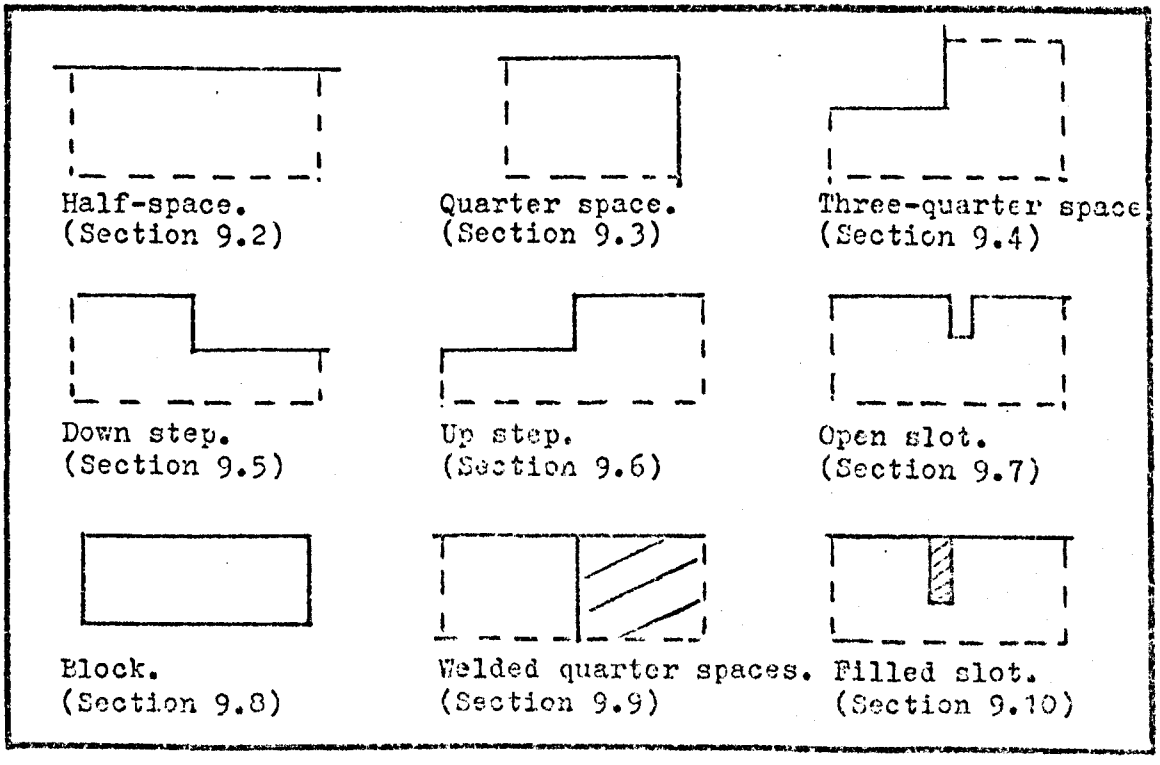

Configurations for which Rayleigh wave propagation and scattering have been investigated in the present study.

FIGURE 9.1.

9.2 Rayleigh waves on half-spaces.

The half-space or free surface, is a configuration on which Rayleigh wave propagation is of prime importance. This is because it is one of the few cases for which Rayleigh wave propagation is described analytically and experimentally. The sucessful modelling of waves in this configuration is therefore a prerequsite for the modelling of all other configurations.

a. Analytical theory.

The basic theory which has developed from the work of Lord Rayleigh (1885) specifies that for a homogeneous, isotropic half-space the propagation of a Rayleigh wave pulse is non-dispersive. This results in the propagation of a pulse the shape of which does not change with distance travelled.

An introduction to the analytical theory for the case of harmonic Rayleigh waves was given in Section 2.3, with extensions to pulse theory being made in Section 4.4.1 and Appendix H.

b. Experimental results.

In the present study a series of experimental measurements were made and these are reported in Section 8.4. For aluminium blocks with smooth surfaces it was found that with 1 MHz centre-frequency pulses of Rayleigh waves the waves would travel over distances up tc about 10 cm (about 4 wavelengths) with no systematic attenuation or pulse-shape change. It was found that in this region that larger changes in pulse amplitude occurred due to coupling errors than due to attenuation.

For pulses of ultrasound it is found that typical values for attenuation are of the order of 0.02 to 0.06 dB per mm. In the present study over distances of about 10 cm, a drop in signal amplitude of 5 to 6 dB was measured.

When longer wavelengths are used, pulses will propagate over rough surfaces, as is shown in the work by Cole (1977) who used electromagnetically induced Rayleigh waves at between 25 and 35 kHz on hot billets.

c. Numerical results.

The results of previous numerical work by Munasinghe (1973), for the propagation of a Ricker-type pulse of Rayleigh waves on a half-space, has shown that when using a pseudo-mode formulation

for the boundary nodes, at 35 nodes per wavelength, that for distances up to 5 wavelengths, in the first half-wavelength below the surface, amplitude errors in the wavenumber spectrum appear to be random and in the range of wavenumbers from 0.5 to 2. K/K_o they were found to be less than 2 %.

It has been found by Munasinghe (1973) that the higher frequency components in the pulse move at a velocity lower than the Rayleigh wave velocity and the velocity error against frequency curve is shown as Figure 9.2. It has also been found, by other workers and in the present study, that when using the pseudo-node formulation for the boundary conditions that the larger distortions occur in the vertical component of displacement.

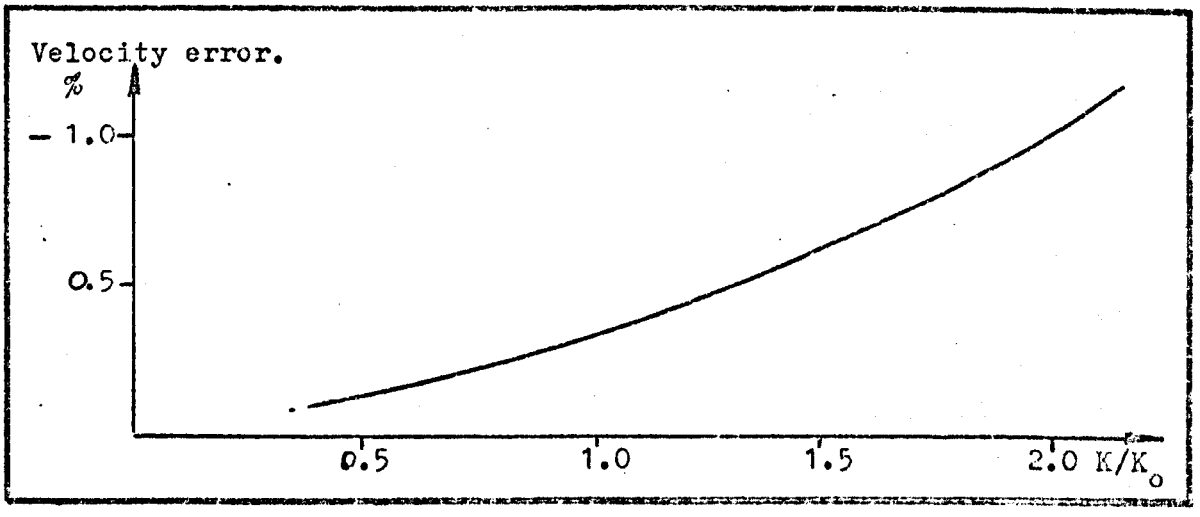

Velocity error found in range of normalised wave number values by Munasinghe (1973), using pseudo-node scheme.

FIGURE 9.2.

In the present study two numerical models of Ricker-type pulses on half-spaces were produced. The first model, the results from which are presented in Section 7.2.1, used the same pseudo-node formulation for boundary nodes as Munasinghe (1973) and the second model, the results from which are presented in Section 7.3.1, used the new composed second order formulation for the boundary nodes, after Ilan and Loewenthal (1976).

Using the pseudo-node scheme it was found that the errors in the present study at 32 nodes per wavelength were much the same as those reported by Munasinghe (1973) when using 35 nodes per wavelength. For the model runs performed using 16 nodes per wavelength the results of spectral measurements were found to be very inaccurate. It was also found that there were changes in

pulse spatial shape that only remained within 10 % of the value for the corresponding point on the input pulse up to about 100 iterations. The errors of all types were found to increase when higher Poisson's ratio material data were used.

Using the new composed second order formulation for the boundary nodes and 16 nodes per wavelength it was found that the pulse shape changes were minimal over distances up to about 4.5 wavelengths, for which measurements were made. Over this distance it was also found that the pulse position, compared with that calculated from the wave velocity and the model time increment, were in agreement to better than 0.5 %, and the obvious lag present in pseudo-node models was absent.

d. Conclusions.

The numerical model produced in the present study, using the new composed formulation for the boundary nodes has been found to give non-dispersive propagation of pulsed Rayleigh waves using half the number of nodes per wavelength, 16 as compared with 32, required in previous studies. This results in the use of a quarter of the number of nodes for a model of the same size half-space, measured in wavelengths. Also the new second order scheme gives the pulse distance travelled in much better agreement with that given by the wave velocity and the model time increment, within 0.5 %, and without the pulse position lag found with pseudo-node schemes.

The model with the new composed formulation for the boundary nodes provides a model that will give nondispersive propagation of pulses over distances of the same order as those for experimental measurements.

9.3 Rayleigh waves on quarter spaces.

The quarter space configuration has a 90^{o} corner at the intersection of two free surfaces. The propagation and scattering of Rayleigh waves on quarter spaces has been considered by a number of workers and a summary of their results, with those of the present study, are presented as Table 31.

The values given for the reflection and transmission coefficients that are presented in Table 31 are plotted against Poisson's ratio and shown as Figure 9.3. The symbols used in Figure 9.3 to indicate the source of a result are the first letters

Source.	Poisson's ratio	Transmission coefficient.	Reflection coefficient.	% mode conv. Loss.
a. Theoretical				
Mal & Knopoff (1966)	0.25	0.46	0.40	63
Viswanathan et al (1971)		0.76	0.56	12
Viswanathan & Roy (1973)		0.34	0.56	58
b. Experimental				
de Bremaecker(1958)	0.17	0.63 ± .06	0.38 ± .04	46
Knopoff & Gangi (1960)	0.266	0.73 ± .02	0.27 ± .02	41
Viktorov (1962)	0.34	0.70	0.65	10
Pilant et al (1964)	0.25	0.67	0.25	
Haydl (1974)		0.64	0.36	
Cuozzo et al (1977)	0.2	-	0.25	
"	0.34	-	0.33	
"	0.34	-	0.35	
"	0.36	-	0.38	
Present study	0.29	-	0.43 ± .05	
	0.34	0.60 ± .1	0.37 ± .05	
c. Numerical				
Alsop & Goodman (1972)	0.25	0.645	-	
Munasinghe & Farnell (1973)	0.245	0.64 ± .02	0.36 ± .02	45
Cuozzo et al (1977)	0.17	0.67 ± .03	0.26 ± .02	
"	0.25	0.72 ± .03	0.27 ± .02	
"	0.34	0.72 ± .03	0.42 ± .03	
Present study (pseudo-node model)	0.24	0.65 ± .05	0.39 ± .05	43
(full results are given in Table 15) (Section 7.2.2.)	0.29	0.47 ± .05	0.56 ± .05	47
	0.34	0.64 ± .05	0.49 ± .05	35
Present study (Second order model)	0.24	0.57 ± .05	0.43 ± .05	50
	0.34	0.59 ± .05	0.47 ± .05	44

Transmission and reflection coefficients on quarter spaces.

TABLE 31.

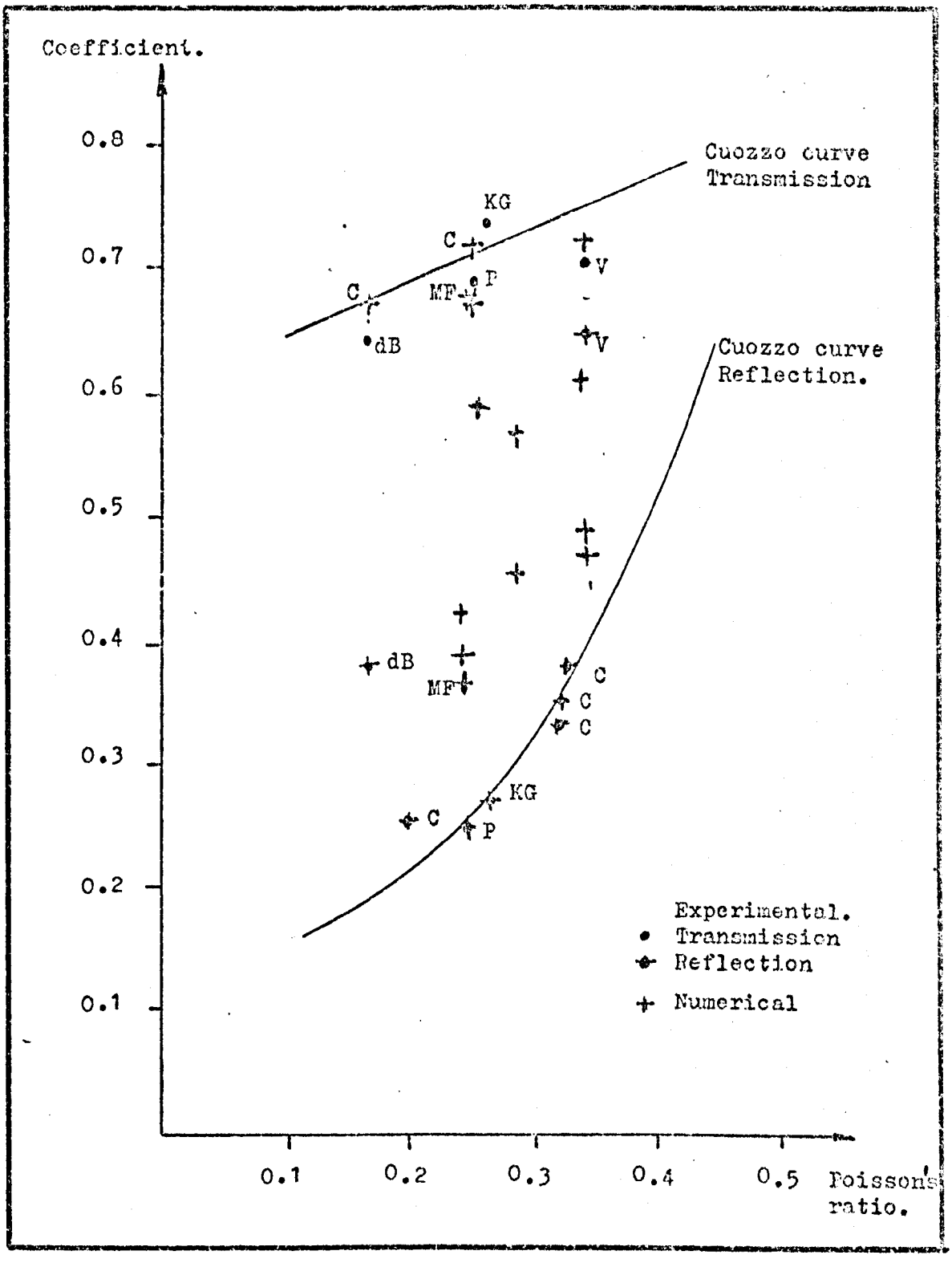

Experimental and numerical transmission and reflection coefficients for Rayleigh waves on quarter spaces. Results are shown without uncertainty which is up to about ± 0.5 on all results.

FIGURE 9.3

of the name of the author of the source paper.

a. Analytical studies.

Although, as was shown in Section 2.4.2, there have been several attempts to provide an analytical description of the scattering of Rayleigh waves on quarter spaces and calculate scattering coefficients, no full solution has been provided. In a recent paper by Ottaviarni (1971) she has commented that the analytical solution of Rayleigh waves on a quarter space presents almost insurmountable difficulties.

The weaknesses in the analytical theory are due to the complications that scattering occurs not only at the corner but also at a section of the vertical surface to a depth of about two wavelengths. Also at the actual corner, the boundary conditions for both free surface apply, which causes the problem to be over conditioned.

b. Experimental studies.

The previous studies on the quarter space fall into two groups which are firstly, those which make amplitude measurements to calculate scattering coefficients and, secondly, those which visualise the waves in transparent models.

From the results of the amplitude measurements, listed in Table 31 and shown on Figure 9.3, it is seen that there is considerable scatter. Also direct comparisons between the results of the different studies is complicated by the different methods and materials used.

From the results of the present study, as reported in Section 8, it was found that scatter can be introduced into the results by such factors as transducer alignment and the sharpness of the corners.

From the visualisation studies, such as that by Hall (1976), it is seen that the basic pattern for the mode converted pulses was compressional and shear waves, which radiate from the corner, PS waves which are due to the mode conversion of the compressional wave at the free surface and transmitted and reflected pulses of Rayleigh waves.

In only one study, that by de Bremaecker, was an estimate of the energy in each of the shear and compressional waves made, and he gave figures of 26 % and 23 % of the input pulse energy in the shear and compressional waves respectively.

c. Numerical studies.

There have been several models produced for Rayleigh waves on quarter spaces and the results of these are presented in Table 31.

Two of the previous models have considered semi-continuous Rayleigh waves and these are the finite element study by Alsop and Goodman (1972), which provided a transmission coefficient, and the finite difference pseudo-node study by Cuozzo et al (1977), who produced the curves for reflection and transmission coefficients against Poisson's ratio which are shown in Figure 9.3.

The only previous study of pulsed Rayleigh waves is that by Munasinghe (1973) who only calculated coefficients with polystyrene ($\sigma = 0.24$) data.

In the present study two computer models were produced, one using pseudo-node formulations after Munasinghe (1973) and one with a second order formulation after Ilan and Loewenthal (1976).

The pseudo-node scheme was used to calculate coefficients for a range of material data with Poisson's ratios from 0.2 to 0.36 which are shown in Table 15. It is found that the main factors which influence the results are the basic finite difference formulation, the number of nodes per wavelength used, the size of the pulse, the distance travelled before the corner and the Poisson's ratio of the data used. It is also found that the errors are larger for higher Poisson's ratios and that the larger errors are found in the vertical component of displacement.

The second order scheme was used with 16 nodes per wavelength, as opposed to the 32 nodes per wavelength used with the pseudo-node scheme, to calculate coefficients with polystyrene and aluminium data. The results for the two schemes were found to have overlapping error bands. The second scheme achieved considerable savings in computer time.

d. Conclusions.

The general pattern of scattered waves on quarter spaces is now well established and confirmed by the results of the present study.

Although there is considerable scatter in the results for quarter spaces, both in previous and the present study, it is now possible to provide a model of this interaction and with further model and experimental measurements it would appear that scattering coefficients can be established.

9.4 Rayleigh waves on three-quarter space.

The three-quarter space is two free surface which intersect at a 270° corner. There have been several studies of this configuration and they have used analytical, experimental and numerical methods.

The results for the transmission and reflection coefficients for Rayleigh waves on three quarter spaces are presented as Table 32. and the results are plotted against Poisson's ratio in Figure 9.4. The point plotted in Figure 9.4 are identified by the first letter of the name of the author of the source paper given in Table 32.

Source.	Poisson's ratio.	Transmission coefficient.	Reflection coefficient.	% mode conv loss.
Knopoff & Gangi (1960)	0.266	0.28	0.1	91
Mal & Knopoff (1965)	0.25	0.25		
Munasinghe & Farnell (1973)	0.245	0.28	0.09	91
Cuozzo et al (1977)	0.17	0.16±.02	0.09±.01	
"	0.25	0.15±.02	0.11±.01	
"	0.34	0.13±.02	0.15±.02	
Present study (Experimental)	0.34	0.20±.05	0.10±.03	
Present study (pseudo-node scheme)	0.24	0.24±.03	0.09±.03	93
	0.34	0.22±.03	0.10±.03	94
Present study (second order scheme)	0.24	0.22±.03	0.09±.03	95
	0.34	0.23±.03	0.11±.03	94

Transmission and reflection coefficients on three-quarter spaces.

TABLE 32.

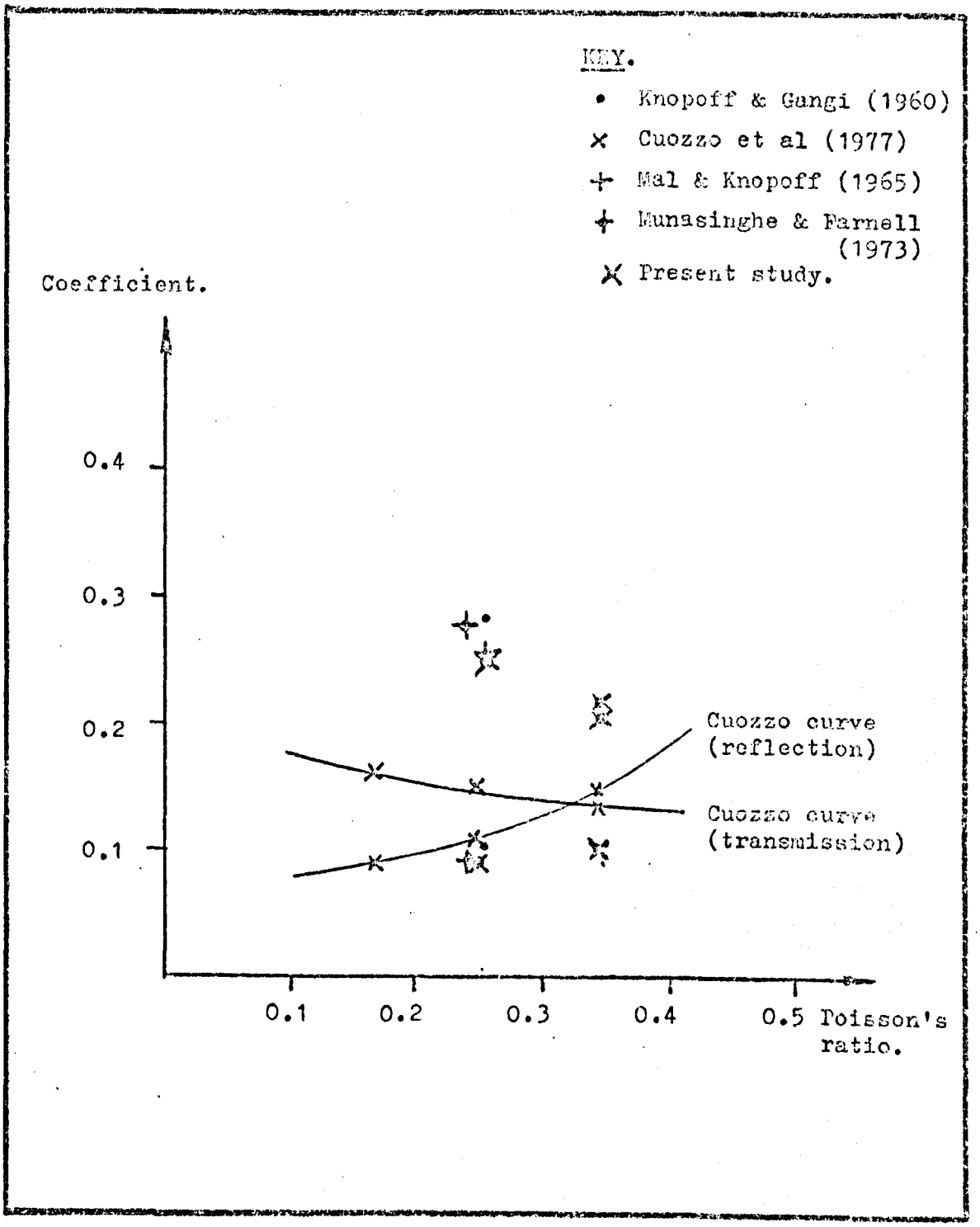

Reflection and transmission coefficients for Rayleigh waves on three-quarter spaces plotted against Poisson's ratio.

FIGURE 9.4.

a. Analytical studies.

Several previous studies have considered pulses on a range of wedges, including the 270° corner, but there have been no studies on just 270° corner. There is no previous study which has provided a satisfactory set of scattering coefficients.

b. Experimental studies.

The experimental results of the two studies by Knopoff and others and the present work are in good general agreement and there is far less scatter in the results on this configuration than those on quarter spaces.

c. Numerical studies.

There have been two previous studies using numerical methods and these have both used pseudo-node finite difference methods. That by Cuozzo et al (1977) considered semi-continuous waves with material data for a range of Poisson's ratios, the resulting curves being shown in Figure 9.4, and that by Munasinghe (1973) who considered pulses on polystyrene three-quarter spaces.

The results from the present study are in good agreement with both the previous experimental and the Munasinghe (1973) numerical results. However the Cuozzo et al (1977) results for transmission coefficient are not in good agreement with other workers. The differences between the Cuozzo et al (1977) results and those of other workers may be due to the use of semi-continuous waves or the use of a nonuniform grid in the finite difference calculations.

d. Conclusions.

The results of all studies, with the exception of that by Cuozzo et al (1977), are in good agreement. All work indicates that there are large, about 90%, energy losses from Rayleigh waves at this type of corner which was found to reduce considerably in experimental measurements with even slightly rounded corners.

9.5 Rayleigh waves at down steps.

The down step is the simplest configuration which can be expected to give wavelength dependent scattering. It is a configuration which has been considered in all the fields where Rayleigh waves are of interest and the reults of previous studies, together with those of of the present study are shown as Figure 9.5. which considers wavelength to step depth ratios from 0.1 to 1.5.

a. Analytical studies.

Various theoretical studies have attempted to describe the scattering of Rayleigh waves at steps, but it is found that in general satisfactory results can only be given for steps with depth to wavelength ratios less than about 0.1 or much larger than 1.5 which are the limits of interest in the present study.

The study by Mal and Knopoff (1965) has used a Green's function method to calculate a transmission coefficient curve which is found to be in good agreement with experimental results and this is shown in Figure 9.5.

b. Experimental studies.

The results of one previous experimental study, with steps in aluminium blocks, are presented in Figure 9.5, and these are due to Frost et al (1975). It is seen in the results due to Frost et al (1975) and the measurements of reflection coefficients in the present study that there is considerable scatter especially for step height ratios over about 0.6.

There have also been photoelastic visualization studies of pulses scattered at down steps, including that by Dally and Lewis (1968), and it is found that the shape of the scattering coefficient curves are in good agreement with those shown in Figure 9.5 and the scattered pulses of shear and compressional waves are generated at the 270° and 90° corners respectively The shear wave from the 90° corner is also shown, as is the mode converting compressional wave, the PS wave.

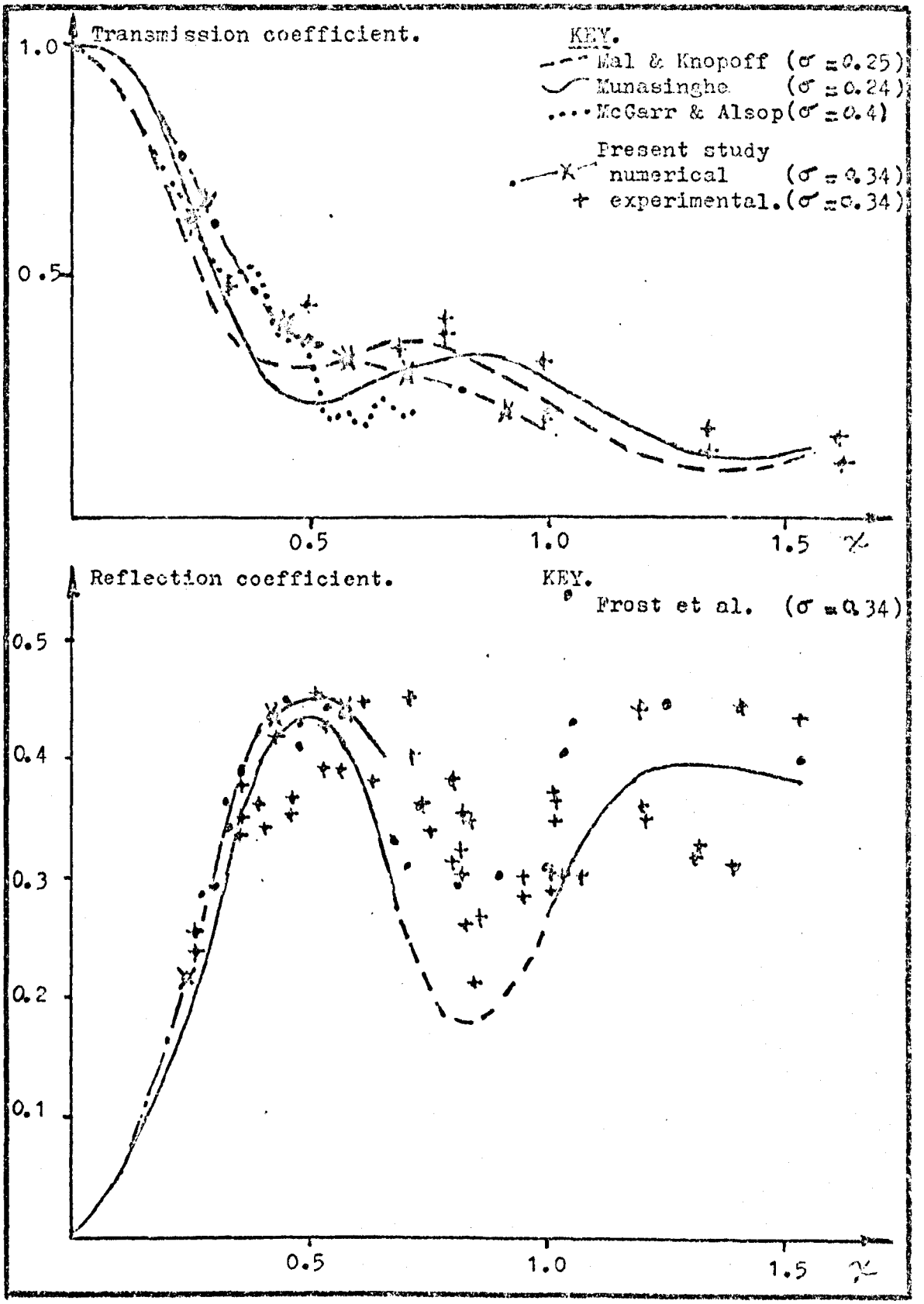

Transmission and reflection coefficients at down steps, with depth measured in wavelengths (χ).

FIGURE 9.5.

c. Numerical studies.

An approximate variational method has been applied by McCarr and Alsop (1967) with the data for Poisson's ratio = 0.4, and this has been found to give quite good results for step depth to wavelength ratios up to about 0.25, but it becomes increasingly inaccurate above this value.

There have been two previous numerical studies using finite difference methods to model Rayleigh waves at down steps. They have both used pseudo-node schemes for the boundary nodes and that by Munasinghe (1973) has used polystyrene data with Ricker type pulses and that by Cuozzo et al (1977) has used quartz data and semicontinuous Rayleigh waves.

The scattering coefficients for the two numerical studies are shown in Figure 9.5 together with three results by Cuozzo et al (1977) for the reflection and transmission coefficients at step depth to wavelength rationvalues of 0.6.

The results for the reflection coefficients given by Cuozzo et al (1977), who used semi-continuous waves and a grid that had different size increments in different regions, are consistantly low when they are compared with those from previous studies and the results of the present experiments and model results.

d. Conclusions.

It is found that the results by Munasinghe (1973), with polystyrene data, Frost et al (1975) using aluminium blocks and the present study are in general agreement with the major features shown in the experimental measurements being followed in the results of the model. The oscillation, which is found to occur in the end of the reflected pulses in the model with step depths between about 0.6 and 1.0, is found in the experimental pulses and the mode converted shear wave pulses shown in the numerical visualisation plots are in good agreement with the pulses shown in the experimental visualisation studies, such as that by Dally and Lewis (1968).

9.6 Rayleigh waves at up steps.

The up step configuration, although when it is combined with the down step forms a wide open slot, has received little attention in previous studies.

There has been no previous analytical study of the up step and only one model using using finite difference methods, that by Cuozzo et al (1977), for semi comtiouous waves, was found in the literature.

The study by Cuozzo et al (1977) modeled the up step using a pseudo-node boundary node formulation and data for quartz (σ=.12). Also only values for the reflection coefficient are give, and these are shown in Figure 9.6.

In the present study both experimental measurements with pulses at up steps on aluminium blocks and model results, using aluminium data, were made. The results of these measurements are shown in Figure 9.6.

It was found that for shallow up steps, the results for which are shown in Figure 9.6, the domanant feature was the 270° corner which caused considerable mode conversion energy loss from Rayleigh waves.

Measurements were also made on deeper steps, with step height to wavelength ration greater than 2.0, and the tip, 270° corner, mode converted shear wave pulse was clearly detected and shown to cut the corner and remode convert into Rayleigh waves on the upper surface. The presence of this pulse has been mentioned by other workers for cracks and it is used by Silk (1976) to measure crack depth.

Conclusions.

The present study experimental and model results have filled a gap in previous knoweledge and shown that contrary to statements by several authors, the energy scattered by an up step or the far side of a crack does not just pass along the surface but cuts the corner to increase the Rayleigh wave energy detected as the transmitted pulse. Also the scattering at the 270° corner shows that the detection of energy reflected by features on the far side of such a corner is difficult if not impossible.

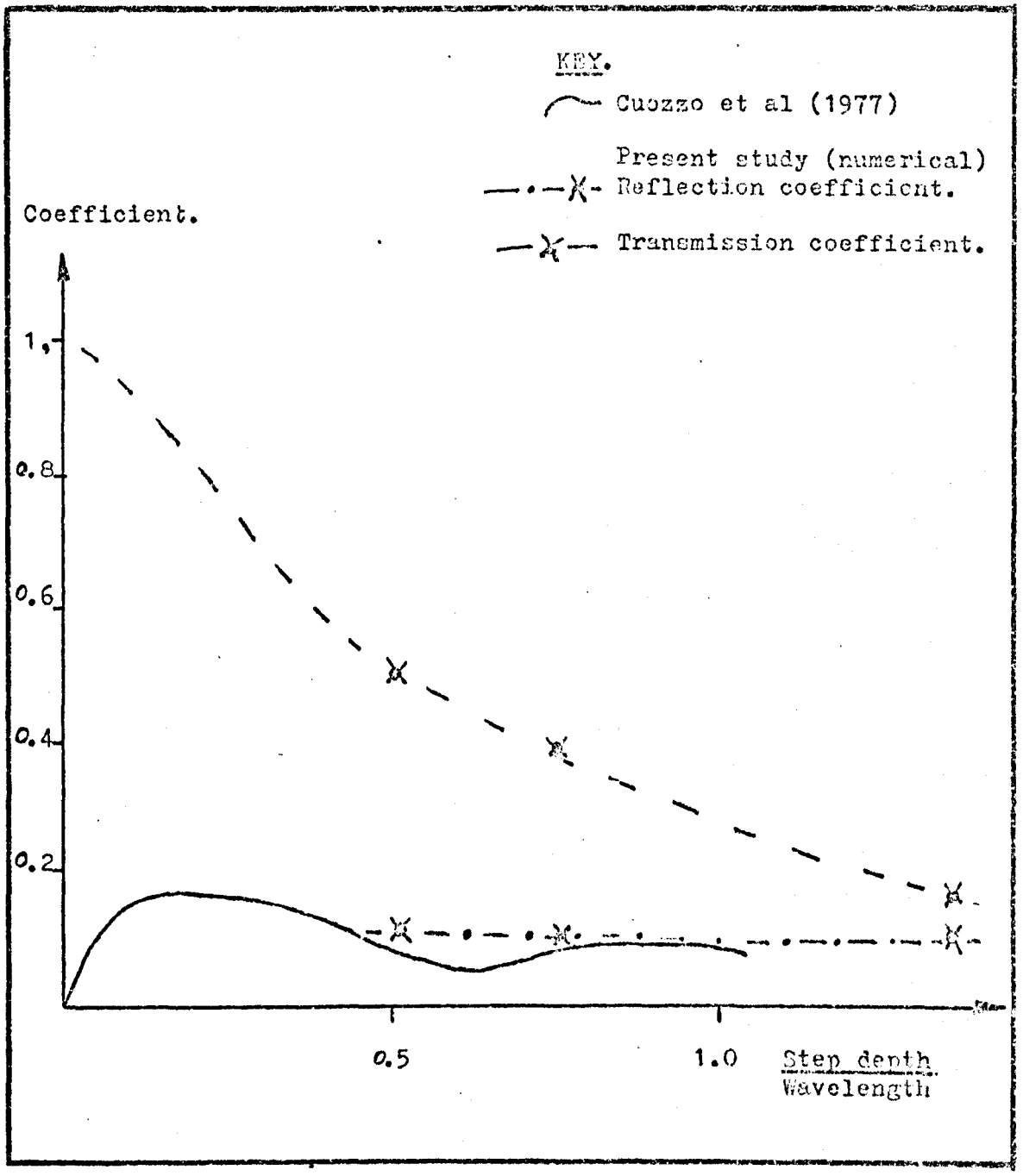

Transmission and reflection coefficients for Rayleigh waves at up steps.

FIGURE 9.6.

9.7 Rayleigh waves at open slots.

The open slot is an idealised crack configuration. However there is very little published work on the scattering of pulses of Rayleigh waves at such features.

There is in the literature, to quote Morgan (1973) 'no satisfactory model for the reflection (of Rayleigh waves) from a slot'.

There is only one published set of reflection and transmission coefficients for pulses in aluminium or dural and this is due to Viktorov (1967) and it is shown in Figure 9.7.

There have been visualisation studies of pulses at open slots including those by Reinhardt and Dally (1970) and Hall (1976). In the present study a series of model runs were performed with aluminium data and a range of 0.125 wavelength wide slots of different depths. The results of these model runs are shown in Figure 9.7.

The general shape of the reflection coefficient curve is similar to that for down steps and for model runs with wide slots, (width larger than .5) wavelengths) the pattern of reflected pulses shown by numerival visualisation is almost identical.

The mode converted pulse used by Silk (1976) was detected both experimentally and seen in the numerical models.

It was also found that the model results were in general agreement with the conclusions of the experimental civil engineering study by Woods (1968) in that a slot of depth-to-wavelength ratio of a minimum of 0.6 was required to reduce the pulse amplitude to 0.25 across the trench (slot). The observation by Woods that there is energy focusing or magnification of the displacements in the region in front of the trench (slot) and on the front side wall of the trench (slot), were confirmed in the model numerical visualisation displays. It was also found that the width of the trench, between wavelength to width ratios of 0.13 tO 0.91, had little influence on the scattering by the trench (slot).

Conclusions.

Morgans statement, that there is no model for waves at an open slot, in now not true and the model results given in the present study are in good agreement with the previous published work. The model results have also shown that it is almost impossible to inspect the far side of a slot (crack) in reflection mode,

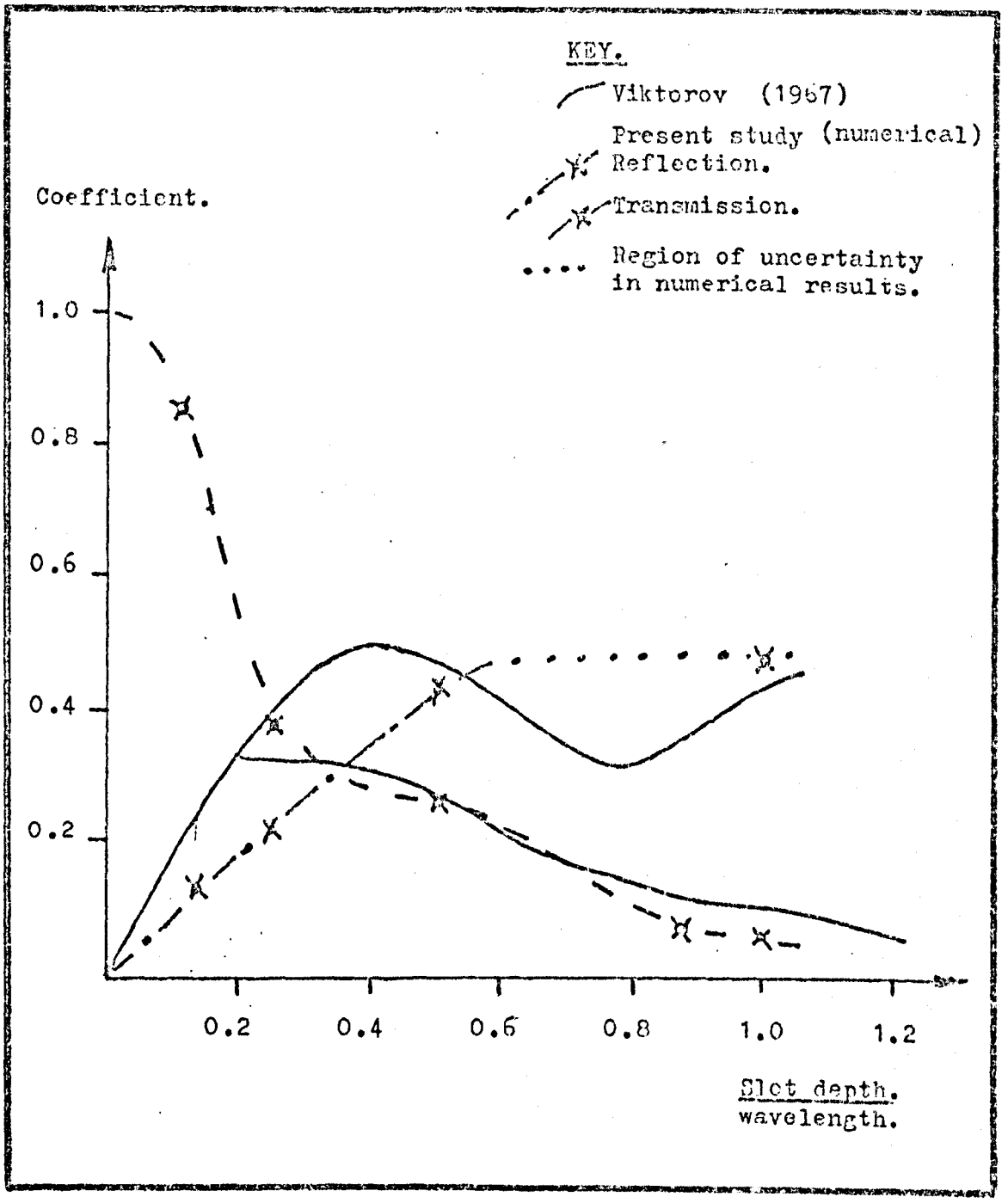

Transmission and reflection coefficients for Rayleigh waves at open slots.

FIGURE 9.7.

due to the domanant scattering at the 270° corners.

9.8 Rayleigh waves on blocks.

The rectangular block, which is common in both the laboratory and in structures has received little attention as a scatterer of elastic waves.

The quarter space, as considered in Section 9.3, has been studied extensively and in the experimental work by Haydl (1974) he has considered pulses at the end of a 'bar' of gallium arsenide. Also in the studies by Hall (1976) using photoelastic visualisation it is seen that complex patterms of mode-converted pulses occur.

In the present study, as reported in Section 8, the detection of experimental pulses can be made difficult due to background noise in the block which is considerably reduced by placing damping material on the unused surfaces of the testblock.

There appears to be no previous numerical model of the pulses on a block. In the present study the time development of the mode converted pulses that occur is followed in the numerical visualisation displays presented in Section 7.3.7. The input pulse of Rayleigh waves is found to mode-convert at the first 90° corner as for a pulse on a quarter space and the resulting mode-converted pulses then move through the block and are scattered or reflected at corners and free surfaces.

A model has therefore been provided which shows the rapid increase in the body wave pulses present in any piece of material of limited spatial extent.

9.9 Rayleigh waves on welded quarter spaces.

Rayleigh waves on welded quarter spaces have been considered by several workers with varying degrees of success. In the present study a new formulation for the free surface/ interface node is presented, in Appendix G, and this was tested by comparison of the results it gave with those of previous studies.

The previous studies are those by McGarr and Alsop (1967), who used an approximate variational method and made a series of experimental measurements and that by Munasinghe (1973) who used the same data as McGarr and Alsop and pulses Rayleigh waves in a finite difference scheme.

Pulses of Rayleigh waves were considered to pass from polystyrene into perspex and vice versa. The model used in the present study considered the same media and the results are presented in Table 33 . The transmission and reflection of the pulses was measured in terms of the ratios of the amplitudes of the vertical components of displacements.

Source.	Polystyrene to perspex		Perspex to polystyrene	
	Reflected.	Transmitted	Reflected.	Transmitted
McGarr & Alsop (1967)				
Experimental	-	0.85±.05	-	1.17±.04
Numerical(variational)	-	0.83	-	1.16
Munasinghe (1973)	0.13±.02	0.81±.02	-	-
Present study	0.08±.03	0.90±.03	0.07±03	1.12±.03

Ratios of the amplitudes of the vertical components of displacement of the transmitted and incident and the reflected and incident pulses of Rayleigh waves on polystyrene and perspex welded quarter spaces.

TABLE 33.

The results given by the model developed in the present study are in good agreement with those by previous workers. Also the results in the present study were achieved using only 16 nodes per wavelength, compared with the 32 used by Munasinghe (1973). This resulted in considerable savings in the computer core required and the job run time.

9.10 Rayleigh waves at filled slots.

The configuration of a filled slot, with a rectangle of polystyrene set in a half space of perspex and vice versa, has not been considered previously either in an experimental or numerical study.

In the present study slots filled with perspex 1.25 wavelengths wide and 4.3 wavelengths deep in a polystyrene half-space and vice versa were considered.

The results for the transmission and reflection coefficients for the slots are presented as Table 25 and those for welded quarter spaces of the same material are presented as Table 33. The scattering coefficients were compared and the results are given in Table 34. The transmitted pulse in the case of the filled slot should have an amplitude the same as a pulse that has passed across two welded quarter space interfaces.

	Reflection welded ¼'s	1st reflection at filled slot
Polystyrene - perspex	0.08	0.10
perspex - polystyrene	0.07	0.08
Using amplitude ratios for ¼'s ;	'Transmitted pulse amplitude'	
Polystyrene in perspex		
McGarr & Alsop (Exp)	0.99	
" (Num)	0.96	
Present study (filled slot)	0.92	
Perspex in polystyrene		
McGarr & Alsop (Exp)	0.99	
" (num)	0.96	
Present study (filled slot)	0.96	

Transmission and reflection coefficients at filled slots and the corresponding results for pairs of welded quarter spaces.

TABLE 34.

The results given in Table 34 show general agreement between those for filled slots and combinations of welded quarter spaces.

The only other result in a previous study that can be compared with the filled slot is the conclusion by Woods (1968) that sheet-wall barriers were not as effective as open trenches in scattering Rayleigh waves.

9.11 Proposed combined method for surface feature characterisation.

Following from the results considered in Sections 9.2 to 9.7 the author proposes a method of surface feature characterisation with several advantages over existing methods, which could be used with either time domain or spectral analysis instrumentation.

The basic arrangement of the proposed equipment is shown in Figure 9.9. The method is a development of those presented by Hudgell et al (1974) and Silk (1976) which uses the advantages of the new Harnik (1977) surface wave receiver.

The basic transducer arrangement would consist of a wedge type transducer as the transmitter and two Harnik-type probes to act as receivers.

The wedge transducer should be a short pulse transmitter that has a centre frequency about 1/10th of the resonant frequency of discs used in the Harnik-type probes.

Idealised expected time-domain signals for the transducer system are shown in Figures 9.9 a to d. Trace a. is the calibration arrangement with the three probes in line on a surface of the type to be investigated but without defects. This arrangement would be used to calibrate any time measurements to be made and to fix the separation of the wedge and receiver 1. Receiver 2 would be arranged so that it could move along the surface in line with the wedge and the fixed receiver.

Trace b. would be for the case of a shallow defect with only a single reflected and a single transmitted pulse detected. The amplitudes of these pulses would vary with defect depth.

Trace c would be the expected trace for a defect with a depth of about two pulse-centre wavelengths. A tip diffracted pulse would be detected and the two components of the transmitted pulse, due to the Rayleigh wave that follows the surface and the mode converted shear wave from the defect tip separate.

Trace d is the expected trace for a deep defect with the three components in the reflected signal due to the tip shear wave, the reflection from the first 90° corner and the Rayleigh wave reflected back from the crack tip. the two components in the transmitted pulse would separate in the time domain.

From the information available in these signals, defect depth measurements should be possible.

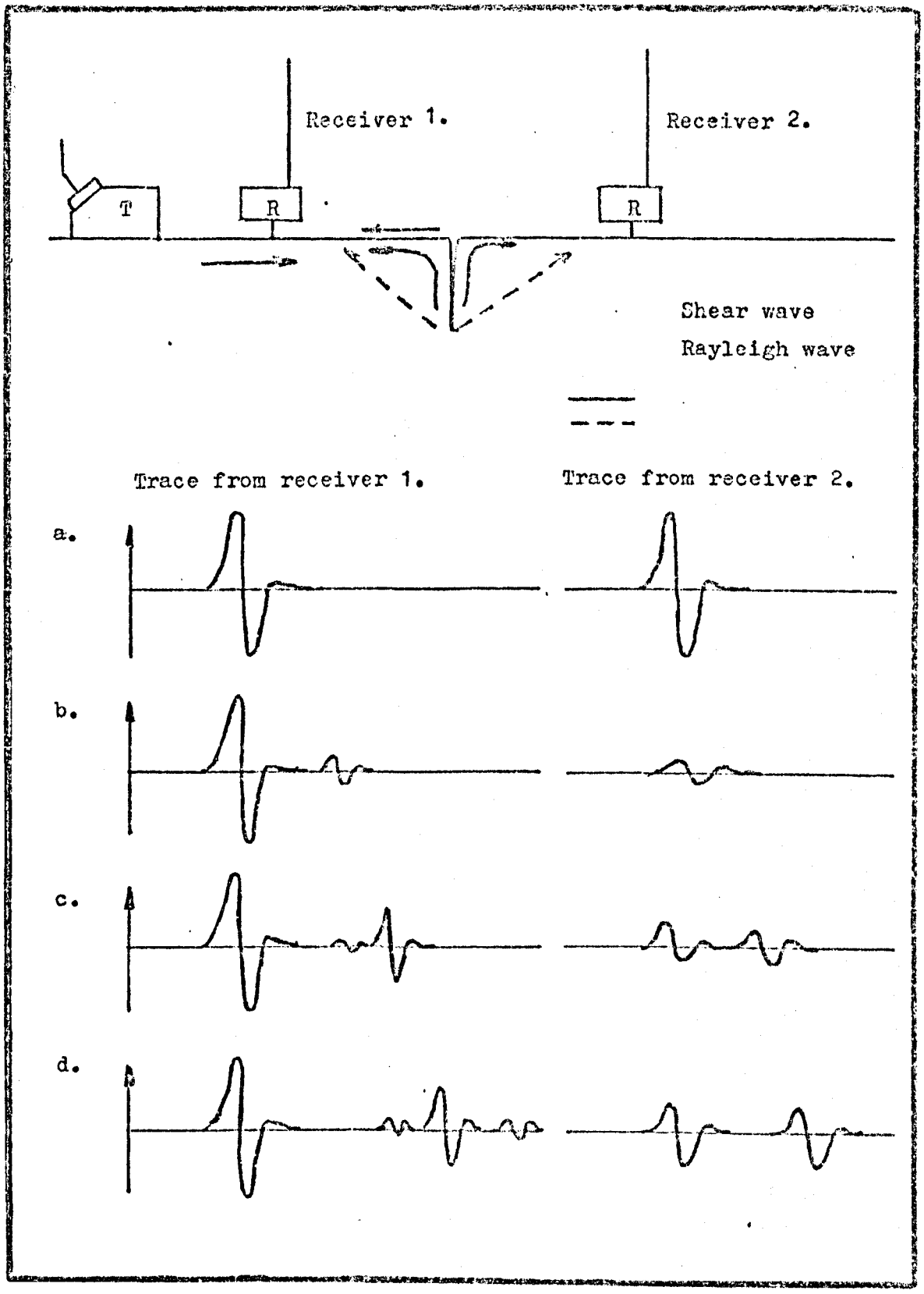

Proposed combined method for surface feature characterisation, with idealised output from receivers for the cases of a. on a smooth surface. b. with a shallow crack. c. with a crack about two wavelengths deep. d. with a deep crack.

FIGURE 9.8

10. CONCLUSIONS.

The finite difference method has been applied to a range of new problems; those which occur in pulsed ultrasonic Rayleigh wave non-destructive testing. The results of the models have provided both quantitativenumerical results and visual information about a wide range of configurations.

The development of a range of new second order formulations for the boundary nodes, including that for the free surface/ interface node in welded quarter spaces, has extended the range of problems which can be considered and the accuracy of the results. The use of the second order formulations at 16 nodes per wavelength compared with the 32 nodes per wavelength used in previous studies, has resulted in considerable reductions in the model computer core requirements and job run times.

For the half, quarter and three quarter spaces, steps and open slots, additional results and understanding have been provided. For Rayleigh waves on welded quarter spaces the new formulation presented has reduced the number of nodes required to model a given size space to a quarter of the previous requirements. The models have been extended to consider the new configurations of the block and the filled slot.

The supporting experimental measurements have resulted in the proposed combined method using the advantages of the new Harnik (1977) transducers.

The power of finite difference modelling, which gives quantative understanding for analyitically intractable problems, has provided results which are valid in all the fields where Rayleigh waves are of interest and the present study provides a firm base for extending the work to consider more complex configurations.

11. SUGGESTIONS FOR FURTHER WORK.

The present study has only started the application of finite difference methods to the modelling of pulsed ultrasonic wave problems, linked with nondestructive testing. The application of the basic methods used in the models in this study need not be restricted to applications that model nondestructive testing configurations; they have possible applications to an almost infinite range of wave propagation problems covering all the subjects discussed in Section 2, geophysics, seismology, civil engineering, nondestructive testing and electronics.

Within the wide range of possible areas for suggestions for further work those given in this section are restricted to three groups. The first group of possible studies are those which would improve or extend the basic numerical schemes. The second group of possible studies are some of the possible straight forward applications of existing models and methods to nondestructive testing linked problems and the third group of possible studies are some extensions of the models to consider more complex configurations, but remaining linked with nondestructive testing.

a. Basic numerical scheme improvements

The basic numerical method is dependent on the development and use of finite difference formulations which describe motion at points (nodes) within the structure under study. There are two basic limitations to extending the use of finite difference schemes and these are the lack of finite difference formulations for a particular type of node, such as the tip of a 30° wedge and the lack of formulations for many nodes that are accurate and stable for material with high Poisson's ratio, above about $\sigma = .3$.

Possible work would be to extend the range of types of nodes which have finite difference formulations, including further work on the formulation for non-90° corners due to Ilan (1977a) and the development of new formulations for interfaces that are neither normal or parallel to the basic grid.

A further possible study would be to develop second order schemes which are more accurate and have a larger region of stability, for such nodes as those at 90° and 270° corners.

b. Further applications of existing schemes.

This group of suggestions is for further application of existing models or the development of models that use mainly existing material.

One possible set of studies in this area would be to perform further work using the existing models for both open and filled slots, with different combinations of width and depth and with different material data.

One extension to the study could be by considering the interaction of body waves with surface features, using existing boundary condition formulations.

c. Extensions to model more complex configurations.

The basic nodal formulations form building blocks which can be combined in many ways, to give models of very complex systems. The extensions to more complex systems can be achieved in two ways, either by the development of a particular type of model or the construction of a complex system from the various basic nodal formulations.

One possible example for extending the study through a series of configurations would be from a Rayleigh wave pulse on a block; to a pulse on a block with a slot in it; to a pulse on a T shape either with or without slots in it.

The direct construction of complex configurations could consider layered configurations, with either surface or body waves, possibly with new formulations for non-90° corners and interfaces.

Within the basic method there is no requirement to use Cartesian type coordinates and models have been made of cylindrical and spherical geophysical configurations using cylindrical coordinate systems. (Alterman & Karal 1970) The use of cylindrical coordinate systems could be extended to model some cylindrical nondestructive testing configurations.

d. Experimental measurements.

In addition to the developments of the numerical models further experimental studies could be developed. A series of

experiments could be performed to use the proposed combined transducer to investigate both open and filled slots to provide data for testing the model results.

The suggestions made in this section are by no means an exhaustive list, but could form the basis for imediate extensions of the present study.

Appendix A.

A. Some basic types of elastic waves.

There are a wide range of different elastic waves which are often known by the name of their discoverer and thesehave particular combinations of components of displacement. Elastic waves in solids can be divided into three classes according to where they propagate and these are body waves, surface waves and interface waves, and some of the waves in these classes are now considered. An extended treatment of elastic waves is given by several authors including Graff (1975).

BODY WAVES.

These are waves which propagate through the bulk of a medium.

Compressional waves. This type of wave has only a longitudinal component of displacement, in the direction of propagation.

They are also known as;

- Longitudinal waves.
- P (Primary) waves.
- α waves, after the symbol given to their velocity in geophysics.

Shear waves. This type of wave has only a transverse component of displacement, normal to the direction of propagation.

They are also known as;

- Transverse waves.
- S (Secondary) waves.
- β waves, after the symbol given to their velocity in geophysics.

SURFACE WAVES.

These are types of elastic waves where the energy propagation is confined to a region near a free surface or surfaces, with the energy propagating parallel to the free surface and decaying rapidly as the body of the medium is penetrated.

Rayleigh waves. This type of wave is a two dimensional wave with only a longitudinal component of displacement in the direction of propagation and a transverse component of displacement normal to the free surface. This wave can also be considered as an interface wave with the second medium a gas or vacuum.

Love waves. This type of wave is a transverse shear wave trapped or guided by a surface layer.

Lamb waves. These propagate in thin plates

INTERFACE WAVES.

These are waves that occur at the boundary between two media, which may be in different phases and their propagation is confined to a region along the interface, the energy in these waves decaying rapidly with distance into the bulk of the media.

Stoneley waves. These are the type of interface waves that occur at an interface between two different solids. Their existence is governed by differences in the shear wave velocities between the two media. The range of existence is considered by Ewing et al (1957, p111-3)

Brekhovskikh waves. This type of wave occurs at a solid/liquid interface and is also known as a Schult wave.

Rayleigh waves. This type of waves can be considered to be the solid/gas or vacuum interface wave or a surface wave.

Appendix B.

B. Nondestructive testing data display.

There are three forms of data display in common use in ultrasonic nondestructive testing and these are known as A, B and C scan's. A outline of each type of display is given in this appendix and further details are given by many authors including Krautkrämer and Krautkrämer (1969).

A Scan. This is a one dimensional display for a pulse echo system. It is illustrated by Figure B.1.

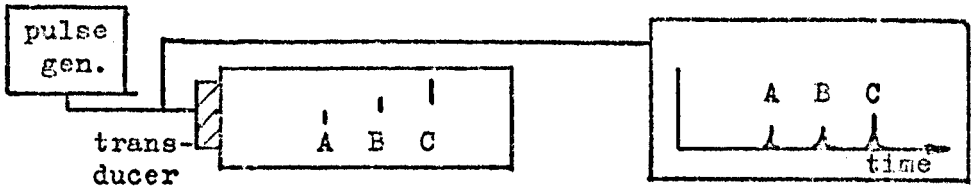

A Scan type of data display.

FIGURE B.1

B Scan. This is a display for a pulse echo system using a single transducer which scans across the test piece in one direction. It is illustrated by Figure B.2. The size of echo recorded relates to the dimensions of the scatters.

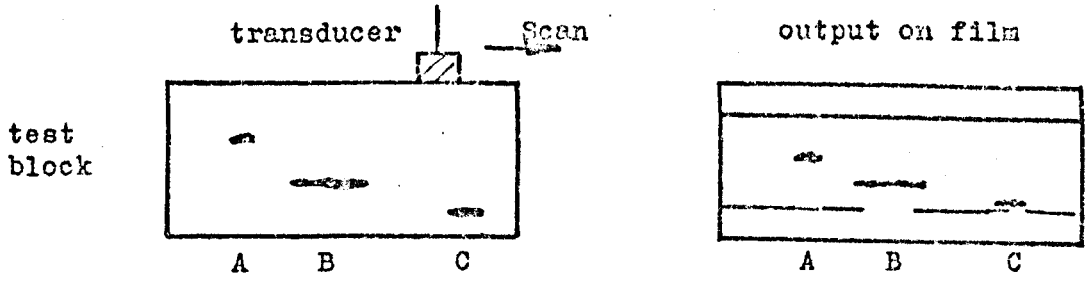

B Scan type of data display.

FIGURE B.2

C Scan. This type of display is formed by either moving a transducer across a specimen or vice versa. The spatial variations in the transmissivity to the ultrasonic beam appear as half tones on recording paper. The position as shown on the recording paper relates in some way to the transducer position. It is illustrated by Figure B.3.

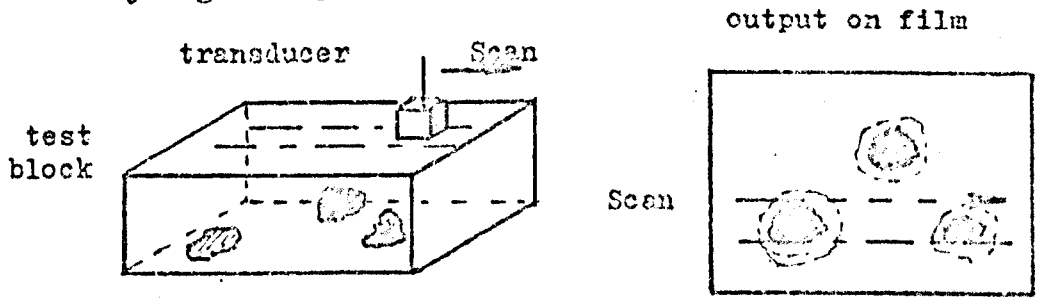

C Scan type of data display.

FIGURE B.3.

Appendix C.

C. Material data.

This appendix lists a range of media, with some material constants and wave velocities, which are of interest in the work reported in this thesis.

The data presented has been collected from a range of sources, but unless otherwise indicated the values given are due to Bradfield (1964).

Material	Poisson's ratio. σ	Density kg/m^3	Wave velocities m/sec. V_c	V_s	V_r	V_s/V_c.
Metals						
(M) Aluminium	0.34	2700	6422	3110	2906	.48
Duralumin	0.345	2700	6398	3122	2917	.488
Copper	0.34	8930	4759	2325	2171	.48
Titanium	0.36	4510	6130	3182	2958	.51
Chromium	0.21	7160	6608	4005	3655	.606
Steel(mild)	0.29	7850	5960	3235	2996	.54
Non-metals						
Glass,crown	0.22	2500	5660	3420	3127	.6
Quartz	0.17	2200	5970	3765	3410	.63
(A) Perspex		1220	2360	1370	1280	.58
(A) Polystyrene	0.245	1080	2030	1180	1084	.58
(K) Concrete			4250 -5250			

Data for some common metals and non-metals.

TABLE 35.

Material	Poisson's ratio. σ	Density kg/m^3	Wave velocities m/sec. V_c	V_s	V_r	V_s/V_c
Geophysical						
(K) Granite			5400			
(G) Granite (Rockfort)	0.243		6050	3360		.55
(G) Quartzitic sandstone	0.118		6080	4000		.65
(G) Dunite	0.262		8050	4570		.56
Medical.						
(K) Bone (human tibia)			4000	1970		.49

Data for some geophysical and medical media.

TABLE 36.

where;

(A) McGarr and Alsop (1967)

(G) Gutenberg Ed. (1951, chapter 4)

(K) Kaye and Laby (1962)

(M) Munasinghe (1973)

Appendix D.

D. Finite difference approximations and body node formulations.

This appendix presents the basic difference forms used and the second order centred difference formulations for the body node. The basic coordinates and coordinate system used are as shown in Figure 4.1.

The basic difference forms used in the formulation of the difference formulations are obtained from the Taylor series expansion for small shifts from a central point P(i,j,k) and the function for displacements is given by Chisholm and Morris (1965) as;

$$\underline{U}(X_1+d, X_2+h, T+s) = \underline{U}(X_1, X_2, T) + \left[d\frac{\partial \underline{U}}{\partial X_1} + h\frac{\partial \underline{U}}{\partial X_2} + s\frac{\partial \underline{U}}{\partial T} \right]_{X_1\ X_2\ T} +$$

$$\frac{1}{2}\left[d^2\frac{\partial^2 \underline{U}}{\partial X_1^2} + h^2\frac{\partial^2 \underline{U}}{\partial X_2^2} + s^2\frac{\partial^2 \underline{U}}{\partial T^2} + dh\frac{\partial^2 \underline{U}}{\partial X_1 \partial X_2} + hs\frac{\partial^2 \underline{U}}{\partial X_2 \partial T} + sd\frac{\partial^2 \underline{U}}{\partial T \partial X_1} \right]_{X\ X_2 T} .$$

$$+ \text{ higher order terms.} \qquad \text{D.1}$$

where d, h and s are the increments in the three coordinate directions X_1, X_2 and T.

By application of the equation D.1 to the node P(i,j,k), in the general case gives the standard difference forms which, when given in the same notation as Munasinghe (1973) are;

$$\frac{\partial \underline{U}(i,j,k)}{\partial X_1} \approx \frac{d_i \cdot \underline{U}(i+1,j,k)}{d_{i-1} \cdot \bar{d}} + \frac{(\bar{d}-d) \cdot \underline{U}(i,j,k)}{d_i \cdot d_{i-1}} - \frac{d_{i-1} \cdot \underline{U}(i-1,j,k)}{d_i \cdot \bar{d}} + O(d^2) \qquad \text{D.2}$$

$$\frac{\partial^2 \underline{U}(i,j,k)}{\partial T^2} \approx 2\left[\frac{\underline{U}(i,j,k-1)}{s_{k-1} \cdot \bar{s}} - \frac{\underline{U}(i,j,k)}{s_k \cdot s_{k-1}} + \frac{\underline{U}(i,j,k-1)}{s_k \cdot \bar{s}} \right] + O(\bar{s}-s) + O(s^2) \qquad \text{D.3}$$

$$\frac{\partial^2 \underline{U}(i,j,k)}{\partial X_1 \partial X_2} \approx \frac{d_i \cdot h_j \cdot \underline{U}(i+1,j+1,k)}{d_{i+1} \cdot \bar{d} \cdot h_{j+1} \cdot \bar{h}} + \frac{\delta d \cdot h_j \cdot \underline{U}(i,j+1,k)}{d_i \cdot d_{i+1} \cdot h_{j+1} \cdot \bar{h}}$$

$$- \frac{d_{i-1} \cdot h_j \cdot \underline{U}(i-1,j+1,h)}{d_i \cdot \bar{d} \cdot h_{j+1} \cdot \bar{h}} + \frac{d_i \cdot \delta h \cdot \underline{U}(i+1,j,k)}{d_{i+1} \cdot \bar{d} \cdot h_j \cdot h_{j+1}} + \frac{\delta d \cdot \delta h \cdot \underline{U}(i,j,k)}{d_i \cdot d_{i+1} \cdot h_j \cdot h_{j+1}}$$

$$- \frac{d_{i+1} \cdot \delta h \cdot \underline{U}(i-1,j,k)}{d_i \cdot \bar{d} \cdot h_j \cdot h_{j+1}} - \frac{d_i \cdot h_{j+1} \cdot \underline{U}(i+1,j-1,k)}{d_{i+1} \cdot \bar{d} \cdot h_j \cdot \bar{h}} - \frac{\delta d \cdot h_{j+1} \cdot \underline{U}(i,j-1,k)}{d_i \cdot d_{i+1} \cdot h_j \cdot \bar{h}}$$

$$+ \frac{d_{i+1} \cdot h_{j+1} \cdot \underline{U}(i-1,j-1,k)}{d_i \cdot \bar{d} \cdot h_j \cdot \bar{h}} + O(\delta d) + O(\delta h) + O(d_i^2) + O(h_j^2) \qquad \text{D.4}$$

where $\bar{d} = d_i + d_{i+1}$; $\bar{h} = h_j + h_{j+1}$; $\bar{s} = s_k + s_{k+1}$

$\delta d = d_{i+1} - d_i$; $\delta h = h_{j+1} - h_j$; $s = s_{k+1} - s_k$

and symbol O( ) denotes order of.

These difference forms, given as equations D.2 to D.4, simplify when restrictions, such as uniform spatial or time steps, are added, and the forms of these relations with the uniform grid restrictions are given as;

$$\frac{\partial \underline{U}(i,j,k)}{\partial X_1} \approx \frac{1}{2d}\left[\underline{U}(i+1,j,k) - \underline{U}(i-1,j,k)\right] + O(d_i^2) \qquad \text{D.5}$$

$$\frac{\partial^2 \underline{U}(i,j,k)}{\partial T^2} \approx \frac{1}{s^2}\left[\underline{U}(i,j,k+1) - 2\,\underline{U}(i,j,k) + \underline{U}(i,j,k-1)\right] + O(s^2) \qquad \text{D.6}$$

$$\frac{\partial^2 \underline{U}(i,j,k)}{\partial X_1 \partial X_2} \approx \frac{1}{4dh}\left[\underline{U}(i+1,j+1,k) - \underline{U}(i-1,j+1,k) - \underline{U}(i+1,j-1,k) + \underline{U}(i-1,j-1,k)\right] + O(d^2) + O(h^2) \qquad \text{D.7}$$

The signs of the components for the mixed derivative are as shown in Figure D.1.

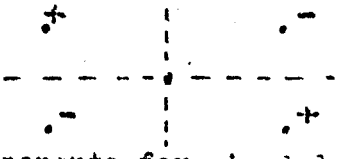

Signs of components for mixed derivative.

FIGURE D.1

The equation for a body node, with uniform spatial and time increments, is given by substitution of equations of type D.6 and D.7, into the basic equation of motion in an elastic solid, which is given as equations 2.3.2 and 2.3.3, and upon manipulation gives;

$$\underline{U}(i,j,k-1) - 2.\underline{U}(i,j,k) - \underline{U}(i,j,k-1) - s^2(Fp(\underline{U})) \qquad D.8$$

where $Fp(\underline{U})$ is an explicit expression, the exact form of which is given by Alterman and Loewenthal (1970) The full form of equation D.8 when written in the notation used by Munasinghe (1973) is;

$$\begin{aligned}\underline{U}(i,j,k+1) = {} & 2\,\underline{U}(i,j,k) - \underline{U}(i,j,k-1) \\ & + \underline{A}\left(\frac{s}{h}\right)^2 \left\{\underline{U}(i+1,j,k) - 2.\underline{U}(i,j,k) + \underline{U}(i-1,j,k)\right\} \\ & + \frac{1}{4}\,\underline{B}\left(\frac{s}{h}\right)^2 \left\{\underline{U}(i+1,j+1,k) - \underline{U}(i+1,j-1,k) - \underline{U}(i-1,j-1,k) \right. \\ & \qquad \left. + \underline{U}(i-1,j-1,k)\right\} \\ & + \underline{C}\left(\frac{s}{h}\right)^2 \left\{\underline{U}(i,j+1,k) - 2.\underline{U}(i,j,k) + \underline{U}(i,j-1,k)\right\} \qquad D.9\end{aligned}$$

where $\underline{U} = \begin{bmatrix} U_1 \\ U_2 \end{bmatrix}$; $\underline{A} = \begin{pmatrix} V_c^2 & o \\ o & V_s^2 \end{pmatrix}$; $\underline{B} = \begin{pmatrix} o & V_c^2 - V_s^2 \\ V_c^2 - V_s^2 & o \end{pmatrix}$

$$\underline{C} = \begin{pmatrix} V_s^2 & o \\ o & V_c^2 \end{pmatrix}$$

Due to the rapid decay of displacements below a surface in some studies of Rayleigh waves, including that by Munasinghe (1973) a nonuniform gird form is used which is given as equation D.10. The nonuniform grid form is also used in the studies of polygonal surfaces with compressional waves by Ilan (1977a, 1977b).

Alternative formulations are possible, using higher order derivatives and or using Lamé constants in the place of velocities using the relations given in Section 2.3 for velocities in terms of the Lamé constants.

The equation for uniform time and nonuniform spatial grids;

$$\underline{U}(i,j,k+1) = 2.\underline{U}(i,j,k) - \underline{U}(i,j.k-1)$$

$$+ s^2\Bigg\{ 2.A\left[\frac{\underline{U}(i+i,j,k)}{d_{i+1}\cdot\bar{d}} - \frac{\underline{U}(i,j,k)}{d_i\cdot d_{i+1}} + \frac{\underline{U}(i-1,j.k)}{d_i\cdot\bar{d}}\right]$$

$$+ 2\,C\left[\frac{\underline{U}(i,j+1,k)}{h_{j+1}\cdot\bar{h}} - \frac{\underline{U}(i,j,k)}{h_j\cdot h_{j-1}} - \frac{\underline{U}(i,j-1,k)}{h_j\cdot\bar{h}}\right]$$

$$+ B\left[\frac{d_i\cdot h_j\cdot\underline{U}(i+1,j+1,k)}{d_{i+1}\cdot\bar{d}\cdot h_{j+1}\cdot\bar{h}} + \frac{\delta h.h_j\cdot\underline{U}(i,j+1,k)}{d_i\cdot d_{i+1}\cdot h_{j+1}\cdot\bar{h}} - \frac{d_{i+1}\cdot h_j\cdot\underline{U}(i-1,j+1,k)}{d_i\cdot\bar{d}\cdot h_{j+1}\cdot\bar{h}}\right.$$

$$+ \frac{d_i\cdot\delta h.\underline{U}(i+1,j,k)}{d_{i+1}\cdot\bar{d}\cdot h_j\cdot h_{j+1}} + \frac{\delta d.\delta h.\underline{U}(i,j,k)}{d_i\cdot d_{i+1}\cdot h_j\cdot h_{j+1}} - \frac{d_{i+1}\cdot h.\underline{U}(i-1,j,k)}{d_i\cdot\bar{d}\cdot h_j\cdot h_{j+1}}$$

$$\left.\left. - \frac{d_i\cdot h_{j+1}\cdot\underline{U}(i+1,j-1,k)}{d_{i+1}\cdot\bar{d}\cdot h_j\cdot\bar{h}} - \frac{\delta d.h_{j+1}\cdot\underline{U}(i,j-1,k)}{d_i\cdot d_{i+1}\cdot h_j\cdot\bar{h}} + \frac{d_{i+1}\cdot h_{j+1}\cdot\underline{U}(i-1,j-1,k)}{d_i\cdot\bar{d}\cdot h_j\cdot\bar{h}}\right]\right\}$$

D.10

Appendix E.

E. First order finite difference formulations for free surface nodes.

This appendix presents the finite difference formulations that are used to calculate displacements at pseudo-nodes outside the free surface of a medium and allow application of the body node formulation to the boundary node.

E.1 Free surface node formulations.

The two pseudo-node schemes which are presented for nodes at free surfaces are both obtained from the boundary conditions for the free surface which are presented in Section 2.3. The first scheme, which uses Centred Difference approximations was originally presented by Alterman and Karal (1968) and is given here in Appendices E.1.1 and E.1.2. The second scheme, which uses One-sided Difference approximations was originally presented by Alterman and Rotenberg (1969) and is given here in Appendices E.1.3 and E.1.4. Both schemes have been used by a number of workers.

E.1.1 Centred Difference scheme for horizontal free surface.

The node configuration for the node outside the top horizontal free surface, node P, is shown in Figure E.1, and the explicit expression for the displacements at this node (P(i,j-1,k)) is obtained from the free surface boundary condition, that the free surface is stress free, which is given as equation 2.3.10 and here as;

$$T_{12} = T_{22} = 0 \qquad \text{E.1.1}$$

where T_{12} and T_{22} are components of the Cartesian stress tensor which is given as equation 2.3.8.

The displacement vector is obtained by substitution of difference forms in equation E.1.1.

$$\underline{U}(i,j-1,k) = \underline{U}(i,j+1,k) + \underline{E}_1 \left[\underline{U}(i+1,j,k) - \underline{U}(i-1,j,k) \right] \qquad E.1.2$$

where $\underline{E}_1 = \begin{bmatrix} 0 & 1/r \\ y^2/r & 0 \end{bmatrix}$; $\underline{U} = \begin{bmatrix} U_1 \\ U_2 \end{bmatrix}$; $r = d/h$; for uniform grid. $= 1$. $y^2 = 1 - 2\,(V_s/V_c)^2$

The right hand side of equation E.1.2 is a linear conbination of displacements inside or on the boundary of the solid.

The nodal configuration for the node outside the bottom horizontal free surface, node Q, is shown in Figure E.1, and the explicit expression for the displacements at this node (Q(i,j+1,k)) is obtained from the same boundary conditions as are used in the case of equation E.1.2.

The resulting equation is given as;

$$\underline{U}(i,j+1,k) = \underline{U}(i,j-1,k) - \underline{E}_1 \left[\underline{U}(i+1,j,k) - \underline{U}(i-1,j,k) \right] \qquad E.1.3$$

where $\underline{E}_1$ is as for equation E.1.2.

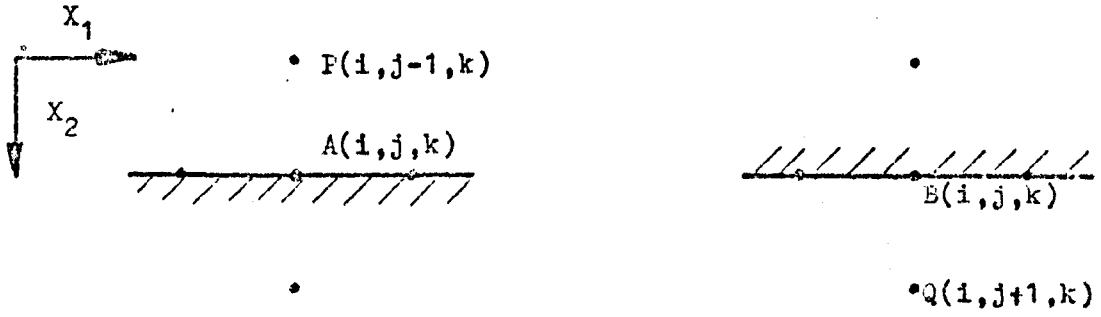

Node arrangement for horizontal free surface.

FIGURE E.1.

E.1.2 Centred Difference scheme for vertical free surface.

Similar expressions to those for the nodes outside horizontal free surfaces are obtained for the cases of vertical free surfaces.

The boundary conditions for vertical free surfaces can be expressed as components of the Cartesian stress tensor, equation 2.3.8, which can be written as;

$$T_{11} = T_{12} = 0 \qquad E.1.4$$

The node configuration for the node outside a right hand free surface, node S, is shown in Figure E.2, and the equation for the displacements at this node (S(i+1,j,k)) which is obtained from equation E.1.4 can be written as;

$$\underline{U}(i+1,j,k) = \underline{U}(i-1,j,k) + \underline{E}_2 \left[\underline{U}(i,j-1,k) - \underline{U}(i,j+1,k) \right] \qquad \text{E.1.5}$$

where $\underline{E}_2 = \begin{bmatrix} 0 & ry^2 \\ r & 0 \end{bmatrix}$; and other parameters are as for equation E.1.2.

As in the case of horizontal boundaries the same boundary condition applies for the other vertical free surface and the explicit expression for the displacements at node T, shown in Figure E.2, can be written as;

$$\underline{U}(i+1,j,k) = \underline{U}(i-1,j,k) + \underline{E}_2 \left[\underline{U}(i,j+1,k) - \underline{U}(i,j+1,k) \right] \qquad \text{E.1.6}$$

where $\underline{E}_2$ is as for equation E.1.5

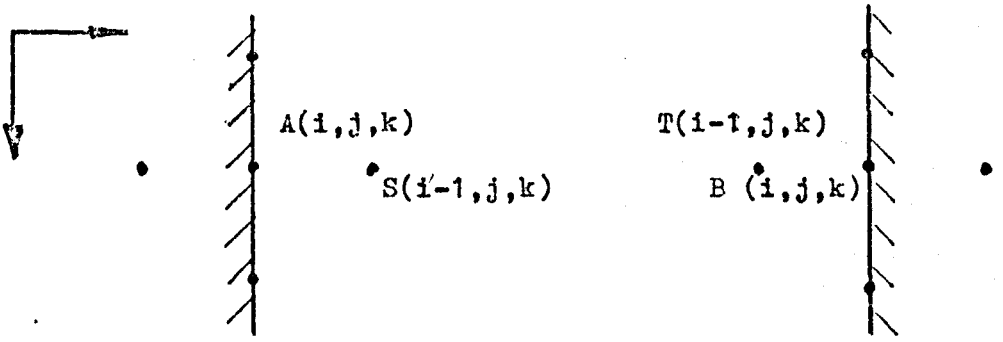

Node arrangement for vertical free surface.

FIGURE E.2.

E.1.3 One-sided Difference scheme for horizontal free surface.

Using the same boundary conditions as given in Appendix E.1.1 but with the substitution of one-sided difference forms in the place of centred differences the explicit expression for the displacements at node P, can be written as;

$$\underline{U}(i,j-1,k) = \underline{U}(i,j,k) - \underline{A}_1 \left[\underline{U}(i+1,j,k) - \underline{U}(i-1,j,k) \right] \qquad \text{E.1.7}$$

where $\underline{A}_1 = \begin{bmatrix} 0 & \frac{1}{2} \\ \frac{1}{2}a & 0 \end{bmatrix}$; $a = \left(\dfrac{V_c^2 - 2V_s^2}{2\,V_c^2} \right)$

E.1.4 One-sided Difference scheme for vertical free surfaces.

Using the same boundary conditions as given in Appendix E.1.2 but with the substitution of one-sided difference forms in the place of centred differences the explicit expression for the displacements at node S, can be written as;

$$\underline{U}(i+1,j,k) = \underline{U}(i,j,k) + \underline{A}_2 \left[\underline{U}(i,j-1,k) - \underline{U}(i,j+1,k) \right] \qquad \text{E.1.8}$$

where $\underline{A}_2 = \begin{bmatrix} 0 & \frac{1}{2}a \\ \frac{1}{2} & 0 \end{bmatrix}$; and a is as for equation E.1.7

Similarly the explicit expression for the displacements at node T can be written as;

$$\underline{U}(i-1,j,k) = \underline{U}(i,j,k) + \underline{A}_2 \left[\underline{U}(i,j+1,k) - \underline{U}(i,j-1,k) \right] \qquad \text{E.1.9}$$

where $\underline{A}_2$ is as for equation E.1.8.

E.2 90° corner node formulation.

This appendix presents the difference formulations for the four 90° corners shown in Figure E.3, using a method due to Alterman and Rotenberg (1969), and extended to the cases of the two inverted nodes, shown as nodes S and T by the author. The notation used follows that given by Munasinghe (1973).

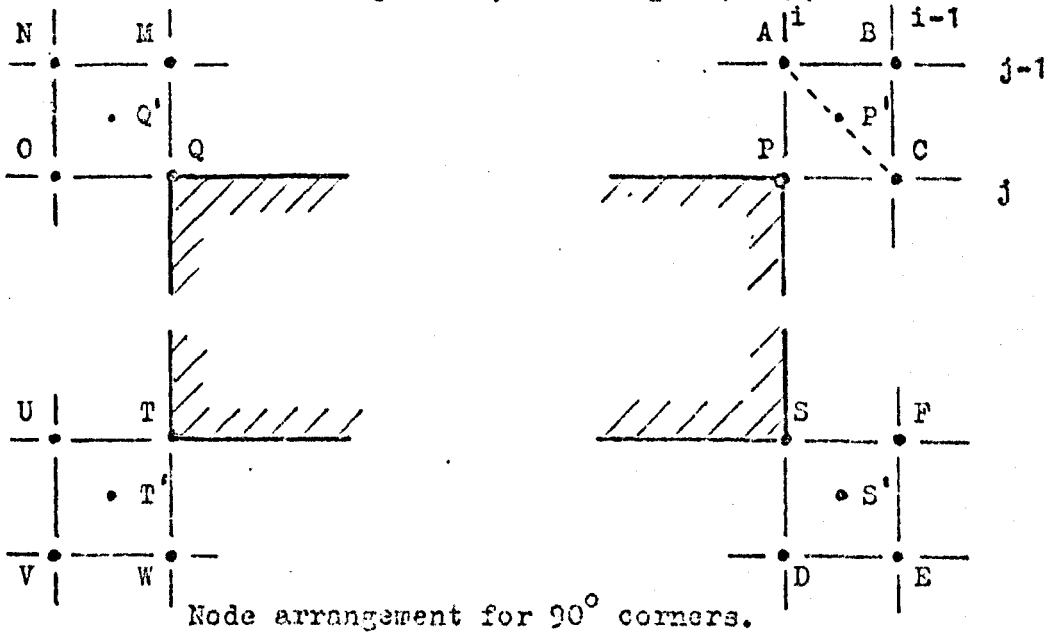

Node arrangement for 90° corners.

FIGURE E.3.

E.2.1 Right hand 90° corners.

For the node P, shown in Figure E.3, which is at the intersection of a horizontal and a vertical interface, both sets of boundary conditions apply simultaneously at this node.

To overcome difficulties in the solution of the equations at node P, a one-sided (off-centred) difference scheme is used in the direction perpendicular to the free surface and a centred scheme is used in the direction parallel to the surface, when each set of conditions are applied.

The displacements at the pseudo-nodes A and C are obtained by the substitution of the approximations, given as equation E.2.1, in the boundary conditions for the horizontal free surface, which were given as equation E.1.1, and the substitution of the approximations, given as equation E.2.2, in the boundary conditions for a vertical free surface, which were given as equation E.1.4.

$$\frac{\partial U}{\partial X_1} = \frac{U(i+1,j,k) - U(i-1,j,k)}{2d}$$

$$\frac{\partial U}{\partial X_2} = \frac{U(i,j,k) - U(i,j-1,k)}{h} \qquad \text{E.2.1}$$

$$\frac{\partial U}{\partial X_1} = \frac{U(i+1,j,k) - U(i,j,k)}{d}$$

$$\frac{\partial U}{\partial X_2} = \frac{U(i,j+1,k) - U(i,j-1,k)}{2h} \qquad \text{E.2.2}$$

The displacements at the pseudo-nodes are then obtained after considerable manipulation of the displacements in the body and on the surface of the medium. The equations for the displacements at nodes A and C are given as equations E.2.3 and E.2.4 respectively

$$\underline{U}(i,j-1,k) = \underline{D}_1\underline{U}(i,j,k) - \underline{D}_2\underline{U}(i,j+1,k) - \underline{D}_3\underline{U}(i-1,j,k) \qquad \text{E.2.3}$$

$$\underline{U}(i+1,j,k) = \underline{D}_4\underline{U}(i,j,k) - \underline{D}_5\underline{U}(i-1,j,k) - \underline{D}_6\underline{U}(i,j+1,k) \qquad \text{E.2.4}$$

where $\underline{D}_1 = \begin{bmatrix} 4/3 & 2/3r \\ a_1/r & a_2 \end{bmatrix}$ $\underline{D}_2 = \begin{bmatrix} 1/3 & 0 \\ 0 & a_3 \end{bmatrix}$ $\underline{D}_3 = \begin{bmatrix} 0 & 2/3 \\ a_1/r & 0 \end{bmatrix}$

$\underline{D}_4 = \begin{bmatrix} a_2 & a_1 r \\ 2r/3 & 4/3 \end{bmatrix}$ $\underline{D}_5 = \begin{bmatrix} a_3 & 0 \\ 0 & 1/3 \end{bmatrix}$ $\underline{D}_6 = \begin{bmatrix} 0 & a_1 r \\ 2r/3 & 0 \end{bmatrix}$

$$a_1 = \frac{2y^2}{(4-y^4)} \; ; \quad a_2 = \frac{4}{(4-y^4)} \; ; \quad a_3 = \frac{4}{(4-y^4)} \; ; \quad y^2 = (1 - 2(V_s/V_c)^2)$$

$r = d/h = 1$ for a uniform grid.

Using a variation of the method due to Alterman and Lowenthal (1970) made by Munasinghe (1973) the displacements at the pseudo-node B are obtained. In this formulation it is seen that the smaller the grid spacing (the larger the number of nodes per wavelength) the more accurate the calculations at the corner will be. The surface tractions at the corner are resolved parallel and perpendicular to a line joining the pseudo-nodes A and C and are set equal to zero.

Using a law for transformation of the invariant stress tensor (Nye 1960), the components of stress are given as;

$$T_{nn} = \left[\frac{(T_{11} + T_{22})}{2}\right] + T_{12} = 0 \; ; \quad T_{np} = \frac{(T_{11} - T_{22})}{2} = 0 \qquad \text{E.2.5}$$

The expressions for the displacements centred at P' for the node B are obtained by the substitution of the difference forms, given as equation E.2.6 in the equations E.2.5.

$$\frac{\partial \underline{U}}{\partial X_1} = \frac{\underline{U}(i+1,j,k) + \underline{U}(i+1,j-1,k) - \underline{U}(i,j,k) - \underline{U}(i,j-1,k)}{2d}$$

$$\frac{\partial \underline{U}}{\partial X_2} = \frac{\underline{U}(i+1,j,k) + \underline{U}(i,j,k) - \underline{U}(i+1,j-1,k) - \underline{U}(i,j-1,k)}{2h} \qquad \text{E.2.6}$$

When the necessary manipulations have been performed the displacements at the pseudo-node B are given as;

$$\underline{U}(i+1,j-1,k) = \underline{U}(i,j,k) + \underline{D}_7\left[\underline{U}(i,j-1,k) - \underline{U}(i+1,j,k)\right] \qquad \text{E.2.7}$$

where in the case of a uniform grid,

$$\underline{D}_7 = \begin{bmatrix} b_1 & -b_2 \\ b_2 & b_3 \end{bmatrix} ; \quad b_1 = 1 - 2r^2/a_1 \; ; \; b_2 = 2r/a_1$$

$$b_3 = 2/a_1 - 1 \; ; \; r = d/h$$

$$a_1 = 1 - \frac{2r(1 + y^2)}{(1 - y^2)} + r^2$$

and in the case of a uniform spatial grid,

$$\underline{D}_7 = \begin{bmatrix} a & b \\ -b & -a \end{bmatrix} ; \quad a = \frac{(1 + y^2)}{2y^2} \; ; \quad b = \frac{(1 - y^2)}{2y^2}$$

By a similar procedure to that given above the author has derived expressions which give the displacements at the set of pseudo-nodes associated with the node S, which is shown in Figure E.3.

The expressions for the displacements at the nodes D and F are obtained by substitution of the difference forms, given as equation E.2.8, in the horizontal free surface boundary conditions, which are given as equation E.1.1, and by the substitution of the difference forms, given as equation E.2.9 in the boundary conditions for a vertical free surface, which are given as equation E.1.4.

$$\frac{\partial U}{\partial X_1} = \frac{U(i+1,j,k) - U(i-1,j,k)}{2d}$$

$$\frac{\partial U}{\partial X_2} = \frac{U(i,j+1,k) - U(i,j,k)}{h} \qquad \text{E.2.8}$$

$$\frac{\partial U}{\partial X_1} = \frac{U(i+1,j,k) - U(i,j,k)}{d}$$

$$\frac{\partial U}{\partial X_2} = \frac{U(i,j+1,k) - U(i,j-1,k)}{2h} \qquad \text{E.2.9}$$

The displacements at the pseudo-nodes D and F are given as;

$$\underline{U}(i,j+1,k) = \underline{D}_1' \underline{U}(i,j,k) - \underline{D}_2' \underline{U}(i,j-1,k) - \underline{D}_3' \underline{U}(i-1,j,k) \qquad \text{E.2.10}$$

$$\underline{U}(i+1,j,k) = \underline{D}_4' \underline{U}(i,j,k) - \underline{D}_5' \underline{U}(i-1,j,k) - \underline{D}_6' \underline{U}(i,j-1,k) \qquad \text{E.2.11}$$

where the constants in the case of a uniform grid are,

$$\underline{D}_1' = \begin{bmatrix} 4/3 & -2/3 \\ a_1 & a_2 \end{bmatrix} \quad \underline{D}_2' = \begin{bmatrix} 1/3 & 0 \\ 0 & a_3 \end{bmatrix} \quad \underline{D}_3' = \begin{bmatrix} 0 & -2/3 \\ -a_1 & 0 \end{bmatrix}$$

$$\underline{D}_4' = \begin{bmatrix} a_2 & -a_1 \\ -2/3 & 4/3 \end{bmatrix} \quad \underline{D}_5' = \begin{bmatrix} a_3 & 0 \\ 0 & 1/3 \end{bmatrix} \quad \underline{D}_6' = \begin{bmatrix} 0 & -a_1 \\ -2/3 & 0 \end{bmatrix}$$

and the constants a_1, a_2, and a_3 are as for equations E.2.3 and E.2.4

A similar procedure to that used for node B is followed to give the equation for the displacements at node E and the derivation is again based on substitution in the stress relations given as equation E.2.5. The expressions for the displacements centred at S' use the substitution of the forms given as;

$$\frac{\partial \underline{U}}{\partial x_1} = \frac{\underline{U}(i+1,j,k) - \underline{U}(i+1,j+1,k) - \underline{U}(i,j,k) - \underline{U}(i,j+1,k)}{2d}$$

$$\frac{\partial \underline{U}}{\partial x_2} = \frac{\underline{U}(i,j+1,k) - \underline{U}(i+1,j+1,k) - \underline{U}(i,j,k) - \underline{U}(i+1,j,k)}{2h} \qquad \text{E.2.12}$$

Following manipulation of the equations the form for the displacements at the pseudo-node E is obtained, which is given as;

$$\underline{U}(i+1,j+1,k) = \underline{U}(i,j,k) - \underline{D}_7' \left[\underline{U}(i,j+1,k) - \underline{U}(i+1,j,k) \right] \qquad \text{E.2.13}$$

where $\underline{D}_7' = \begin{bmatrix} a & b \\ -b & -a \end{bmatrix}$; $a = \frac{(1 + y^2)}{2}$ $b = \frac{(1 - y^2)}{2}$

and y^2 is as for equation E.2.4

E.2.2 Left hand 90° corners.

These are the pair of corners shown as Q and T in Figure E.3. These corners are treated in a similar manner to the right hand corners considered in Appendix E.2.1, and corresponding sets of expressions for the displacements at the associated pseudo-nodes are obtained. The expressions for the displacements at the node Q follow the work of Munasinghe (1973) and those at the node T are derived by the author.

The expressions for the displacements at the pseudo-nodes M and O are given respectively as;

$$\underline{U}(i,j-1,k) = \underline{D}_1'\underline{U}(i,j,k) - \underline{D}_2'\underline{U}(i,j+1,k) - \underline{D}_3'\underline{U}(i+1,j,k) \qquad \text{E.2.14}$$

$$\underline{U}(i-1,j,k) = \underline{D}_4'\underline{U}(i,j,k) - \underline{D}_5'\underline{U}(i+1,j,k) - \underline{D}_6'\underline{U}(i,j+1,k) \qquad \text{E.2.15}$$

The expression for the pseudo-node N is given as;

$$\underline{U}(i-1,j-1,k) = \underline{U}(i,j,k) + \underline{D}_8 \left[\underline{U}(i,j-1,k) - \underline{U}(i-1,j,k) \right] \qquad \text{E.2.16}$$

where the constants in equations E.2.14 and E.2.15 are as for equations E.2.10 and E.2.11. and;

$$\underline{D}_8 = \begin{bmatrix} b_5 & b_6 \\ b_6 & b_7 \end{bmatrix} ; \quad b_5 = \frac{(1 - 2r)}{a_2} \quad b_6 = \frac{2r}{a_2} \quad b_7 = \frac{2}{a_2 - 1}$$

$$a_2 = 1 + \frac{2r(1 + y^2)}{1 - y^2} + r^2 \quad , \text{ for a uniform grid } r = d/h = 1$$

and b_5, b_6 and b_7 simplify to;

$$\underline{D}_8 = \begin{bmatrix} b_5' & b_6' \\ b_6' & -b_5' \end{bmatrix} ; \quad b_5' = \frac{(1 - y^2)}{2} \qquad b_6' = \frac{(1 - y^2)}{2}$$

For the case of the node T, shown in Figure E.3 the expressions for the pseudo-nodes U and W are given respectively as;

$$\underline{U}(i-1,j,k) = \underline{D}_1\underline{U}(i,j,k) - \underline{D}_2\underline{U}(i,j-1,k) - \underline{D}_3\underline{U}(i+1,j,k) \qquad \text{E.2.17}$$

$$\underline{U}(i,j+1,k) = \underline{D}_4\underline{U}(i,j,k) - \underline{D}_5\underline{U}(i+1,j,k) - \underline{D}_6\underline{U}(i,j-1,k) \qquad \text{E.2.18}$$

where the constants are as for equations E.2.3 and E.2.4.

The expression for the pseudo-node V is given as;

$$\underline{U}(i-1,j+1,k) = \underline{U}(i,j,k) + \underline{D}_8'\left[\underline{U}(i,j+1,k) - \underline{U}(i-1,j,k)\right] \qquad \text{E.2.19}$$

where $\underline{D}_8' = \underline{D}_7$ in the case of a uniform grid.

E.3 270° corners.

In the case of 270° corners both the horizontal and vertical free surface boundary conditions apply at the corner. For the nodes P and Q, shown in Figure E.4, Munasinghe (1973) has produced a triple pseudo-node formulation at the nodes E and H.

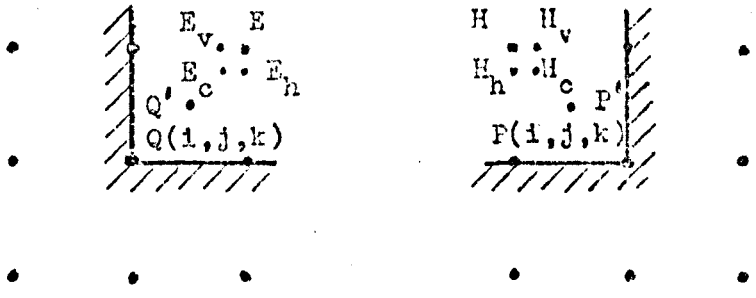

Node arrangement for 270° corners.

FIGURE E.4.

E.3.1 Right hand 270° corner.

The triple node, as developed by Munasinghe (1973), at node E is developed so that the necessary boundary conditions for the three nodes that use the values of displacements at that node can be reflected in that node.

The displacements at node E_v and E_h are obtained by the application of the boundary formulations for the vertical and horizontal free surfaces as given in Appendix E.1, as equations E.1.5 and E.1.2. The pseudo-node corresponding to the corner point Q is treated in the same way as the 90° corner and Q' becomes the effective corner.

The expression for the displacements at the node E_c, in the case of a uniform grid is given as;

$$\underline{U}(i+1,j-1,k) = \underline{U}(i,j,k) + \underline{L}_1 \left[\underline{U}(i,j-1,k) - \underline{U}(i+1,j,k) \right] \quad \text{E.3.1}$$

where $\underline{L}_1 = \underline{D}_7$ as used for equation E.2.7.

E.3.2. Left hand 270° corner.

This corner is the corresponding dual problem to the right hand case and the set of equations used for the nodes H_v and H_h are the boundary formulations for the vertical and horizontal free surfaces given in Appendix E.1. The pseudo-node corresponding to the corner point P is treated in the same way as the 90° corner and P' becomes the effective corner.

The expression for the displacements at the node E_c, in the case of a uniform grid is given as;

$$\underline{U}(i-1,j-1,k) - \underline{U}(i,j,k) + \underline{L}_2 \left[\underline{U}(i,j-1,k) - \underline{U}(i-1,j,k) \right] \quad \text{E.3.2}$$

where $\underline{L}_2 = \underline{D}_8$ as used for equation E.2.16.

Appendix F.

F. Second order finite difference formulations for free surface nodes.

This appendix presents schemes for second order boundary condition formulations, initially due to Ilan et al (1975), and extended by Ilan and Loewenthal (1976), and in this study by the author to cover a larger range of types of nodes.

F.1 Free surface node formulations.

Two sets of free surface formulations are presented in this appendix. The basic formulation is the second order composed approximation due to Ilan et al (1975), which is found to have a very limited region of stability.

The second formulation is the new composed formulation which was developed for the horizontal free surface by Ilan and Loewenthal (1976) to extend the region of stability and this scheme has been applied to vertical free surfaces by the author. The new formulation uses the formulation for the component of displacement parallel to the free surface from the composed approximation and a new formulation for the component of displacement normal to the surface.

The basic node arrangements, which do not include pseudo-nodes, for surface formulations, are shown in Figure F.1.

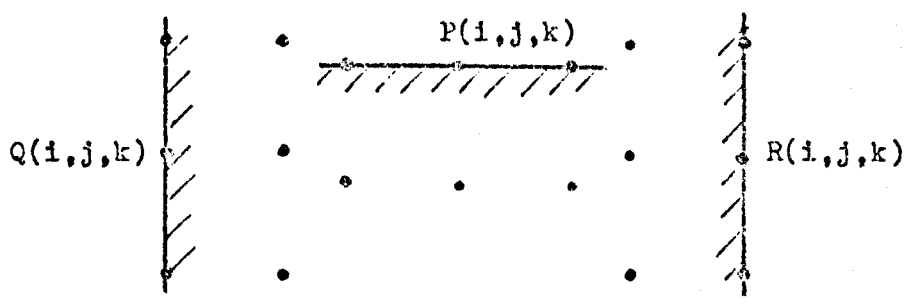

Node arrangements for second order surface formulations.

FIGURE F.1

F.1.1 Composed approximation for horizontal free surface.

In the development of a boundary node formulation which does not use pseudo-nodes, as the derivatives with respect to X_2 on the free surface $X_2 = 0$ can only be approximated by one-sided differences, they are replaced by derivatives with respect to X_1 and time, for which centred difference forms can be applied.

On the horizontal free surface, node P(i,j,k), shown in Figure F.1, the boundary condition for a stress free surface applies and this is given as equation F.1.1, where the components are components of the stress tensor as defined in equation 2.3.8.

$$T_{21} = T_{22} = 0 \qquad \text{F.1.1}$$

The components can be written in full and are given as;

$$\frac{\partial U_2}{\partial X_1} + \frac{\partial U_1}{\partial X_2} = 0 \qquad \text{F.1.2}$$

$$\frac{\partial U_2}{\partial X_2} + (1 - 2 (V_s^2/V_c^2)) \frac{\partial U_1}{\partial X_1} = 0 \qquad \text{F.1.3}$$

These equations, equations F.1.2 and F.1.3, are differentiated with respect to X_1 on $X_2 = 0$, and give;

$$\frac{\partial^2 U_1}{\partial X_1 \partial X_2} = - \frac{\partial^2 U_2}{\partial X_1^2} \qquad \text{F.1.4}$$

$$\frac{\partial^2 U_2}{\partial X_1 \partial X_2} = - (1 - 2 (V_s^2/V_c^2)) \frac{\partial^2 U_1}{\partial X_1^2} \qquad \text{F.1.5}$$

The basic equations of motion for the system are defined in Section 2.3 and are given here as;

$$\frac{\partial^2 U_1}{\partial t^2} = V_c^2 \frac{\partial^2 U_1}{\partial X_1^2} + V_s^2 \frac{\partial^2 U_1}{\partial X_2^2} + (V_c^2 - V_s^2) \frac{\partial^2 U_2}{\partial X_1 \partial X_2} \qquad \text{F.1.6}$$

$$\frac{\partial^2 U_2}{\partial t^2} = V_c^2 \frac{\partial^2 U_2}{\partial X_2^2} + V_s^2 \frac{\partial^2 U_2}{\partial X_1^2} + (V_c^2 - V_s^2) \frac{\partial^2 U_1}{\partial X_1 \partial X_2} \qquad \text{F.1.7}$$

From Taylor series expansions it is necessary to define expansions for $U_1(i,j+1,k)$ and $U_2(i,j+1,k)$ and these are given as;

$$U_1(i,j+1,k) = U_1(i,j,k) + h\frac{\partial U_1}{\partial X_2} + \tfrac{1}{2}h^2\frac{\partial^2 U_1}{\partial X_2^2} + O(h^3) \qquad \text{F.1.8}$$

$$U_2(i,j+1,k) = U_2(i,j,k) + h\frac{\partial U_2}{\partial X_2} + \tfrac{1}{2}h^2\frac{\partial^2 U_2}{\partial X_2^2} + O(h^3) \qquad \text{F.1.9}$$

The equations F.1.2 to F.1.9 define two sets of eight equations and these contain eight unknowns, the last two of which occur in the finite difference forms of the second order time derivatives in equations F.1.6 and F.1.7. The system of linear equations can be reduced to give equations for each of the two components and these are;

$$U_1(i,j+i,k) = U_1(i,j,k) - h\frac{\partial U_2}{\partial X_1} + \tfrac{1}{2}h^2\left[\frac{1}{V_s^2}\frac{\partial^2 U_1}{\partial t^2} - \frac{\partial^2 U_1}{\partial X_1^2}\left[\frac{3V_c^2 - 2V_s^2}{V_c^2}\right]\right] + O(h^3) \qquad \text{F.1.10}$$

$$U_2(i,j+1,k) = U_2(i,j,k) - h(1 - 2(V_s^2/V_c^2))\frac{\partial U_1}{\partial X_1} + \tfrac{1}{2}h^2\left[\frac{1}{V_c^2}\frac{\partial^2 U_2}{\partial t^2} + (1 - 2(V_s^2/V_c^2))\frac{\partial^2 U_2}{\partial X_1^2}\right] + O(h^3) \qquad \text{F.1.11}$$

In equations F.1.10 and F.1.11 there are only two unknowns after finite difference substitution and these are $U_1(i,j,k+1)$ and $U_2(i,j,k+1)$. The explicit forms for the displacements at a free surface are then obtained and these are given as;

$$U_1(i,j,k+1) = 2V_s^2\left[\frac{s}{h}\right]^2 U_1(i,j+1,k)$$

$$+2V_s^2\left[\frac{s}{h}\right]^2\left[\left[\frac{h}{s}\right]^2\frac{1}{V_s^2} - 1 - \left[\frac{h}{d}\right]^2\left[\frac{3V_c^2 - 2V_s^2}{V_c^2}\right]\right]U_1(i,j,k)$$

$$+ V_s^2\left[\frac{s}{h}\right]^2\left[\frac{h}{d}\right]\left[U_2(i+1,j,k) - U_2(i-1,j,k)\right] - U_1(i,j,k-1)$$

$$+ V_s^2\left[\frac{s}{d}\right]^2\left[\frac{3V_c^2 - 2V_s^2}{V_c^2}\right]\left[U_1(i+1,j,k) - U_1(i-1,j,k)\right] \qquad \text{F.1.12}$$

$$U_2(i,j,k+1) = 2V_c^2\left[\frac{s}{h}\right]^2 U_2(i,j+1,k) - U_2(i,j,k-1)$$

$$+2V_c^2\left[\frac{s}{h}\right]^2\left[\left[\frac{h}{s}\right]^2\frac{1}{V_c^2} - 1 + \left[\frac{h}{d}\right]^2\left[1 - 2\frac{V_s^2}{V_c^2}\right]\right]U_2(i,j,k)$$

$$+ V_c^2\left[1 - 2\frac{V_s^2}{V_c^2}\right]\left[\frac{s}{h}\right]^2\left[U_1(i+1,j,k) - U_1(i-1,j,k)\right]$$

$$- V_c^2\left[1 - 2\frac{V_s^2}{V_c^2}\right]\left[\frac{s}{h}\right]^2\left[U_2(i+1,j,k) - U_2(i-1,j,k)\right] \qquad \text{F.1.13}$$

F.1.2 New composed approximation for horizontal free surface.

It has been found by Ilan and Loewenthal (1976) that the region of stability for the composed formulation, given as equations F.1.12 and F.1.13, has severe limitations and hence cannot be used with the data for many common materials that have a Poisson's ratio larger than 0.27. It is found that it is the vertical component of displacement that is the most sensitive part of the composed scheme and a reformulation for this component has been proposed by Ilan and Loewenthal (1976).

Following the procedure of Ilan and Loewenthal (1976), the author has derived a new composed formulation adapted for the coordinate system used in the present study.

A Taylor series expansion for the vertical component about the point P(i,j,k) is given as;

$$U_2(i,j+1,k) = U_2(i,j,k) + h\frac{\partial U_2}{\partial X_2} + \tfrac{1}{2}h^2\frac{\partial^2 U_2}{\partial X_2^2} + O(h^3) \qquad \text{F.1.14}$$

The boundary condition, given as equation F.1.3, is rewritten in a form for substitution in equation F.1.14 and is given as;

$$\frac{\partial U_2}{\partial x_2} = -\left[\frac{V_c^2 - 2V_s^2}{V_c^2}\right]\frac{\partial U_1}{\partial x_1} \qquad \text{F.1.15}$$

The equation of motion, given as equation F.1.7, is also rewritten in a form for substitution into equation F.1.14 and is given as;

$$\frac{\partial^2 U_2}{\partial x_2^2} = \frac{1}{V_c^2}\frac{\partial^2 U_2}{\partial t^2} - \frac{V_s^2}{V_c^2}\frac{\partial^2 U_2}{\partial x_1^2} - \left[\frac{V_c^2 - V_s^2}{V_c^2}\right]\frac{\partial^2 U_1}{\partial x_1 \partial x_2} \qquad \text{F.1.16}$$

The approximation used for the mixed derivative in the equation of motion is given as;

$$\frac{\partial^2 U_1}{\partial x_1 \partial x_2} = \frac{1}{2dh}\Big[U_1(i+1,j+1,k) - U_1(i+1,j,k) - U_1(i-1,j+1,k) + U_1(i-1,j,k)\Big] \qquad \text{F.1.17}$$

The equations F.1.14 to F.1.17 are a system of linear equations that reduce to the form given as;

$$U_2(i,j+1,k) = U_2(i,j,k) - h\left[\frac{V_c^2 - 2V_s^2}{V_c^2}\right]\frac{\partial U_1}{\partial x_1} + \frac{h^2}{2}\left[\frac{1}{V_c^2}\frac{\partial^2 U_2}{\partial t^2} - \frac{V_s^2}{V_c^2}\frac{\partial^2 U_2}{\partial x_1^2} - \left[\frac{V_c^2 - V_s^2}{V_c^2}\right]\frac{\partial^2 U_1}{\partial x_1 \partial x_2}\right] \qquad \text{F.1.18}$$

Difference forms are substituted in equation F.1.18 and the terms rearranged to give the expression for the vertical component of displacement for the surface node P(i,j,k) which is given as;

$$\begin{aligned} U_2(i,j,k+1) = {} & 2\left[1 - s^2/h^2V_c^2 - s^2/h^2V_s^2\right]U_2(i,j,k) - U_2(i,j,k-1) \\ & + 2\,s^2/h^2V_c^2\,U_2(i,j+1,k) + V_s^2 s^2/h^2\left[U_2(i+1,j,k) + U_2(i-1,j,k)\right] \\ & + s^2/h^2\,(V_c^2 - 3V_s^2)\tfrac{1}{2}\left[U_1(i+1,j,k) - U_1(i-1,j,k)\right] \\ & + \tfrac{1}{2}\,s^2/h^2(V_c^2 - V_s^2)\left[U_1(i+1,j+1,k) - U_1(i-1,j+1,k)\right] \end{aligned} \qquad \text{F.1.19}$$

F.1.3 Composed approximation for vertical free surfaces.

For the vertical free surface nodes, nodes Q and R in Figure F.1, the formulations can be obtained in two ways, either by the direct solution of the system of linear equations, by the method used to derive rquations F.1.12 and F.1.13, or by the application of a set of transformations derived by Ilan et al (1975), to equations F.1.12 and F.1.13.

The set of equations for node Q are presented as equations F.1.20 and F.1.21, and the sign changes necessary for their application to node R are indicated by a second sign in the appropriate places.

$$U_1(i,j,k+1) = 2V_c^2(s/d)^2 U_1(i\mp1,j,k) - U_1(i,j,k-1)$$
$$+ 2\left[1 - V_c^2(s/d)^2 - (s/h)^2(V_c^2 - 2V_s^2)\right] U_1(i,j,k)$$
$$\mp (s/d)^2(d/h)\,(V_c^2 - 2V_s^2)\left[U_2(i,j+1,k) - U_2(i,j-1,k)\right]$$
$$- (s/h)^2(V_c^2 - 2V_s^2)\left[U_1(i,j+1,k) + U_1(i,j-1,k)\right] \qquad \text{F.1.20}$$

$$U_2(i,j,k+1) = 2V_s^2(s/d)^2 U_2(i\mp1,j,k) - U_2(i,j,k-1)$$
$$+2V_s^2(s/h)^2\left[(h/s)^2 1/V_s^2 - 1 - (3V_c^2 - 2V_s^2)/V_c^2\right] U_2(i,j,k)$$
$$\mp V_s^2(s/d)^2 d/h\left[U_1(i,j+1,k) - U_1(i,j-1,k)\right]$$
$$\pm V_s^2(3V_c^2 - 2V_s^2)/V_c^2\,(s/h)^2\left[U_2(i,j+1,k) + U_2(i,j-1,k)\right]$$

F.1.21

F.1.4 New composed approximation for vertical free surfaces.

For the vertical free surface nodes the author has derived new composed type formulations using the same procedure as that given for equation F.1.19, in Appendix F.1.2.

For node Q, shown in Figure F.1, the new composed form is given as;

$$U_1(i,j,k+1) = 2V_c^2(s/d)^2U_1(i+1,j,k) - U_1(i,j,k-1)$$
$$+2\left[1 - V_c^2(s/d)^2 - V_s^2(s/d)^2\right]U_1(i,j,k)$$
$$+ (s/d)^2\tfrac{1}{2}(V_c^2 - 3V_s^2)\left[U_2(i,j+1,k) - U_2(i,j-1,k)\right]$$
$$+ (s/d)^2V_s^2\left[U_1(i,j+1,k) + U_1(i,j-1,k)\right]$$
$$- \tfrac{1}{2}(s/d)^2(V_c^2 - V_s^2)\left[U_2(i+1,j-1,k) - U_2(i+1,j+1,k)\right] \qquad \text{F.1.22}$$

For node R, shown in Figure F.1, the new composed for is given as;

$$U_1(i,j,k+1) = 2V_c^2(s/d)^2U_1(i-1,j,k) - U_1(i,j,k-1)$$
$$+2\left[1 - V_c^2(s/d)^2 - V_s^2(s/d)^2\right]U_1(i,j,k)$$
$$- (s/d)^2\tfrac{1}{2}(V_c^2 - 3V_s^2)\left[U_2(i,j+1,k) - U_2(i,j-1,k)\right]$$
$$+ (s/d)^2V_s^2\left[U_1(i,j+1,k) + U_1(i,j-1,k)\right]$$
$$+ \tfrac{1}{2}(s/d)^2(V_c^2 - V_s^2)\left[U_2(i-1,j-1,k) - U_2(i-1,j+1,k)\right] \qquad \text{F.1.23}$$

The equations F.1.22 and F.1.23 are used with the corresponding forms for the vertical components of displacement given as equation F.1.21.

F.2 Second order formulation for 270° corners.

In the study by Ilan et al (1975) a second order formulation was proposed for use at the corner node for a quarter space set in a three quarter space and in the present study it was applied to nodes S and T shown in Figure F.2.

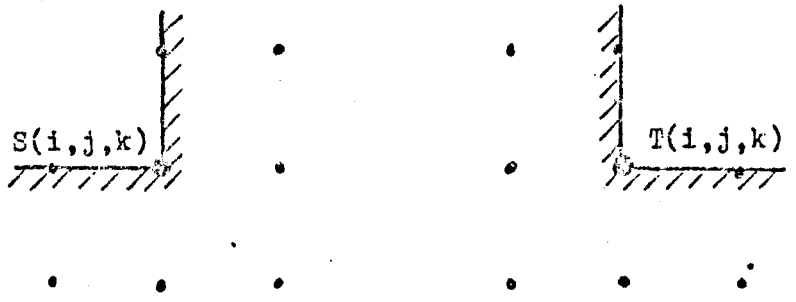

Node arrangements for second order 270° corner formulations.

FIGURE F.2.

The equations for the application of a second order scheme to nodes S and T, shown in Figure F.2, are obtained directly from the equations of motion, given as equations F.1.6 and F.1.7 by the use of a different form for the mixed derivative.

The form of approximation used for the mixed derivative is after Ilan et al (1975) and for node S given as;

$$\frac{\partial^2 U_2}{\partial X_1 \partial X_2} = \frac{1}{4hd}\Big[2U_2(i+1,j+1,k) - U_2(i,j+1,k) - U_2(i+1,j-1,k)$$

$$+ U_2(i,j-1,k) - U_2(i+1,j,k) - U_2(i-1,j+1,k) + U_2(i-1,j,k)\Big]$$

$$+ O(h) \qquad \text{F.2.1}$$

with a similar expression for the other component.

The full equation for node S is given as;

$$U_1(i,j,k+1) = 2U_1(i,j,k) - U_1(i,j,k-1)$$
$$+ V_c^2(s/h)^2\left[U_1(i+1,j,k) - 2U_1(i,j,k) + U_1(i-1,j,k)\right]$$
$$+ V_s^2(s/h)^2\left[U_1(i,j+1,k) - 2U_1(i,j,k) + U_1(i,j-1,k)\right]$$
$$+ (V_c^2 - V_s^2)\, s^2/4dh\Big[2U_2(i+1,j+1,k) - U_2(i,j+1,k)$$
$$- U_2(i+1,j-1,k) + U_2(i,j-1,k) - U_2(i+1,j,k) - U_2(i-1,j+1,k)$$
$$+ U_2(i-1,j,k)\Big] \qquad \text{F.2.2}$$

The expression for the $U_2(i,j,k+1)$ term is obtained by the replacement of all U_1 by U_2 and U_2 by U_1 in equation F.2.2.

The expressions for node T are obtained by the replacement of the mixed derivative in equation F.2.2 by the expression given as;

$$\frac{\partial^2 U_2}{\partial x_1 \partial x_2} = \frac{1}{4dh}\Big[2U_2(i-1,j+1,k) - U_2(i,j+1,k) - U_2(i+1,j+1,k) - U_2(i-1,j,k) - U_2(i-1,j,k) - U_2(i-1,j-1,k) + U_2(i,j-1,k)\Big] + O(h) \qquad \text{F.2.3}$$

F.3 Second order formulation for 90° corner.

Two second order formulations for the 90° corner have been considered by Ilan (1978, in press) in a recent study of body waves at corners.

The problem in the solution of the boundary conditions and equations of motion is that at the corner the boundary conditions for both the vertical and horizontal free surfaces apply which over conditions the problem. Some form of approximation must there therefore be made.

In the present study the author, following discussions with Ilan, has adopted the use of the following scheme, for the corner node, node O shown in Figure F.3.

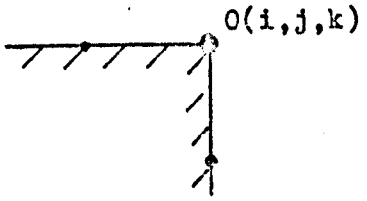

Node arrangement at a 90° corner.

FIGURE F.3.

The new composed formulations for the horizontal and vertical free surfaces, presented in Appendices F.1.2 and F.1.4 respectively are applied to nodes A and D.

The components of displacement at node O(i,j,k) are then calculated using the expressions given as;

$$U_1(i,j,k+1) = U_1(i-1,j,k+1) \qquad \text{F.3.1}$$

$$U_2(i,j,k+1) = U_2(i,j+1,k+1) \qquad \text{F.3.2}$$

Appendix G.

G. Second order finite difference formulations for interface nodes.

This appendix presents second order finite difference forms for nodes located at the interface between two media, and those at the point where an interface between two media meets a free surface.

The initial work on extending second order formulations to interfaces is due to Ilan et al (1975) and the author has reformulated their equations to make them consi tant with the coordinate system used in the present study and to express the constants in terms of wave velocities in place of Lamé constants. The author has also extended the scheme to consider the free surface/interface node for welded quarter spaces. The range of two media configurations for which formulations are presented are shown in Figure 4.7 in Section 4.3.4.

G.1.1 Second order formulations for horizontal interfaces.

The horizontal interface formulation is due to Ilan et al (1975) and in the present study the method used to derive the formulation for node P(i,j,k), shown in Figure G.1,has followed their method.

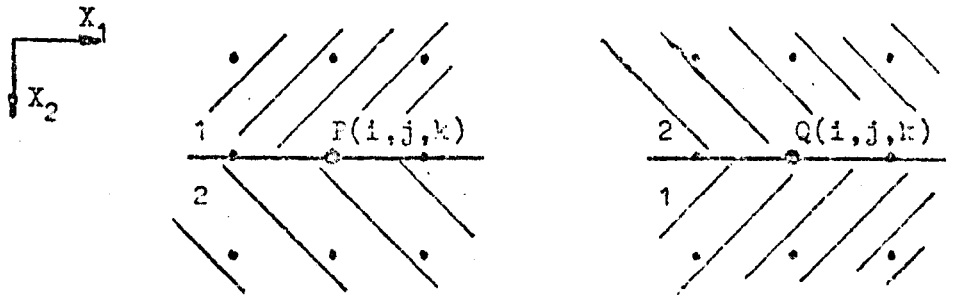

Node arrangements for horizontal interfaces with second order formulations.

FIGURE G.1.

The boundary conditions for a horizontal interface, along X_2 = constant for node P(i,j,k), are for the continuity of stress and displacement and these are given as;

$$(V_s^2\rho)_1\left[\frac{\partial U_2^1}{\partial X_1} - \frac{\partial U_1^1}{\partial X_2}\right] = (V_s^2\rho)_2\left[\frac{\partial U_2^2}{\partial X_1} - \frac{\partial U_1^2}{\partial X_2}\right] \qquad \text{G.1.1.}$$

$$(V_c^2\rho)_1\frac{\partial U_2^1}{\partial X_2} + \rho(V_c^2 - 2V_s^2)_1\frac{\partial U_1^1}{\partial X_1} = (V_c^2\rho)_2\frac{\partial U_2^2}{\partial X_2} + \rho(V_c^2 - 2V_s^2)_2\frac{\partial U_1^2}{\partial X_1} \qquad \text{G.1.2.}$$

$$U_1^1 = U_1^2 \qquad \text{G.1.3}$$

$$U_2^1 = U_2^2 \qquad \text{G.1.4}$$

At the interface the displacements are denoted as;

$$U_1^c = U_1^1 = U_1^2$$
$$U_2^c = U_2^1 = U_2^2 \qquad \text{G.1.5}$$

where U_1^c and U_2^c are not differentiable on the interface with respect to X_2 but they are continuously differentiable with respect to X_1 and t.

Equations G.1.1 and G.1.2 can be rewritten in the forms given as;

$$(V_s^2\rho)_1\frac{\partial U_1^1}{\partial X_2} - (V_s^2\rho)_2\frac{\partial U_1^2}{\partial X_2} = -\left[(V_s^2\rho)_1 - (V_s^2\rho)_2\right]\frac{\partial U_2^c}{\partial X_1} \qquad \text{G.1.6}$$

$$(V_c^2\rho)_1\frac{\partial U_2^1}{\partial X_2} - (V_c^2\rho)_2\frac{\partial U_2^2}{\partial X_2} - \left[(\rho(V_c^2 - 2V_s^1))_1 - (\rho(V_c^2 - 2V_s^2))\right]\frac{\partial U_1^c}{\partial X_1} \qquad \text{G.1.7}$$

The equations of motion for the two media can be written in the forms given as;

$$\frac{\partial^2 U_1^j}{\partial X_2^2} + \left(\frac{V_c^2 - V_s^2}{V_s^2}\right)_j\frac{\partial^2 U_2^j}{\partial X_1 \partial X_2} = \frac{1}{V_{sj}^2}\frac{\partial^2 U_1^c}{\partial t^2} - \left(\frac{V_c^2}{V_s^2}\right)_j\frac{\partial^2 U_1^c}{\partial X_1^2} \qquad \text{G.1.8}$$

$$\frac{\partial^2 U_2^j}{\partial X_2^2} + \left(\frac{V_c^2 - V_s^2}{V_c^2}\right)_j\frac{\partial^2 U_1^j}{\partial X_1 \partial X_2} = \frac{1}{V_{cj}^2}\frac{\partial^2 U_2^c}{\partial t^2} - \left(\frac{V_s^2}{V_c^2}\right)_j\frac{\partial^2 U_2^c}{\partial X_1^2} \qquad \text{G.1.9}$$

where the superscripts and subscripts j = 1 or 2 indicated the media involved.

Equations C.1.6 and C.1.7 are differentiated with respect to X_1 to give the forms given as;

$$(V_s^2\rho)_1 \frac{\partial^2 U_1^1}{\partial X_2 \partial X_1} - (V_s^2\rho)_2 \frac{\partial^2 U_1^2}{\partial X_2 \partial X_1} = -\left[(V_s^2\rho)_1 - (V_s^2\rho)_2\right] \frac{\partial^2 U_2^2}{\partial X_1^2} \qquad \text{C.1.10}$$

$$(V_c^2\rho)_1 \frac{\partial^2 U_2^1}{\partial X_2 \partial X_1} - (V_c^2\rho)_2 \frac{\partial^2 U_2^2}{\partial X_2 \partial X_1} = -\left[(\rho(V_c^2 - 2V_s^2))_1 - (\rho(V_c^2 - 2V_s^2))_2\right] \frac{\partial^2 U_1^c}{\partial X_1^2}$$

C.1.11

Also a set of Taylor series expansions are required and these are given as;

$$\pm h \frac{\partial U_1^m}{\partial X_2} - \frac{h^2}{2} \frac{\partial^2 U_1^m}{\partial X_2^2} = U_1^m(i,j\pm1,k) - U_1^c(i,j,k) + O(h^3) \qquad \text{C.1.12}$$

$$\pm h \frac{\partial U_2^m}{\partial X_2} - \frac{h^2}{2} \frac{\partial^2 U_2^m}{\partial X_2^2} = U_2^m(i,j\pm1,k) - U_2^c(i,j,k) + O(h^3) \qquad \text{C.1.13}$$

where m = 1,2 for the two media and the second sign indicated the form required for the forward term.

The finite difference approximations used for the mixed terms are given as;

$$\pm 2dh \frac{\partial^2 U_1^m}{\partial X_1 \partial X_2} = \left[U_1^m(i+1,j\pm1,k) - U_1^m(i-1,j\pm1,k) - U_1^c(i+1,j,k) + U_1^c(i-1,j,k)\right] + O((dh)^2) \qquad \text{C.1.14}$$

$$\pm 2dh \frac{\partial^2 U_2^m}{\partial X_1 \partial X_2} = \left[U_2^m(i+1,j\pm1,k) - U_2^m(i-1,j\pm1,k) - U_2^c(i+1,j,k) + U_2^c(i-1,j,k)\right] + O((dh)^2) \qquad \text{C.1.15}$$

The system of equations up to equation C.1.15 provides two sets of linear equations, based on the equations of motion, each of which is a set of fourteen equations which contain fourteen unknowns.

By the solution of these sets of equations expressions for t the time development of the displacements at node P(i,j,k) are given.

The expressions for the displacements for a point on a horizontal interface (P(i,j,k)) are given as;

$$U_1(i,j,k+1) = 2U_1(i,j,k) - U_1(i,j,k-1)$$

$$+ \frac{2}{\rho_1 + \rho_2}\left[\frac{s}{h}\right]^2\Big[\rho_2 V_{s2}^2\, U_1(i,j+1,k) + \rho_1 V_{s1}^2\, U_1(i,j-1,k)$$

$$- (\rho_1 V_{s1}^2 + \rho_2 V_{s2}^2)U_1(i,j,k)$$

$$+ \tfrac{1}{2}(h/d)\Big[\rho_2 V_{s2}^2 - \rho_1 V_{s1}^2\Big]\Big[U_2(i-1,j,k) - U_2(i-1,j,k)\Big]\Big]$$

$$+ \frac{\rho_1 V_{c1}^2 + \rho_2 V_{c2}^2}{\rho_1 - \rho_2}\left[\frac{s}{h}\right]^2\Big[U_1(i+1,j,k) - 2U_1(i,j,k) + U_1(i-1,j,k)\Big]$$

$$+ \frac{s^2}{\rho_1 + \rho_2}\, G \qquad \text{G.1.16}$$

$$U_2(i,j,k+1) = 2U_2(i,j,k) - U_2(i,j,k-1)$$

$$+ \frac{2}{\rho_1 + \rho_2}\left[\frac{s}{h}\right]^2\Big[\rho_2 V_{c2}^2 U_2(i,j+1,k) + \rho_1 V_{s1}^2 U_2(i,j-1,k)$$

$$- (\rho_1 V_{c1}^2 + \rho_2 V_{c2}^2)\, U_2(i,j,k)$$

$$+ \tfrac{1}{2}(h/d)\Big[(\rho_2(V_{c2}^2 - 2V_{s2}^2)) - (\rho_1(V_{c1}^2 - 2V_{s1}^2))\Big]\Big[U_1(i+1,j,k) - U_1(i-1,j,k)\Big]\Big]$$

$$+ \left[\frac{\rho_1 V_{s1}^2 + \rho_2 V_{s2}^2}{\rho_1 + \rho_2}\right]\left[\frac{s}{h}\right]^2\Big[U_2(i+1,j,k) - 2U_2(i,j,k) + U_2(i-1,j,k)\Big]$$

$$+ \frac{s^2}{\rho_1 - \rho_2}\, H \qquad \text{G.1.17}$$

where $G = (G_1 + G_2)/2$ and $H = (H_1 + H_2)/2$ and G_1, G_2, H_1 and H_2 are defined in equations G.1.18 to G.1.21 respectively.

The terms G_1 and H_1 and the terms G_2 and H_2 are obtained by the use of the forward and reverse approximations for the mixed derivatives, which are given as equations G.1.14 and G.1.15.

$$G_1 = \frac{1}{2dh}\left[\rho_2(V_{c2}^2 - V_{s2}^2) + \left[(V_{c1}^2 - V_{s1}^2)(\rho_2 V_{c2}^2) \Big/ V_{c1}^2\right]\right]$$
$$\left[U_2^2(i+1,j+1,k) - U_2^2(i-1,j+1,k) - U_2^c(i+1,j,k) + U_2^c(i-1,j,k)\right]$$
$$+ \left[\frac{(V_{c1}^2 - V_{s1}^2)(\rho_2(V_{c2}^2 - 2V_{s2}^2) - \rho_1(V_{c2}^2 - 2V_{s1}^2))}{V_{c1}^2}\right]\frac{\partial^2 U_1^c}{\partial X_1^2} + O(h)$$

G.1.18

$$G_2 = \frac{1}{2dh}\left[\rho_1(V_{c1}^2 - V_{s1}^2) + \left[(V_{c2}^2 - V_{s2}^2)(\rho_1 V_{c1}^2) \Big/ V_{c2}^2\right]\right]$$
$$\left[U_2^c(i+1,j,k) - U_2^c(i-1,j,k) - U_2^1(i+1,j-1,k) + U_2^1(i-1,j-1,k)\right]$$
$$+ \left[\frac{(V_{c2}^2 - V_{s2}^2)(\rho_1(V_{c1}^2 - 2V_{s1}^2) - \rho_2(V_{c2}^2 - 2V_{s2}^2))}{V_{c2}^2}\right]\frac{\partial^2 U_1^c}{\partial X_1^2} + O(h)$$

G.1.19

$$H_1 = \frac{1}{2dh}\left[\rho_2(V_{c2}^2 - V_{s2}^2) - \left[(V_{c1}^2 - V_{s1}^2)(\rho_2 V_{s2}^2) \Big/ V_{s1}^2\right]\right]$$
$$\left[U_1^2(i+1,j+1,k) - U_1^2(i-1,j+1,k) - U_1^c(i+1,j,k) + U_1^c(i-1,j,k)\right]$$
$$+ (V_{c1}^2 - V_{s1}^2)(\rho_2 V_{s2}^2 - \rho_1 V_{s1}^2)\Big/(V_{s1}^2)\ \frac{\partial^2 U_2^c}{\partial X_1^2} + O(h)$$

G.1.20

$$H_2 = \frac{1}{2dh}\left[\rho_1(V_{c1}^2 - V_{s1}^2) - \left[(V_{c2}^2 - V_{s2}^2)(\rho_1 V_{s1}^2) \Big/ V_{s2}^2\right]\right]$$
$$\left[U_1^c(i+1,j,k) - U_1^c(i-1,j,k) - U_1^1(i+1,j-1,k) + U_1^1(i-1,j-1,k)\right]$$
$$+ (V_{c2}^2 - V_{s2}^2)(\rho_1 V_{s1}^2 - \rho_2 V_{s2}^2)\Big/(V_{s2}^2)\ \frac{\partial^2 U_2^c}{\partial X_1^2} + O(h)$$

G.1.21

The equations which describe the displacements at node Q(i,j,k), shown in Figure G.1, are obtained by the solution of a similar set of equations to those used for equations G.1.16 and G.1.17 or by the reversing of the material parameters in the final equations.

G.1.2 Second order formulations for vertical interfaces.

Two vertical interface arrangements were considered in the present study and as with the equations used for the horizontal interface they are based on those derived by Ilan et al (1975) adapted to fit the coordinate scheme used in the present study.

The two nodes considered are shown in Figure G.2.

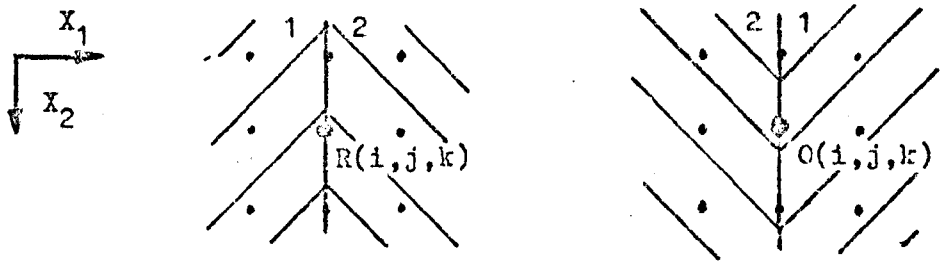

Node arrangements for vertical interfaces with second order formulations.

FIGURE G.2.

The equations for the displacements at the nodes R and shown in Figure G.2, can be obtained either by the system of fourteen equations which describes the configuration or by the application of transforms which are given by Ilan et al (1975).

For node R the transforms used are;

$$U_1 \longrightarrow U_2; \quad U_2 \longrightarrow U_1; \quad d \longrightarrow h; \quad \text{"i's"} \longrightarrow \text{"j's"} \qquad \text{G.1.22}$$

For node S the same transforms that are used for node R, equation G.1.22, followed by the reversing of the material parameters and velocities for the two media.

G.2.1 Quarter spaces welded in three-quarter spaces.

It is shown in the study by Ilan et al (1975) that a second order formulation, based on the equation of motion can be applied to a quarter space set into a three quarter space by using a different form for the mixed derivative term.

Two cases are considered in the present study and the node arrangements are shown as Figure G.3.

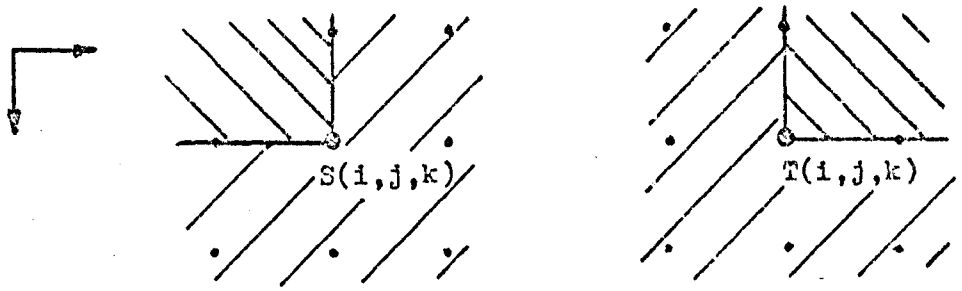

Node arrangements for quarter spaces welded in three-quarter spaces, with second order formulations.

FIGURE G.3.

The nodes used in the difference formulations are all assumed to be in the three-quarter space. Using this assumption, that all nodes are in the three quarter space, the formulations were applied to 270° corners and the detailed approximations are presented in Appendix F.2, as equations F.2.1 to F.2.3. (Page 254). which considers second order formulations for 270° corners.

G.3 The free surface/interface node for welded quarter spaces, a new second order formulation.

This appendix presents the derivation of a new second order formulation for the node P(i,j,k), shown in Figure C.4, at the intersection of a free surface and a vertical interface between two media.

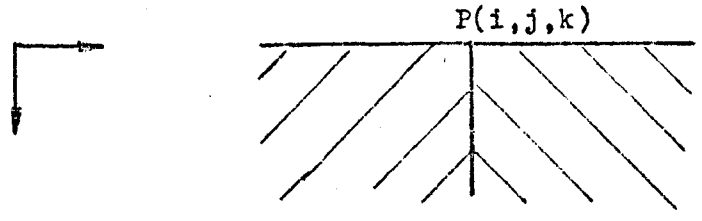

Node arrangement for the free surface/interface node in welded quarter spaces.

FIGURE G.4.

The equations which describe the time development of the displacements at node P(i,j,k) are obtained by the direct solution of the equations of motion, subject to the free surface and vertical interface boundary conditions.

The equations of motion are given as;

$$\frac{\partial^2 U_1^c}{\partial t^2} = V_{cj}^2 \frac{\partial^2 U_1^j}{\partial X_1^2} + V_{sj}^2 \frac{\partial^2 U_1^j}{\partial X_2^2} + (V_{cj}^2 - V_{sj}^2) \frac{\partial^2 U_2^j}{\partial X_1 \partial X_2} \qquad \text{G.3.1}$$

$$\frac{\partial^2 U_2^c}{\partial t^2} = V_{cj}^2 \frac{\partial^2 U_2^j}{\partial X_2^2} + V_{sj}^2 \frac{\partial^2 U_2^j}{\partial X_1^2} + (V_{cj}^2 - V_{sj}^2) \frac{\partial^2 U_1^j}{\partial X_1 \partial X_2} \qquad \text{G.3.2}$$

where $j = 1,2$ for the two media.

At the vertical interface the boundary conditions require the continuity of displacements so at the interface;

$$U_1^c = U_1^1 = U_1^2 \quad ; \quad U_2^c = U_2^1 = U_2^2 \qquad \text{G.3.3}$$

In thecequations G.3.1 and G.3.2 all the components are always differentiable with respect to time.

The boundary conditions for a stress free surface along $X_2 = 0$ are given as;

$$\frac{\partial U_2^j}{\partial X_1} = \frac{\partial U_1^j}{\partial X_2} = 0 \qquad \text{G.3.4}$$

$$\frac{\partial U_2^j}{\partial X_2} + (1 - 2(V_s^2/V_c^2)) \frac{\partial U_1^j}{\partial X_1} = 0 \qquad \text{G.3.5}$$

where $j = 1,2$ for the two media.

The equations for the stress free boundary condition can be differentiated with respect to X_1 to give;

$$\frac{\partial^2 U_1^j}{\partial X_1 \partial X_2} = -\frac{\partial^2 U_2^j}{\partial X_1^2} \qquad \text{G.3.6}$$

$$\frac{\partial^2 U_2^j}{\partial X_1 \partial X_2} = -(1 - 2(V_s^2/V_c^2)) \frac{\partial^2 U_1^j}{\partial X_1^2} \qquad \text{G.3.7}$$

The vertical boundary of the media is on X = constant, at the point P(i,j,k), and this has boundary conditions which are given as;

$$(\rho_1 V_{s1}^2)\frac{\partial U_1^1}{\partial X_2} - (\rho_2 V_{s2}^2)\frac{\partial U_1^2}{\partial X_2} = -\left[(\rho_1 V_{s1}^2) - (\rho_2 V_{s2}^2)\right]\frac{\partial U_2^c}{\partial X_1} \qquad \text{G.3.8}$$

$$(\rho_1 V_{c1}^2)\frac{\partial U_2^1}{\partial X_2} - (\rho_2 V_{c2}^2)\frac{\partial U_2^2}{\partial X_2} = -\left[(\rho_1(V_{c1}^2 - 2V_{s1}^2)) - (\rho_2(V_{c2}^2 - 2V_{s2}^2))\right]\frac{\partial U_1^c}{\partial X_1} \qquad \text{G.3.9}$$

The equations for the vertical interface boundary conditions can be differentiated with respect to X_2 to give;

$$(\rho_1 V_{s1}^2)\frac{\partial^2 U_1^1}{\partial X_2^2} - (\rho_2 V_{s2}^2)\frac{\partial^2 U_1^2}{\partial X_2^2} = -\left[(\rho_1 V_{s1}^2) - (\rho_2 V_{s2}^2)\right]\frac{\partial^2 U_2^c}{\partial X_1 \partial X_2} \qquad \text{G.3.10}$$

$$(\rho_1 V_{c1}^2)\frac{\partial^2 U_2^1}{\partial X_2^2} - (\rho_2 V_{c2}^2)\frac{\partial^2 U_2}{\partial X_2^2} = -\left[(\rho_1(V_{c1}^2 - 2V_{s1}^2)) - (\rho_2(V_{c2}^2 - 2V_{s1}^2))\right]\frac{\partial^2 U_1^c}{\partial X_1 \partial X_2} \qquad \text{G.3.11}$$

From Taylor series expansions it is necessary to define the expansions given as;

$$h\frac{\partial U_1^2}{\partial X_2} + \tfrac{1}{2}h^2\frac{\partial^2 U_1^2}{\partial X_2^2} = U_1^2(i,j+1,k) - U_1^c(i,j,k) \qquad \text{G.3.12}$$

$$\mp dh\frac{\partial^2 U_2}{\partial X_1 \partial X_2} = \left[-U_2^j(i\mp1,j,k) + U_2^j(i\mp1,j+1,k) + U_2^c(i,j,k) - U_2^c(i,j+1,k)\right] \qquad \text{G.3.13}$$

$$h\frac{\partial U_2^2}{\partial X_2} - \tfrac{1}{2}h^2\frac{\partial^2 U_2^2}{\partial X_2^2} = U_2^2(i,j-1,k) - U_2^c(i,j,k) \qquad \text{G.3.14}$$

$$\mp dh\frac{\partial^2 U_1}{\partial X_1 \partial X_2} = \left[-U_1^j(i\mp1,j,k) + U_1^j(i\mp1,j+1,k) + U_1^c(i,j,k) - U_1^c(i,j+1,k)\right] \qquad \text{G.3.15}$$

where j = 1,2 for the reverse and forward difference forms.

The equations given as equations G.3.1 to G.3.15 form the two sets of equations which describe the time development of the displacements at node P(i,j,k).

The horizontal component of displacement at node P(i,j,k) is obtained by the addition of the equations of motion for the two

media which are given by j = 1 and 2 in equation G.3.1. The resulting resulting equation is given as;

$$\left[\frac{1}{V_{s1}^2}+\frac{1}{V_{s2}^2}\right]\frac{\partial^2 U_1^c}{\partial t^2} - \left[\frac{\partial^2 U_1^1}{\partial X_2^2}+\frac{\partial^2 U_1^2}{\partial X_2^2}\right] =$$

$$\left[\frac{V_{c1}^2}{V_{s1}^2}\frac{\partial^2 U_1^1}{\partial X_1^2}+\frac{V_{c2}^2}{V_{s2}^2}\frac{\partial^2 U_1^2}{\partial X_1^2}\right]+\left[\frac{V_{c1}^2 - V_{s1}^2}{V_{s1}^2}\right]\frac{\partial^2 U_2^1}{\partial X_1 \partial X_2}+\left[\frac{V_{c2}^2 - V_{s2}^2}{V_{s2}^2}\right]\frac{\partial^2 U_2^1}{\partial X_1 \partial X_2} \quad \text{G.3.16}$$

The terms in equation are reduced by substitution of the equations for the boundary conditions and the Taylor series expansions to be in terms of derivatives of X_1 and a mixed term. This results in the equation given as;

$$\left[\frac{1}{V_{s1}^2}+\frac{1}{V_{s2}^2}\right]\frac{\partial^2 U_1^c}{\partial t^2} =$$

$$\left(1+\frac{\rho_2 V_{s2}^2}{\rho_1 V_{s1}^2}\right)\left[\frac{2}{h^2}\left\{U_1(i,j+1,k) - U_1(i,j,k) - h/2\left[\frac{(\rho_1 V_{s1}) - (\rho_2 V_{s2})\frac{\partial U_2}{\partial X_1} - (\rho_1 V_{s1})\frac{\partial U_2}{\partial X_1}}{(\rho_2 V_{s2}^2)} - \frac{\partial U_2}{\partial X_1}\right]\right\}\right]$$

$$+\frac{\partial^2 U_1^1}{\partial X_1^2}\left[\left[\frac{V_{c1}^2}{V_{s1}^2}\right]-\left[\frac{V_{c1}^2 - V_{s1}^2}{V_{s1}^2}\right]\left[\frac{V_{c1}^2 - 2V_{s1}^2}{V_{c1}^2}\right]\right]$$

$$+\frac{\partial^2 U_2^2}{\partial X_1 \partial X_2}\left[\left[\frac{V_{c2}^2 - V_{s2}^2}{V_{s2}^2}\right]-\left[\frac{V_{c2}^2}{V_{s2}^2}\right]\left[\frac{V_{c2}^2}{V_{c2}^2 - 2V_{s2}^2}\right]\right] \quad \text{G.3.17}$$

The finite difference form of equation G.3.17 is obtained by the substitution of the difference forms, given in Appendix D, for all the derivatives except the mixed term. It is found that the use of either the forward or the reverse expansions given as equation G.3.13 in equation G.3.17 for the case when the same material data is used for the two media results in small scattered pulses. The scattered pulses were eliminated by the use of an expression given as $G = (G_1 + G_2)/2$ where G_1 and G_2 are the forward and reverse expressions given as equation G.3.13.

The resulting finite difference form for the horizontal component of displacement is given as;

$$U_1(i,j,k+1) = 2\,U_1(i,j,k) - U_1(i,j,k-1)$$
$$+\left[\frac{s^2}{\frac{1}{V_{s1}^2}+\frac{1}{V_{s2}^2}}\right]\left\{\left(1-\frac{\rho_2 V_{s2}^2}{\rho_1 V_{s1}^2}\right)\left(\frac{2}{h^2}\right)\left[U_1(i,j+1,k)-U_1(i,j,k)+\frac{h}{2d}\left\{U_2(i+1,j,k)-U_2(i-1,j,k)\right\}\right]\right.$$
$$\left.+\left[\frac{1}{d^2}\right]\left[\frac{3-2V_{s1}^2}{V_{c1}^2}\right]\left[U_1(i+1,j,k)-2U_1(i,j,k)+U_1(i-1,j,k)\right]-G\right\} \qquad \text{G.3.18}$$

where $G = (G_1 + G_2)/2$

and $G_1 = \left[(3V_{c1}^2 - 2V_{s1}^2)/(V_{c1}^2 - 2V_{s1}^2) \div (\rho_1 V_{s1} - \rho_2 V_{s2})/\rho_2 V_{s2}\right]$

$\times$ (reverse form of equation G.3.13)

and similarly for G_2 except that the wave velocities and densities used in each term are those of the other medium, and the difference form used is that for the forward difference which is given in equation G.3.13.

A similar procedure to that used to derive equation G.3.18 is used to derive the equation for the vertical component of displacement which is given as;

$$U_2(i,j,k+1) = 2\,U_2(i,j,k) - U_2(i,j,k-1)$$
$$+\left[\frac{s^2}{\frac{1}{V_{c1}^2}+\frac{1}{V_{c2}^2}}\right]\left\{\left[\frac{2}{h^2}\right]\left\{U_2(i,j-1,k)-U_2(i,j,k)-\left[\frac{h}{2d}\right]\left[\frac{V_{c2}^2-V_{s2}^2}{V_{c2}^2}\right]\left[1-\frac{\rho_2 V_{c2}^2}{\rho_1 V_{c1}^2}\right]\left[U_1(i-1,j,k)-U_1(i-1,j,k)\right]\right\}\right.$$
$$\left.+\frac{1}{d^2}\left[\frac{V_{c1}^2-2V_{s1}^2}{V_{c1}^2}\right]\left[U_2(i+1,j,k)-2U_2(i,j,k)+U_2(i-1,j,k)\right]+H\right] \qquad \text{G.3.19}$$

where $H = (H_1 + H_2)/2$

and $H_1 = (V_{c2}^2 - 2V_{s2}^2)/V_{c2}^2 - \left[\rho_2(V_{c1}^2 - 2V_{s1}^2) - \rho_2(V_{c2}^2 - 2V_{s2}^2)/\rho_1 V_{c1}^2\right]$

$\times$ (reverse form of equation G.3.15)

and similarly for H_2 except that the wave velocities and densities used in each term are for the other medium, and the difference form used is that for the forward difference which is given in equation G.3.15.

Appendix H.

H. The Ricker Pulse.

The pulse of Rayleigh waves used in the present study is the Ricker pulse which was first described by Ricker (1945) in a geophysical study and has since been used by Boore (1970), in a numerical Love wave study, and by Munasinghe (1973), in a numerical study of Rayleigh waves on surface acoustic wave device configurations.

This appendix extends the description of the pulse used in the present study which is given in Section 4.4.1. The material presented here is in two parts, Appendix H.1, which considers the analytical equations of the Ricker pulse and Appendix H.2, which presents the digitised equations used for pulse synthesis.

H.1 Analytical equations for the Ricker pulse.

The vertical component of displacement for the Ricker pulse, at a horizontal free surface, is defined as;

$$R(X_1,0,0) = -(A\sqrt{\pi}) \left[\left(\frac{\pi X}{\gamma_o} \right)^2 - \frac{1}{2} \right] \exp \left[1 - \left(\frac{\pi X}{\gamma_o} \right)^2 \right] \qquad \text{H.1.1}$$

and this has a corresponding wavenumber amplitude spectrum, given as;

$$S(K) = \left(\frac{K}{K_o} \right)^2 \exp \left[1 - \left(\frac{K}{K_o} \right)^2 \right] \qquad \text{H.1.2}$$

where $\gamma_o = 2\pi/K_o$; A is a constant.

γ_o is the wavenumber, and K_o is the wave number at the centre frequency.

The surface displacements and the wavenumber amplitude spectrum for the basic pulse are shown as Figure H.1.

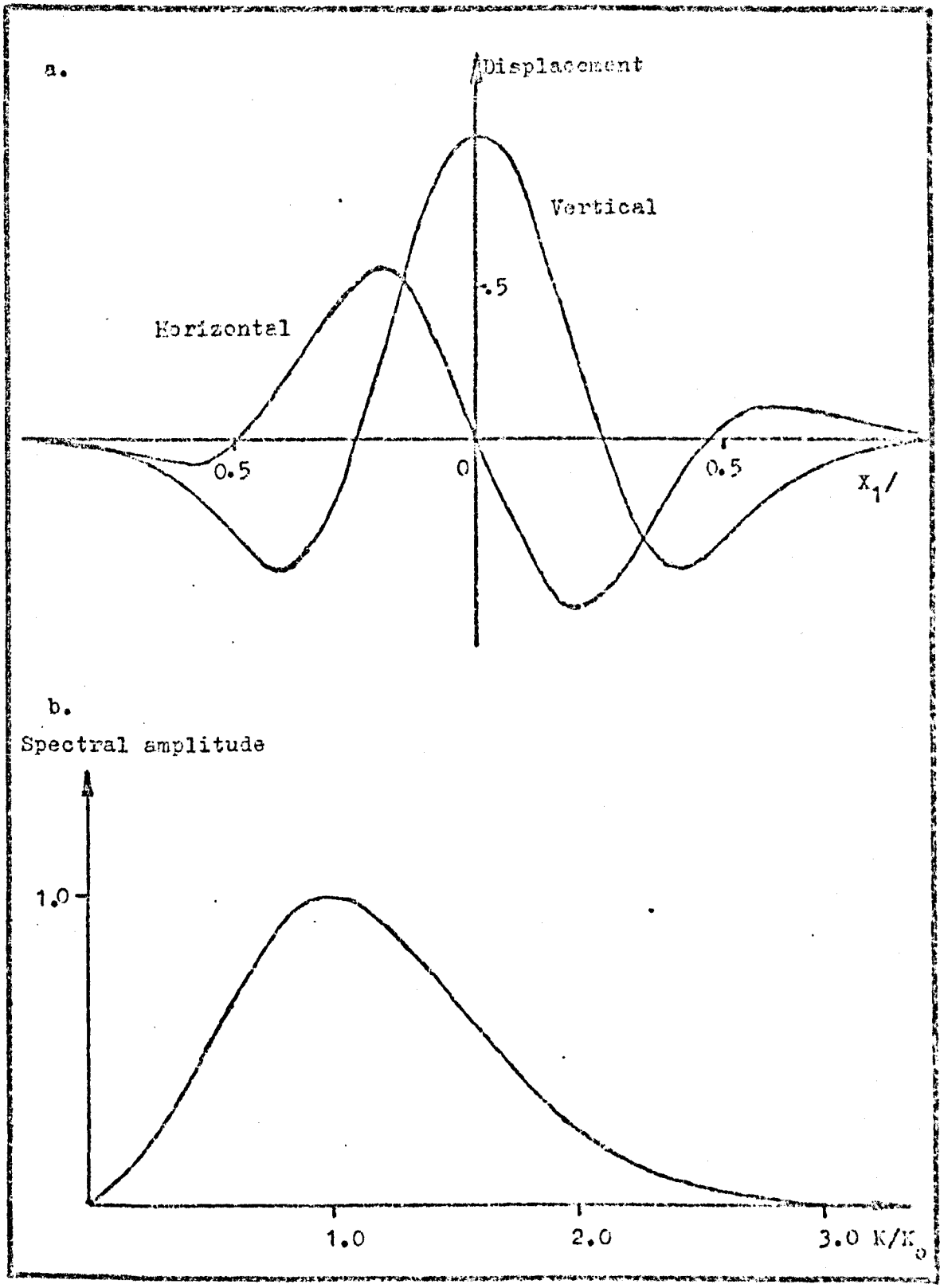

Normalised analytical forms of the Ricker pulse; a. Surface displacement wave forms. b. Wave number amplitude spectrum.

FIGURE H.1.

The operation of passing from a set of displacements to a wavenumber amplitude spectrum is achieved by integration. This integration has the form given as;

$$R(x,y,0) = A \int_{-\infty}^{+\infty} \left(\frac{K}{K_o}\right)^2 \exp\left[1 - \left(\frac{K}{K_o}\right)^2\right] \exp i\left(\frac{K}{K_o}\right)x \; d(K/K_o) \qquad H.1.3$$

where $x = KX/(K/K_o) = K_oX = 2\pi X/\gamma_o$ and X is a genuine length.

The integration is performed by the method of integration by parts, using the form given by Philips (1951).

The general form obtained being given as;

$$R(x) = A\frac{\sqrt{4\pi}}{2}\left[1 - \frac{x^2}{2}\right] \exp\left[1 - \frac{x^2}{4}\right] \qquad H.1.4$$

where A is an amplitude function.

One of the most important properties of this wavelet, as defined in Section 4.4.1, is that it is not too extensive in either the real or the wavenumber space.

The two dimensional Ricker pulse, which has surface displacements defined by equation H.1.1, can be synthesised by a method similar to that used by Boore (1970), who considered a one dimensional pulse. This method of pulse synthesis has been extended by Munasinghe (1973) to two dimensions and it is from the work by Munasinghe that the method presented here is derived.

It is known from the analytical theory for Rayleigh waves on a half-space, that, in the case of a homogeneous, isotropic, semi-infinite half-space that the lossless propagation of harmonic Rayleigh waves occurs. These analytically exact solutions to the half-space problem are known as Rayleigh eigenmodes. It has also been shown that the unit displacement eigenmodes($\underset{\sim}{\Phi}^K$) propagating in the positive X_1 direction, which satisfy the equations of motion and the boundary conditions for the stress free surface of a half-space, have the real form given by Munasinghe (1973) as;

$$\underset{\sim}{\Phi}^K = \begin{bmatrix} -B_1(KX_2) \sin K(X_1 - vt) \\ B_2(KX_2) \cos K(X_1 - vt) \end{bmatrix} \qquad H.1.5$$

where K is the wavenumber,

$v = W/K = V(K)$ is the Rayleigh wave velocity $= V_r$

W is the radian frequency,

B_1 and B_2 are real amplitude functions which decay with increasing depth X_2, normalised at the surface to $B_2 = 1$.

In the case of the homogeneous half-space the non-dispersive Rayleigh wave velocity is obtained from the equation given in Section 2.3 as equation 2.3.16 or by the use of the approximation, due to Bergmann (1949), which is given as equation 2.3.17.

The amplitude factors, in equation H.1.5, are given explicitly by Viktorov (1967) as;

$$\underline{B}(KX_2) = \begin{bmatrix} B_1 \\ B_2 \end{bmatrix} = \frac{1}{|K|(i\bar{Z}-R_c)} \begin{bmatrix} K & -(i\bar{Z})R\,K \\ -R_c|K| & (i\bar{Z})|K| \end{bmatrix} \begin{bmatrix} \exp(-|K|R_c X_2) \\ \exp(-|K|R_s X_2) \end{bmatrix} \qquad \text{H.1.6}$$

where $R_c^2 = 1 - (V_r/V_c)^2$; $R_s^2 = 1 - (V_r/V_s)^2$; $\bar{Z} = -i2R_c/(1+R_s^2)$

In the more general case of layered media both wave velocity and amplitude factors require numerical calculation (Sun 1970).

Extending consideration from the eigenmodes which make up a Rayleigh wave to those which are in a pulse, it is clear that a wave packet, such as the Ricker pulse, consisting of any linear combination of the appropriate eigenmodes ($\underline{\alpha}^K$) will give non-dispersive propagation on a half-space.

Thus the pulse defined by the Rayleigh eigenmodes, weighted with the wavenumber spectrum, is given as;

$$R(X_1,X_2,t) = \frac{1}{\pi} \int_0^\infty \underline{\alpha}^K(X_1,X_2,t)\, S(K)dK \qquad \text{H.1.7}$$

where $\underline{\alpha}^K = \begin{bmatrix} \alpha_1^K \\ \alpha_2^K \end{bmatrix}$

The equation H.1.7 can be transformed into the double sided Fourier integral which has the form given as;

$$R_1(X_1,X_2,t) = (\tfrac{1}{2}\pi) \int_{-\infty}^\infty iA_1(K\,X_2) \exp(iK(X_1 - vt)dK$$

$$R_2(X_1,X_2,t) = (\tfrac{1}{2}\pi) \int_{-\infty}^\infty A_2(K\,X_2) \exp(iK(X_1 - vt)dK \qquad \text{H.1.8}$$

where

$$A_1(K\,X_2) = S(K)\, B_1(KX_2) = -A_1(-KX_2)$$

$$A_2(K\,X_2) = S(K)\, B_2(KX_2) = A_2(-KX_2)$$

At the free surface the vertical component at t = 0, defined by equation H.1.7, reduces to the form given as;

$$R_2(X_1,0,0) = (1/2\pi)\int_{-\infty}^{+\infty} S(K)\exp(iKX_1)dK \qquad \text{H.1.9}$$

It is seen from the tables of integral transforms (Erdelyi 1954) that the Fourier transform in equation H.1.9 is identical to equation H.1.1. It is also seen that the terms on the right hand s side of equation H.1.8 are either known explicitly or can be computed numerically and this enables the synthesis of the displacements for a Ricker type pulse at t = 0 and t=s using Fourier transforms.

H.2 Pulse synthesis.

The Ricker type pulse used in the present study is produced by the use of digitised forms of the analytical equations which are given in Appendix H.1.

Each wave number component is calculated at each depth level and for the two time steps using the explicit expressions for the real and imaginary (Jth) wavenumber developed by Kumasinghe, which is given as;

$$\begin{bmatrix} \text{Re Data}_1(J) \\ \text{Im Data}_1(J) \\ \text{Re Data}_2(J) \\ \text{Im Data}_2(J) \end{bmatrix} = \left[(J-1)^2/N\gamma_o n_k^2\right]\exp\left[1-\left[\frac{(J-1)}{n_k}\right]^2\right] \times$$

$$\begin{bmatrix} C_1\sin(r_v(J-1)t) & -C_2\sin(r_v(J-1)t) \\ C_1\cos(r_v(J-1)t) & -C_2\cos(r_v(J-1)t) \\ -D_1\cos(r_v(J-1)t) & D_2\cos(r_v(J-1)t) \\ -D_1\sin(r_v(j-1)t) & D_2\sin(r_v(J-1)t) \end{bmatrix} \begin{bmatrix} \exp(-r_c X_2'(J-1) \\ \exp(-r_s X_2'(J-1) \end{bmatrix}$$

H.2.1

where $n_k = K_o/\Delta K = N/N_x$, the number of wavenumber points per unit centre wavelength.

$N_x = \gamma_o/\Delta X$ number of nodes per pulse centre wavelength.

$\Delta X = \gamma_o/N_x$ and $\Delta K = 2\pi/N(\Delta X)$ spatial and wavenumber increments.

$X_2' = X_2/\gamma_o$ depth, scaled in units of wavelengths (γ_o).

The constants used in equation H.2.1 are defined as;

$$C_1 = (1 + R_s^2)/R_c(1 - R_s^2) \qquad C_2 = 2R_s/(1 - R_s^2)$$

$$D_1 = (1 + R_s^2)/(1 - R_s^2) \qquad D_2 = 2/(1 - R_s^2)$$

$$r_v = 2\pi V_r/N_k \text{ o} \qquad r_c = 2\pi R_c/N_k \qquad r_s = 2\pi R_s/N_k$$

$$R_s^2 = 1 - (V_r/V_s)^2 \qquad R_c^2 = 1 - (V_r/V_c)^2$$

The data array (Data (J)) is evaluated for the full range of J values, for both the real and imaginary components, at each depth and for each time level. For each array of N real and complex components, which correspond to one depth and one time, the set of displacement for this depth and at this time are obtained by the operation of the discrete Fourier transform. This operation can be written as;

$$\text{Trans}(M) = \sum_{J-1}^{N} \text{Data}(J) \exp \pm 2\pi i(J-1)(M-1)/N \qquad \text{H.2.2}$$

for M = 1,2....N and where the positive and negative signs refer to the forward and inverse transforms respectively.

In the present study the operation defined by equation H.2.2 was performed by a version of the Cooley-Tukey(1965) method which folds data about ((N/2) + 1) and is a standard NAG subroutine (ULCC 1976).

The use of the NAG subroutine results in the need to reorder the basic data and this is considered in Figure 4.9.

The application of the digitised form, given as equation H.2.1, is considered further in Section 4.4.1.

References.

Alford R.M, Kelly K, Boore D.(1974)
Accuracy of finite difference modelling of the acoustic wave equation (seismology).
Geophysics (USA) 39 (6) 834-42.

Alsop I.E, Goodman A.S.(1972)
Finite difference formular for Neumann conditions on irregularly shaped boundaries.
I.B.M. J.Res.& Dev. 16 365-371.

Alterman Z.S, Karal F.C.(1968)
Propagation of elastic waves in layered media by finite difference methods.
Bull. Seis. Soc Am. 58 367-398.

Alterman Z.S, Karal F.C.(1970)
Propagation of elastic waves in a semi-infinite cylindrical rod using finite difference methods.
J. Sound Vib. 13 (2) 115-145.

Alterman Z.S, Loewenthal D. (1970)
Seismic waves in a quarter and three-quarter plane.
Geophys. J. Royal Astr. Soc. 20 (2) 101-26.

Alterman Z.S, Loewenthal D. (1972)
Computer generated seismograms.
Methods in Computational Physics. Vol 12. 35-164.
Ed. B.Bolt Academic Press,(New York London)

Alterman Z.S, Rotenberg A. (1969)
Seismic waves in a quarter plane.
Bull. Seis. Soc. Am. 59 (1) 347-368.

Ames W.F. (1969) Numerical methods for partial differential equations.
Barnes and Noble (New York)

Auld B.A. (1962) Application of microwave concepts to the theory of Acoustic Fields and waves in Solids.
IEEE Trans. Microwave Theory Tech., MTT-17, 800

Baborovsky V.M, Marsh D.M, Slater E.A. (1973)
Schlieren and computer studies of the interaction of ultrasound with defects.
Non-Destr. Test. 6 (4) 200-7.

Benson C. (1950) Supersonic Testing. U.S. Patent 2,527,896.

Bergmann L. (1949) Ultraschall und seine Anwendung in Wissenschaft und Technik.
Edwards. Ann Arbor. Mich. (In German)

Bertholf L.D, Benzely S.E. (1968)
Toody 2, A computer code for two dimensional wave propagation.
Sc-RR-68-41, Scandia Labs. Albuquerque N.M.(USA)

Brinczewski G.I. (1957) Standardization and application of ultrasonic surface-wave inspection.
Non-Destr. Test. 15 (1) 36-42.

Böhme W. (1958) Nondestructive testing of aluminium articles with ultrasonic pulses.
Aluminium 34 (4) 200- 205. (In German)

Bolt B.A. (1978) Editor, Special Volume to commemorate the life and and work of the late Professor Z.S.Alterman.
J. Comp. Physics. (In press)

Boore D.M. (1970) Love waves in nonuniform wave guides; Finite difference calculations.
J. Geophys. Res. 75 1512-1527.

Boore D.M. (1972) Finite difference method for seismic wave propagation in heterogeneous materials.
Methods in Computational Physics. Vol 11.
Ed. B.A.Bolt Academic Press (New York, London)

Bradfield G. (1964) Use in industry of elasticity measurements in metals with the help of mechanical vibrations.
N.P.L. Notes on Applied Science No. 30.

Bremaecker J.A.de (1958)
Transmission and reflection of Rayleigh waves at corners.
Geophysics 23 (2) 253-266.

Bridge B. El-Dardiry S.M.A. (1976)
An investigation of the surface structure of machined bright steel, using 5 MHz Rayleigh waves.
Symposium paper, Non destructive testing control of materials. Slovak Scientific and Technical Society Publishing Centre. Bratislava.

Brown A.F. (1973) Materials testing by ultrasonic spectroscopy.
Ultrasonics 11 202-210.

Brown A.F. (1976) Ultrasonic spectroscopy.
Contributed to; Ultrasonic Testing Ed. J.Szilard.

Brown A.F. (1978) Ultrasonic spectroscopy in nondestructive testing.
Sci. Proj. (Oxf) 65 (In press)

Brummer S.B, Bell R.O, Cocks F.H, Cordellos A. (1969)
Study of the general mechanism of stress corrosion of aluminium alloys and the development of techniques for its detection. NASA-CR-102693, contract no, NAS8-20297
Toyco Labs. Inc.

Bykov N.S, Shneider Yu.G. (1960)
An experimental investigation of the effect of surface quality on the attenuation of surface waves.
Soviet Phys. Acoust. 6 (4) 500-502.

Chisolm J.S.R, Morris R.M. (1965)
Mathematical Methods in Physics.
W.B.Saunders (Philadelphia)

Cole P.T.C (1977) Use of electromagnetic-acoustic surface waves in the inspection of hot semi-finished steel products. Meeting on Surface Acoustic waves, Physical Acoustics Group Institute of Acoustics Essex Univ. 26 Sept.

Cook D. (1972) Crack depth measurements with surface waves.
Brit.Aco.Soc. Spring Meeting 5th-7th April
Loughborough university.

Cook E.G, Valkenburg H.E. (1954)
Surface waves at ultrasonic frequencies.
ASTM Bull. 198 (5) 81-84.

Cooley J.W, Tukey J.W. (1965) An algorithm for machine calculation of complex Fourier series.
Math. of Comp. 19 (9) 297-301.

Cordellos A.D, Bell R.O, Brummer S.B. (1969)
Use of Rayleigh waves for the detection of stress-corrosion cracking (S.C.C.) in aluminium alloys.
Materials evaluation 27 (4) 85-90

Cottrell A.H. (1964)
The Mechanical Properties of Matter.
John Wiley & Sons. (New York London Sydney)

Courant R, Friedricks K.O. Lewy H. (1928)
Uber die partiellen Differenzengieichungen der mathematischen Physik.
Math. Ann 100 32- (In German)

Courant R, Hilbert D. (1962)
Methods of Mathematical Physics Vol. 2.
Interscience (New York)

Cuozzo F.C, Cambiaggio E.L, Damiano J.P, Rivier E. (1977)
Influence of Elastic Properties on Rayleigh wave Scattering by Normal Discontinuities.
IEEE Tran. Son. & Ultrason. SU-24 (4) 280-289

Curtis G.J. (1975)
A review of current ultrasonic nondestructive testing in the U.K.
Report AERE-R-7946. HMSO.

Davis L. West L. (1973)
Observed effects of topography on ground motion.
Bull. Seis. Soc. Am. 63 (1) 283-298.

Dally J.W, Lewis D. (1968)
A photoelastic analysis of propagation of Rayleigh waves past a step change in elevation.
Bull. Seis. Soc. Am. 58 (2) 539-564.

Dory Jacques. (1973) The scope of application of frequency analysis in NDT by ultrasonic examination.
Paper G24, 7th International Conference on NDT, Warsaw. 4th-8th June.

Drake L.A. (1972) Rayleigh waves at a continental boundary by the finite element method.
Bull. Seismol. Soc. Am. 62 (5) 1259-68.

Erdélyi A. Ed. (1954) Tables of integral transforms, Vol.1.
McGraw-Hill (New York)

Ewing W.M, Jardetzky W.S, Press F. (1957)
Elastic waves in layered media.
McGraw-Hill (New York)

Farnell G, Adler E. (1972) Physical Acoustics, Vol 9 Part A.
Ed. W.Mason and R.N.Thurston.
Academic Press (New York)

Firestone F. (1942) Flaw detection device and measuring instrument.
U.S. Patent No 2,280,226. 21st April.

Firestone F. (1945) The supersonic reflectorscopy for interior inspection.
Metal Progress, September 505-12.

Firestone F, Frederick J.R. (1946)
Refinements in supersonic reflectoscopy.
J. Acoust. Soc. Am. 18 (1) 200-211.

Frank R.H. (1952) Ultrasonics- inspection applications grow.
Steel 130 (24) 99-102.

Friedrichs K.O, Keller H.B. (1966)
A finite difference scheme for generalized Neumann problems. Numerical solutions of partial differential equations.
Academic Press (New York)

Frost H.M, Sethares J, Szabo T.L. (1975)
Applications for new electromagnetic SAW transducers.
Proc. Ultrasonics Symp. 1975 IEEE 604-607.

Fuchs K, Muller G. Editors (1977) Proceedings of the Eleventh International Symposium on Mathematical Geophysics, 18-27 August 1976, Seeheim/Odenwald F.R.Germany
Published as; Journal of Geophysics 43 (1/2)

Gangi A.F. (1967) Experimental determination of P wave/Rayleigh wave conversion coefficients at a stress-free wedge.
J. Geophys. Res. 72 5685-92

Gericke O.R. (1963) Determination of the geometry of hidden defects by ultrasonic pulse analysis testing.
J.Acoust.Soc.Am. 35 364-368.

Gericke O.R. (1965) Materials research and standards 5 (1) 23-30.
Pergamon Press (Oxford)

Gericke O.R. (1971) Ultrasonic Spectroscopy.
Encyclopaedic Dictionary of Physics, Supplement 4.
Pergamon Press (Oxford) 502-506.

Gilbert J.C. (1976) The Calcomp 1670 Microfilm Plotter.
University of London Computer Centre Bull. M.8/2.

Graff Karl F. (1975) Wave motion in elastic solids.
Clarendon Press (Oxford)

Gutenberg B, Richter C.F. (1939) Seismic waves Part 4.
Gerlands Beitr Z. Geophys. 54 (2) 94-136.

Gutenberg B. Ed. (1951) Internal Constitution of the Earth.
Dover Pub. Inc. (New York)

Haines N.F. (1976) Ultrasonic spectroscopy.
Physics in Technology 7 (3) 108-115.

Hall K.G. (1976) Crack depth measurement in rail steel by Rayleigh waves aided by photoelastic visualization.
Non-destructive Testing 9 (3) 121-126.

Harnik E. (1977) A broadband probe for studies of accustic surface waves.
J. Phys. E. (J.Sci.Inst.) 10 1217-1218

Haydl W.H. (1974) Surface wave reflection from right angle corners in GaAs.
IEEE Sonics. & Ultrason. SU-21 (2) 120-124.

Hentzi A.N, Dally J.W. (1971)
A photoelastic study of stress wave propagation in a quarter plane.
Geophysics 36 296-

Herrera I. (1964) On a method to obtain a Green's function for a multi-layered half-space.
Bull. Seism.Soc.Am. 54 1087-1096

Hudgell R.J, Morgan L.L, Lumb R.F. (1974)
Non-destructive measurement of the depth of surface-breaking cracks using ultrasonic Rayleigh waves.
Brit. J. NDT. 16 (5) 144-149.

Hudson J.A, Knopoff L. (1964)
Transmission and reflection of surface waves at a corner. 1. Love waves, 2. Rayleigh waves.
J.Geophys.Res. 69 (2) 275-280,281-290.

Hudson J.A. (1970) The attenuation of surface waves by scattering.
Proc.Cambridge Phil.Soc. 67 (1) 215-223.

Hudson J.A. (1977) Ray theory/perturbation techniques for surface waves in solids. Colloquia 23rd Feb. The City Univ.

Ilan A. (1977a) Representation of boundary conditions in finite difference schemes for seismological problems.
Ph.D. Thesis Tel-Aviv Univ. Israel. January 1977.

Ilan A. (1977b) Finite difference modelling for P-pulse propagation in elastic media with arbitrary polygonal surface.
Proceedings of 11th International Symposium on Mathematical Geophysics. Published as J.Geophysics 43 (1/2)

Ilan A. (1978, In press) Stability of finite difference schemes for the problem of elastic wave propagation in a quarter plane. J.Comp.Phys.

Ilan A, Loewenthal D. (1976) Stability of finite difference schemes due to boundary conditions in elastic media. Geophysical Prospecting 24 431-453.

Ilan A, Ungar A, Alterman Z.S. (1975) An improved representation of boundary conditions in finite difference schemes for seismological problems. Geophys.J.R.Astr.Soc. 93 727-795.

Julian B.R, Gubbins D. (1977) Three dimensional seismic ray tracing. Proceedings of 11th International Symposium on Mathematical Geophysics. Published as J.Geophysics 43 (1/2) 95-114.

Kane J, Spence J. (1963) Rayleigh wave transmission on elastic wedges. Geophysics. 28 (5) Part 1 715-723.

Kaye G, Laby T.(1962) Tables of physical and chemical constants. Longmans (London)

Kennett B.L.N. (1974) Reflections, rays and reverberations (Seismic waves). Bull.Seismol.Soc.Am. 64 (6) 1685-96.

Key S.W. (1975) HONDO- A finite element computer program for the large deformation response of axisymmetric solids. Scandia Labs. SLA-74-0039 (Second printing Aug. 1975)

Knopoff L, Gangi A.F. (1960) Transmission and reflection of Rayleigh waves by wedges. Geophysics 25 (6) 1203-1214.

Krautkramer J.& H. (1969) Ultrasonic testing of materials. Heidelberg (New York)

Lapwood E.R. (1961) The transmission of a Rayleigh pulse round a corner. Geophys.J. 4 174-196

Lax P.D, Wendroff B.(1964) Difference schemes for hyperbolic equations with high order of accuracy. Comm. Pure and App. Math. 17 381-398

Li R.C.M. (1972) Analysis of surface wave reflection from a series of grooves. Proc.IEEE Ultr Symp 72 CHO 807-8SU 263-

Lidington B.H, Silk M.G. (1975) Crack depth measurements using a single surface wave probe. Brit.J.NDT. 17 (6) 165-167.

Lloyd E.A. (1970) Wide band ultrasonic techniques. Proc.Symp. The future of Ultrasonic spectroscopy. Ed. P.M. Reynolds, Brit.Non-ferrous Metals Res.Ass. 14th October. London.

Lloyd E.A. (1974) Non-destructive testing of bonded joints.
Non-destructive Testing 7 (6) 331-334.

Lloyd E.A. (1975) Developments in ultrasonic spectroscopy.
Proc. Ultrasonics Int. London April
IPC. 54-57.

Love A.E.H (1934) A treatise on the mathematical theory of elasticity.
Cambridge University Press (London)

Lumb R.F. (1977) Inspection of pipelines using nondestructive
techniques. Physics in Technology 8 249-256.

Lysmer J. (1970) Lumped mass method for Rayleigh waves.
Bull.Seismol.Soc.Am. 60 89-104.

Lysmer J, Drake L.A. (1972) A finite element method in seismology.
Methods in Computational Physics, Vol. 11. Ed. B.A. Bolt.
Academic Press (New York London)

Mal A.K, Knopoff L. (1965) Transmission of Rayleigh waves past a
step change in elevation.
Bull.Seismol.Soc.Am. 55 (2) 319-334.

McGarr A, Alsop L.E. (1967) Transmission and reflection of
Rayleigh waves at vertical boundaries.
J.Geophys.Res. 72 (8) 2169-2180.

Minton W.C. (1954) Inspection of metals with ultrasonic surface
waves. Nondestructive Testing (July-August) 13-16.

Morgan L.L. (1970) Surface acoustic wave transducers.
M.Sc. Thesis Univ. of London.

Morgan L.L. (1973) Crack size evaluation using ultrasonic surface
wave spectroscopy.
Ph.D. Thesis, The City University.

Mow C, Pao Y. (1971) The diffraction of elastic waves and dynamic
Stress concentrations.
RAND Report R-482-PR.

Munasinghe M. (1973) Numerical solution for acoustic Rayleigh wave
scattering in discontinuous media.
Ph.D. Thesis, McGill Univ. Canada.

Munasinghe M. (1976) Numerical solutions for acoustic Rayleigh wave
problems in anisotropic and layered media.
Ultrasonics 14 (1) 9-14.

Munasinghe M, Farnell G.W. (1972)
Surface wave scattering at vertical discontinuities.
Proc. IEEE Ultr Symp 72 CHO 708-8SU 267-270.

Munasinghe M, Farnell G.W. (1973)
Acoustic surface-wave scattering on a homogeneous
three-quarter space.
J.Applied Phys. 44 (5) 2025-2031.

Musil F.J. (1967) Eddy current and ultrasonic techniques for inspection of large parts.
J.Mater. 2 (1) 65-80.

Nye J.F. (1960) Physical properties of crystals.
Clarendon Press (Oxford)

Ottaviarni M. (1971) Elastic wave propagation in two evenly welded quarter spaces.
Bull.Seismol.Soc.Am. 61 (5) 1119-1152.

Philips E.G. (1951) Functions of a complex variable.
Oliver and Boyd (London)

Pilant W.L, Knopoff L, Schwab F. (1964)
Transmission and reflection of surface waves at a corner, 3. Rayleigh waves (experimental).
J.Geophys Res. 69 (2) 291-298.

Pohlman R. (1963) Detection of surface cracks in nitrated heat treated steels by means of ultrasonic surface waves.
Z.Instrumentenk 71 (12) 322-329. (In German)

Quentin G, de Billy M, Tenoudji F.C, Doucet J, Jungman A. (1975)
Experimental results on the scattering of ultrasound by randomly or periodically rough surfaces in frequency range 2 to 25 Mhz.
Proc.1975 Ultrasonics Symp. 102-106.

Rasmussen I.G. (1962) Prediction of fatigue failure using ultrasonic surface waves.
Non-destr. Test. 20 (2) 103-110.

Rayleigh Lord. (1885) On waves propagated along the plane surface of an elastic solid.
Proc.London Math.Soc. 17 4-11.

Reinhardt H.W, Dally J.W. (1970) Some characteristics of Rayleigh wave interaction with surface flaws.
Mater.Eval. 28 (10) 213-220.

Richtmyer R.D, Morton K.W. (1967)
Difference methods for initial value problems.
Interscience Pub. (New York London Sydney)

Ricker N. (1945) The computation of output disturbances from amplifiers for true wavelet inputs.
Geophys 10 207-220.

Ronnekliev A, Souquet J. (1975)
Surface wave to bulk wave scattering from grooves.
Proc.IEEE Ultrasonics Symp. 73 Cho 994-4SU, 434-437.

Rose J.L. (1971) Elastic wave propagation in multi layered spheres and cylinders MCDIT-24 Computer code.
Drexil Univ. Mech. & Structures Res Report No 71-1.

Rose J.L, Meyer P.A. (1973) Ultrasonic procedures for predicting adhesive bond strength.
Mat. Eval. 31 (6) 109-114.

Rose J.L, Meyer P.A. (1974) Ultrasonic signal processing concepts for measuring the thickness of thin layers. Mater.Eval. 32 (12) 249-255 & 258.

Rose J.L, Meyer P.A. (1975) Model for ultrasonic field analysis in solids. J.Acoust.Soc.Am. 57 (3) 598-605.

Rykunov L.N, Tkhukh F. (1972) A study of the effect of local heterogeneities on the Rayleigh wave field. Acad.Sci.USSR Phys.Solid Earth 5 309-14

Sabina F.J, Willis J.R. (1977) Scattering of Rayleigh waves by a ridge. Proc. 11th International Symp. on Mathematical Geophysics. Published as J.Geophys. 43 (1/2) 401-420.

Scherneck H.G. (1976) Notes on computer model for geophysics. Frankfurt Univ. (Unpublished, In German)

Seville A.H. (1977) Ultrasonic Spectroscopy. Physics in Technology 8 34-35.

Shraiber D.S. (1959) Flaw detection in metals. From Collection of papers on Ultrasonic flaw detection . Gos.Izd.Oboron.Prom (Moscow) 214-355.

Silk M.G. (1976) The determination of crack penetration using ultrasonic surface waves. NDT International 10 290-297.

Smith W.D. (1975) The application of finite element analysis to body wave propagation problems. Geophys.J.R.Astr.Soc. 42 747-768.

Sokolinskii A.G. (1958) Technique for the excitation and reception of surface waves. Author's Cert. No. 19297(1958) USSR.

Sommerfeld A. (1950) Mechanics of deformable bodies. Academic Press (New York)

Stockl H. (1977) Finite difference calculation of stress relaxation earthquake models. Proc. 11th International Symp. on Mathematical Geophysics. Published in J.Geophys. 43 (1/2) 311-328.

Stoneley R. (1924) Elastic waves at the surface of separation of two solids. Proc.Roy.Soc. A 106 416-28.

Sun I.H. (1970) Elastic waves guided by isotropic layers. M.Eng. Thesis Elec.Eng.Dept. McGill University.

Thompson D.O. (1976) Proceedings of the ARPA/AFML review of quantitive NDE. Science Centre, Rockwell International Tech Report No. AFML-TR-75-212.

Tolley J. (1972) Ultrasonic Rayleigh and Lamb waves in N.D.T.
The City University Centre for Information Science.

Tuan H-S. (1975) On bulk waves excited at a groove by Rayleigh waves.
J.Appl.Phys.(USA) 46 (1) 36-41.

Tuan H-S, Parekh J.P. (1975)
Influence of groove profile on surface to bulk wave conversion of Rayleigh waves at shallow grooves.
Proc.IEEE Ultrasonics Symp. 1975 75 CHO 994-4SU

ULCC (1976) Fortran extended version 4 reference manual CDC.
Mass storage input/output Section 111.7.
University of London Computer Centre.

Urazakov E.I, Falkovskii L.A. (1973)
Propagation of a Rayleigh wave along a rough surface.
Sov. Phys. JETP 36 (6) 1214-16.

Viktorov I.A. (1967) Rayleigh and Lamb waves.
Trans. by Consultants Bureau.
Plenum Press (New York)

Viswanathan K. (1966) Wave propagation in welded quarter spaces.
Geophys J.R.Astr.Soc. 11 293-322.

Viswanathan K, Kuo J.T, Lapwood E.R. (1971)
Reflection and transmission of Rayleigh waves in a wedge 1.
Geophys.J.R.Astr.Soc. 24 (4) 401-14.

Viswanathan K, Roy A. (1973)
Reflection and transmission of Rayleigh waves in a wedge 2.
Geophys.J.R.Astr.Soc. 32 (4) 459-78.

Vybornov B.I. (1969) Ultrasonic method for the early detection of failure of the material in fatigue tests.
Industr. Lab. 35 (6) 838-841.

Vybornov B.I, Ogurtsov K.A. (1962)
The small size UZDL-61 ultrasonic defectoscope for testing gas turbine blades.
Industr. Lab. 28 (8) 1056-1058.

Waddell D. (1974) An introductory guide to Update.
Univ. London Computer Centre Bull. B.2.7/1.

Waas G. (1972) Earth vibration effects and abatement for military facilities Report No 3. Analysis method for footing vibrations through layered media.
US Army Eng. Waterways Exp. Station Tech. Rep. S 71-14.

Weight J.P. (1975) Instrumentation associated with the development of wideband ultrasonic techniques (ultrasonic spectroscopy)
M.Phil. Thesis. The City University.

White R.M. (1970) Surface elastic waves.
Proc. IEEE 58 (8) 1238-1276.

Woods R.D. (1968) Screening of surface waves in soils.
J.Soil Mech.Found.Div.ASME. 94 915-979.

Yoneyama T, Nishida S. (1976)
Further calculations on Rayleigh wave diffraction by elastic wedges.
J.Acoust.Soc.Am. 59 (1) 206-208.

Young J. (1977) The significance of Defects Symposium.
Report in Brit.J.NDT. 19 (4) 184.

Zienkiewicz O.C. (1971) The finite element method in engineering science.
McGraw-Hill (London)